Novel Aluminium Phosphonate Materials

A thesis submitted in application for the title of Ph.D.

by

Dipl.-Chem. Nadja Zakowsky

University of St. Andrews

Supervised by Prof. Russell E. Morris

Submitted January 2002

Declaration

I, Nadja Zakowsky, hereby certify that this thesis, which is approximately 35,000 words in length, has been written by me, that it is the record of work carried out be me and that it has not been submitted in any previous application for a higher degree.

Date 31.5.2002 Signature of Candidate

I was admitted as a research student in September 1998 and as a candidate for the degree of Doctor of Philosophy in September 1999; the higher study for which this is a record was carried out in the University of St. Andrews between 1998 and 2001.

Date 31.5.2002 Signature of Candidate

I hereby certify that the candidate has fulfilled the conditions of the Resolution and Regulations appropriate for the degree of Doctor of Philosophy in the University of St. Andrews and that the candidate is qualified to submit this thesis in application for that degree.

Date 31 May 2002 Signature of Supervisor

In submitting this thesis to the University of St. Andrews I understand that I am giving permission for it to be made available for use in accordance with the regulations of the University Library for the time being in force, subject to any copyright vested in the work not being affected thereby. I also understand that the title and abstract will be published, and that a copy of the work may be made and supplied by any *bona fide* library or research worker.

Date 31.5.2002 Signature of Candidate

Acknowledgements

I would like to express my thanks to Prof. Russell E. Morris for his enthusiastic supervision and constant encouragement and to Dr. Gary B. Hix for patiently answering many questions during my first year. Thanks also go to Dr. Paul A. Connor, my colleagues from the Morris group, Dr. Martin P. Attfield, Dr. Simon S. Teat at the CCLRC in Daresbury, Dr. David Apperley at the EPSRC Solid State NMR Service Durham, Dr. Alex Slawin (single crystal XRD) and Sylvia Williamson (CHN analysis) at the University of St. Andrews. Dr. P.A. Cox kindly permitted the use of some of his results in this thesis.

I'm very grateful to my parents who always are supportive. – Ich bin meinen Eltern für ihre liebevolle Unterstützung sehr dankbar.

Furthermore, there are many people who made my time as a PhD student in St. Andrews a pleasant one; especially Angela, Catherine, Dan, Frances, Jennifer, Rafa, Sneh and Takumo as well as quite a few others. My uncle, Ekkehard Maurer, shows continuous interest in my work and I'd like to take this opportunity to thank him very much.

In the end I would like to thank the organisations who funded my work; the EPSRC, the School of Chemistry at the University of St. Andrews, and the Dr. Wamsler Stiftung GmbH in Munich, Germany, which made life as an overseas student so much easier.

Table of Contents

Abbreviations and key to graphs

AlaPrPO	Aluminium 3-aminopropylphosphonate
AlBzPO	Aluminium benzylphosphonate
approx.	approximately
CHN	Microanalysis; percentage of carbon, hydrogen, and nitrogen in a compound
DCC	Dicyclohexylcarbodiimide
FOM	Figure of merit
HCl	Hydrochloric acid
HNO_3	Nitric acid
H_2SO_4	Sulphuric acid
IR	Infrared
LB	Langmuir-Blodgett
MAS NMR	Magic angle spinning nuclear magnetic resonance
N-H···	N-H group with H bonding
O-H···	O-H group with H bonding
PA	Phosphonic acid
Pr_3N	Tripropylamine
PTFE	Polytetrafluoroethylene
r.t.	Room temperature
TGA	Thermogravimetric analysis
TMS	Tetramethylsilane
XRD	X-ray diffraction
α-ZrP	α-zirconium phosphate

γ-ZrP γ-zirconium phosphate

The key for graphs containing structures is the following;

light or dark blue spheres…	metal atoms,
yellow spheres…	phosphorus atoms,
red spheres…	oxygen atoms,
black spheres…	carbon atoms and
white spheres…	hydrogen atoms.

Other kinds of atoms are specified in the figure captions. The exact nature of the metal atom can be found in the sum formula of the material given in the figure caption.

Abstract

A number of functionalised layered aluminium phosphonates have been synthesised from various aluminium sources (*e.g.* gibbsite, aluminium chloride) with different phosphonic acids by hydrothermal treatment, under reflux and in one instant by melting the phosphonic acid with aluminium nitrate. The products were analysed using powder, microcrystal and single crystal X-ray diffraction, ^{27}Al, ^{31}P, ^{15}N and ^{13}C MAS NMR, CHN analysis, TGA and IR spectroscopy.

The possibilities opened by the variation of the synthesis conditions were explored to prepare materials with different structures from the same phosphonic acid/aluminium source system. A first series of experiments was carried out investigating the influence of aluminium source, pH value and Al:P ratio on products prepared from benzylphosphonic acid. Two new phases have been fully characterised; $Al_3H(PO_3CH_2C_6H_5)_5.H_2O$, monoclinic $P2_1/c$, a = 17.2497 (13) Å, b = 25.7851 (18) Å, c = 9.4339 (7) Å, β = 103.567 (1)° and $Al(OH)(O_3PCH_2C_6H_5).H_2O$, monoclinic $P2_1/c$, a = 14.985 (9) Å, b = 7.066 (5) Å, c = 9.613 (9) Å, β = 113.9 (3)°. The nature of two other phases could not be determined.

Attempts to transfer the results obtained from the aluminium benzylphosphonates to reactions with amino-functionalised phosphonic acids were only partly successful. Nevertheless, it was possible to prepare a new aluminium 3-aminopropylphosphonate phase; $Al(O_3P(CH_2)_3NH_3).SO_4.H_2O$, orthorhombic *Pnma*, a = 10.3082 Å, b = 6.2577 Å, c = 16.486 Å. Another two 3-aminopropylphosphonate phases were obtained in mixtures with the first one, but could not be further characterised. The powder pattern

of an aluminium vinylphosphonate could be indexed to monoclinic, a = 10.054 Å, b = 19.502 Å, c = 7.048 Å and β = 107.33°. However, due to the paucity of data from the powder pattern, the systematic absences are consistent with three space groups, $P2_1/c$, $P2_1/a$ and $P2_1/n$. Further experiments to solve the structure are underway.

In addition, although their structures could not be determined solid materials were prepared in the following systems; aluminium aminomethylphosphonate, aluminium 2-aminoethyl-phosphonate, aluminium 1-aminobutylphosphonate, aluminium 4-aminobenzyl-phosphonate, aluminium iminobis(methylphosphonate) and aluminium carboxymethylphosphonate.

Finally, some preliminary experiments were carried out to investigate the reactions of three different aluminium phosphonates with functionalised carboxylic acids. It was concluded from the IR spectra of the products that a reaction had taken place, although an increase in the interlayer distance could only be observed for the products prepared from aluminium aminomethylphosphonate.

Chapter 1. Introduction

This chapter contains an overview of the current knowledge of the crystal chemistry of phosphonates, including those that are further described later on in this thesis.

Metal phosphonates ($M^{n+}(PO_3R^{2-})_{n/2}.nS$) are a diverse group of solids that display varied and potentially important properties. Phosphonate ions (PO_3R^{2-}) are the anions of a phosphonic acid (H_2PO_3R). A phosphonic acid can be looked at as a derivative of orthophosphoric acid (H_3PO_4), in which an organic group R replaces one hydroxyl group. This group R can be an alkyl or an aryl group and it may contain a variety of functional groups such as carboxyl[1] and sulphonate groups.[2] In the materials there are strong ionic interactions between the positively charged metal ions (M^{n+}) and the negatively charged phosphonate groups. The phosphonate group (PO_3R) can be thought of as containing both an inorganic part ($-PO_3$), which can form part of an inorganic framework, and an organic part that allows the preparation of novel materials.

The choice of the organic group R can greatly affect the properties of the resulting material. The vast majority of these solids are layered, although there are a number that have microporous architectures. Additionally, metal phosphates and phosphonates might contain one or more solvent molecules (S) per formula unit. The solvent is usually water, but depending on the synthesis conditions it may also be another solvent. The inner and outer surfaces of the phosphonates are lined with the organic groups, which leads to a surface with a greatly different hydrophobicity than the purely inorganic compound would have.

The bonding within the organic part of the starting material is, in general, retained after the syntheses of these compounds. If a layered inorganic starting material is used it may also be possible that the layered structure is maintained during the synthesis. The fixed structures of metal phosphonates enable the arrangement of the organic groups within the materials sometimes to be predicted. This is a step towards the design of desired structures.

The interest in phosphonates lies in the possible use of these compounds as catalysts,[3,4] molecular sieves,[5] proton conductors[2,3,6,7,8] and in molecular recognition.[5] Additionally, the range of applications is enhanced by the capability of metal phosphonates to form thin films. Monolayers as well as multilayered films that are analogues of Langmuir-Blodgett (LB) films can be formed by the stepwise growth of layers.[4,9,10,11,12] These films may exhibit interesting molecular sieving properties[5] and are able to exclude solution species from coated electrodes.[4,5] They could find application as insulators[13] in sandwich devices,[5] be used to align organic molecules for topotactical intralayer reactions,[5] polar chromophores with non-linear optical properties,[4,5] and to study electron transfer reactions in the solid state.[4] The alignment can also give rise to magnetic ordering.[11,12] Some metal phosphonates are thermally stable up to 500 °C depending on their composition.[1,14]

1.1. Metal(IV) phosphonates

Yamanaka published an article about the synthesis of organic derivatives of zirconium phosphate in 1976.[15] He reacted ethylene oxide with both α- and γ-

zirconium phosphate, which resulted for the first time in a product where an organic group was covalently bonded to a layered inorganic material *via* P-O-C bonds.

In 1978 Alberti *et al.* first reported the synthesis of a layered zirconium phenyl-phosphonate.[16] The structure proposed at this time (see Figure 1.1a) only differed in the position of the phenyl groups from the structure that was determined for this compound from powder X-ray diffraction data in 1993[17] (see Figure 1.1b). If the structure of the zirconium phenyl-phosphonate is compared with the structure of α-zirconium phosphate ($Zr(HPO_4)_2.H_2O$, α-ZrP)[18] it can be seen that the structure of the inorganic layer is retained with the phenyl groups in the phenylphosphonate replacing the hydroxyl groups of the phosphate (Figure 1.1c). Therefore α-ZrP can be considered as the parent compound of the phenylphosphonate.

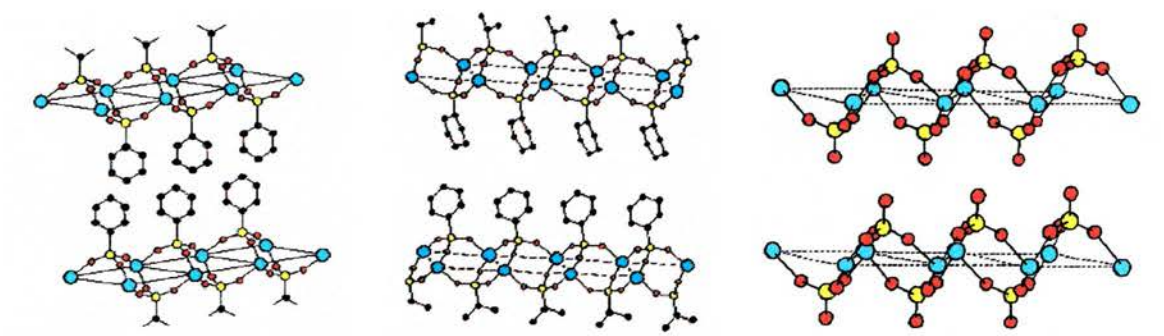

(a) (b) (c)

Figure 1.1: Structure of zirconium phenylphosphonate in comparison to the structure of α-ZrP;

(a) Structure of $Zr(O_3PC_6H_5)$ as proposed by Alberti et al.[16]

(b) Structure of $Zr(O_3PC_6H_5)$ as determined by Clearfield et al.[17]

(c) Structure of $Zr(HPO_4)_2.H_2O$ (α-ZrP)[18]

Hydrogen was omitted for clarity. Key see pg. 4.

Since then a great number of other metal(IV) phosphonates have been prepared. The organic groups, which have been used include aryl rings[1,19] and alkyl chains.[1,20]

They may contain for example halide,[1] acyl chloride,[21] carboxyl,[1,6] sulphonate,[1,2] cyanide[1] and vinyl groups.[1]

Shortly after the characterisation of α-ZrP, the zirconium phosphate γ-ZrP was characterised as $Zr(PO_4)(H_2PO_4).2H_2O$.[22] Its structure is shown in Figure 1.2. Phosphonate derivatives of this compound can be formed by topotactic replacement of the dihydrogen phosphate groups with monohydrogen phosphonate groups (HO_3PR).[3,23] It is possible to prepare γ-zirconium phosphonates with pendant methyl, propyl and cyclohexyl[20] as well as phenyl groups[23] using this method. In another paper the method was used to introduce sulphoaryl groups.[2] The replacement of the H_2PO_4 groups by O_3PR_2 groups increases the interlayer distance of the material while X-ray experiments confirmed that the γ-layer framework stays intact,[2,3,20] although the introduction of sulphoaryl groups led to a distinct loss in crystallinity.

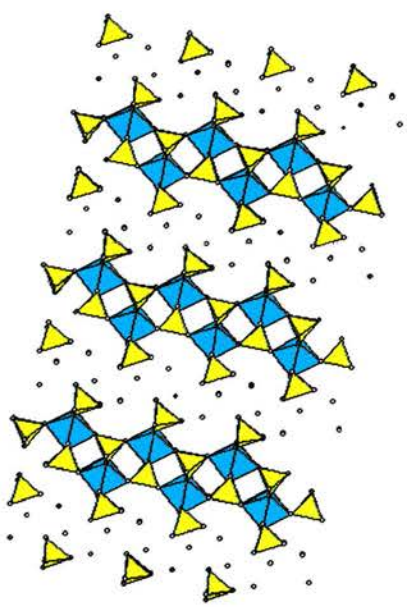

Figure 1.2: Structure of γ-ZrP[22]

The yellow tetrahedra denote $[PO_4]$ and $[H_2PO_4]$, the pale blue octahedra denote $[ZrO_6]$. The oxygens of the ligands (H_2O) are shown as spheres and hydrogens are omitted for clarity.

Even though γ-type phosphonates can be easily prepared by topotactic synthesis from γ-ZrP, the α-type compounds are usually synthesised by direct synthesis, i.e. precipitation from a solution containing the starting materials. There have however been some exceptions, where α-type phosphonates were prepared via topotactic synthesis.[19,24]

It can be assumed that metal(IV) phosphonates form α-type compounds if the area required by the organic group is smaller than the area that is provided by a phosphate group. The distance between adjacent phosphorus atoms within one layer is 5.3 Å in α-ZrP and therefore the free area around each phosphorus can be calculated to be 24 $Å^2$. If the cross-section of an organic group exceeds this area, it is not possible that two of these groups occupy adjacent sites in an inorganic α-type layer.[1,3,25] It has also been found that metal phosphonate films, which would normally adopt an α structure can incorporate oversized organic groups,[26] possibly by forming zirconium rich crystalline materials.[27]

In case of short lateral distances between neighbouring organic groups interpenetration of the groups belonging to adjacent inorganic layers is not possible and a double film is obtained. If organic groups containing alkyl chains are inserted in the inorganic material, an odd/even effect in the interlayer distances can be observed. This means that the increase in the interlayer space is not directly proportional to the length of the alkyl chain due to the different conformations, which can be adopted by odd and even membered chains (Figure 1.3). This has been shown for a homologous series of $Zr(O_3P(CH_2)_nCOOH)_2$ with n = 1-5.[6]

Mixed metal(IV) phosphonates

Mixed phosphonates ($M(RPO_3)_{2-x}(R'PO_3)_x$) can be prepared easily if different phosphonic acids are used in the synthesis. For R groups with similar size and chemical properties, the value of x may change continuously, although generally discontinuous x-values are more likely to occur. This is particularly apparent for materials with high crystallinity. It was also found that mixed phosphonates occasionally form asymmetrical layers, where regions rich in the different R groups alternate.[3,25] Another possibility for the distribution of R groups in mixed phosphonates is a regular one with each group surrounded by six groups of the other kind. This kind of distribution is of special importance if the cross-section of one of the groups exceeds the limit of 24 $Å^2$.[3] According to Thompson,[4] homogeneous mixed phosphonates are often kinetically favoured but return to segregated regions for the organic groups upon heating. Still, in some cases the homogeneous phase can also be the thermodynamically stable one. Mixed α-Ti^{IV} phosphate-phenylphosphonates were reported in 1996.[19] The interlayer distance of the materials lies between the values for the pure phosphate and phosphonate samples. For products containing more phosphonate than phosphate groups the interlayer spacings approached those of the pure phosphonate.

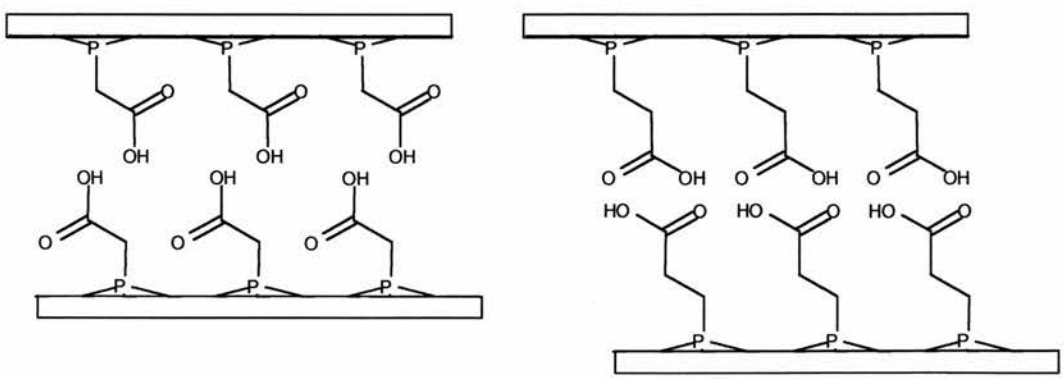

(a) (b)

Figure 1.3: Possible arrangement of the carboxyalkyl chains in compounds with an (a) odd and (b) even number of carbon atoms.[6]

Alberti et al. investigated the influence of the size of the R group on the results of topotactic exchange reactions in γ-ZrP.[20] Methyl- and propylphosphonic acids yielded products where all H_2PO_4 groups could be replaced by phosphonate groups. However, in the cyclohexylphosphonate, only partial replacement of 66 % of the phosphate groups took place. This is consistent with results earlier obtained for phenylphosphonic acid.[28] It seems therefore that complete replacement is indeed only prevented by the steric hindrance due to the bulky phenyl and cyclohexyl groups respectively.

Thermal stability

According to Dines and DiGiacomo,[1] phosphonates exhibit higher thermal stability than their analogous phosphate compound (decomposition occurs approximately 100 °C higher). The particular values depend on the nature of the R group, but 300 °C is a good average in the absence of interlayer water. Two examples highlighting the possible differences in the decomposition temperature are Zr allylphosphonate ($Zr(O_3PCH_2CH{=}CH_2)_2$ and Zr vinylphosphonate ($Zr(O_3PCH{=}CH_2)_2$. The allyl compound starts to decompose at 250 °C and loses 100 % of the mass calculated for its organic moiety up to 450 °C. Contrary to this, the vinyl compound starts to decompose at about 400 °C and looses only about 30 % of its organic matter by 650 °C. Apart from decomposition mechanisms specific to the organic groups, Dines and DiGiacomo also state that more stable compounds result if the R groups are fixed at distances larger than the *van der Waals* contact, because then no collisional routes to dissociation are provided.[1]

Porosity

To enhance the available surface of materials used as catalysts or sorbents it is useful to introduce porosity into these compounds. This can be achieved by the

intercalation of various compounds into the interlayer region. However, it has been shown for α-ZrP fully intercalated with $NH_2(CH_2)_nNH_2$ (n = 2, 4,... , 10) that the packing density of the inserted diamine is so high that hardly any porosity is introduced. About 90 % of the volume created by the expansion is occupied by the diamine itself. Therefore, it is necessary to use the incompletely intercalated compounds, which are capable of inserting polar molecules such as water or short chain alcohols.[29] This is further emphasised by the finding that an increase in the loading with propylamine caused a progressive decrease in the hydration of intercalated α-ZrP.[30]

The same problems are experienced when a layered material is reacted with reagents such as diphosphonic acids[25] that contain rigid segments, which act as pillars to keep the phosphonate layers apart[3] and lead to microporous solids. An approach to porous phosphonates avoiding this dilemma was reported by Dines *et al.*[31] Diphosphonic acids and their corresponding phosphate esters were reacted with a Zr salt and the phosphate subsequently hydrolysed with hydrobromic acid. The hydrolysed product showed a significant increase in the surface area compared to the intermediate product. However, this increase was later[3] found to be mainly due to inter-crystal mesoporosity arising from low crystallinity. An elegant solution for these difficulties was eventually found by Alberti *et al.*, who prepared mixed phosphonates containing 'based pillars', *i.e.* diphosphonic acids that posses a base with a cross-section larger than 24 $Å^2$ but become narrower towards the centre of the pillar. This way, the pillars cannot occupy adjacent positions and significant porosity can be created in the interlayer space.[32]

None of the problems connected to pillaring were experienced with γ-ZrP. Alberti *et al.* synthesised pillared phases by topotactic replacement of $H_2PO_4^-$ with

diphosphonic acids.[33] For 4,4'-biphenyldiphosphonic acid, stable anhydrous phases could be obtained for pillaring percentages of 25 % and above.[34] The pillaring percentage is equivalent to the percentage of topotactic replacement of $H_2PO_4^-$ with diphosphonate groups for replacements of less than 50 %. The maximum possible interlayer porosity was created at the minimum concentration of pillars in the dehydrated phase, *i.e.* 25 to 28 % pillaring. At lower percentages the pillared phase is only stable in the presence of intercalated solvent.

Intercalation

It has been mentioned that Zr phosphonates intercalate nonpolar[1] or neutral guests.[25] It was also reported that α-Zr polyetherphosphonates readily intercalate electrolytes and coordination complexes, although no mention was made as to their nature.[35] However, the preparation of ionic conductors by the incorporation of electrolytes into polyethers was mentioned elsewhere.[36] The polyether derivatives of α-ZrP become more hydrophilic with increasing chain length. This leads to a higher uptake of water (swelling). The subsequent increase in the interlayer distance allows other molecules to diffuse into and migrate in the materials more freely. Incorporation of chains with nine or more members results in the formation of colloids in water.[35]

In general, Alberti and Costantino state that the process of intercalation into phosphonates can simply be driven by the interaction between the intercalated species and the R groups, provided that it is stronger than the interaction among the R groups belonging to adjacent layers.[25] A paper by Jaimez *et al.* investigates the influence of steric and electronic effects in mixed phosphonates on the intercalation behaviour of amines into Ti^{IV} phosphate-phosphonate.[19] In some cases, pre-intercalation can

facilitate reactions within phosphonates that would otherwise be blocked.[21] Johnson *et al.* thermally removed benzyl alcohol from vanadyl phosphonates with the formula $VO(O_3PR).H_2O.C_6H_5CH_2OH$ to create a free coordination site.[37] This vacancy could then be used for coordinative intercalation of primary alcohols that bind to these sites while secondary alcohols are excluded due to their increased bulk and subsequent steric hindrance. The use of this method was also reported for layered divalent metal phosphonates (see Section 1.2, pg. 29).

1.2. Metal(II) phosphonates

Under acidic conditions, metal(II) phosphonates are more soluble than the corresponding metal(IV) compounds. This makes it possible to prepare products with a higher degree of crystallinity and to obtain crystal structures more easily. Metal(II) phosphonate crystals redissolve in dilute acids and may therefore be prepared as single crystals.[38] Metal(II) phosphonates may include a variety of functionalities such as; amino,[39,40] carboxyl[41,42,43,44] and halide groups,[41,42] apart from the more common phenyl or alkyl groups.

Investigations into metal(II) phosphonates started some years after the research in the metal(IV) phosphonates had begun. In 1979 Cunningham *et al.* published a report concerning the preparation of various divalent metal phenylphosphonates including magnesium, zinc, iron, copper, manganese, cobalt, nickel and cadmium.[45] It was discovered that these compounds form isostructural hydrates $M^{II}(O_3PPh).H_2O$. The Zn and Cu phosphonates can furthermore be directly prepared as anhydrous compounds, while the other anhydrous phosphonates are only available *via* dehydration of their hydrates. The anhydrous phosphonates are less crystalline than the hydrated

compounds. The dehydration is reversible for most compounds except for the anhydrous Cu phenylphosphonate. At that time of their discovery it was not possible to solve the structures of these materials.

In 1988, Cao *et al.*[46] tried to establish whether the structures of the metal(II) phosphonates prepared by Cunningham[45] were related to the layered structure of newburyite ($M^{II}(O_3POH).3H_2O$)[47] (M = Mg, Mn) in the same way as metal(IV) phosphonates are often related to the α-ZrP structure (see Chapter 1.1, pg. 9). This was however not the case. X-ray powder diffraction studies confirmed that there exist different structures for a homologous series, $M^{II}(O_3PR).H_2O$ (M = Mg, Mn, Zn and Cd), $Ca(O_3PR).H_2O$ and for $Ca(HO_3PR)_2$. For the series a crystal structure was solved for $Mn(O_3PC_6H_5).H_2O$, showing a layered compound with the phenyl groups perpendicular to the layers. It contains Mn atoms coordinated distorted octahedrally by five phosphonate oxygens and the water molecule. Two oxygen atoms from each phosphonate group are chelating two manganese atoms each. Therefore two of the oxygens connected to every Mn atom belong to the same phosphonate group. This leads to a kinked layer, which in turn forces the pending organic groups close to each other[46] (Figure 1.4).

For the other Mn, Mg and Zn compounds unit cell dimensions could be established from their indexed powder patterns. They were similar to the values for the Mn phenylphosphonate although with different *b* dimensions according to the length of the organic groups. It was therefore assumed that all of them have the same layer structure.[38,46] The crystal structure of Zn phenyl-phosphonate was solved from a single crystal and found to exactly match the previously described structure for

$M^{II}(O_3PR).H_2O$ phosphonates. There also exist copper compounds that are isomorphous to the zinc phenylphosphonate.[48]

Similarly, a variety of Ni phosphonates such as phenyl[42,45,48] and others (methyl, benzyl, carboxymethyl and bromoethyl)[42] all have essentially the same type of layered structure with octahedrally coordinated nickel. For the nickel carboxymethylphosphonate this is a pronounced difference to the previously known zinc[41] and cobalt[44] 2-carboxyethylphosphonates that contain both tetrahedrally and octahedrally coordinated metal atoms and have a much smaller interlayer spacing (see pg. 25). It can therefore be expected that the carboxyl groups in the nickel compound do not coordinate to the metal.[42] The same structure is also adopted by the LB films of these phosphonates.[12]

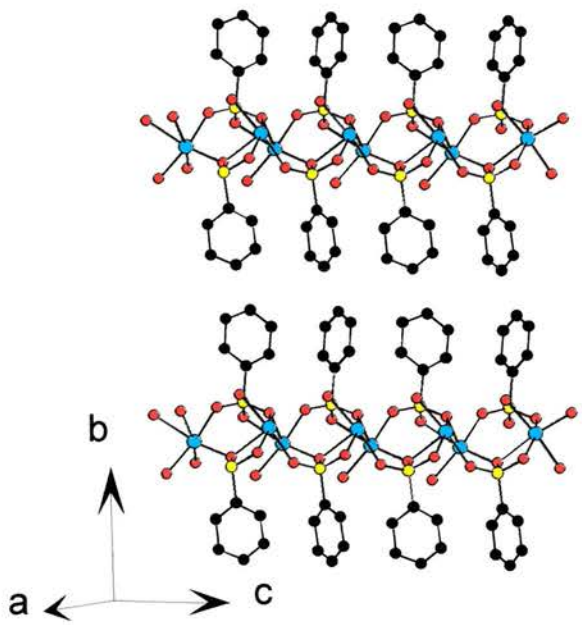

Figure 1.4: Layered structure of $Mn^{II}(O_3PC_6H_5).H_2O$ with manganese in distorted octahedral coordination.[46] Only one of the many possible orientations of the phenyl groups is shown and hydrogen atoms are omitted for clarity. Key see pg. 4.

The structure of the Ca phosphonates was established by Cao and co-workers in 1990.[49] It was found that they adopt a structure different from the Mn^{II}, Mg and Zn phosphonates due to the larger ionic radius of Ca^{2+}. In a homologous series of Ca alkylphosphonates two different structures can be found depending on the length of the alkyl chain. For methyl up to pentylphosphonates (n = 1-5) the formula is $Ca(O_3PR).H_2O$, while for chains with more than 5 carbon molecules it is $Ca(HO_3PR)_2$. A picture of $Ca(HO_3P(C_6H_{13})_2$ is shown in Figure 1.5. Both structures were determined.

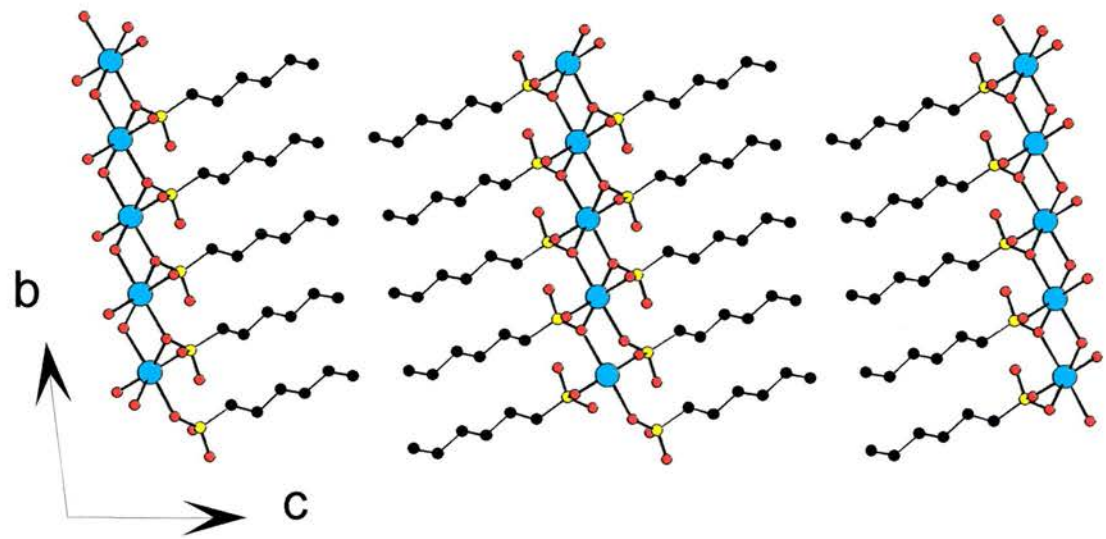

Figure 1.5: Layered structure of $Ca(HO_3PC_6H_{13})_2$.[49] *Key see pg. 4.*

The calcium atoms of $Ca(O_3PCH_3).H_2O$ have a distorted pentagonal-bipyramidal coordination and are coordinated by six chelating phosphonate oxygens and one water molecule. This results in a layered structure where the methyl groups point towards the interlayer space. It should however be noted that the fifth coplanar oxygen atom has a significantly longer Ca-O bond (2.7 Å as opposed to 2.3-2.4 Å for the other four). Although this is still within the range for such bonds, disregarding it would lead to a very distorted octahedron, thus establishing the relation to the $M^{II}(O_3PR).H_2O$ series described above.

The Ca hexylphosphonate (Figure 1.5) with a Ca: P ratio 1:2 has a structure where the calcium ion is coordinated by a distorted octahedron of six $C_6H_{13}PO_3H^-$ groups. The hydroxyl group is non-coordinating, therefore one of the two remaining oxygens is bridging two calcium ions while the other is only coordinated to one calcium. The hexyl chains are extending into the interlayer space. This structure is closely related to that of α-ZrP and the $M^{IV}(O_3PR)_2$ phosphonates (see Section 1.1). Ca phosphonate films adopt the same structures depending on the length of the alkyl chains.[12]

Le Bideau and co-workers prepared metal(II) *t*-butylphosphonates.[50] The structures of these compounds differ from materials with less bulky R groups. For $Co(O_3PC(CH_3)_3).H_2O$ the structure was solved. It contains three differently coordinated cobalt atoms (one octahedral and two tetrahedral) and three phosphonate groups bonding to them in different ways. This leads to undulating layers from which the *t*-butyl groups extend into the interlayer space (Figure 1.6). Based on analytical evidence, the corresponding manganese and zinc compounds are assumed to adopt the same and a similar structure respectively. However, the copper *t*-butylphosphonate has a different structure with a Cu:P ratio of 1.75:1.

An enantiomerically pure Zn phosphonate was prepared by Fredoueil *et al.* in 1999 (Figure 1.7).[51] Its structure is completely different from the racemic materials described in a previous paragraph [38,46,48] and also from a racemic compound with the same formula but a lower water content than the enantiomerically pure compound. This shows the extent to which the structure of a phosphonate is influenced by the properties of the organic group. *(R)*-$Zn[O_3PCH_2P(O)(CH_3)(C_6H_5)].H_2O$ consists of zinc atoms tetrahedrally coordinated by three phosphonate oxygens and the phosphane oxygen.

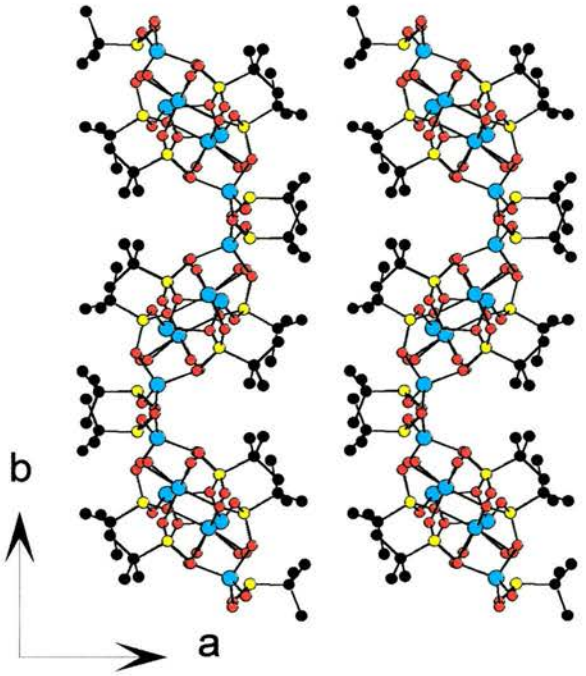

Figure 1.6: The undulating structure of $Co(O_3PC(CH_3)_3).H_2O$.[50] *Key see pg. 4.*

The layers are built from corner-sharing ZnO_4 and PO_3C tetrahedra forming 12-membered rings. The phenyl groups are alternatively placed on the two faces of the layer. This allows close packing because they can interlace with the groups from the opposite layer. The water molecules are situated in the interlayer space, forming weak hydrogen bonds with the phosphonate oxygens.

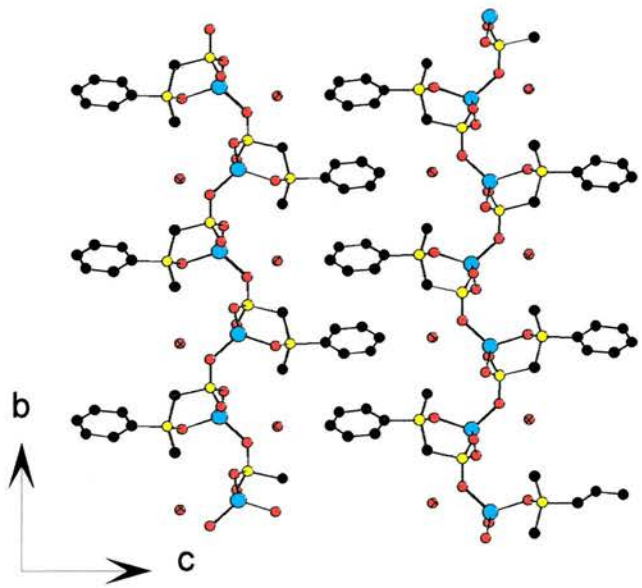

Figure 1.7: Structure of the first enantiomerically pure M^{II} phosphonate, $Zn[O_3PCH_2P(O)(CH_3)C_6H_5)].H_2O$.[51] *Key see pg. 4.*

Zhang and Clearfield discovered Cu phosphonates, α-$Cu(O_3PR).H_2O$, with a layered structure where the metal is 5-coordinated in a distorted tetragonal pyramid (Figure 1.8).[52] The layers are made up from four- and eight-membered rings. The organic groups (methyl or phenyl) extend into the interlayer space. There is hydrogen bonding between the water and the oxygen molecules of the eight-membered rings within the same layer. The layers are held together by *van der Waals* interactions only. Dehydration of the α-Cu^{II} phosphonates leads to compounds with a highly distorted trigonal pyramidal coordination for copper.[52,53] The anhydrous α-Cu^{II} ethyl- and *n*-butylphosphonates can be prepared either directly or by dehydration of the hydrated compound.[53] Le Bideau *et al.* furthermore report a layered Cu^{II} methylphosphonate with both distorted 4- and 6-coordinate metal atoms.[53]

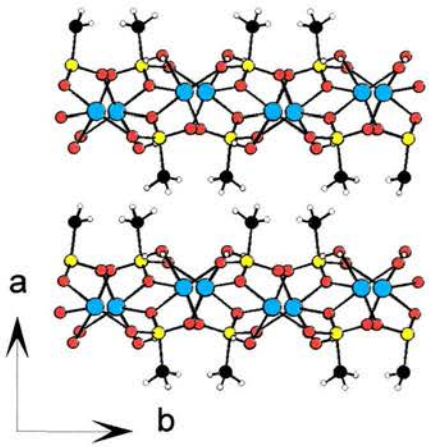

Figure 1.8: Structure of α-$Cu(O_3PCH_3).H_2O$.[52] Key see pg. 4.

Another different structure was found for a family of Zn organophosphates with the formulae $Zn(O_3POC_2H_5).H_2O$ and $Zn(O_3POC_2H_4NH_3)(O_2CCH_3)$.[39] The materials both contain tetrahedrally coordinated Zn atoms. Three of the coordination sites are taken up by oxygens from three different phosphonate groups. This leads to an undulating inorganic layer. The fourth Zn-O bond links the zinc atom to a water molecule or one acetate oxygen respectively. The ethyl and the acetate groups fill the interlayer space of

their respective compounds. The aminoethyl group is doubled back around itself, which provides the maximum number of possible hydrogen bonds. The layers are held together by *van der Waals* forces only (Figure 1.9).

Metal(II) phosphonates can be prepared by direct precipitation from combined solutions of metal salts and phosphonic acids.[38,46,52] Another method is *via* the intercalation of layered metal(II) salts with the sodium phosphonates.[54,55] For these reactions the molar ratio of sodium phosphonate to metal salt and the initial pH of the reaction mixture are of a crucial influence with respect to the phases obtained.[54] In addition to these approaches, work has been published concerning the synthesis of Ni^{II} phosphonates from molten phosphonic acid.[42] Furthermore, the synthesis of copper(II) phosphonates has also been attempted using templates.[56] It was found that the choice of the template had a significant effect on the structure of the resulting phosphonate under similar reaction conditions. Addition of ammonia led to chain structures, while bigger molecules such as 1,4-butylenediamine created layered structures.

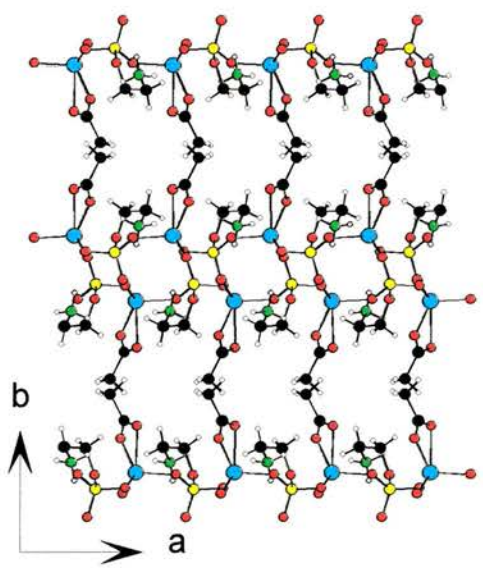

Figure 1.9: Structure of $Zn(O_3POC_2H_4NH_3)(O_2CCH_3)$.[39] Key see pg. 4.

As already pointed out for the metal(IV) phosphonates, very bulky organic groups cannot be accommodated in the normal layered structure. The critical cross-section for metal(II) phosphonates of the structure $M^{II}(O_3PR).H_2O$ is 28 $Å^2$.[38] It was found that extra space for bulky groups can be created by extensive hydration of the metal. The inorganic sheets then consist of hydrated metal cations, phosphonate oxygen atoms, P-OH groups and additional water molecules, all held together by hydrogen bonding.[38]

Microporous compounds

In 1994, it was possible to prepare the first microporous Cu^{II} methylphosphonate, β-$Cu(O_3PCH_3)$ (Figure 1.10).[53] It contains 5-coordinate copper atoms with a distorted tetragonal pyramidal environment and the structure is very similar to the layered Cu^{II} methylphosphonate described above.[52] Two of the phosphonate oxygens bridge two copper atoms each. Every copper atom is connected to the two neighbouring copper atoms by two of those oxygens *via* four-membered rings, thus forming chains. These chains are connected by O-P-O bonds in the other two dimensions, which leads to hexagonal tunnels with a diameter of 5.97 Å between two opposite methyl carbons.

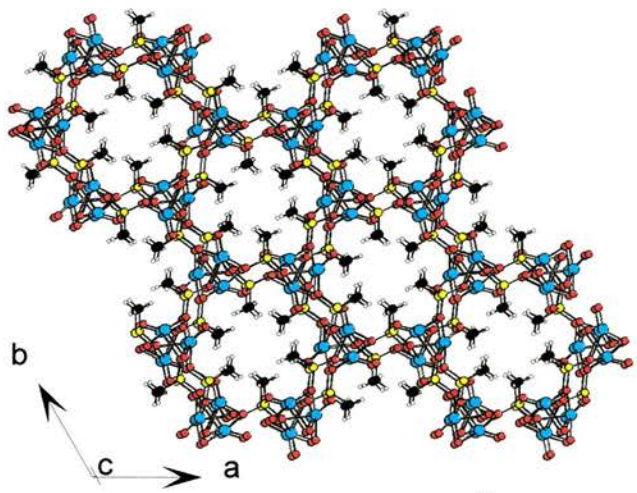

Figure 1.10: Structure of the microporous β-$Cu(O_3PCH_3)$.[53] *Key see pg.4.*

A three-dimensional zinc phosphonate with carboxyethyl-functionality was described by Drumel and co-workers in 1995.[41] $Zn_3(O_3P(CH_2)_2CO_2)_2$ contains both four- and six-coordinate zinc. It forms layers that are connected by the carboxyl groups (Figure 1.11). Another three-dimensional metal(II) phosphonate with the same structure was discovered in the same year; Rabu et al. announced the preparation of the Co^{II} carboxyethylphosphonate $Co_3(O_3P(CH_2)_2CO_2)_2$.[44]

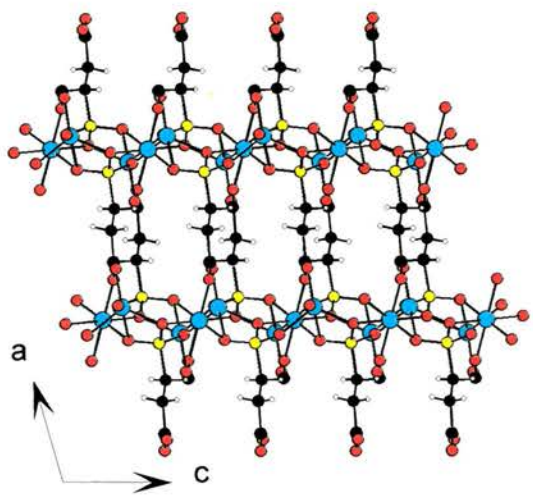

Figure 1.11: Structure of $Zn_3(O_3P(CH_2)_2CO_2)_2$.[41] *Key see pg. 4.*

Also in 1995, the structure of a zeolite-like phosphonate was published.[40] $Zn(O_3P(CH_2)_2NH_2)$ consists of layers of 16- and 8-membered rings created by the connection of each zinc atom to three oxygens from different phosphonate groups (Figure 1.12). These sheets are linked together by the fourth coordination of the tetrahedral zinc to the amino group of the phosphonate in another sheet, thereby forming 8-membered rings. This is similar to the structure of $Zn(O_3P(CH_2)_2CO_2H).1.5H_2O$[41] (see above). The stacking of the 16-membered rings gives rise to elliptical channels with a cross-section of 3.6 by 5.3 Å. Along those channels run two rows of nitrogen atoms from the amino groups.

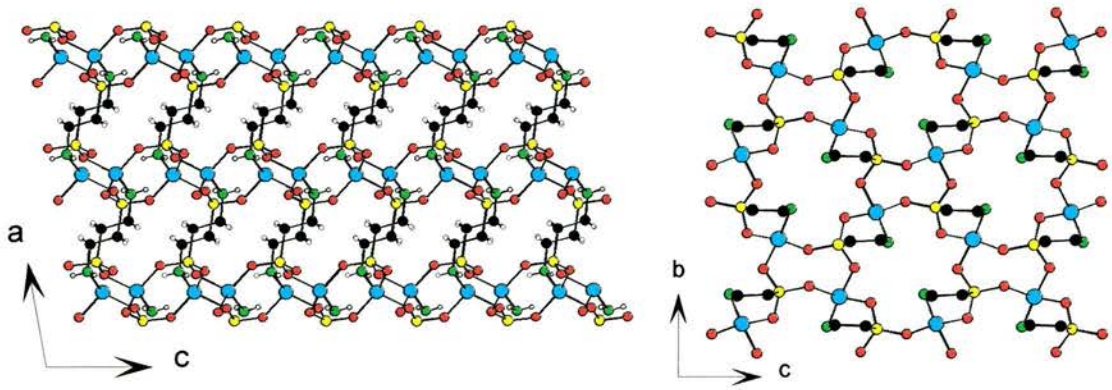

(a) (b)

Figure 1.12: Structure of $Zn(O_3P(CH_2)_2NH_2)$. (a) Layered structure. (b) Structure of the layers; water molecules and hydrogen atoms are omitted for clarity.[40]
Key see pg. 4.

Ayyappan and co-workers reported a three-dimensional open-framework Pb^{II} carboxyethylphosphonate in 1999.[43] It contains lead atoms in tetrahedral, trigonal-bipyramidal and octahedral coordination geometries with a lone pair occupying one site in each arrangement. The coordination by oxygens from phosphonate and carboxyl groups leads to layers with narrow channels that are connected by the fifth bond of the octahedral lead (Figure 1.13).

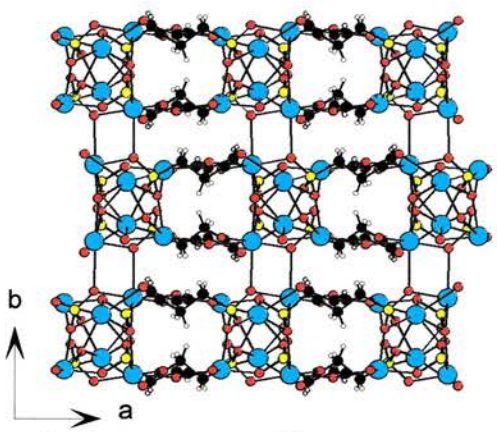

Figure 1.13: Structure of $Pb^{II}(O_3P(CH_2)_2CO_2)$.[43] *Key see pg. 4.*

An open-framework zinc material was prepared using carboxymethylphosphonic acid, benzenetricarboxylic acid and ethylendiamine.[57] The framework is built from zinc atoms in three different coordination environments, one of them octahedral and two

tetrahedral, and the phosphonic acid moieties using both the phosphonate oxygens and the oxygens from the carboxymethyl groups ($-CH_2COO^-$). It forms parallel 24-, 12- and 8-ring channels. The framework also includes the diprotonated ethylendiamine molecules that are connected to framework oxygen by hydrogen bonds in the walls of the 24-rings. The carboxymethyl groups ($-CH_2COOH$) extend into the 24-ring channels. In addition, the benzenetricarboxylic acid molecules can be found at the centre of these channels.

In 2001, Riou-Cavallec *et al.* published the preparation of an open-framework Cu^{II} carboxyethylphosphonate containing sodium cations (Figure 1.14).[58] The copper atoms have a square-pyramidal coordination and bond to three oxygens from phosphonate groups and two from carboxyl groups. This leads to double chains of alternating copper polyhedra and phosphonate tetrahedra that are held together in three dimensions by bridging carboxylate groups. The structure contains two types of parallel channels. The sodium ions are situated in the smaller channel and coordinated by eight oxygen atoms.

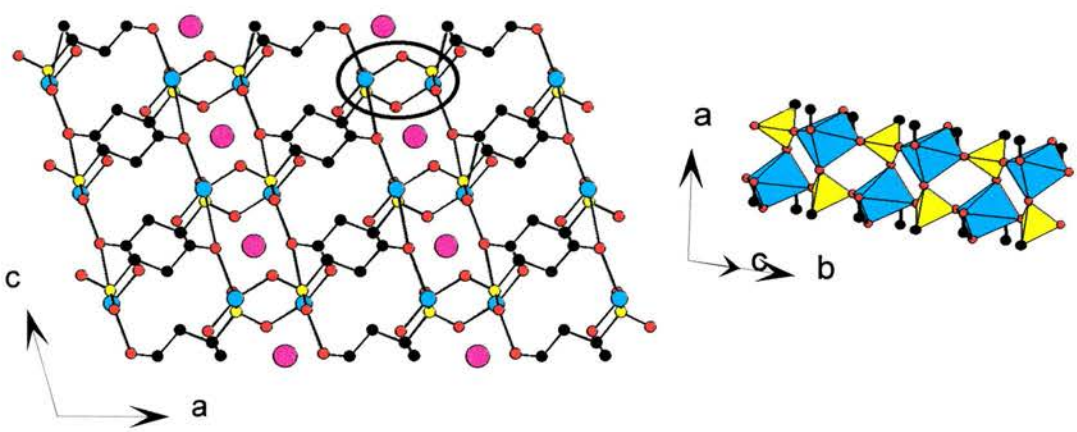

(a) (b)

Figure 1.14: Structure of $Na[Cu(O_3P(CH_2)_2CO_2)]$. (a) View along the b*-axis; the sodium ions in the channels are depicted in purple. The inorganic double chain is circled. (b) Detail of the double chain made up of copper polyhedra and phosphonate tetrahedra.*[58] *Key see pg. 4, additional; purple spheres denote sodium, yellow tetrahedra phosphonate groups and pale blue polyhedra copper coordinated by oxygen.*

Functionalised layered metal(II) phosphonates

Drumel and co-workers were able to prepare functionalised zinc and copper phosphonates containing carboxyl, bromine and protonated amino groups.[41] The structures of these compounds are related to the non-functionalised $Zn(O_3PR).H_2O$[38,46,48] and $Cu(O_3PR).H_2O$[52] structures respectively (see pg. 17 and pg. 22 in this section). For the hydrated zinc carboxyethylphosphonate $Zn(O_3P(CH_2)_2CO_2H).1.5H_2O$[41] it was noticed that the carboxyl group is coordinated to the metal and therefore not able to undergo any reactions. However, this is not the case for the anhydrous compound. A material containing aniline was prepared from the hydrated Zn carboxyethylphosphonate by replacing the water (for similar reactions see "Intercalation" below). The formation of an amide link resulting in $Zn(O_3P(CH_2)_2CONHC_6H_5)$ was only possible by direct synthesis from the metal salt, the phosphonic acid and aniline. For the modification of the carboxy-functionalised phosphonates prior activation of the carboxyl groups may be necessary.[41]

Thermal stability

The thermal stability of the metal(II) phosphonates varies widely. Water of hydration is lost readily, while lattice water (water that is coordinated to the metal atoms) is more strongly bound and in some cases partly retained up to 300 °C.[38] Cunningham *et al.* reported that most hydrates lost water between 130 and 160 °C, with some exceptions starting at 25 to 80 °C.[45] The organic part usually decomposes between 360 and 620 °C. Alkylphosphonates tend to be less stable than the aryl compounds[38] and copper phosphonates less stable than for example the corresponding cobalt and zinc compounds,[59] which was also noted by Cunningham *et al.*[45] This may in some cases be due to strong hydrogen bonding, but the most likely cause is that

different structures may result in metal coordination geometries of different energy upon the loss of water.

Intercalation

The dehydration of metal(II) phosphonates with water coordinated to the metal atoms leads to compounds with a vacant coordination site that can be used for coordinative intercalation.[60] This approach is similar to the method used for metal(IV) phosphonates[37] (see Section 1.1, pg. 16). It was also possible to replace the water molecule coordinated to Zn carboxyethylphosphonate with aniline.[41] Furthermore, it was noticed that primary amines without branching in the α-position are selectively intercalated into anhydrous Zn and Co^{II} methylphosphonates, although primary amines with branching were excluded.[60] Complementary experiments were carried out on Zn and Co^{II} phenylphosphonates. Ammonia was absorbed into the material from the gas phase but alkyl amines were excluded.[61]

The Cu^{II} phosphonates α-$Cu(O_3PCH_3).H_2O$ prepared by Zhang and Clearfield[52] already contain a free coordination site due to their tetragonal pyramidal coordination (see pg. 22). Dehydration of the materials makes a second coordination site available for intercalation. Experiments showed that the intercalation of butylamine into the layered hydrated methylphosphonate was reversible upon standing in air. However, for the dehydrated compound no loss of amine could be perceived after exposure to air.[52] Further investigations showed that the interlayer spacing of $Cu(O_3PCH_3)$ increases linearly with the number of carbon atoms in a homologous series of alkyl amines.[59] Intercalation led to equivalent products from solution and from the gas phase. For $Cu(O_3PC_6H_5)$ it was found that *n*-alkylamines are intercalated slowly from the gas

phase and faster from the liquid phase. The gas-solid intercalation reaction was considerably slower than for the methyl compound.[59]

1.3. Metal(III) phosphonates

1.3.1. Aluminium phosphonates

Aluminium phosphates

A major reason for studying aluminium phosphonates is the assumption that there will be similarities between the phosphonates and the well-known microporous family of aluminium phosphates, and that therefore it might be possible to prepare interesting materials in this system. The first aluminium phosphate molecular sieves were reported by Wilson *et al.* in 1982.[62] To date there are around 250 aluminophosphates known. Most aluminium phosphates have tetrahedral frameworks, although examples of 5-,[63,64] and 6-coordinate aluminium[64,65] are known. The versatility of the coordination environment of aluminium in phosphates makes more complex structures possible than found in zeolites (aluminium silicates). This may also be the reason why the first large pore molecular sieves were discovered in the aluminium phosphate system.[66] A review of the synthesis of aluminium phosphate molecular sieves was published by Davis and Lobo in 1992.[67]

Most of the layered structures consist of AlO_4 and PO_4 tetrahedra without any direct Al-O-Al linkages (Löwenstein's rule). However, in 1999 a new type of framework was reported.[68] It contains Al_2O_7 units as well as the customary AlO_4 and

PO_4 and the layers feature Al-O-Al links connecting rows of fused four-rings. Another aluminium phosphate with Al-O-Al bonds was discovered by Kongshaug *et al.* in the same year.[64] These are examples of how reactions at high temperatures can occasionally lead to the formation of energetically unfavourable structures, allowing for completely unexpected new materials.

Microporous aluminium phosphonates

Despite the early interest and extensive investigations into the aluminium phosphate system and the obvious similarities to the aluminium phosphonate system, research in the area of aluminium phosphonates started only much later. In 1994 Maeda *et al.* published an article about the synthesis of the first microporous aluminium methylphosphonate (AlMePO-β; see Figure 1.15) with the composition $Al_2(CH_3PO_3)_3.H_2O$.[14] The fact that the first[14,69] and also the second[70] aluminium phosphonate to be discovered were both microporous is remarkable, as most known aluminium phosphonates are layered. The next microporous aluminium phosphonate ($Al_2[O_3PC_2H_4PO_3](H_2O)_2F_2.H_2O$) was only published in 2000.[71] Contrary to this, a multitude of new, layered aluminium phosphonates was described in the literature during those six years (for examples see pp. 36).

In the three-dimensional network of AlMePO-β the aluminium and phosphonate groups alternate, but the network is not exclusively 4-connected due to the terminal methyl groups. It has been determined that this compound contains six crystallographically independent CH_3PO_3 tetrahedra and four independent aluminium atoms, of which one is 6-coordinated and three are 4-coordinated. All aluminium atoms are connected to phosphonate groups. The phosphonate groups share their oxygen

atoms with three adjacent aluminium atoms of which two are 4- and one is 6-coordinated. The result of this linkage are ladder-like chains made up of phosphonate tetrahedra and aluminate tetrahedra and octahedra, respectively, connected by four-rings that include all the aluminium atoms and five of the six independent phosphorus atoms. These chains are connected to each other both by the remaining phosphorus and the 6-coordinated aluminium.[69]

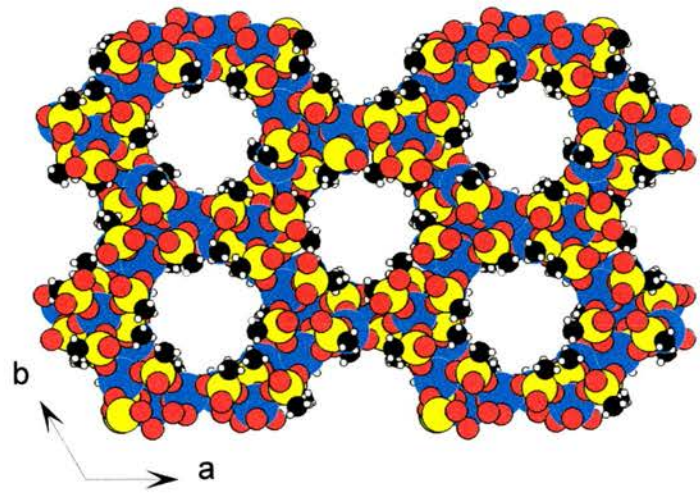

Figure 1.15: Structure of AlMePO-β. View along the c-axis.[69]
Key see pg. 4.

The inorganic skeleton of AlMePO-β forms unidimensional 18-ring channels parallel to the c-axis as shown in Figure 1.15. These 18-ring channels consist of alternating aluminium and phosphorus atoms, more specifically three 6-coordinated aluminium atoms, six 4-coordinated aluminium atoms and nine phosphorus atoms. The methyl groups that line the channel walls are covalently bonded to the skeleton. They point towards the centre of the channel, which is also confirmed by the fact that the adsorption isotherm of water in AlMePO-β has a hydrophobic character.[14] This results in channels with approximately triangular cross sections with a side length of about 7.0 Å and a diameter of about 5.8 Å. However, the adsorption of 2,2-dimethylpropane

(diameter 6.2 Å) into the channels demonstrates that these methyl groups possess a high degree of flexibility. Additional 8-ring channels possess an estimated diameter of only 1.4 Å, which is too narrow for even small molecules.[14,69]

AlMePO-β can be prepared hydrothermally both through the original method used by Maeda and co-workers from pseudo-boehmite and methylphosphonic acid in water[14] and from gibbsite and methylphosphonic acid in the presence of 1,4-dioxane, also in water.[72] The latter product contains dioxane molecules in the channels that can be removed thermally in an inert atmosphere. As degassing at 500 °C does not lead to changes in the powder XDR pattern, it seems that the framework of AlMePO-β is thermally stable up to this temperature.[14]

In 1995, Maeda *et al.* synthesised another aluminium methylphosphonate called AlMePO-α (Figure 1.16).[70] AlMePO-α and AlMePO-β are both prepared under hydrothermal conditions with small differences in the molar aluminium to phosphorus ratio and other reaction conditions[14,70] and their structures are very closely related. This was highlighted in a publication by Carter *et al.*[72] They noticed that it is possible to transform AlMePO-β into AlMePO-α by thermal treatment in the presence of water. This transformation is very unusual, as such framework solids often tend to collapse at elevated temperatures.

In AlMePO-α, the connectivity is the same as in AlMePO-β, *i.e.* one of the three oxygen atoms in each phosphonate group is connected to a 6-coordinated aluminium atom, while the other two are bound to 4-coordinated aluminium. However, this results in a three-dimensional framework based on alternating aluminate and phosphonate

groups. These groups are arranged in successive layers along the c-axis. This resembles the starting material, boehmite that consists of layers of AlO(OH).[73]

The framework of AlMePO-α contains unidimensional 18-ring channels parallel to the c-axis (Figure 1.16). The features of these channels are the same as in AlMePO-β. The triangular rings have side lengths of approx. 7.0 Å. After degassing at 400 °C the materials can accommodate 2,2-dimethylpropane (diameter 6.2 Å). Between the 18-rings in AlMePO-α there are also 6-rings that are too small to accommodate adsorbed molecules, especially as they are also lined by methyl groups. Like AlMePO-β, the framework of AlMePO-α is thermally stable up to 500 °C under vacuum.[70]

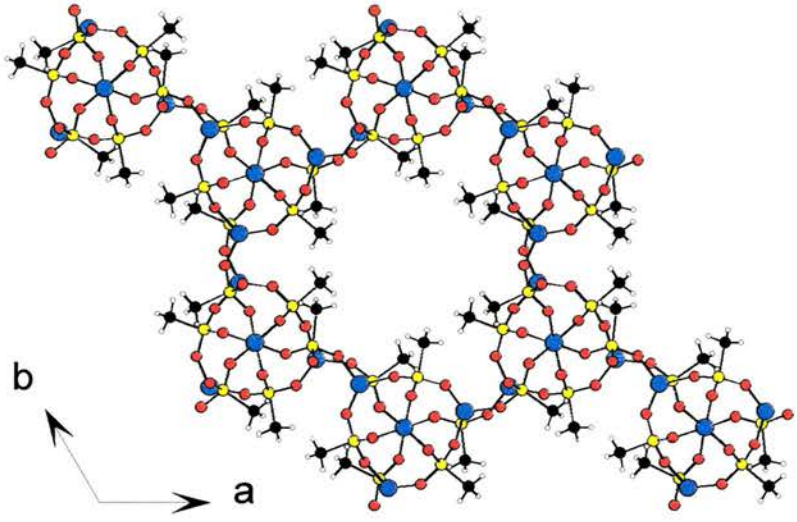

Figure 1.16: Structure of $AlMePO_4$-α.. View along the c-axis.[70]
Key see pg. 4.

Harvey and co-workers were able to prepare an open-framework aluminium diphosphonate with the formula $Al_2(O_3PC_2H_4PO_3)(H_2O)_2F_2.H_2O$ under hydrothermal conditions from the HF/pyridine system.[71] It contains two different types of octahedral aluminium. One of them is coordinated to two fluorine atoms in *trans* configuration and four phosphonate oxygens. The other aluminium atom is surrounded by two

fluorine atoms in *cis* configuration, two phosphonate oxygens in the remaining equatorial positions and two water molecules in the axial positions. This means that the aluminium octahedra form corner-sharing chains *via* the fluorine atoms along the [010] direction, which are connected by the phosphonate groups along [001] and [100] through corner-sharing phosphonate tetrahedra and diphosphonate bridges respectively. A view along the [100] direction is shown in Figure 1.17.

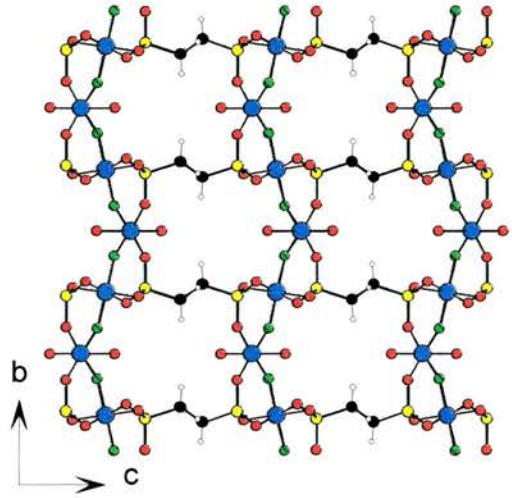

Figure 1.17: Structure of $Al_2(O_3PC_2H_4PO_3)(H_2O)_2F_2..H_2O$ viewed along the [100] direction.[71]

Key see pg. 4. In addition, green spheres denote fluorine.

The structure contains small channels along the [100] direction with a cross-section of 5.7 × 5.3 Å where the extra-framework water molecules are located. However, the dehydration of the material at 190 °C (loss of extra-framework water) is not reversible, due to the small dimension and hydrophobic character of the channels. The framework decomposes at temperatures above 380 °C.[71]

Layered aluminium phosphonates

So far, only a few functionalities were introduced into layered aluminium

phosphonates. They include methyl groups[74,75] and phenyl groups[76,77,78] as well as carboxymethyl,[79] benzyl,[80, 81] bromobenzyl[80] and 3-aminopropyl groups.[82]

Aluminium methylphosphonates were synthesised either hydrothermally,[74] or by melting a phosphonic acid together with aluminium hydroxide.[75] Some of the aluminium phenylphosphonates were prepared under reflux[76,77,78] and others hydrothermally.[77,80] Aluminium carboxymethylphosphonate,[79] benzylphosphonate[80,81] bromobenzylphosphonate[80] and 3-aminopropylphosphonate[82] can likewise be prepared under hydrothermal conditions.

The structure of the aluminium methylphosphonate $Al(OH)(PO_3CH_3).H_2O$ was solved by Sawers *et al. ab initio* from powder X-ray diffraction data in 1996.[74] It consists of chains of distorted AlO_6 octahedra that are linked by bridging oxygens from the hydroxyl groups. Additionally, each aluminium is connected to one neighbour in the chain *via* corner-sharing phosphonate tetrahedra. The third oxygen of the phosphonate group provides the bond to a neighbouring chain. The sixth coordination site of the aluminium is filled by a water molecule. Within the layers, 12-ring cavities are formed by two pairs of oxygen-linked aluminium atoms from adjacent chains and the two phosphorus and four oxygen atoms belonging to the phosphonate groups that are linking these chains/aluminium atoms. Two water molecules belonging to aluminium atoms from different chains are placed in each of the cavities (Figure 1.18). The methyl groups connected to the phosphonate alternately point above and below the inorganic layers.

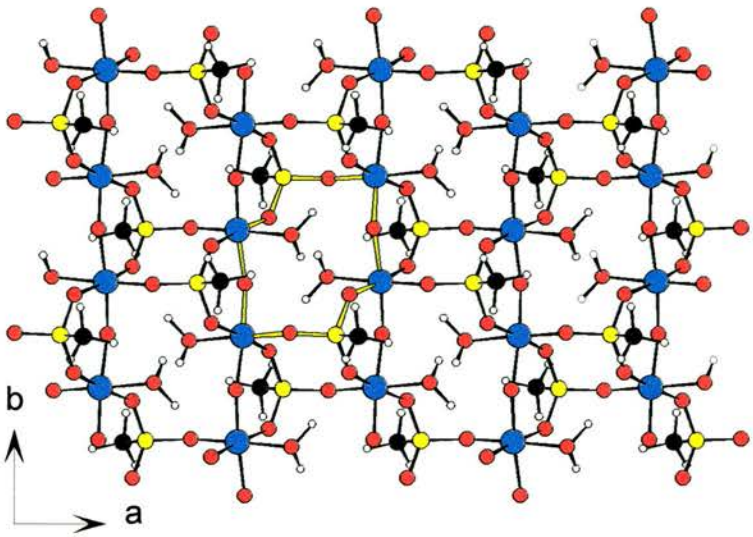

Figure 1.18: View onto an $Al(OH)(PO_3CH_3).H_2O$ layer along the c-axis. The bonds in one of the 12-ring cavities are shown in yellow.[74]
Key see pg. 4. Hydrogen was omitted for clarity.

The layered aluminium methylphosphonate $Al(O_3PCH_3)(HO_3PCH_3).H_2O$[75] (Figure 1.19) is made up of chains of AlO_6 octahedra coordinated by five phosphonate oxygens and one water molecule. Within these chains, the octahedra are bridged by two oxygen atoms belonging to two different phosphonate groups. In one of those groups all three oxygens are coordinated to aluminium atoms and in the other one only two of them are coordinated to aluminium and one is part of a hydroxyl group. The chains are cross-linked by the third oxygen of the phosphonate groups with three P-O-Al bonds. The hydroxyl groups point into the interlayer space as do the methyl groups. However, methyl groups attached to phosphorus atoms with three bonds to aluminium have P-C bonds perpendicular to the inorganic layers while the methyl groups on phosphorus atoms carrying a hydroxide groups have P-C bonds parallel to the layers. The layers are held together by hydrogen bonds between the hydroxyl groups from adjacent layers. These hydrogen bonds form elliptical channels that are lined with the methyl groups. The shortest distance across these channels is 2.81 Å (H-H).

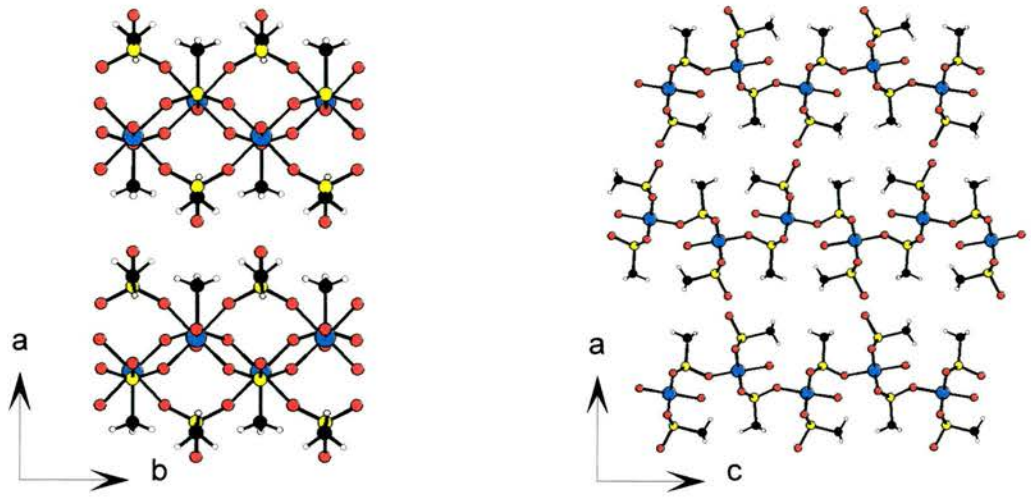

(a) (b)

Figure 1.19: Structure of the layered aluminium methylphosphonate $Al(O_3PCH_3)(HO_3PCH_3).H_2O$.[75] *Key see pg. 4.*

In 1996, Raki and Detellier published the preparation of an aluminium phenylphosphonate with the formula $Al_2(O_3PC_6H_5)_3.4H_2O$.[76] It was the first layered aluminium phosphonate structure to be reported and is prepared from bayerite $Al(OH)_3$. Bayerite consists of layers of aluminium octahedrically coordinated by hydroxyl groups that are held together by hydrogen bonds.[83] It was assumed by the authors that the intercalated material retains the basic structure of the inorganic layer while it contains covalently bonded chelating phosphonate groups that replace all but one of the water molecules coordinated to the aluminium. The phenyl groups are presumed to extend into the interlayer space.

Haky and Brady prepared a new aluminium phenylphosphonate in 1997.[78] The structure of $AlH(O_3PC_6H_5)_2.H_2O$ was assumed from powder XRD, NMR and IR spectroscopy, TGA and CHN analysis to consist of layers of aluminium atoms octahedrally coordinated by phosphonate groups. The structure suggested in the paper for the aluminium phenylphosphonate exactly matches the structure for α-ZrP proposed

by Alberti *et al.*[16] (see Figure 1.1b). The phenyl groups are expected to point towards the interlayer space, which corresponds to the observed interlayer distance of ~ 15 Å. No mention was made about the position of the hydrogen atom. The crystallinity of the product could be enhanced by refluxing it in an aqueous solution of *n*-propylamine, although it was not possible to prepare single crystals. Thermal studies showed that the material loses its water of hydration between 130 and 200 °C and is then stable up to 625 °C.

In 1998, Cabeza *et al.* published an article about a family of aluminium phenylphosphonates.[77] Depending on the synthesis conditions they were able to prepare six different phases: (i) $Al_2(O_3PC_6H_5)_3.2H_2O$, (ii) $Al_2(O_3PC_6H_5)_3$, (iii) α-$Al(HO_3PC_6H_5)(O_3PC_6H_5).H_2O$, (iv) β-$Al(HO_3PC_6H_5)(O_3PC_6H_5).H_2O$, (v) $Al(HO_3PC_6H_5)_3.H_2O$ and (vi) $Al(OH)(O_3PC_6H_5)$. Compounds (i) and (v) were prepared under reflux with a molar ratio of the starting material of Al:P 5:1 using absolute ethanol and toluene as respective solvents. All other compounds were prepared from aqueous solutions under hydrothermal conditions with ratios Al:P of 10:1 and 1:3. The variables in the reaction conditions included aluminium source, pH value and reaction time. The results of the TGA analyses of the samples varied widely. For example phase (i) loses its water of hydration at 40 °C while phase (v) loses water only above 210 °C. The combustion of the organic groups starts between 470 and 660 °C for the different materials. The structure of phase (iii) was solved from high-resolution powder synchrotron diffraction data. It corresponds to the structure of the related aluminium methylphosphonate $Al(HO_3PCH_3)(O_3PCH_3).H_2O$[75] that is described on pg. 37.

The layered aluminium carboxymethylphosphonate with the formula

$Al(O_3PCH_2CO_2).3H_2O$ consists of chains of AlO_6 octahedra that are cross-linked by phosphonate groups *via* shared oxygen atoms. Each phosphonate group has bonds to three different aluminium atoms. One oxygen of the carboxyl group is also coordinated to one of these aluminium atoms. The remaining two coordination sites of the aluminium are filled by water. The second oxygen atom of every carboxyl group is deprotonated and points towards the interlayer space on alternating sides of the layer. The inorganic layers are held together by hydrogen bonding between these carboxylate ions and water molecules that are situated in the interlayer space (Figure 1.20).[79] The difference to the previously known metal(II) carboxyethylphosphonates[41,44] (see pg. 25) is that the carboxymethyl compound coordinates to an aluminium atom in the same layer as the phosphorus atom it belongs to, rather than bridging two layers.

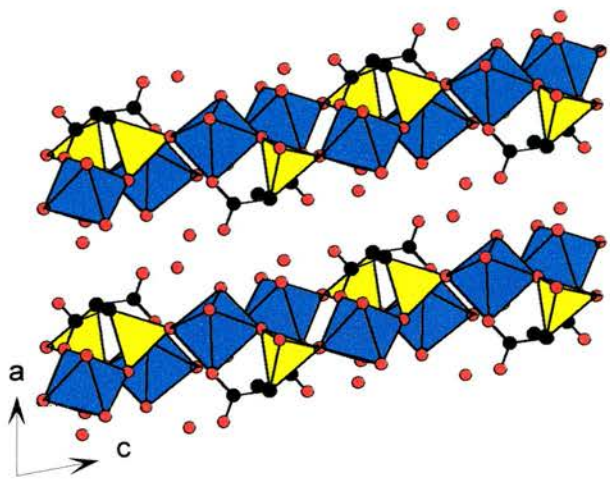

Figure 1.20: Structure of the layered aluminium carboxymethylphosphonate $Al(O_3PCH_2CO_2).3H_2O$.[79] The aluminate octahedra are blue, phosphonate tetrahedra yellow, oxygen atoms are denoted by red spheres and carbon atoms by black ones.

Chaplais *et al.*[80] reported the preparation and structural characterisation of an aluminium bromobenzylphosphonate with the molecular formula $Al(OH)(O_3PCH_2C_6H_4Br).H_2O$. The structure of this material is similar to that of the corresponding aluminium methylphosphonate,[74] although there are some distortions due

to the bulk of the bromobenzyl groups. The preparation of an aluminium benzyl- and a phenylphosphonate were also mentioned. The structure of the phenylphosphonate $Al_2(O_3PC_6H_5)_3.H_2O$ was assumed to be different from the structure of $Al_2(O_3PC_6H_5)_3.2H_2O$.[77] The aluminium benzylphosphonate $Al(OH)(O_3PCH_2C_6H_5).H_2O$ was expected to show similar structural features to both the bromobenzyl and the methylphosphonate.[74]

In an independent investigation the structure of $Al(OH)(O_3PCH_2C_6H_5).H_2O$ was solved from powder X-ray diffraction data.[81] Its structure is very similar to the related aluminium methylphosphonate (Figure 1.18).[74] A detailed description of the material can be found in Chapter 4.1.1. It was also possible to elucidate the unusual undulating structure of a new aluminium benzylphosphonate ($Al_3H(O_3PCH_2C_6H_5)_5.H_2O$; Figure 1.21), which is discussed in Chapter 4.1.2.[81] A similar structure was found for the cobalt *t*-butylphosphonate[50] (Figure 1.6, pg. 21).

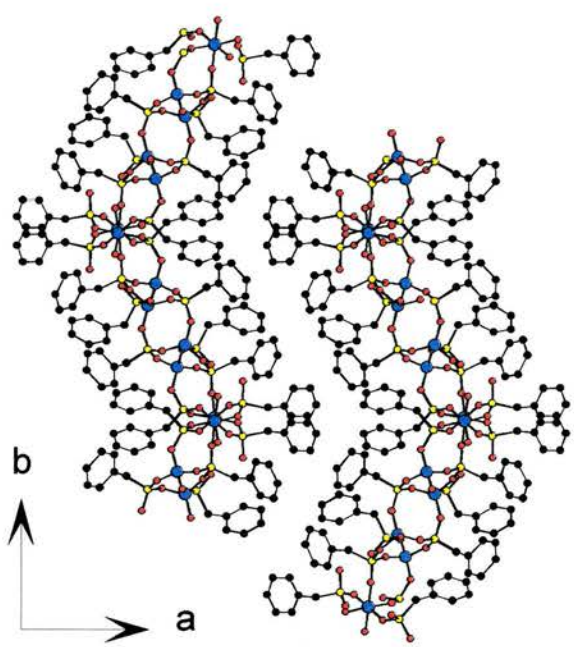

Figure 1.21: The undulating structure of $Al_3H(O_3PCH_2C_6H_5)_5.H_2O$ viewed along the a-axis.[81]

Key see pg. 4. Hydrogen was omitted for clarity.

An aluminium 3-aminopropylphosphonate sulphate hydrate with an uncommon chain structure ($Al(O_3P(CH_2)_3NH_3).SO_4.3H_2O$)[82] was prepared recently. It contains highly unusual positively charged phosphonate moieties that are balanced by negatively charged sulphate groups occluded in the material (Figure 1.22). Again, a more detailed discussion of the material and its special features can be found in Chapter 4.2.1.

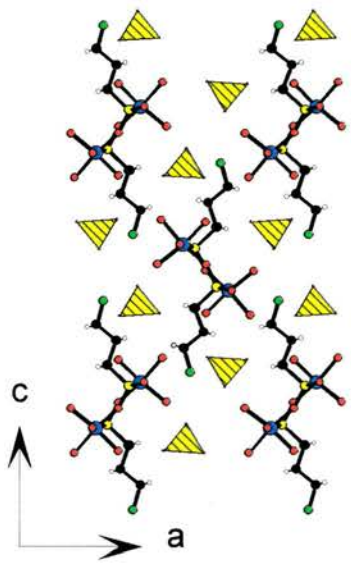

Figure 1.22: The structure of $Al(O_3P(CH_2)_3NH_3).SO_4.3H_2O$ with sulphate tetrahedra occluded between the phosphonate chains.[82]
Key see pg. 4. The green spheres denote nitrogen. The sulphate groups are shown as hashed yellow tetrahedra.

1.3.2. Gallium phosphonates

Recently, research interest has also been focused on gallium phosphonates. The structures of the first two gallium phosphonates were determined in 1998.[84] The layered compounds have the formulas $Ga(OH)(O_3PC_2H_4CO_2H).H_2O$ (a) and $Ga_3(OH)_3(O_3PC_2H_4CO_2)_2.2H_2O$ (b). The structure of (a) is very similar to $Al(OH)(O_3PCH_2C_6H_5).H_2O$[81] and the corresponding aluminium methyl-,[74] (Figure 1.18), benzyl-,[81] and bromobenzylphosphonates.[80] The organic groups extend into the

interlayer space and the carboxyl groups are not coordinated. In compound (b) the carboxyl groups are coordinated, probably to gallium atoms. This is expected to lead to a pillared material if the gallium atoms belong to an adjacent layer. It was also found that there is only one independent gallium environment in (b), although no further conjectures were made as to its structure. In zinc and cobalt carboxyethylphosphonate the layers are held together by the carboxyl groups (Figure 1.11).

1.4. References for Chapter 1

[1] M.B. Dines and P.M. DiGiacomo, *Inorg. Chem.*, **1981**, 20, 92-97

[2] G. Alberti, L. Boccali, M. Casciola, L. Massinelli and E. Montoneri, *Solid State Ionics*, **1996**, 84, 97-104

[3] G. Alberti, M. Casciola, U. Costantino and R. Vivani, *Adv. Mater.*, **1996**, 8, 291-303

[4] M.E. Thompson, *Chem. Mater.*, **1994**, 6, 1168-1175, and references therein

[5] G. Cao, H.-G. Hong and T.E. Mallouk, *Acc. Chem. Res.*, **1992**, 25, 420-427, and references therein

[6] G. Alberti, U. Costantino, M. Casciola and R. Vivani, *Solid State Ionics*, **1991**, 46, 61-68

[7] G. Alberti, M. Casciola, U. Costantino, A. Peraio and E. Montoneri, *Solid State Ionics*, **1992**, 50, 315-322

[8] G. Alberti, M. Casciola, R. Palombari and A. Peraio, *Solid State Ionics*, **1992**, 58, 339-344

[9] H. Lee, L.J. Kepley, H.-G. Hong, S. Akhter and T.E. Mallouk, *J. Phys. Chem.*, **1988**, 92, 2597-2601

[10] H. Lee, L.J. Kepley, H.-G. Hong and T.E. Mallouk, *J. Am. Chem. Soc.*, **1988**, 110, 618-620

[11] G.E. Fanucci, M.A. Petruska, M.W. Meisel and D.R. Talham, *J. Solid State Chem.*, **1999**, 145, 443-451

[12] C.T. Seip, G.E. Granroth, M.W. Meisel and D.R. Talham, *J. Am. Chem. Soc.*, **1997**, 119, 7084-7094

[13] H.E. Katz and M.L. Schilling, *Chem. Mater.*, **1993**, 5, 1162-1166

[14] K. Maeda, Y. Kiyozumi and F. Mizukami, *Angew. Chem. Int. Ed. Engl.*, **1994**, 33, 2335-2337

[15] S. Yamanaka, *Inorg. Chem.*, **1976**, 15, 2811-2817

[16] G. Alberti U. Costantino, S. Allulli and N. Tomassini, *J. Inorg. Nucl. Chem.*, **1978**, 40, 1113-1117

[17] M.D. Poojary, H.-L. Hu, F.L. Campbell and A. Clearfield, *Acta Cryst.*, **1993**, B49, 996-1001

[18] J.M. Troup and A. Clearfield, *Inorg. Chem.*, **1977**, 16, 3311-3314

[19] E. Jaimez, A. Bortun, G.B. Hix, J.R. Garcia, J. Rodriguez and R.T.C. Slade, *J. Chem. Soc., Dalton Trans.*, **1996**, 2285-2292

[20] G. Alberti, M. Casciola and R. Vivani, *Inorg. Chem.*, **1993**, 32, 4600-4604

[21] D.A. Burwell and M.E. Thompson, *Chem. Mater.*, **1991**, 3, 14-17

[22] D.M. Poojary, B. Shpeizer and A. Clearfield, *J. Chem. Soc., Dalton Trans.*, **1995**, 111-113

[23] S. Yamanaka and M. Hattori, *Inorg. Chem.*, **1981**, 20, 1929-1931

[24] G.B. Hix, S.J. Kitchin and K.D.M. Harris, *Chem. Soc., Dalton Trans.*, **1998**, 2315-2319

[25] G. Alberti and U. Costantino in *Inclusion compounds: Inorganic and physical aspects of inclusion,* eds. J.L. Atwood, J.E.D. Davies and D.D. MacNicol, Oxford University Press,Oxford, **1991**, vol.5, ch. 5, 136-176

[26] S.B. Ungashe *et al.*, *J. Am. Chem. Soc.*, **1992**, 114, 8717-8719

[27] H.E. Katz *et al.*, *Chem. Mater.*, **1991**, 3, 699-703

[28] G. Alberti *et al.*, *React. Polym.*, **1993**, 19, 1-12

[29] M. Casciola, U. Costantino, L. DiCroce and F. Marmottini, *J. Incl. Phenom.*, **1988**, 6, 291-306

[30] M. Casciola, U. Costantino and S. D'Amico, *Solid State Ionics*, **1986**, 22, 127-133

[31] M.B. Dines, R.E. Cooksey, P.C. Griffith and R.H. Lane, *Inorg. Chem.*, **1983**, 22, 1003-1004

[32] G. Alberti *et al.*, *Angew. Chem. Int. Ed. Engl.*, **1993**, 32, 1357-1358

[33] G. Alberti *et al.*, *Mater. Chem. Phys.*, **1993**, 35, 187-192

[34] G. Alberti, F. Marmottini, S. Murcia-Mascaros and R. Vivani, *Angew. Chem. Int. Ed. Engl.*, **1994**, 33, 1594-1597

[35] C.Y. Ortiz-Avila and A. Clearfield, *Inorg. Chem.*, **1985**, 24, 1773-1778

[36] T. Wong *et al.*, *Solid State Ionics*, **1981**, 5, 689-692

[37] J.W. Johnson, A.J. Jacobson, W.M. Butler, S.E. Rosenthal, J.F. Brody and J.T. Lewandowski, *J. Am. Chem. Soc.*, **1989**, 111, 381-383

[38] G. Cao, H. Lee, V.M. Lynch and T.E. Mallouk, *Solid State Ionics*, **1988**, 26, 63-69

[39] Y. Ortiz-Avila, P.R. Rudolf and A. Clearfield, *Inorg. Chem.*,**1989**, 28, 2137-2141

[40] S. Drumel, P. Janvier, D. Deniaud and B. Bujoli, *J. Chem. Soc., Chem. Commun.*, **1995**, 1051-1052

[41] S. Drumel, P. Janvier, P. Barboux, M. Bujoli-Doeuff and B. Bujoli, *Inorg. Chem.*, **1995**, 34, 148-156

[42] G.B. Hix and K.D.M. Harris, *J. Mater. Chem.*, **1998**, 8, 579-584

[43] S. Ayyappan, G. Diaz de Delgado, A.K. Cheetham, G. Ferey and C.N.R Rao, *J. Chem. Soc., Dalton Trans.*, **1999**, 2905-2907

[44] P. Rabu, P. Janvier and B. Bujoli, *J. Mater. Chem.*, **1999**, 9, 1323-1326

[45] D. Cunningham, P.J.D. Hennelly and T. Deeney, *Inorganica Chimica Acta*, **1979**, 37, 95-102

[46] G. Cao, H. Lee, V.M. Lynch and T.E. Mallouk, *Inorg. Chem.*, **1988**, 27, 2791-2785

[47] D.J. Sutor, *Acta Cryst.*, **1967**, 23, 418-422

[48] K.J. Martin, P.J. Squattrito and A. Clearfield, *Inorg. Chim. Acta*, **1989**, 155, 7-9

[49] G. Cao, V.M. Lynch, J.S. Swinnea and T.E. Mallouk, *Inorg. Chem.*, **1990**, 29, 2112-2127

[50] J. LeBideau, A. Jouanneaux, C. Payen and B. Bujoli, *J. Mater. Chem.*, **1994**, 4, 1319-1323

[51] F. Fredoueil, M. Evain, M. Bujoli-Doeuff and B. Bujoli, *Eur. J. Inorg. Chem.*, **1999**, 1077-1079

[52] Y. Zhang and A. Clearfield, *Inorg. Chem.*, **1992**, 31, 2821-2826

[53] J. Le Bideau, C. Payen, P. Palvadeau and B. Bujoli, *Inorg. Chem.*, **1994**, 33, 4885-4890

[54] H. Hayashi and M.J. Hudson, *J. Mater. Chem.*, **1995**, 5, 115-119

[55] B. Bujoli *et al.*, *Chem. Mater.*, **1993**, 5, 583-587

[56] L.-M. Zheng, H.-H. Song, C.-Y. Duan and X.-Q. Xin, *Inorg. Chem.*, **1999**, 38, 5061-5066

[57] J. Zhu, X. Bu, P. Feng and G.D. Stucky, *J. Am. Chem. Soc.*, **2000**, 122, 11563-11564

[58] M. Riou-Cavellec, M. Sanselme, N. Guillou and G. Férey, *Inorg. Chem.*, **2001**, 40, 723-725

[59] Y. Zhang, K.J. Scott and A. Clearfield, *Chem. Mater.*, **1993**, 5, 495-499

[60] G. Cao and T.E. Mallouk, *Inorg. Chem.*, **1991**, 30, 1434-1438

[61] K.J. Frink, R.-C-. Wang, J. L. Cólon and A. Clearfield, *Inorg. Chem.*, **1991**, 30, 1438-1441

[62] S.T. Wilson, B.M. Lok, C.A. Messina, T.R. Cannan and E.M. Flanigen, *J. Am. Chem. Soc.*, **1982**, 104, 1146-1147

[63] J.M. Bennett *et al.*, *Inorg. Chem.*, **1985**, 24, 188-193

[64] K.O. Kongshaug, H. Fjellvåg and K.P. Lillerud, *J. Mater. Chem.*, **1999**, 9, 1591-1598

[65] D. Riou, T. Loiseau and G. Férey, *Solid State Chem.*, **1993**, 102, 4-8

[66] M.E. Davis, *Nature*, **1988**, 331, 698-699

[67] M.E. Davis and R.F. Lobo, *Chem. Mater.*, **1992**, 4, 756-768

[68] Q. Huang and S.-J. Hwa, *J. Chem. Soc., Chem. Commun.*, **1999**, 2343-2344

[69] K. Maeda, J. Akimoto, Y. Kiyozumi and F. Mizukami, *J. Chem. Soc., Chem. Commun.*, **1995**, 1033-1034

[70] K. Maeda, J. Akimoto, Y. Kiyozumi and F. Mizukami, *Angew Chem. Int. Ed. Engl.*, **1995**, 34, 1199-1201

[71] H.G. Harvey, S.J. Teat and M.P. Attfield, *J. Mater. Chem.*, **2000**, 10, 2632-2633

[72] V.J. Carter, P.A. Wright, J.D. Gale, R.E. Morris, E. Sastre and J. Perez-Pariente, *J. Mater. Chem.*, **1997**, 7, 2287-2292

[73] N.N. Greenwood and A. Earnshaw, *Chemistry of Elements*, Pergamon Press, Oxford **1984**

[74] L.-J. Sawers, V.J. Carter, A.R. Armstrong, P.G. Bruce, P.A. Wright and B.E. Gore, *J. Chem. Soc., Dalton Trans.*, **1996**, 3159-3161

[75] G.B. Hix, V.J. Carter, D.S. Wragg, R.E. Morris and P.A. Wright, *J. Mater. Chem.*, **1999**, 9, 179-185

[76] L. Raki and C. Detellier, *Chem. Commun.*, **1996**, 2475-2476

[77] A. Cabeza, M.A.G. Aranda, S. Bruque, D.M. Poojary, A. Clearfield and J. Sanz, *Inorg. Chem.*, **1998**, 37, 4168-4178

[78] J.E., Haky, J.B. Brady, N. Dando and D. Weaver, *Mater. Res. Bull.*, **1997**, 32, 297-303

[79] G.B. Hix, D.S. Wragg, R.E. Morris and P.A. Wright, *J. Chem. Soc,. Dalton Trans.*, **1998**, 3359-3361

[80] G. Chaplais, J. Le Bideau, D. Leclercq, H Mutin and A. Vioux, *J. Mater. Chem.*, **2000**, 10, 1-10

[81] N. Zakowsky, G.B. Hix and R.E. Morris, *J. Mater. Chem.*, **2000**, 10, 2375-2380

[82] N. Zakowsky, P.S. Wheatley, I. Bull, M.P. Attfield and R.E. Morris, *J. Chem. Soc., Dalton Trans.*, **2001**, 2899-2902

[83] J.D. Gale, A.L. Rohl, V. Milman and M.C. Warren, *J. Phys. Chem. B*, **2001**, 105, 10236-10242

[84] F. Fredoueil, D. Massiot, D. Poojary, M. Bujoli-Doeuff, A. Clearfield and B. Bujoli, *Chem. Commun.*, **1998**, 175-176

Chapter 2. Aims of the research

The great versatility of aluminium phosphonates due to the incorporation of 4- and/or 6-coordinate aluminium as well as the variety of possible connections between aluminium and phosphorus atoms leads to a wide range of conceivable structures. The organic part of the phosphonate also allows to easily incorporate functional groups that could change the hydrophobicity of a given material, act as receptors, sensors, or catalytic sites, or simply be used to further modify the material by post-synthetic reactions. Furthermore, it is known that;

- Aluminium phosphonates can form crystalline, microporous or layered materials.
- These materials show good thermal stability, e.g. AlMePO-α is stable to $\sim$ 500°C, an essential property for catalysis at high temperatures.
- The porosity of the materials may potentially be controlled by using diphosphonic acids to form covalent bridges between the inorganic layers at regular intervals and also by the use of templates in the syntheses of the materials.

Aluminium phosphonates therefore seemed interesting and important enough to conduct some in-depth research into their synthesis. Special interest was given to;

- The investigation into the influence of the reaction conditions on the synthesis of aluminium phosphonates and the determination of the conditions for the preparation of different phases.
- The synthesis of new functionalised aluminium phosphonates.
- The characterisation and (where possible) full structure determination of the new materials.

In addition, preliminary experiments were directed at the possibility of post-synthetic modification of some functionalised aluminium phosphonates prepared during the course of this research.

Chapter 3. Experimental

3.1. Hydrothermal Synthesis

The term 'hydrothermal synthesis' refers to reactions that take place in aqueous solution at high temperatures and pressures. They are normally carried out in PTFE-lined autoclaves, which are loaded with the reaction mixture, sealed and then heated in an oven for a set time at a certain temperature. The method is often used for the synthesis of aluminium phosphonates,[1,2] (see Chapter 1.3.1, pp. 33) but is also variously applied to the preparation of e.g. aluminium,[3,4,5] gallium,[6] cobalt,[7] tin,[8] and zinc[9] phosphates. Occasionally it is used to prepare other phosphonates, such as cobalt *t*-butylphosphonate hydrate,[10] sodium copper(II) carboxyethyl-phosphonate,[11] or α-zirconium phenylphosphonate.[9]

3.2. Synthesis of aluminium benzylphosphonates

For the preparation of aluminium benzylphosphonates from benzylphosphonic acid (benzyl PA) through hydrothermal synthesis (adapted from Maeda *et al.*[12]) qualitative and quantitative reaction parameters were varied. The qualitative factor was represented by the aluminium source; gibbsite (aluminium hydroxide), aluminium nitrate and sulphate, and a 1 M aqueous solution of aluminium chloride. The quantitative parameters included the ratio Al:P (varied between 1:1 and 1:50), the pH value (1.5, 2.5 or 4.5), the absolute amount of starting material per autoclave (approx. 0.3 g and 1.7 g respectively) and the reaction time (2 days to 13 days). The reaction temperature was kept constant at 160 °C.

Benzyl PA was prepared from diethyl benzylphosphonate (0.08 mol; 20 g) and hydrochloric acid (37 %, 0.8 mol; 75 ml). The chemicals were used as obtained from the manufacturer (see Chemicals, pg. 180). The mixture was refluxed for two days, allowed to cool down and the resulting solid was filtered off. It was then dissolved in water and the solution was evaporated on a rotavapor to remove residual HCl. This procedure was repeated 5 times before the white product was dried at 60 °C in air for five days.[13]

The following procedure is typical for the preparation of all samples. The sample containing the AlBzPO-2 ($Al_3H(PO_3CH_2C_6H_5)_5.H_2O$) single crystals was prepared as follows; 9.6×10^{-3} mol (1.650 g) benzyl PA and 4.8×10^{-4} mol (0.036 g) gibbsite (Al:P ratio 1:20) were ground together in a mortar and pestle. The mixture was then transferred into a Teflon-lined stainless steel autoclave with a volume of 23 ml and mixed with 10 ml of distilled water. After adjusting the pH to 1.5 with 0.06 ml NaOH solution (5 M) under stirring the autoclave was closed and left in an oven at 160 °C for 10 days. For some experiments, 0.5 ml acetone was added before the autoclave was closed. This was intended to decrease the surface tension of the solution and to prevent the phosphonate crystals from floating on the surface of the solution after the reaction and from sticking to the surfaces of the containers used for the workup.[14] However, it was found that this did not make any difference and the acetone was therefore omitted in subsequent experiments. The white crystalline product was removed by filtration, washed with distilled water and acetone and dried in air at 60 °C. Sample characterisation was carried out using powder X-ray diffraction, microcrystal diffraction, ^{27}Al, ^{31}P and ^{13}C MAS NMR spectroscopy, TGA, CHN analysis, and IR spectroscopy.

3.3. Synthesis of aluminium 3-aminopropylphosphonates

The synthesis of aluminium 3-aminopropylphosphonates was attempted in two ways, *via* hydrothermal synthesis (similar to the procedure in 3.2) and under reflux using a method adapted from Raki and Detellier.[15] As in Chapter 3.2, reaction parameters were varied. All experiments used 3-aminopropylphosphonic acid as source of phosphorus. The aluminium sources included gibbsite (aluminium hydroxide), aluminium nitrate and aluminium sulphate and a 1 M aqueous aluminium chloride solution. The ratio Al:P varied between 1:1 and 1:10, the pH value was adjusted to values between 1.5 and 7.0 and the absolute amount of starting material per autoclave varied between 0.2 g and 0.5 g. The reaction time was varied between 2 days and 29 days. The reaction temperature for the hydrothermal syntheses was kept at 160 °C for the first series of experiments. For all subsequent experiments it was reduced to 150 °C due to the necessity of sharing an oven with other researchers, but the change did not influence the results.

Hydrothermal syntheses at 160 °C were carried out similar to the procedure for aluminium benzylphosphonates (see Section 3.2). For the preparations at 150 °C, the amount of water was reduced to 5 ml and no acetone was added. A typical synthesis yielding AlaPrPO-1 was carried out by dissolving 7.2×10^{-4} mol (0.100 g) of 3-aminopropylphosphonic acid and 3.6×10^{-4} mol (0.240 g) of aluminium sulphate octadecahydrate (Al:P ratio 1:1) in 5 ml of distilled water in a Teflon-lined stainless steel autoclave with a volume of 23 ml. The pH value was then adjusted to 3.6 by addition of 0.16 ml of 5 M sodium hydroxide solution and the autoclave closed and heated in an oven at 150 °C for 11 days. After it was allowed to cool down, the

crystalline white product was removed by filtration, washed with distilled water and acetone and left to dry in air at 60 °C.

For the reflux experiments, the following procedure was followed; 1.44×10^{-3} mol (0.200 g) of 3-aminopropyl PA were dissolved in 20 ml of distilled water and 4.8×10^{-4} mol (0.319 g) of aluminium sulphate octadecahydrate (Al:P ratio 2:3) suspended in the solution under stirring. The suspension was then stirred under reflux for 3 days. After cooling, the white crystalline product was removed by filtration or centrifugation, washed with distilled water and acetone and dried in air at 60 °C. The aluminium 3-aminopropylphosphonates were characterised using microcrystal diffraction, powder X-ray diffraction, ^{27}Al, ^{31}P, ^{15}N and ^{13}C MAS NMR spectroscopy, TGA, CHN analysis and IR spectroscopy.

3.4. Synthesis of aluminium 2-aminoethylphosphonates

The hydrothermal synthesis of aluminium 2-aminoethylphosphonates followed the same procedures as described in Section 3.3 for aluminium 3-aminopropylphosphonates. Reflux experiments were also carried out according to the relevant method used for the aluminium 3-aminopropylphosphonates. In both cases 2-aminoethylphosphonic acid was used as the phosphorus source. The starting materials for the reflux reactions were gibbsite, aluminium sulphate, aluminium chloride and aluminium nitrate. Hydrothermal reactions were carried out at 150 °C using gibbsite and aluminium chloride. With the exception of some reactions with gibbsite, which were performed at an Al:P ratio of 1:2, the ratio was kept constant at

1:1.5. The pH value varied between 1.8 and 4.9. The reaction time was 3 days for all reflux experiments, but was increased to up to 10 days for some of the hydrothermal reactions. All products were white. Powder X-ray diffraction, ^{27}Al, ^{31}P and ^{13}C MAS NMR, TGA, CHN analysis and IR spectroscopy were used for the characterisation of the products.

3.5. Synthesis of aluminium aminomethylphosphonates

The preparation of aluminium aminomethylphosphonates was attempted both under hydrothermal conditions (procedure see Section 3.2) and under reflux (procedure see Section 3.3). The starting materials for all experiments were aminomethylphosphonic acid and gibbsite, at an Al:P ratio of 1:1.5 for the hydrothermal synthesis and 1:2 for the synthesis under reflux. The pH value was not monitored, there was no acetone added to the solutions and the reaction time varied from 18 h to 69 h. All products were white. The products were characterised using powder X-ray diffraction, CHN analysis, TGA, ^{27}Al, ^{15}N, ^{31}P and ^{13}C MAS NMR and IR spectroscopy.

3.6. Synthesis of aluminium 1-aminobutylphosphonates

For syntheses under reflux, gibbsite was used at the Al:P ratios 1:1.5 and 1:2. The hydrothermal synthesis was carried out with gibbsite and 1-aminobutylphosphonic acid at a ratio Al:P of 1:2. The preparation of the samples followed the procedure in Sections 3.2 and 3.3 for hydrothermal synthesis and synthesis under reflux respectively,

without addition of acetone, no monitoring of the pH value and reaction times varying from 22 h to 66 h. All 1-amino-butylphosphonates were white. The characterisation of the products took place by powder X-ray diffraction, ^{27}Al, ^{31}P and ^{13}C MAS NMR, TGA, CHN analysis and IR spectroscopy.

3.7. Synthesis of aluminium 4-aminobenzylphosphonates

4-Aminobenzylphosphonic acid was reacted with gibbsite under hydrothermal conditions (procedure see Section 3.2) and under reflux with gibbsite and aluminium chloride. The reflux reaction was carried out both in the same way as for the other aminophosphonic acids (see Section 3.3) and with some changes to the procedure (see below) as it is insoluble in water. For all reactions the molar ratio of aluminium to phosphorus was kept at 1:2. The reaction time varied from 24 to 90 h. The pH value was monitored for reactions involving mineral acids and varied from 1.0 to 6.0. The products were pale yellow.

The following changes were made to the conditions of the reflux reactions;

- use of a mixture of 10 ml of H_2O and 10 ml of dioxane as solvent,
- use of 25 ml of water and addition of 0.5 ml of a mineral acid (HCl, H_2SO_4, HNO_3),
- addition of sodium hydroxide solution to adjust the pH value if necessary.

Where the pH was 1 the reactions yielded a clear colourless solution. It was then necessary to increase the pH to 4 with sodium hydroxide solution and to reflux the solution for a further 24 h in order to obtain a precipitate. Powder X-ray diffraction,

^{27}Al, ^{31}P, and ^{13}C MAS NMR, TGA, CHN analysis, and IR spectroscopy were used for the characterisation of the samples.

3.8. Synthesis of aluminium iminobis(methylphosphonates)

Aluminium iminobis(methylphosphonates) were prepared under hydrothermal conditions at Al:P ratios of 1:1, 1:1.5, 1:2 and 1:5. Beside iminobis(methylphosphonic acid), the starting materials included gibbsite, aluminium chloride, aluminium nitrate and aluminium sulphate. The pH value of the reaction mixtures was varied between 0.5 and 2.7 by addition of small amounts of 5 M NaOH solution. The reaction temperature was kept at 150 °C for most reactions, although some experiments were carried out at 130 °C and 170 °C respectively. All reactions yielded a white amorphous product. A typical reaction would proceed as follows; 1.219×10^{-3} mol (0.250 g) of iminobis(methylphosphonic acid) and 3.05×10^{-4} mol (0.203 g) of aluminium sulphate octadecahydrate (Al:P ratio 1:2) were dissolved in 5 ml of distilled water in a Teflon-lined stainless steel autoclave with a volume of 23 ml. The pH value was adjusted to 1.5 by addition of 0.42 ml of 5 M sodium hydroxide solution, the autoclave sealed and heated in an oven at 150 °C for 3 days. After cooling down, the white product was removed by filtration, washed with distilled water and acetone and dried in air at 60 °C. Characterisation of the products was carried out using ^{27}Al, ^{31}P, ^{15}N and ^{13}C MAS NMR, powder XRD, TGA, CHN analysis and IR spectroscopy.

3.9. Synthesis of aluminium vinylphosphonates

Aluminium vinylphosphonate microcrystals were prepared under hydrothermal conditions in 6 ml of water from gibbsite (6.41×10^{-3} mol; 0.500 g) and 4.27 ml of a 1.5 M aqueous solution of vinylphosphonic acid (6.41×10^{-3} mol; 0.692 g; Al:P ratio 1:1). The pH of the reaction mixture was 2.5. It was stirred in a Teflon-lined stainless steel autoclave, sealed and heated in an oven for 17 days at 150 °C. The white product was recovered by filtration, washed with water and acetone and dried in air at 60 °C. A polycrystalline material was obtained at a reaction time of 60 h. The reaction of gibbsite (1.00×10^{-2} mol; 0.780 g) and 10 ml of the vinylphosphonic acid solution (1.50×10^{-2} mol; 1.620 g; Al:P ratio 2:3) under the same conditions yielded a white product of low crystallinity that was not investigated further. The characterisation of the products was carried out using powder X-ray diffraction, ^{27}Al, ^{31}P and ^{13}C solid state NMR spectroscopy, TGA, CHN analysis and IR spectroscopy. Attempts to employ microcrystal X-ray diffraction and HRTEM were not successful due to the disorder of the material in the third dimension and its instability towards the electron beam respectively.

3.10. Synthesis of aluminium carboxymethylphosphonates

The synthesis of aluminium carboxymethylphosphonates was attempted both following a method by Stucky *et al.*[16] and the method applied for the synthesis of aluminium iminobis(methylphosphonates) at pH values of 1.5 (see Section 3.8). The latter experiments led to a crystalline product, whose structure could be solved from

single crystals on a laboratory X-ray source. It was then recognised to be a phase previously prepared by Hix *et al.*[17] from gibbsite, carboxymethylphosphonic acid and *n*-butylamine under hydrothermal conditions.

The preparation of an aluminium carboxymethylphosphonate using the method of Stucky yielded polycrystalline materials. 1.681×10^{-3} mol (0.630 g) aluminium nitrate nonahydrate, 1.900×10^{-3} mol (0.266 g) carboxymethylphosphonic acid and 1.919×10^{-3} mol (0.403 g) 1,3,5-benzenetricarboxylic acid (BTC) were suspended in 2.0 ml of water and 7.2 ml of ethylene glycol in a Teflon-lined stainless steel autoclave (v = 23 ml). Subsequently, 7.05×10^{-3} mol (0.424 g) of ethylene diamine were added before the autoclave was sealed. The pH value of the reaction mixture was 7.2. After heating at 170 °C for 6 days, the autoclave was allowed to cool down and the product removed by filtration and washed with water and acetone. The caramel-coloured product was then dried in air at 60 °C. The material was characterised using ^{27}Al, ^{31}P, ^{15}N and ^{13}C MAS NMR, powder and single crystal XRD, TGA, IR spectroscopy and CHN analysis.

3.11. Amidation of amino-functionalised aluminium phosphonates with functionalised carboxylic acids

The starting material (e.g. aluminium aminomethylphosphonate, 8.5×10^{-5} mol; 0.020 g) was suspended in 1.5 ml of distilled water and under continuous stirring the following solutions were added in this order;

i) 10 ml of a dioxane-water-mixture (2:1 or 1:1),

ii) 3 ml of a solution of a carboxylic acid (0.05 M in water or dioxane) or a mixture of three carboxylic acids (0.05 M in water or dioxane, 3 × 1 ml; see Table 3.1) and

iii) 1.5 ml (7.5×10^{-4} mol; 0.155 g) of a solution of DCC (dicyclohexylcarbodiimide) (0.05 M in dioxane).

The reaction mixture was then placed in an oven at 60 °C and left there for 69 h. The product was recovered by filtration and dried in air at 60 °C. IR spectroscopy and powder X-ray diffraction were used for the characterisation of the products.

Table 3.1: Amidation experiments carried out with a variety of acids/acid mixtures and different starting materials

Starting material	**Carboxylic acid / mixture of carboxylic acids**			
	Octanoic acid	3-Hydroxy-carboxylic acid	4-Hydroxy-carboxylic acid	Imidazolecarb-oxylic acid
Aluminium methylphosphonate	×			
		×		
			×	
				×
	×		×	×
Aluminium 1-amino-butylphosphonate	×		×	×
	×		×	×

3.12. Techniques

3.12.1. X-ray diffraction

Diffraction studies are the pre-eminent method for the determination of average atomic positions and from them distances and bond angles in crystalline inorganic solids. Natural X-rays occur in a range from 0.1 to 100 Å. The artificial sources used

in structure determination have a wavelength of approximately 1 Å, which is in the order of magnitude for interatomic separations.

Regularly spaced arrangements of 'points' act as diffraction grating for waves with a wavelength similar to the repeat distance between those 'points'. Therefore, a diffraction pattern occurs when the X-ray beam is scattered by the electrons surrounding atoms or ions in a crystalline material and there is subsequent interference between the beams diffracted by different atoms.

X-rays can be generated by bombarding a metal target, often Cu or Mo, with an electron beam from a heated filament. Thereby, electrons from the 1 *s* shell of the Cu atoms are ionised and X-rays are emitted when the vacancies are filled by electrons dropping from the 2 *p* (K_α) and 3 *p* (K_β) levels. A monochromatic beam can be selected by either reflection on a crystal monochromator according to Bragg's law (see below) or by using a filter (Ni for Cu radiation, *i.e.* the atomic number *Z* of the target -1). With increasing atomic number of the target the energy of the emission increases and its wavelength decreases.

Bragg's law: $\lambda = 2d \sin\theta$

λ...wavelength, θ...scattering angle,

d...repeat distance in the regularly spaced arrangement.

The scattering power f_x decreases with increasing scattering angle (2θ). At $\sin\theta / \lambda = 0$, the scattering factor f_x is proportional to the atomic number *Z* of the respective atom and therefore very small for light elements, e.g. hydrogen and lithium. The scattering factor f_x is approximately independent of λ, but for accurate work

corrections must be made for anomalous scattering ($f_x = f_x + f_x' + i f_x''$). The interference between waves scattered by different atoms is given by the structure factor F_{hkl}, depending on the scattering factors and the positions of the atoms involved;

$$F_{hkl} = \Sigma f_n \cos 2\pi (hx_n + ky_n + lz_n)$$

with $F^2_{hkl} \sim I_{hkl}$ (I_{hkl} ... intensity of the reflection)

F_{hkl} is the Fourier transform of the electron density ρ_{hkl}. However, only the amplitude $| F_{hkl} |$ is available from measurements, while the sign (phase) cannot be determined directly (the so-called phase problem). This can be solved by computational methods such as, direct methods or the Patterson synthesis. Direct methods attempt to estimate approximate phases from a set of X-ray intensities by purely mathematical means with no prior knowledge about the crystal structure itself, apart from the discrete atomic nature of matter and its implications for diffraction effects. The phases and intensities can then be combined to give an electron density map. The Patterson synthesis can provide information on approximate positions of some of the atoms in a structure if there are a few heavy atoms among many light atoms or when it can be expected that a large proportion of the structure is well-defined, *e.g.* for a known rigid internal geometry. Here, the amplitudes are replaced by their squares and the phases omitted. The result of these calculations is closely related to the electron density.

The relation between the crystal lattice of the investigated material and the reciprocal lattice of the diffraction pattern can be explained as follows (Figure 3.1); an imaginary sphere or shell with a radius of $1/\lambda$ is placed around the sample. Where the exiting beam intersects with this shell, the reciprocal lattice is situated depicted here with the c^* - axis perpendicular to the beam. The lattice point for the (001) reflection

can be found on this axis at a distance of $1/d_{001}$. The reciprocal lattice can be rotated to place this point onto the surface of the imaginary sphere and at the same time the crystal in the diffracting position. The distance of the intersection of the shell with the exiting beam and the intersection of the shell with the diffracted beam equals the distance $1/d_{001}$ (reciprocal lattice vector, shown in red). This vector can be translated to originate in the centre of the sphere, with the reciprocal lattice perpendicular to it. Since the angle between the diffracted beam and the exiting beam is 2 θ, then due to geometric relationships the smallest angle of the triangle formed from, the diameter of the circle $(2/\lambda)$, $1/d_{001}$, and the connection l between the intersection of the incident beam with the shell and the diffracted beam with the shell, equals θ. As both l and the reciprocal lattice vector c^* are perpendicular to the 001 plane, the angle between the incident beam and the lattice planes and the angle between the diffracted beam and the lattice planes equals in both cases θ. This can also be used for a mathematical derivation of Bragg's law. The product of the sine of an angle enclosing the hypotenuse with the length of the hypotenuse equals the length of the side of the triangle opposite that angle. Applied to the triangle drawn in red that leads to Bragg's law;

$$\sin\theta = (1/d_{001}) / (2/\lambda) = \lambda / 2d_{001} \quad \rightarrow \quad (n)\ \lambda = 2d_{001}\ \sin\theta.$$

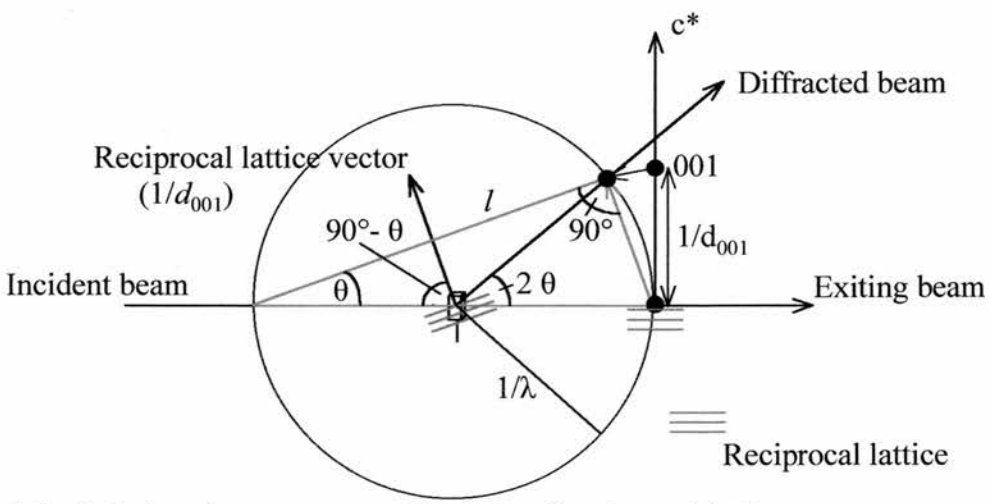

Figure 3.1: Relations between crystal lattice and reciprocal lattice.

Constructive interference is achieved if the Bragg equation is satisfied. As high-order scattering (n = 2,3,...) is indistinguishable from first-order scattering (n = 1), this equation represents the condition for diffraction to take place.

Diffraction at different angles θ leads to a regular pattern of discrete spots with different intensities. The geometry of the pattern reflects the symmetry of the crystalline material investigated. That means that the reciprocal lattice contains information about the size and symmetry of the unit cell. Lattice points may lie on atoms, but more often are placed on symmetry elements. Therefore information about the atoms in the unit cell is contained only in the intensities of the reflections, and not in the pattern itself. The coordinate system *xyz* (**x**) of the crystal mounting and *hkl* (**h**) of the reciprocal lattice are related to each other by a matrix A as follows; $\mathbf{x} = A \cdot \mathbf{h}$. The matrix A varies as **x** is diffractometer specific, because *x*, *y* and *z* are related to the diffractometer angles 2θ, ω, φ and χ.

Crystals can be imagined to be made up from small repeating units (unit cells) with the three translations *a*, *b* and *c* and the three angles α, β and γ. The unit cell includes a complete set of lattice points/atoms whose translation in three dimensions leads to the crystal structure. Lattice points can be imagined to be connected by lattice planes. Sets of these planes are parallel to each other and equally spaced. Different planes can be laid through different sets of lattice points. The planes cut the cell axes in fractional parts, the reciprocals of which are called the *Miller Indices h*, *k* and *l*, which define the placement of the plane. The spacing between two planes is the *d*-spacing, d_{hkl}. In single crystals, each set of *hkl* planes can be brought into the reflecting position using three degrees of freedom of a four-circle diffractometer (φ, χ and ω). The counter can then

scan across the remaining degree of freedom (2θ).[18,19]

3.12.1.1. Powder X-ray Diffraction

Powder X-ray diffraction is a valuable tool for probing the structure of microcrystalline solids. Such a powder contains an infinite number of crystallites at random orientations and the scattered intensity of the X-rays can be detected as a function of the scattering angle.[18]

Due to their random orientations, some of the crystallites should always be in an appropriate position for diffraction. The diffractometer therefore has only two variables, 2θ and ω. Initial screening of the products was carried out on all samples. Promising samples were then investigated further. For capillary samples the Debye-Scherrer-method was used. In this case, only 2θ is moved, resulting in a cone of scattering for each *hkl* value. The cones at different 2θ values can be intercepted to give intensities at these angles, resulting in a powder pattern. For samples mounted between discs of plastic foil fixed by Vaseline (Transmission method), the intensity of the scattered beams is also measured as a function of the angle 2θ as ω is fixed.

The initial powder X-ray diffraction patterns were recorded on a Philips diffractometer equipped with a Xe proportional detector and a secondary beam monochromator utilising CuK_α radiation. The Philips diffractometer uses flat plate samples in a reflective collection mode. The samples are affixed by coating the plate with a slurry made from finely ground sample and acetone and letting the acetone evaporate. Patterns suitable for Rietveld refinement were re-recorded on a STOE

diffractometer with a position-sensitive linear detector covering 6° in 2θ and employing Ge-monochromated Cu-$K_{\alpha 1}$ radiation (λ = 1.54056 Å). Samples were mounted either fixed with Vaseline between Mylar discs or in a glass capillary in order to reduce any preferred orientation effects, where such are observed. Indexing of powder patterns was carried out using the program TREOR90,[20] and Rietveld refinement was carried out using the GSAS suite of programs.[21]

3.12.1.2. Single Crystal Diffraction

By collecting data from a single crystal in a range of orientations, data may be obtained for the full 3-dimensional lattice structure. The use of CCD (charge coupled device) area detectors allows detection of many diffracted beams in a single exposure. The crystal can therefore be mounted in a two-circle set-up. The intensities of the diffracted beams are separated from the background by thresholding software and measured by integration of the intensities.[22] Data were collected on a Bruker AXS SMART CCD area detector diffractometer using molybdenum K_α radiation.

3.12.1.3. Microcrystal Diffraction

Microcrystal X-ray diffraction data were collected at low temperature (160 K) using a Bruker AXS SMART CCD area-detector diffractometer on the high-flux single-crystal diffraction station 9.8 at CCLRC Daresbury Laboratory Synchrotron Radiation Source, Cheshire, UK. The experiment used X-rays of wavelength 0.6944 Å selected by a horizontally focusing silicon (111) monochromator and vertically focused by a cylindrically bent palladium-coated zerodur mirror. The data sets covered more than a

hemisphere of reciprocal space with several series of exposures, each series with a different crystal orientation and each exposure taken over 0.2° rotation. Corrections were made for the synchrotron beam intensity decay as part of standard inter-frame scaling procedures.[22]

3.12.2. Nuclear Magnetic Resonance Spectroscopy

For solid materials whose structure is accessible by XRD, NMR studies can add valuable information about the short-range structure or confirm structural features found using XRD methods. In amorphous systems, it can be the main source of structural information. In the solid state, the line-widths of NMR signals can vary widely for different nuclei and for extremely crystalline and heterogeneous or amorphous systems respectively. For MAS (Magic Angle Spinning) NMR spectra that could be a range between 0.5 and 10 ppm, while for static solid state NMR spectra line widths of 100's of ppm are possible. Isotropic chemical shift values are specific for the solid state, *i.e.* they can reflect the local effects of the lattice. Furthermore, multiple peaks may occur due to crystallographically inequivalent sites in the unit cell and packing in the lattice can lead to different conformations and loss of symmetry in the material. It is possible for different conformations to occur within a single crystal, or for different polymorphs within one solid.

Nuclei with unpaired protons or neutrons behave similarly to bar magnets; they have a magnetic moment. These nuclei possess an intrinsic angular momentum known as spin. When exposed to a magnetic field the nuclei adopt one of a number of orientations. The simplest example is ^{1}H, which can adopt only one of two possible

orientations; a low energy orientation aligned with the magnetic field or a high energy orientation opposed to the magnetic field. When the nuclei are then exposed to a radio frequency signal the distribution of nuclei between the opposed and aligned orientations will change. This occurs when the radio frequency matches the energy difference between the two ($E = h\nu$; E...energy, h...Planck's constant, ν...frequency). When nuclei are promoted to a higher energy state, a small portion of the radio signal is absorbed. The signal is then measured (see below) from the re-emission of radiation as the nuclei relax to the ground state again.

The spectra are obtained through Fourier transformation. In the former the frequency range is scanned by either varying the frequency of the transmitter or by varying the magnetic field. In Fourier transformation NMR the transmitter and receiver are aligned with their axes at right angles to each other, usually the *x*-axis and *y*-axis respectively. The receiver sees no signal as long as the bulk magnetic vector *M* spins around the *z*-axis because there is no fluctuation in the magnetic field. When *M* is flipped into the *xy* plane by a 90° pulse from the transmitter, it starts to precess in the *xy* plane around the *z*-axis because the applied magnetic field B_0 tries to force it back into its original direction. This precession causes a fluctuation along the *x*-axis and the detector receives a signal. Finally relaxation processes occur and *M* gradually returns to its position along the *z*-axis. Over the acquisition period, the detector picks up the oscillations during relaxation. This signal is called the free induction decay (FID). The FID can be Fourier transformed and displayed as the frequency spectrum of the nuclei.

When an electron cloud is placed in a magnetic field, it circulates in a direction that produces a field opposing the applied field (diamagnetic circulation). Therefore, the

total field experienced by a nucleus is less strong. The induced field is directly proportional to the applied field, leading to the equation;

$B_i = B_0 - B_{induced} = B_0 - \sigma_i B_0 = B_0(1-\sigma_i)$ where B_i is the field experienced by a nucleus i.

Thus the nucleus is shielded from the applied field by the diamagnetic electronic circulation. The extent of the shielding depends on the electron density around a nucleus. The lower the electron density around a certain nucleus is, the greater the field experienced by this nucleus and the smaller the frequency of its precession. Differences in the shifts of various nuclei, *e.g.* ^{1}H (spanning a range of approx. 10 ppm), ^{13}C (250 ppm) or ^{31}P (400 ppm), are caused by the increasing number and the greater mobility of electrons in these atoms, leading to greater variation in the diamagnetic shielding. The interaction of the magnetic moment of a nucleus with an applied static magnetic field is called Zeeman interaction. It is responsible for the initial splitting of the energy level in a nucleus and determines the frequency of observation of that nucleus in a given magnetic field strength.

In the solid state the nuclear spin is dependent on the (fixed) orientation of the nuclear spin vector in the magnetic field and the random distribution of possible orientations leading to spectral broadening. It is therefore important to find ways to manipulate the spin systems to remove or average the solid state interactions so that the chemical shifts and spin-spin couplings can be retrieved.

Broad resonances are a major difficulty in solid-state NMR. Several factors contribute to the line width. The main factor is dipolar coupling, along with chemical

shift anisotropy. Dipolar interaction occurs between two like or unlike spins and leads to two lines with a characteristic peak separation. It takes place pair-wise between a nucleus and all its near neighbours (distance dependence $1 / r^3$).

Although there are nearly equal amounts of up and down spins averaged over the sample, their proportion may vary considerably through the sample. Therefore, some nuclei will experience a larger field than others resulting in a Gaussian distribution of coupling constants that leads to broad resonances with Gaussian shapes. For ^{1}H NMR broad peaks can lead to strong overlapping, although peaks can often be resolved by mathematical methods. In liquids and gases no dipolar coupling takes place due to molecular tumbling.

In solids, each molecule has a fixed orientation. The electron circulation, and with it the chemical shift are dependent on that orientation. Molecules with different orientations experience different shielding and therefore have different resonance frequencies. This effect is called 'chemical shift anisotropy'. It is caused by the modification of the applied magnetic field for a specific nucleus by its surrounding electrons. Because of this, the averaging of the possible random orientations in a polycrystalline sample leads to field-dependent line broadening. For ^{1}H NMR spectra, the frequency range of the line broadening has approx. the same order of magnitude as the isotropic shift range for solution NMR. It is the dominant broadening factor for spin ½ nuclei. The basic problem of solid state NMR therefore is to remove dipolar interactions for non-quadrupolar nuclei and to produce isotropic average values for other interactions (see below).

Indirect electron-coupled spin-spin interactions (spin-spin coupling) take place between two nuclear spins in solids as well as in solution. They are orientation-dependent according to the two spin vectors, generally small, and most important for spin ½. They can be important for the elucidation of chemical structures. For nuclei with a spin > ½, quadrupolar interactions occur in addition to spin-spin coupling.

Quadrupolar interactions arise from the interaction of a nuclear spin with the non-spherical symmetry field gradient at the nucleus. It is important for non-integral spins. Its orientation dependence is due to the fixed molar and spin orientation in the solid state. These interactions can be described as taking place between vector quantities described by 3×3 matrices. Some of these matrices can be averaged to zero. The non-zero results are the isotropic chemical shifts and the spin-spin couplings of these nuclei.

Molecular spin systems can be separated into two categories; 'abundant' and 'dilute' spin systems. In abundant spin systems, there is a high density of nuclei of high isotropic abundance (*e.g.* ^{1}H), making the dipolar term dominant for homonuclear interactions. This precludes the use of those nuclei in routine solid state NMR spectroscopy. This is illustrated by the following example; a short relaxation time in ^{1}H spectra can be caused by dipolar relaxation. If neighbouring nuclei have similar precessional frequencies their rotating magnetic components are close in frequency and they can exchange spin energy very efficiently leading to broad spectral lines.

Dilute spin systems contain low concentrations of the observed nucleus, either because of its low isotopic abundance or because of its low absolute concentration in the sample. For this reason, no or only very small homonuclear interactions occur.

Large heteronuclear interactions can be removed by decoupling the H-resonance frequency. Further more, the $(1 / r^3)$ - dependence of dipolar interactions leads to large reductions for abundant nuclei that are not directly bonded.

Chemical shift anisotropy is the main remaining interaction leading to line broadening after the removal of dipolar interactions for spin ½ nuclei. It can be overcome by the use of magic angle spinning (MAS) NMR spectroscopy. In powder patterns, the absorptions for random orientations give rise to broad 'anisotropy patterns'. MAS NMR can average the anisotropic chemical shift to the isotropic value. For this, the sample is spun around an axis inclined at an angle θ to the magnetic field axis at a frequency similar to the value of the shift anisotropy. Thereby, the shift anisotropy can be modified by a term $(3 \cos^2\theta - 1)$. If $\theta = 54°44'$, this term becomes zero, leaving only the term for the isotropic shift to influence the spectrum. Depending on the spinning frequency, spinning side bands may or may not appear. A sample spinning at the magic angle also imitates the motion of molecular tumbling, which is a simpler explanation for why remaining dipolar interactions can be removed.

Cross-polarisation (CP) increases the signal-to-noise ratio for dilute nuclei, but does not influence the resolution of a spectrum. It is used to enhance the magnetisation of dilute nuclei from the magnetisation reservoir of the abundant proton spin system, as the long relaxation time of dilute nuclei brings practical disadvantages (multi-pulse spectra can only be obtained with very long delays between the pulses). To this end, the proton spin magnetisation is rotated by 90° to be aligned with the proton magnetisation (it is 'spin-locked'). Simultaneous application of an on-resonance pulse with matching magnitude (*e.g.* the precession rate of ^{13}C is only ¼ of the rate of protons, therefore the

amplitude of the pulse is four times the amplitude of the pulse used to magnetise the protons) to the dilute nucleus allows the magnetisation of this nucleus to grow by transfer of magnetisation from the proton reservoir during the contact time (when both pulses are on). The pulse for the dilute nucleus is then turned off and the proton field is used for decoupling during the acquisition time. The dilute nuclei will now precess at the rate of the protons, thus ensuring their efficient relaxation.[23,24]

In materials without hydrogen there are no CP experiments possible and proton decoupling is not necessary. Simple MAS NMR experiments are therefore sufficient to remove shift anisotropy and dipolar interactions. The experiments should be carried out at the highest possible field strength, as that leads to a gain in resolution for spin ½ nuclei due to the higher stability and homogeneity of those fields as well as the minimisation of minor interaction such as dipolar interactions to quadrupolar nuclei. Additionally, the chemical shift dispersion is maximised.

The quadrupolar interactions for nuclei with non-integral spin (e.g. ^{11}B with $I = 3/2$, ^{27}Al and ^{17}O with $I = 5/2$) lead to changes in the Zeeman splitting. This can be illustrated on the example of ^{11}B, where the four energy levels 3/2, 1/2, -1/2 and -3/2 should theoretically be equidistant. However, first order quadrupolar interaction leads to a shift. The 3/2 and -3/2 levels stay at the same value and the 1/2 and –1/2 levels are shifted in the same direction by the same amount. Therefore, only the ½ to 3/2 and the -3/2 to -1/2 transitions are affected, leading to broad, non-observable bands far from the resonance frequency. The line shape of the +1/2 to –1/2 transition is distorted and the centre of gravity of the signal shifted due to second order quadrupolar interactions. These second order interactions are however inversely field dependent and therefore

minimised at high fields. For quadrupolar nuclei, the nuclear spin is not quantified along the Zeeman field direction and MAS only reduces the interaction, but does not remove it. [25] In ^{27}Al NMR spectra of silicates and phosphonates, the main distinction is between octahedral coordination with shifts between –60 and 10 ppm and tetrahedral coordination at around 40 to 65 ppm.

Solid-state ^{31}P NMR has been used to characterise zinc phosphonates.[26] In the study, the ^{31}P NMR spectra of crystalline zinc phosphonates with known structures were measured in order to obtain the chemical shift for PO_3 groups with different connectivities. These data were then used as references for the determination of the connectivity in amorphous zinc phosphonates. The methods used included both magic angle spinning (MAS) NMR and static NMR.

The oxygens in the PO_3 group can be connected to metal atoms in three ways;

(i) each oxygen is coordinated to one zinc atom (111),

(ii) one oxygen is bridging two zinc atoms and the other two are each connected to one zinc atom (211) and

(iii) two oxygens are each bridging two zinc atoms and one oxygen is only connected to one zinc atom (221).

The references were measured at different spinning rates and the isotropic chemical shifts were extracted from the MAS NMR. For the different connectivities different chemical shifts were observed. For (i) δ had a range from 27.0 to 29.8 ppm, for (ii) the range was 32.4 to 34.4 ppm and for (iii) δ varied between 35.9 and 37.7 ppm. From these data it appears that the isotropic chemical shifts move downfield with increasing

connectivity. The static NMR spectra showed the same trend.[26]

In 1989 R. K. Harris *et al.* published an article about solid state ^{13}C and ^{31}P NMR of phosphonic and phosphinic acids.[27] It was found that the phosphorus line widths were in the range of 50 – 80 Hz. Therefore, coupling constants were not resolved from the ^{31}P spectra. Due to line widths of 20 – 30 Hz the resolution of the ^{13}C spectra often was not sufficient to separate the lines of the spectra. The phosphorus spin-lattice relaxation time determined for ethane diphosphonic acid was greater than 900 s, which might be due to a highly rigid lattice caused by strong hydrogen bonding. Cross-polarisation techniques were used to allow shorter delays between cycles.

^{27}Al, ^{31}P, ^{15}N and ^{13}C MAS NMR experiments were carried out through the EPSRC Solid State Service (Durham) on a Varian Unityplus 300 spectrometer. Chemical shifts are reported with respect to 1 M aqueous $AlCl_3$, 85 % H_3PO_4, CH_3NO_2 indirectly through labelled NH_4NO_3, and TMS (Tetramethylsilane) for ^{27}Al, ^{31}P, ^{15}N and ^{13}C spectra respectively. For solid state NMR these are usually external standards. All spectra were measured at ambient temperature.

3.12.3. Infrared Spectroscopy

In Infrared (IR) spectroscopy samples are exposed to radiation with frequencies of 3×10^{12} to 3×10^{14} Hz (wavelengths 1×10^{2} to 1×10^{4} cm^{-1}), which causes the molecules of the sample to vibrate and to change their configuration. Vibrations that lead to a dipole change in the molecule are IR active and can be measured with an IR spectrometer. The observed vibrations can be roughly divided into skeletal vibrations (1400...700 cm^{-1})

that arise from linear or branched structures in the backbone of a molecule and groups frequencies that are found in the spectrum above and below the skeletal vibrations. The group frequencies are typical for functional groups like O-H or C=O and small structural units like triple bonds or methylene groups.

An IR spectrometer consists generally of a source of radiation, an optical unit that serves to focus the beam on the sample and a detector. The source of radiation is a laser that emits a very precisely defined frequency. In Fourier Transform spectroscopy the radiation is led from the source *via* aluminised or silvered mirrors (glass absorbs strongly in the IR region) to a half-transparent beam splitter. From there the radiation goes to 50 % to a fixed and to 50 % to a movable mirror. The recombined leaving radiation shows constructive or destructive interference depending on the path lengths a and b from the beam splitter to the two mirrors. Constructive interference occurs for $a = n \times b$ when n is an integral number of the wavelength; destructive interference if n is a half-integral number. The beam is then sent through the sample, which absorbs energy according to its structure, and the intensity of the leaving radiation is measured with the detector. The detector can be photoconductive or thermal, measuring the heating effect of the radiation. Interference of water and carbon dioxide vibrations can be reduced by sweeping the spectrometer with dry or inert gas or by the use of a double-beam spectrometer.

In Fourier Transform spectroscopy the sum of all waves is recorded as a function of time. This spectrum can be transformed mathematically into the frequency domain, where the amplitude of a vibration is given with respect to the wavelength at which it occurs.

The number of possible vibrations in a molecule is determined by its degrees of freedom. A molecule with n atoms has $3\times n$ degrees of freedom, which are distributed as 3 rotational, 3 translational and $3n$-6 vibrational moods. Therefore there should be $3n$-6 different frequencies for non-linear molecules ($3n$-5 for linear molecules). As mentioned before, vibrations are only IR active if a change of the dipole moment occurs and so the number of active frequencies depends on the symmetry of a molecule. In liquids and solids there is also an influence by an external field caused by neighbouring molecules. In crystals additional selection rules exist because of the regularity in the arrangement.

Different vibrations can interact with each other leading to combination bands (the sum or difference of fundamental vibrations). In addition, so-called overtones are multiples of fundamental vibration frequencies. Both are always weaker than the fundamental bands and hence may not be observed.

The following observations can be made for covalently linked atoms, which exhibit stretching or bending vibrations. The stretching frequency of X-H bonds increases with the electronegativity of X and decreases with its increasing atomic weight. Frequencies of X-Y bonds occur at much lower wavenumbers. In general, stronger bonds lead to higher frequencies, e.g. X=Y bonds have higher frequencies than X-Y bonds and H bonding leads to higher frequencies for X-H vibrations. Bending vibrations occur at wavenumbers that are about one order of magnitude smaller than the corresponding stretching vibrations and they are more sensitive to changes in the environment.[23,28]

IR spectra were obtained on a Perkin-Elmer PE 1710 Fourier transform IR spectrometer. The samples were run as KBr disks containing approximately 1 % sample at a resolution of 2.0 cm^{-1}. Bands were assigned using a variety of tables[23,28,29] combined with assumptions based on comparisons of recurring features in the IR spectra of the phosphonic acids and aluminium phosphonates investigated here.

3.12.4. Thermal Analysis

Thermogravimetric analysis (TGA) involves heating a small sample of an (unknown) material at a controlled rate in a controlled atmosphere and observing the changes in mass that occur during heating. The observed mass losses can be related to the loss of solvent adhering to the surface of the material, water of crystallisation and the combustion of the organic parts of the material. Sometimes it is possible to deduce the molecular formula of the compound from the losses and the amount of residue remaining after the heating cycle. The method is especially useful in combination with CHN analysis (see Chapter 3.12.5). Differential temperature analysis (DTA) data can be obtained at the same time as the TGA and gives information on the energy changes at a thermal event (exothermic/endothermic).

The TGA experiments were carried out on a TA Instruments SDT 2960 Simultaneous DTA-TGA thermogravimetric analyser. Samples were heated in an alumina crucible, at a rate of 10 °C min^{-1}, to a maximum temperature of 1200 °C, in an atmosphere of flowing oxygen (100 ml min^{-1}). Recalcined aluminium oxide was used as the reference material.

3.12.5. Microanalysis (CHN Analysis)

CHN analysis provides data on the relative amounts of carbon, hydrogen and nitrogen present in a material. The results can be used in conjunction with TGA to allow the stochiometry of a sample to be ascertained. The CHN analyses were obtained on a Carlo Erba model 1106 elemental analyser.

3.13. References for Chapter 3

[1] H.G. Harvey, S.J. Teat and M.P. Attfield, *J. Mater. Chem.*, **2000**, 10, 2632-2633

[2] K. Maeda, J. Akimoto, Y. Kiyozumi and F. Mizukami, *Angew Chem. Int. Ed. Engl.*, **1995**, 34, 1199-1201

[3] S.T. Wilson, B.M. Lok, C.A. Messina, T.R. Cannan and E.M. Flanigen, *J. Am. Chem. Soc.*, **1982**, 104, 1146-1147

[4] H.-M. Yuan, J.S. Chen, Z. Shi, W. Chen, Y. Wang, P. Zhang, J.-H. Yu and R.-R. Xu, *J. Chem. Soc., Dalton Trans.*, **2000**, 1981-1984

[5] A.A. Ayi, A. Choudhury and S. Natarajan, *J. Solid State Chem.*, **2001**, 156, 185-193

[6] D. Wragg and R.E. Morris, *J. Mater. Chem.*, **2001**, 11, 513-517

[7] Y.-H. Xu, Z. Yu, X.-F. Chen, S.-H. Liu and X.-Z. Yon, *Solid State Chem.*, **1999**, 146, 157-162

[8] R. Vaidhyanathan and S. Natarajan, *J. Mater. Chem.*, **1999**, 9, 1807-1811

[9] S. Neeraj, S. Natarajan and C.N.R. Rao, *J. Chem. Soc., Chem. Commun.*, **1999**, 165-166

[10] J. LeBideau, A. Jouanneaux, C. Payen and B. Bujoli, *J. Mater. Chem.*, **1994**, 4, 1319-1323

[11] M. Riou-Cavellec, M. Sanselme, N. Guillou and G. Férey, *Inorg. Chem.*, **2001**, 40, 723-725

[12] K. Maeda, J. Akimoto, Y. Kiyozumi and F. Mizukami, *J. Chem. Soc., Chem. Commun.*, **1995**, 1033-1034

[13] adapted from Organikum, H.G.O. Becker *et al.*, 19th edition, Deutscher Verlag der Wissenschaften, **1993**, pg. 433

[14] S. Yamanaka, K. Sakamoto and M. Hattori, *J. Phys. Chem.*, **1984**, 88, 2067-2070

[15] L. Raki and C. Detellier, *Chem. Commun.*, **1996**, 2475-2476

[16] J. Zhu, X. Bu, P. Feng and G.D. Stucky, *J. Am. Chem. Soc.*, **2000**, 122, 11563-11564

[17] G.B. Hix, D.S. Wragg, R.E. Morris and P.A. Wright, *J. Chem. Soc,. Dalton Trans.*, **1998**, 3359-3361

[18] A.K. Cheetham, *Diffraction methods, in* Solid State Chemistry – Techniques, eds. A.K. Cheetham and P. Day, Oxford University Press, **1988**, pp. 39

[19] Material from the 8th BCA/CCG Intensive Course in X-ray Structure Analysis, Durham, **2001**

[20] TREOR90, P.E. Werner, University of Stockholm, Sweden, **1990**

[21] GSAS, R.B. von Dreele and A.C. Larson, Regents of the University of California, USA, **1995**

[22] SAINT, BRUKER, Karlsruhe, Germany, **2000**

[23] C.N. Banwell and E.M. McCash, *Fundamentals of molecular spectroscopy*, 4th edition, McGraw-Hill Book Company Europe, **1994**

[24] D.H. Williams and I. Fleming, *Spectroscopic methods in organic chemistry*, 4th edition, McGraw-Hill Book Company Europe, **1989**

[25] C.A. Fyfe and R.E. Wasylishen, *High-resolution solid-state MAS NMR investigations of inorganic systems*, *in* Solid State Chemistry – Techniques, eds. A.K.Cheetham and P.Day, Oxford University Press, **1988**, pp. 190

[26] D. Massiot, S. Drumel, P. Janvier, M. Bujoli-Doeuff and B. Bujoli, *Chem. Mater.*, **1997**, 9, 6-7

[27] R.K. Harris, L.H. Merwin and G. Haegele, *J. Chem. Soc., Faraday Trans. I*, **1989**, 85, 1409-1423

[28] C.N.R. Rao, *Chemical applications of infrared spectroscopy*, Academic Press, London, **1963**

[29] M. Otto, *Analytische Chemie*, VCH Verlagsgesellschaft mbH, Weinheim, **1995**, pp. 247

Chapter 4. Results and Discussion

Each section in this chapter relates to a phosphonate/group of phosphonates with a different functionality. All details relating to the synthesis, analysis, and structure of any of these phosphonates are discussed together in the respective section. If different phases were prepared for the same functionality, their structures are discussed in different sections.

4.1. Synthesis of aluminium benzylphosphonates

Depending on the synthesis conditions a variety of different aluminium benzylphosphonate phases can be obtained by combining benzylphosphonic acid with a suitable aluminium source. The pH, Al:P ratio, and aluminium source all have dramatic effects on the nature of the phases produced. Figure 4.1 shows the effect of pH and Al:P ratio on the phases prepared from gibbsite and Figure 4.2 gives an impression of the change in the interlayer distance depending on the reaction conditions. One of the phases was present in most of the samples, and in a number of cases was the only phosphorus-containing product (however some Al-containing starting material was still present in a number of preparations). This phase has been identified as $Al(OH)(O_3PCH_2C_6H_5).H_2O$ and is referred to as AlBzPO-1. The unit cell of this phase was determined and a model for the structure elucidated from the X-ray powder diffraction data (see Section 4.1.1). At lower Al:P ratios, phases with presumably increasing phosphorus content are also evident. However, the presence of AlBzPO-1 as a minor phase in almost all the preparations complicates the characterisation of these

phases considerably, and only in the case of $Al_3H(PO_3CH_2C_6H_5)_5.H_2O$ (AlBzPO-2), where small single crystals suitable for X-ray diffraction at a synchrotron source were recovered, was full structural characterisation possible (see Section 4.1.2). The mixtures can include two more phases AlBzPO-3 and AlBzPO-4, identified from their different powder X-ray diffraction patterns. AlBzPO-3 is the major phase prepared at low pH values and at Al:P ratios between 1:5 and 1:10 and a minor phase at higher phosphorus concentrations. Unfortunately, it was impossible to prepare this material either as a pure phase or containing any single crystals suitable for structural characterisation. AlBzPO-4 has only been observed as a minor phase in combination with AlBzPO-1 prepared at pH values of 2.5 or higher and at Al:P ratios around 1:1. Many of the samples prepared at Al:P ratios between 1:1 and 1:2 also contained pseudo-boehmite (AlO(OH)).

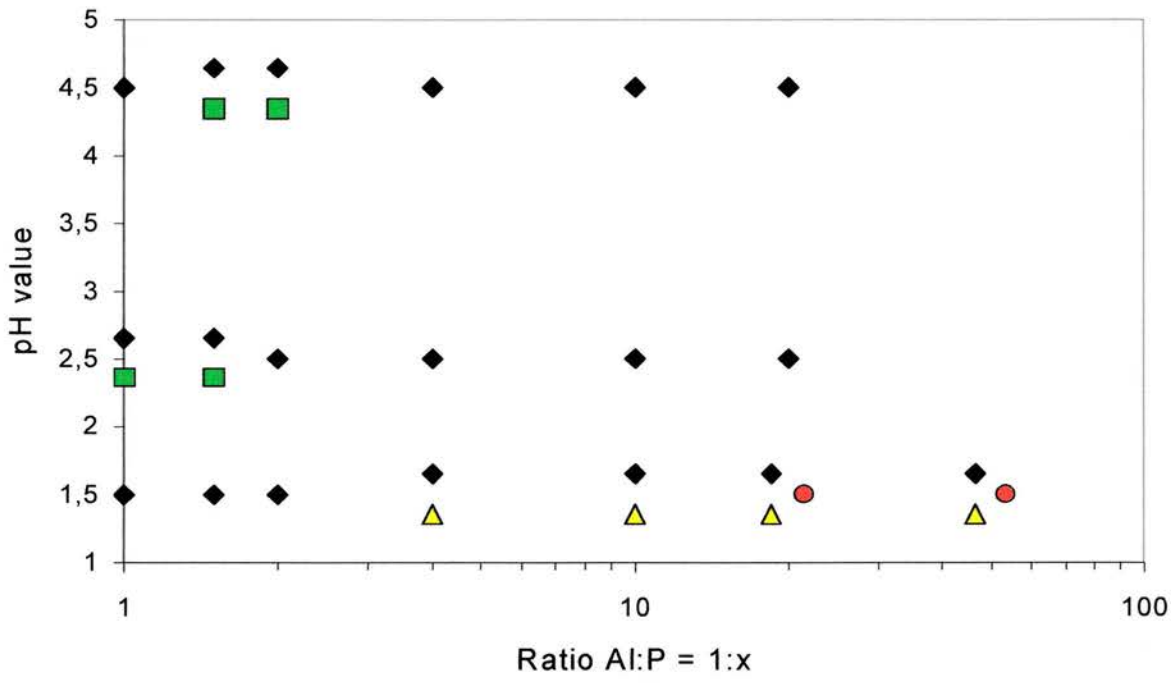

Figure 4.1: Illustration of the variety of phases that can be prepared from benzylphosphonic acid and gibbsite depending on the pH and the Al:P ratio of the starting materials, when all other conditions are kept constant as described in the text. Key: AlBzPO-1 (◆), AlBzPO-2 (●), AlBzPO-3 (▲) and AlBzPO-4 (■).

The variety of phases/phase mixtures that can be obtained also depends strongly on the aluminium source. With aluminium nitrate and sulphate only AlBzPO-1 is observed. When aluminium chloride is used, mixtures of AlBzPO-1 and AlBzPO-3 can be prepared. The phase diagram is then similar to the pattern for gibbsite: AlBzPO-3 can be found at pH 1.5 for ratios Al:P between 1:4 and 1:10 (see Figure 4.3).

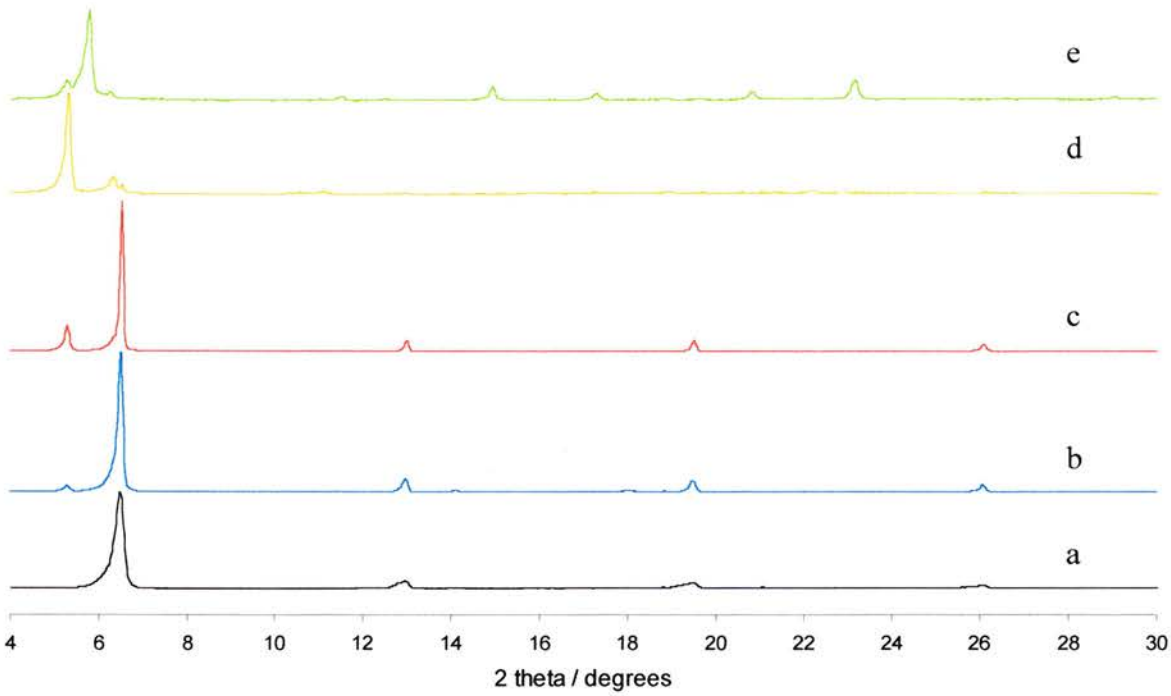

Figure 4.2: Powder XRD patterns of the aluminium benzylphosphonate phases prepared from gibbsite depending on the reaction conditions;

(a) AlBzPO-1, pH 4.5, ratio Al:P 1:4, c_{Al}=0.045 mol/l

(b) AlBzPO-1 and -3, pH 1.5, ratio Al:P 1:4, c_{Al}=0.045 mol/l

(c) AlBzPO-1and -3, pH 1.5, ratio Al:P 1:10, c_{Al}=0.016 mol/l

(d) AlBzPO-1, -3 and 4, pH 1.5, ratio Al:P 1:20, c_{Al}=0.008 mol/l

(e) AlBzPO-2, -3 and 4, pH 1.5, ratio Al:P 1:20, c_{Al}=0.048 mol/l.

Although the reaction time for most experiments was left constant at 2 days, there seems to be an influence on the composition of the product if the reaction time is increased. Samples with a ratio Al:P 1:20 and an absolute concentration of 1.7 g of

material per autoclave at pH 1.5 were left in the oven for 2, 5 and 10 days. The first and the second sample each yielded a mixture of AlBzPO-3 with some AlBzPO-1, whereas the third contained mainly AlBzPO-2 accompanied by AlBzPO-3 and AlBzPO-1. This may mean that AlBzPO-2 is thermodynamically more stable than AlBzPO-3. However, it is hard to tell without knowing the structure of AlBzPO-3. More complicated structures tend to be less thermodynamically stable than less complicated ones.

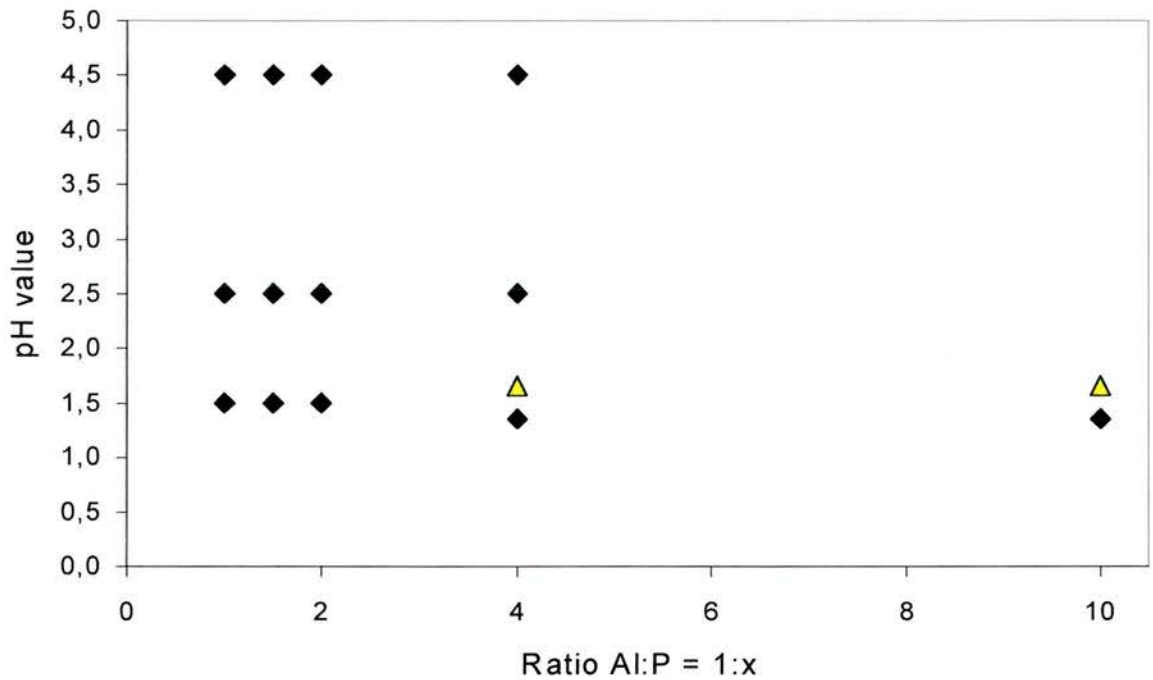

Figure 4.3: Graphic illustration of the phases that were prepared from benzylphosphonic acid and aluminium chloride depending on the pH and the Al:P ratio of the starting material, when all other conditions were kept constant as described in the text.

Key: AlBzPO-1 (◆) and AlBzPO-3 (▲).

4.1.1. Structure of $Al(OH)(O_3PCH_2C_6H_5).H_2O$ (AlBzPO-1)

Structural characterisation of AlBzPO-1 from powder X-ray diffraction data

Samples of AlBzPO-1 were synthesised as described in Chapter 3.2, and small single crystals that could be recovered were investigated using single-crystal X-ray diffraction. However, closer inspection of the thin plates indicated that they were not single, and consisted of very thin lamellar sections, which had grown into one another. A laboratory powder X-ray diffraction data set was subsequently collected on a Stoe diffractometer and the resulting powder pattern indexed using the program TREOR90[1] with a monoclinic unit cell. The final refined lattice parameters are a = 14.985(9) Å, b = 7.066(5) Å, c = 9.613(9) Å, β = 113.9(3)°. The systematic absences were consistent with space group $P2_1/c$ (#14). Initial attempts to solve the structure *ab initio* using direct methods were unsuccessful.

However, the indexed unit cell is very similar in two directions to that for the aluminium methylphosphonate, $Al(OH)(O_3PCH_3).H_2O$ solved by Wright and co-workers.[2] This suggests that AlBzPO-1 is layered, with the same layer structure as the aluminium methylphosphonate but with a larger interlayer spacing to accommodate the large benzyl groups. The atomic positions for aluminium methylphosphonate,[2] suitably modified to take into account for the difference in interlayer spacing between aluminium methyl- and benzylphosphonates, were used by Dr. D.S. Wragg and Prof. R.E. Morris as a starting point for Rietveld refinement against the powder X-ray diffraction data using GSAS.[3] The Rietveld plot for AlBzPO-1 is shown in Figure 4.3 a. The remaining six carbons of the phenyl group were then located from difference Fourier maps. This process was not straightforward, and despite finding possible

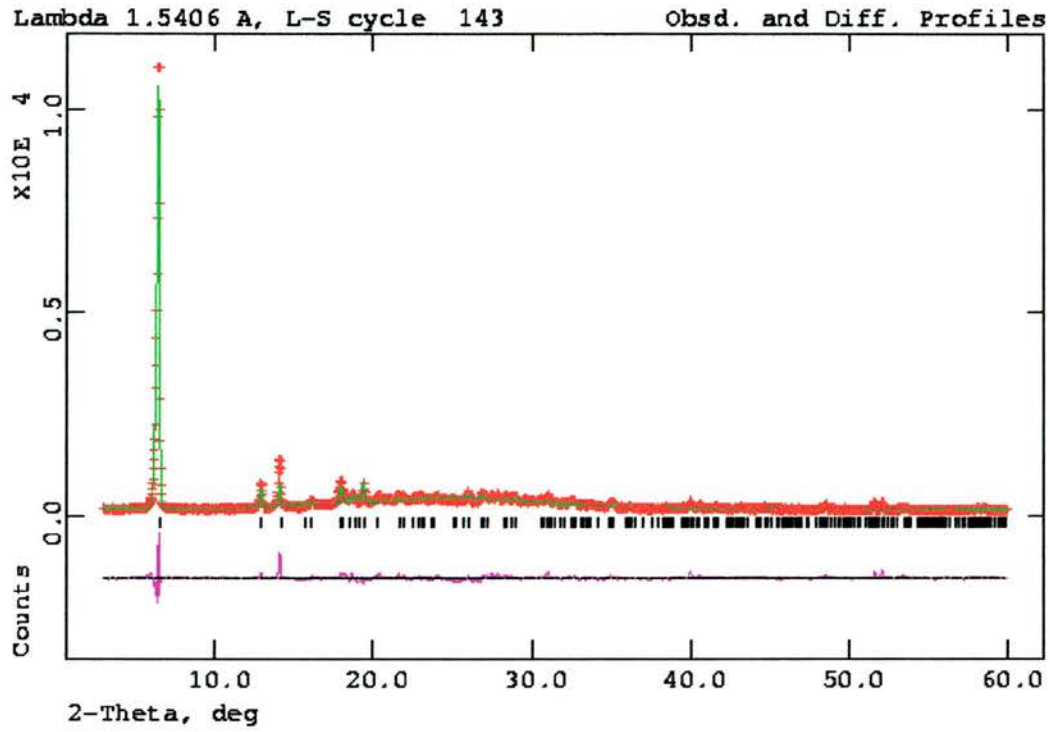

Figure 4.3a: Rietveld plot for the refinement of AlBzPO-1.

positions for the benzyl group the refinement was not quite as good as expected. This may be due to some unresolvable disorder in the benzyl group, similar to that seen in AlBzPO-2 (see Section 4.1.2), or simply to the inherent lack of information presented by powder X-ray diffraction. The refinement was also complicated by the presence of a small amount of a non-phosphorus containing impurity that was identified as pseudo-boehmite. Considering these difficulties, it is not surprising that the final refinement required reasonably strong chemical restraints to remain stable. The final Rietveld refinement least-squares cycles led to agreement factors of R_p = 0.100 and R_{wp} = 0.133.

Because of the need for restraints and the slight uncertainty in the carbon positions, the model proposed here should be regarded as a rough estimate of the benzyl carbon positions rather than a detailed structural determination. However, considering the consistency of the results with the other experimental techniques (see below) and the

similarity between the unit cells of the AlBzPO-1, aluminium methylphosphonate[2] and aluminium bromobenzylphosphonate,[4] together with reasonable refinement of the layer itself, lead to the belief that the layered model is indeed a good representation of this structure. Details of the data collection and structure solution are given in Table 4.1. Atomic coordinates of AlBzPO-1 with their equivalent isotropic displacement parameters can be found in Table 4.2a and bond lengths in Table 4.3. Recently, the proposed structure for AlBzPO-1 was supported through modelling experiments by P.A. Cox *et al.* at the University of Portsmouth. They used a quantum mechanical approach to investigate the structure and properties of AlBzPO-1 and their results were in good agreement with the experimental values obtained in our studies (see Table 4.2b).

Table 4.1: Details of data collection and structure solution for AlBzPO-1

Identification code	AlBzPO-1
Empirical formula	$Al(OH)(O_3PCH_2C_6H_5).H_2O$
Formula weight	232.10 g/mol
Temperature	ambient
Wavelength	1.54056 Å
Crystal system, space group	monoclinic, $P2_1/c$
Unit cell dimensions	a = 14.985 (9) Å α = 90°
	b = 7.066 (5) Å β = 113.9 (3)°
	c = 9.613 (9) Å γ = 90°
Unit cell volume	930.79 $Å^3$
Z, calculated density	4, 1.65 g/cm^3
$F_{(000)}$	304
2 theta range for data collection	5.00° to 60.00°
Refinement method	Rietveld
R_{wp}	0.133
R_p	0.100
χ^2	4.99
Restraints	- bond distances and applied ESD's; P-O 1.510(1), Al-O 1.900(1), P-C 1.800(1), C-C 1.390(1) (ESD's on individual atom positions are highly biased towards these weights)
	- angles were restrained to values seen in other Al phosphonates
	- isotropic temperature factors were set to be equal for each element type

The asymmetric unit contains one crystallographically independent benzylphosphonate group and one aluminium atom. The structure of AlBzPO-1 is made up of layers that contain chains of *trans* vertex-sharing AlO_6 octahedra, which are linked together by bridging phosphonate units (Figure 4.4a). The shared vertices of the aluminium-centred octahedra are hydroxide oxygens.[2] The Al-O-Al chains run parallel to the crystallographic *b*-axis of the structure and the layers are parallel to the *bc* plane of the unit cell. The benzyl groups point into the interlayer region of the structure (Figure 4.4b).

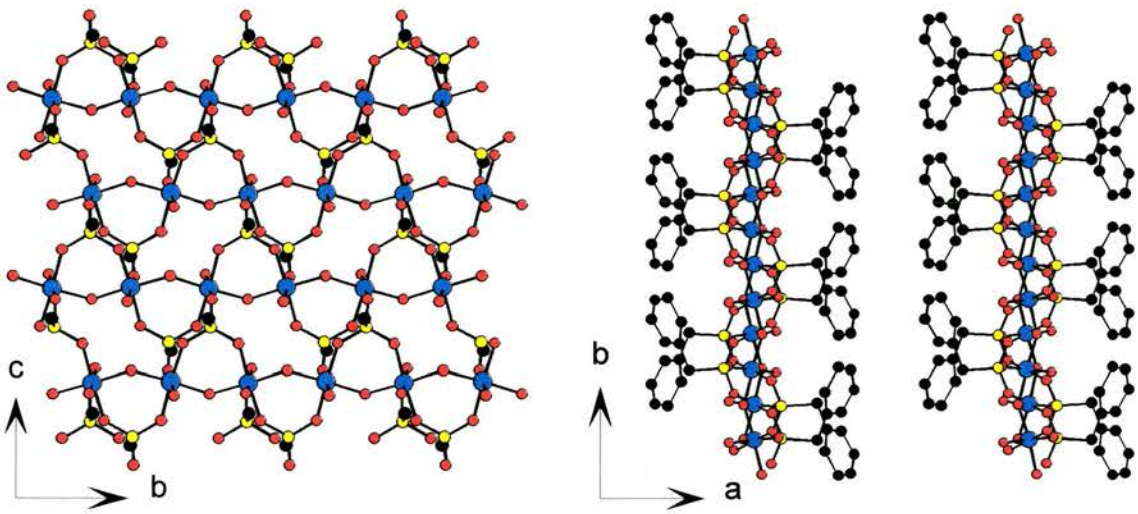

(a) (b)

Figure 4.4: Structure of AlBzPO-1; (a) a layer of Al-O-Al chains linked by phosphonate groups and (b) view along the layers with the benzyl groups pointing towards the interlayer space.

Key see pg. 4. Hydrogen was omitted for clarity.

Results of the quantum mechanical study of AlBzPO-1 by P.A. Cox et al. *at the University of Portsmouth*

The structure of AlBzPO-1 was investigated using a semi-empirical quantum mechanical method (implemented in the program GULP[5]). The results of the computational studies strongly support the structure proposed in the previous paragraphs. The theoretical atomic coordinates closely match those obtained through

X-ray diffraction (Figure 4.5). It was also found from the electronic distribution in AlBzPO-1 that the aluminium acts as a Lewis acid in the co-ordination of water. 0.21 e (electron charges) are transferred from the water molecule to the framework atoms (Figure 4.6). Furthermore, the barrier height for the rotation of a benzyl group (Figure 4.7 a and b) was calculated to be 200.7 kJ mol^{-1}. The value for the rotational barrier of a

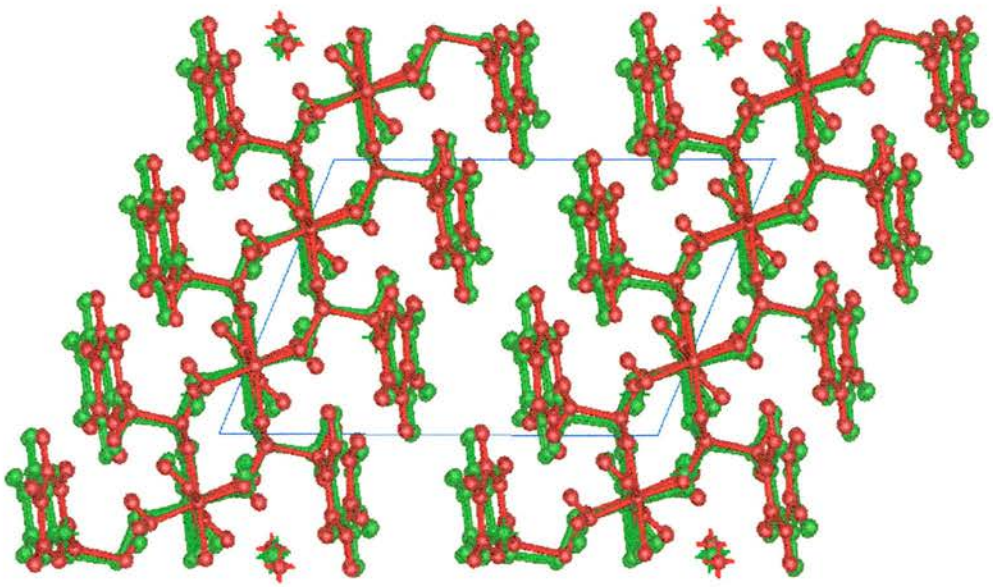

Figure 4.5: Comparison of the structures for AlBzPO-1 obtained experimentally (red) and from computational results (green). (Picture used with permission of P.A. Cox.)

Table 4.2a: Atomic coordinates and equivalent isotropic displacement parameters (in $Å^2$) for AlBzPO-1.

Atom	x	y	z	U_{iso}
P(1)	0.106	0.366	0.541	0.00442
Al(1)	0.004	0.122	0.246	0.00437
O(1)	0.092	0.359	0.689	0.00429
O(2)	-0.087	0.103	0.321	0.00479
O(3)	0.069	0.547	0.453	0.00766
O(4)	0.072	0.185	0.452	0.00840
O(5)	-0.034	0.373	0.189	0.00775
C(1)	0.234	0.381	0.585	0.00775
C(2)	0.357	-0.120	0.762	0.00775
C(3)	0.269	0.194	0.647	0.00775
C(4)	0.322	0.181	0.803	0.00775
C(5)	0.311	-0.135	0.601	0.00775
C(6)	0.370	0.019	0.872	0.00775
C(7)	0.261	0.038	0.544	0.00775

methyl group in the aluminium methylphosphonate $Al(OH)(O_3PCH_3).H_2O$[2] and AlMePO-β[6,7] is 8.9 kJ mol^{-1} and 8.1 kJ mol^{-1} respectively. It can therefore be expected that rotation in AlBzPO-1 is severely hindered even at elevated temperatures, due to steric constraints.

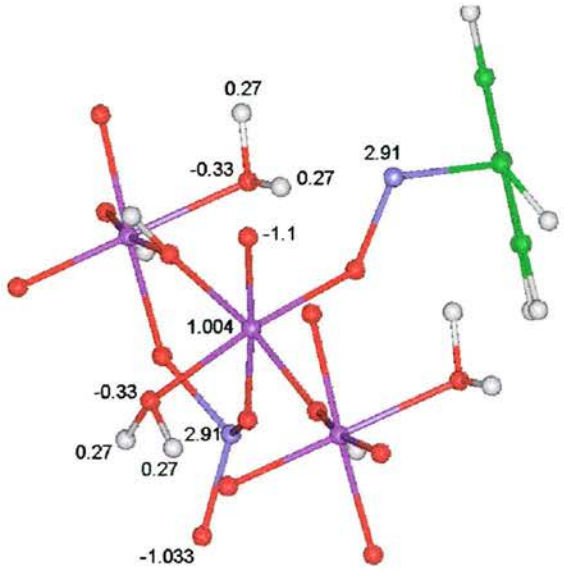

Figure 4.6: Electron distribution in AlBzPO-1. (Picture used with permission of P.A. Cox.)

Key: purple spheres with octahedral coordination denote aluminium, purple spheres with a charge of 2.91 e denote phosphorus, red spheres denote oxygen, green carbon and white hydrogen.

Table 4.2b: Comparison of experimental and computational values for the atomic coordinates of AlBzPO-1 (used with permission of P.A. Cox).

Experimental values			GULP[5] values		
x	y	z	x	y	z
0.1060	0.3660	0.5410	0.1107	0.3786	0.5418
0.0040	0.1200	0.2460	0.0087	0.1265	0.2476
0.0920	0.3590	0.6890	0.1119	0.3555	0.7059
0.9130	0.1030	0.3210	0.9060	0.0819	0.3091
0.0690	0.5470	0.4530	0.0561	0.5547	0.4497
0.0720	0.1850	0.4520	0.0663	0.2016	0.4436
0.9660	0.3730	0.1890	0.9638	0.3731	0.1887
0.2340	0.3810	0.5850	0.2275	0.3884	0.5645
0.3570	0.8800	0.7620	0.3690	0.8931	0.7848
0.2690	0.1940	0.6470	0.2840	0.2174	0.6390
0.3220	0.1810	0.8030	0.3416	0.2173	0.7959
0.3110	0.8650	0.6010	0.3357	0.8932	0.6278

(continued)

Experimental values			GULP[5] values		
x	y	z	x	y	z
0.3700	0.0190	0.8720	0.3918	0.0553	0.8684
0.2610	0.0380	0.5440	0.2829	0.0531	0.5556
0.2690	0.4930	0.6670	0.2648	0.5173	0.6309
0.2470	0.4110	0.4840	0.2305	0.4043	0.4496
0.3920	0.7470	0.8140	0.4306	0.7661	0.8421
0.3260	0.3604	0.8730	0.3456	0.3452	0.8636
0.3140	0.7430	0.5330	0.3340	0.7660	0.5605
0.4120	0.0010	0.9940	0.4325	0.0563	0.9930
0.2170	0.0540	0.4230	0.2365	0.0492	0.4321
0.8910	0.2360	0.3370	0.9174	0.1556	0.4009
0.8540	0.0290	0.2460	0.9088	0.9500	0.3438
0.8940	0.3760	0.1140	0.9030	0.3707	0.1015

Table 4.3: Bond lengths for AlBzPO-1 (in Å; constrained to an esd of 0.010 for all atoms except carbon, which was constrained to 0.005).

P(1) - O(1)	1.510	Al(1) - O(5)	1.873
P(1) - O(3)	1.498	C(1) - C(3)	1.453
P(1) - O(4)	1.507	C(2) - C(5)	1.402
P(1) - C(1)	1.793	C(2) - C(6)	1.394
Al(1) - O(1)	1.624	C(3) - C(4)	1.367
Al(1) - O(2)	1.798	C(3) - C(7)	1.446
Al(1) - O(3)	1.835	C(4) - C(6)	1.368
Al(1) - O(4)	1.852	C(5) - C(7)	1.421

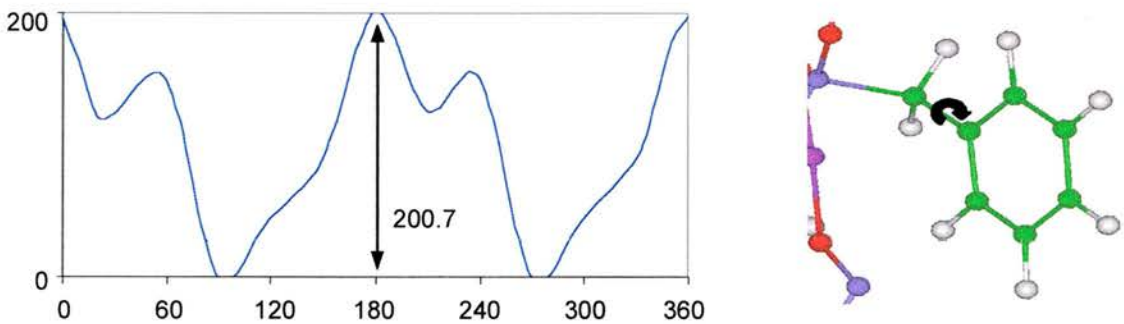

Figure 4.7: (a) Barrier height and (b) point of rotation for the rotation of the benzyl group in AlBzPO-1. (Pictures used with permission of P.A. Cox.)
Key: Green spheres denote carbon and white hydrogen.

Solid State MAS NMR spectroscopy of AlBzPO-1

The symmetry of the X-ray diffraction model structure is consistent with NMR experiments. The ^{27}Al MAS NMR spectrum in Figure 4.8 clearly shows a resonance from one octahedral aluminium atom (together with a small amount of a second

octahedral site from a pseudo-boehmite impurity, which is also just detectable in the XRD experiments). From the simulation of the bandshape the site was determined to have a quadrupole coupling of 6.4 MHz, an asymmetry of 0.76 and an isotropic chemical shift of δ_{Al} 0.0 ppm. These values are very similar to those for $Al(OH)(O_3PCH_3).H_2O$ (quadrupole coupling 5.86 MHz, asymmetry 1.0, and δ_{Al} -0.16 ppm)[2] confirming the similar coordination environment of the aluminium in both materials. There is only one resonance present in the ^{31}P MAS NMR (δ 10.27 ppm), indicating only one crystallographically independent phosphorus atom, which is also consistent with the X-ray structure (Figure 4.9a). As expected, the ^{13}C MAS NMR shows the peaks for the phenyl carbons between 120 and 140 ppm and a broad resonance for the methylene group that should be an overlapping doublet centred at δ 35.96 ppm (Figure 4.10).

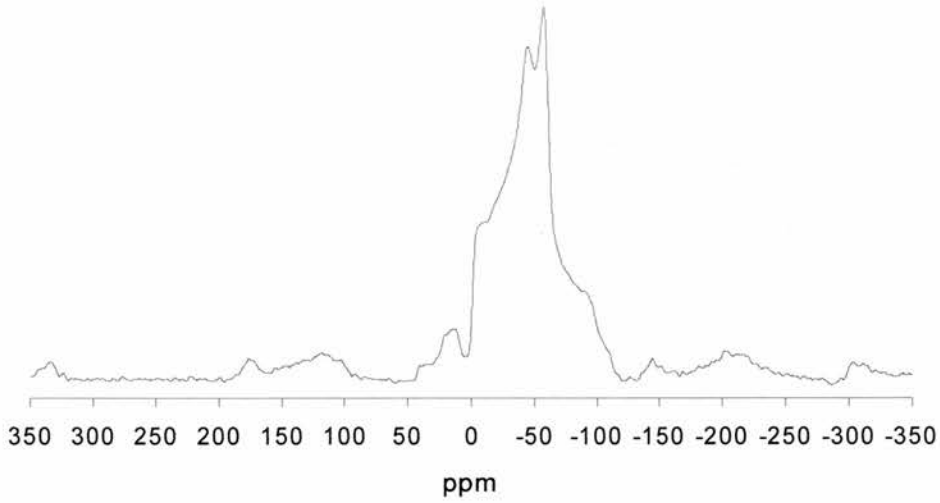

Figure 4.8: ^{27}Al MAS NMR spectrum of AlBzPO-1 at 78.16 MHz

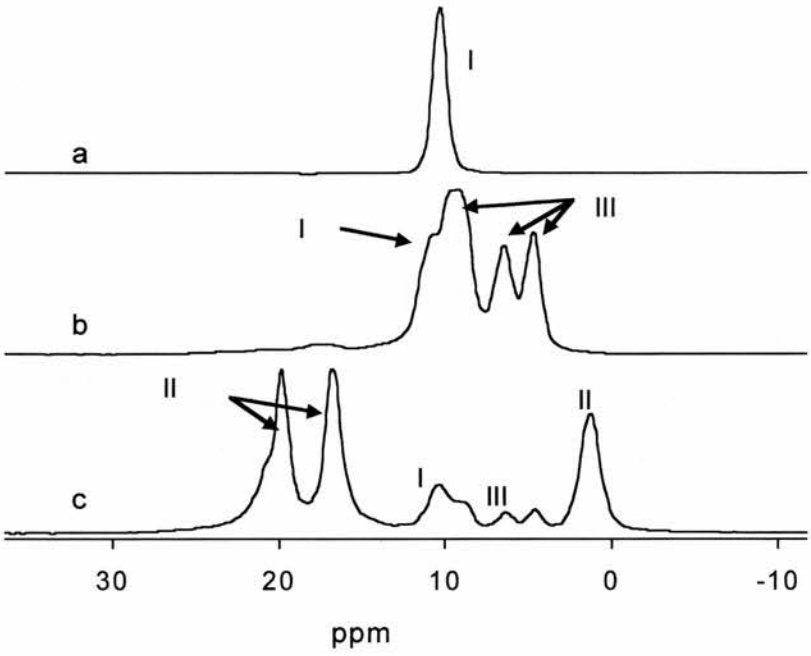

Figure 4.9: ^{31}P MAS NMR spectra of (a) a pure sample of AlBzPO-1, (b) a mixture of AlBzPO-1 and -3, and (c) a mixture of AlBzPO-1, -2 and -3, all at 121.42 MHz. Resonances from each of the phases are labelled.

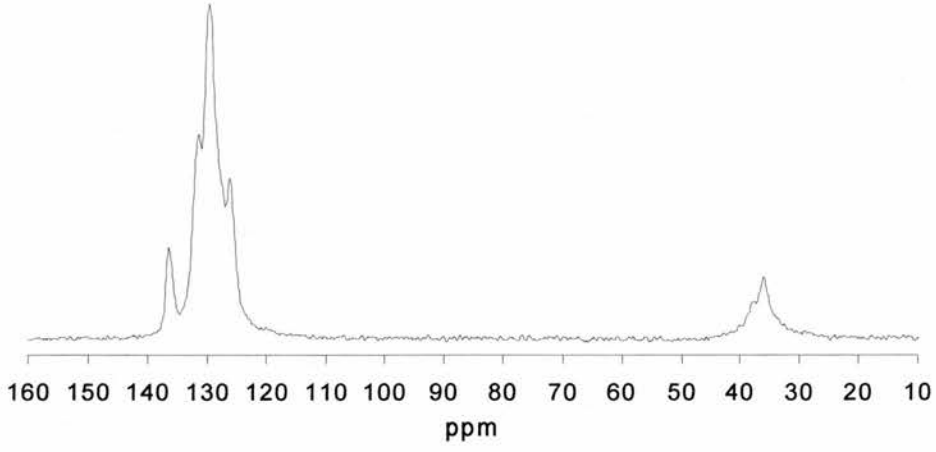

Figure 4.10: ^{13}C MAS NMR of AlBzPO-1 at 75.43 MHz

Thermogravimetric and CHN analysis of AlBzPO-1

The thermogravimetric analysis of AlBzPO-1 is also consistent with the X-ray diffraction structure. The values observed in the TGA of AlBzPO-1 (see Figure 4.11) are within 1 % of the values calculated for $Al(OH)(O_3PCH_2C_6H_5).H_2O$. The three mass losses in the TGA correspond to a loss of one molecule of water per formula unit at

130 °C (observed loss 7.8 %, calculated 7.72 %), the loss of half a molecule of water per formula unit (arising from the condensation of two hydroxyl groups, observed 3.7 %, calculated 3.88 %) at 300 °C and finally the combustion of the phosphonate groups at 500 °C (observed 35.92 %, calculated 35.82 %). The mass of the residue (52.63 %) corresponds to the value calculated for one molecule of $AlPO_4$ per formula unit (52.54 %). This was confirmed by an X-ray powder pattern of the residue. Comparison with the patterns of known compounds established it as $AlPO_4$. The results of the CHN analysis of AlBzPO-1 were also consistent with the formula mentioned above. The observed values are 36.33 % C and 4.20 % H. The composition calculated for $Al(OH)(O_3PCH_2C_6H_5).H_2O$ is; 36.22 % C and 4.34 % H.

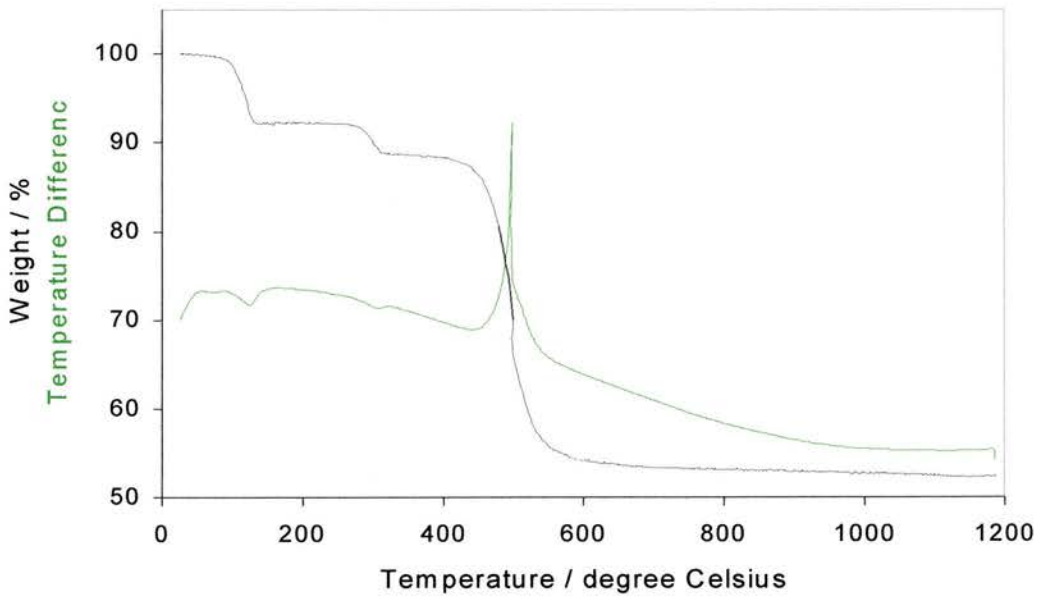

Figure 4.11: TGA trace of AlBzPO-1. The individual mass losses are described in the text.

IR spectroscopy of AlBzPO-1

In the spectrum of AlBzPO-1 (Figure 4.12), the very sharp band at 3652 cm^{-1} is due to the free O-H stretching vibration of water molecules in the material. There are also additional broad bands for O-H··· stretching vibrations (with H-bonds) at 3508 cm^{-1} and

at 3391 cm^{-1}. In the spectrum of benzyl PA, there is only one broad band in this area at 3446 cm^{-1}. At approx. 3035 cm^{-1} there are the sharp aromatic C-H stretching bands in the spectra of both the acid and the phosphonate. The C-H vibration of the CH_2 group is another sharp band found at 2915 cm^{-1} for both compounds.

The H_2O deformation vibration becomes visible as a broad band at 1635 cm^{-1} and 1645 cm^{-1} for the acid and AlBzPO-1, respectively. The C-H deformation band of the P-CH_2 group can be found in both spectra at approx. 1455 cm^{-1}. A sharp band occurs at 1262 cm^{-1} in the acid and at 1247 cm^{-1} in the phosphonate and the C-H deformation vibration of the monosubstituted aromatic ring is situated at 1105 cm^{-1} and at 1128 cm^{-1}, respectively. The O-P-O stretching vibration shows at 1075 cm^{-1} (acid) and at 1093 cm^{-1} (phosphonate). A strong band at 1065 cm^{-1} is only present in the phosphonate, while another strong band at 943 cm^{-1} is also present in the acid (923 cm^{-1}). Another vibration for the C-H deformation of the monosubstituted aromatic ring can only be detected for the phosphonate, at 800 cm^{-1}. Table 4.4 gives a comparison of the bands

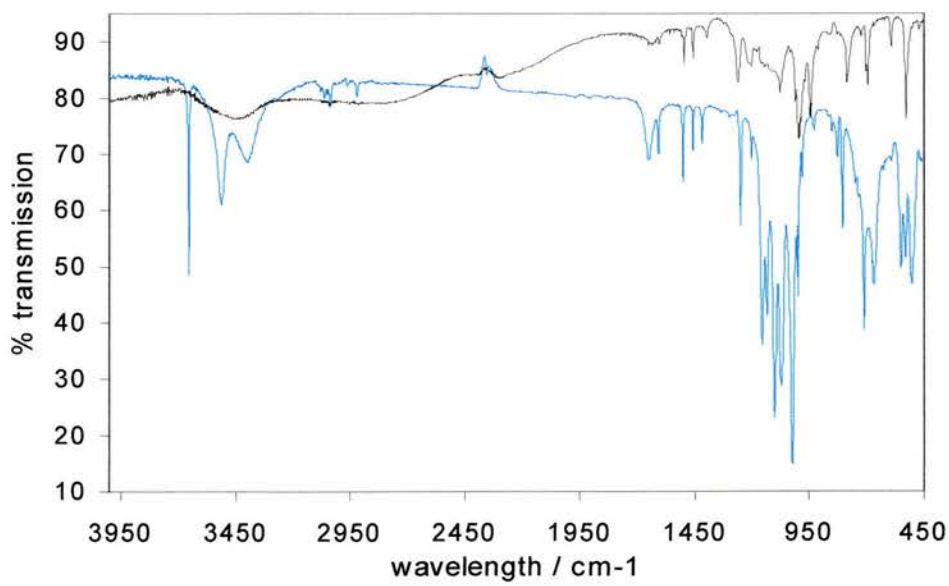

Figure 4.12: IR spectra of AlBzPO-1 (blue) and benzylphosphonic acid (black).

in the IR spectra of benzyl PA and AlBzPO-1. The respective spectra of both compounds are shown in Figure 4.12.

Table 4.4: Comparison of the IR spectra of benzyl PA and AlBzPO-1.

Assigned vibration	**Benzyl PA**	**AlBzPO-1**
Free O-H stretching		3652 cm^{-1}
O-H stretching/ H bonding		3508 cm^{-1}
O-H stretching/ H bonding	3446 cm^{-1}	3391 cm^{-1}
C-H stretching/ aromatic	3035 cm^{-1}	3031 cm^{-1}
C-H stretching/ CH_2	2914 cm^{-1}	2915 cm^{-1}
H_2O deformation	1635 cm^{-1}	1645 cm^{-1}
C-H deformation/ P-CH_2	1458 cm^{-1}	1455 cm^{-1}
	1262 cm^{-1}	1247 cm^{-1}
C-H deformation monosubstituted aromatic ring	1105 cm^{-1}	1128 cm^{-1}
O-P-O stretching	1075 cm^{-1}	1093 cm^{-1}
		1065 cm^{-1}
	943 cm^{-1}	923 cm^{-1}
C-H deformation monosubstituted aromatic ring		800 cm^{-1}

4.1.2. Structure of $Al_3H(PO_3CH_2C_6H_5)_5.H_2O$ (AlBzPO-2)

Structural characterisation of AlBzPO-2 from microcrystal diffraction

AlBzPO-2 was synthesised at relatively low starting Al:P ratios (< 1:5) and at relatively acidic pH. Unfortunately, despite numerous attempts it was not possible to prepare this material as a single pure phase - it is always contaminated to some extent by AlBzPO-1, and another phase, AlBzPO-3. However, it was possible to pick out some very small (< 20 μm maximum dimension) crystals from some of these mixtures, which were suitable for single crystal X-ray diffraction experiments using station 9.8 at the Daresbury synchrotron radiation laboratory. Data were collected on a plate-like crystal of approximate dimensions 15 × 15 × 5 μm, and the structure solved and refined using direct methods (SHELXS[8]) and least-squares techniques (SHELXL[8]) by I. Bull and Prof R.E. Morris. The small size of the crystal, even for synchrotron techniques, led to fairly weak data with no appreciable scattering beyond 40° 2 θ. The paucity of

data, together with the disorder that is present in some of the benzyl groups, is probably the cause of the need for restraints on the aromatic rings and thermal displacement parameters, and the fact that the precision on the atomic positions (and consequently the bond distances and angles) is slightly worse than would be expected for a more strongly diffracting crystal. However, the bond distances and angles are of a magnitude expected for a structure of this type.

The final single crystal X-ray diffraction data for compound AlBzPO-2, $Al_3H(PO_3CH_2C_6H_5)_5.H_2O$, are M_r = 950.48, monoclinic $P2_1/c$, a = 17.2497(13) Å, b = 25.7851(18) Å, c = 9.4339(7) Å and β = 103.567(1)°. The final cycles of least-squares refinement against F^2 included anisotropic thermal displacement parameters for Al, P, O and C atoms. Where possible, hydrogen atoms were placed using geometric methods and their positions recalculated at the end of each cycle of least-squares refinement. The final cycle of refinement also included restraints to ensure planarity of the aromatic rings in the structure, and some light restraints to prevent non-positive definite thermal parameters. Details of the data collection and structure solution are listed in Table 4.5.

Table 4.5: Details of the data collection and structure solution for AlBzPO-2.

Identification code	AlBzPO-2	
Empirical formula	$Al_3H(PO_3CH_2C_6H_5)_5.H_2O$	
Formula weight	950.48 g/mol	
Temperature	150(2) °C	
Wavelength	0.6944 Å	
Crystal system, space group	monoclinic, $P2_1/c$	
Unit cell dimensions	a = 17.2497(13) Å	α = 90°
	b = 25.7851(18) Å	β = 103.5670°
	c = 9.4339(7) Å	γ = 90°
Unit cell volume	4079.0(5) Å^3	
Z, calculated density	4, 1.55 g/cm^3	
Absorption coefficient	0.378 mm^{-1}	

(continued)

$F_{(000)}$	1988
Crystal size	15 × 15 × 5 μm
2 theta range for data collection	4.0° to 40.0°
Limiting indices	$-16 \leq h \leq 16$, $-24 \leq k \leq 24$, $-9 \leq l \leq 9$
Reflections collected / unique	12898 / 3800
Refinement method	Full-matrix least squares on F^2
Data / restraints / parameters	3800 / 447 / 683
Goodness-of-fit on F^2	1.197
Final R indices [$I>2\sigma(I)$]	$R_1 = 0.0835$, $wR^2 = 0.1819$
R indices (all data)	$R_1 = 0.1349$, $wR^2 = 0.202$
Largest difference peak and hole	0.736 and -1.104 eÅ^{-3}

The asymmetric unit of AlBzPO-2 (Figure 4.13) consists of two aluminium atoms in tetrahedral coordination, and one in octahedral coordination, together with five phosphorus atoms, all of which are present as benzylphosphonate units. Three of these phosphonate units have all three of their oxygen atoms bound to aluminium atoms, while the remaining phosphonates have only two of their oxygen atoms bound to aluminium atoms. The hydrogen atom needed for charge balancing the structure is most likely situated between these two hanging oxygens, which are 2.72 Å apart, a good distance for a hydrogen bond. Two of the five benzyl groups are disordered into two distinct positions that could be resolved in the experiment. A third benzyl group showed significantly larger thermal displacement parameters than the others, probably indicating some unresolvable disorder. The other two benzyl rings show no evidence of disorder.

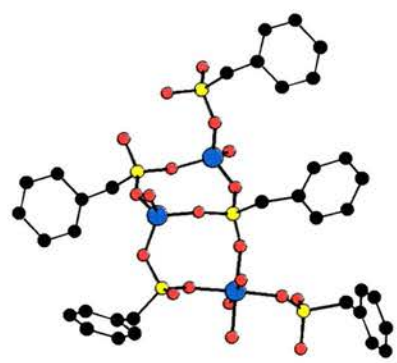

Figure 4.13: The asymmetric unit of AlBzPO-2. For clarity, hydrogens are left out and only one orientation is shown for the benzyl groups. Key see pg. 4.

The overall structure of AlBzPO-2 (Figure 4.14) consists of unusual undulating layers that run parallel to the bc plane of the crystallographic unit cell, with the undulations running parallel to the b-axis. The pitch of the undulations is equal in length to the b-axis (25.785 Å). As in AlBzPO-1, the benzyl groups are oriented towards the interlamellar region. A similar undulating structure was reported previously for $Co[(CH_3)_3CPO_3].H_2O$[9] (Figure 3.6). The layers themselves consist of

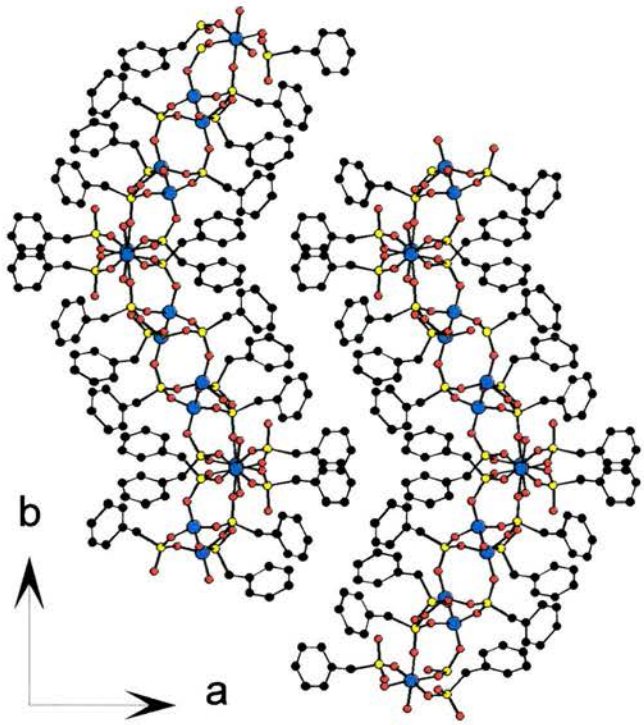

Figure 4.14: The undulating structure of AlBzPO-2 viewed along the c-axis.

Key see pg. 4. Hydrogen was omitted for clarity.

small subunits comprising five edge sharing four-ring units in a short ladder-like arrangement (Figure 4.15, also circled in Figure 4.16). These units are linked into a two- dimensional array to form the layers (Figure 4.16). Unlike in AlBzPO-1, the arrangement of aluminium and phosphorous is strictly alternating (i.e. there are no Al-O-Al linkages). The water molecule, which is coordinated to the octahedral aluminium, is enclosed within the layer. It is forming hydrogen bonds to the hanging

oxygens of two phosphonate groups (Figure 4.16). The atomic coordinates are listed in Table 4.6 ((a) isotropic and (b) anisotropic displacement parameters). The bond distances and angles are shown in Table 4.7a and b respectively.

Table 4.6a: Atomic coordinates and displacement parameters (in Å) for AlBzPO 2. Isotropic displacement parameters are given for hydrogen atoms. Equivalent displacement parameters are given for all other atoms. The occupancy is shown if it differs from 1. Hydrogen U_{iso}'s were calculated as 1.2 times the U_{iso} of the attached carbon atom. Carbon atoms were restrained for the benzyl rings to be flat and all carbon atoms were restrained to be positive definite, although some are very close to being npd.

Atom	x	y	z	U_{eq}	U_{iso}	occupancy
Al(1)	-0.1922(3)	0.2554(2)	0.3042(6)	0.0104(16)		
Al(2)	-0.0433(4)	0.3884(2)	0.1903(7)	0.0152(17)		
Al(3)	-0.0737(4)	0.4464(2)	0.6075(7)	0.0135(16)		
P(1)	0.0745(3)	0.4347(2)	0.4675(6)	0.0122(14)		
P(2)	-0.0683(3)	0.2770(2)	0.1054(6)	0.0119(14)		
P(3)	-0.1201(3)	0.4379(2)	0.8988(6)	0.0154(15)		
P(4)	-0.1780(3)	0.3764(2)	0.3726(6)	0.0135(15)		
P(5)	-0.3045(3)	0.2932(2)	-0.0108(6)	0.0163(15)		
O(1)	0.0171(7)	0.4318(5)	0.5686(14)	0.015(3)		
O(2)	0.0980(8)	0.4903(5)	0.4492(15)	0.017(4)		
O(3)	0.0395(8)	0.4109(5)	0.3186(15)	0.019(4)		
O(4)	-0.0983(7)	0.2659(5)	0.2414(15)	0.014(3)		
O(5)	-0.1327(7)	0.2799(5)	-0.0340(14)	0.013(3)		
O(6)	-0.0210(7)	0.3283(5)	0.1298(14)	0.012(3)		
O(7)	-0.1788(8)	0.3956(5)	0.8649(16)	0.022(4)		
O(8)	-0.0647(8)	0.4402(5)	0.7920(15)	0.019(3)		
O(9)	-0.0633(8)	0.4338(5)	1.0528(15)	0.017(3)		
O(10)	-0.1817(7)	0.3198(5)	0.4099(14)	0.013(3)		
O(11)	-0.1228(8)	0.3874(5)	0.2706(15)	0.019(4)		
O(12)	-0.1475(8)	0.4063(5)	0.5163(15)	0.018(4)		
O(13)	-0.3060(8)	0.3512(5)	-0.0577(15)	0.020(4)		
O(14)	-0.2508(8)	0.2880(5)	0.1410(15)	0.017(3)		
O(15)	-0.2846(7)	0.2415(5)	0.3751(14)	0.013(3)		
O(16)	-0.2061(8)	0.1889(5)	0.1993(15)	0.017(3)		
C(1)	0.1604(12)	0.3992(8)	0.556(3)	0.022(6)		
H(1A)	0.1917	0.4197	0.6381		0.033	
H(1B)	0.1439	0.3665	0.5953		0.033	
C(2)	-0.0016(11)	0.2275(7)	0.080(2)	0.014(5)		
H(2A)	-0.0333	0.1953	0.0556		0.021	
H(2B)	0.0183	0.2369	-0.0064		0.021	
C(3)	-0.1674(12)	0.5001(8)	0.887(2)	0.020(6)		
H(3A)	-0.1271	0.5254	0.9384		0.03	
H(3B)	-0.1818	0.5103	0.7833		0.03	
C(4)	-0.2721(13)	0.4037(9)	0.283(3)	0.028(6)		
H(4A)	-0.2623	0.4394	0.253		0.042	
H(4B)	-0.293	0.3835	0.1932		0.042	

(continued)

Atom	x	y	z	U_{eq}	U_{iso}	occupancy
C(5)	-0.4040(12)	0.2808(9)	0.007(2)	0.023(6)		
H(5A)	-0.4048	0.2453	0.0472		0.034	
H(5B)	-0.4149	0.305	0.0816		0.034	
C(11)	0.208(8)	0.388(6)	0.456(9)	0.01(3)		0.4(3)
C(12)	0.211(7)	0.345(5)	0.372(5)	0.03(4)		0.5(4)
H(12)	0.1726	0.3189	0.378		0.047	
C(13)	0.258(6)	0.334(4)	0.283(7)	0.00(4)		0.28(16)
H(13)	0.2561	0.3039	0.225		0	
C(14)	0.318(3)	0.380(2)	0.292(4)	0.03(2)		0.68(17)
H(14)	0.3603	0.3751	0.243		0.038	
C(15)	0.316(5)	0.424(2)	0.360(6)	0.01(3)		0.43(14)
H(15)	0.3483	0.452	0.3422		0.017	
C(16)	0.266(4)	0.430(3)	0.460(6)	0.03(2)		0.61(19)
H(16)	0.2701	0.4589	0.5241		0.042	
C(21)	0.0696(11)	0.2141(7)	0.200(2)	0.013(5)		
C(22)	0.1444(13)	0.2287(8)	0.196(3)	0.032(6)		
H(22)	0.1519	0.2509	0.1205		0.048	
C(23)	0.2106(15)	0.2123(9)	0.301(3)	0.037(7)		
H(23)	0.2625	0.2233	0.2963		0.056	
C(24)	0.2001(16)	0.1797(10)	0.410(3)	0.046(7)		
H(24)	0.2455	0.1678	0.4806		0.069	
C(25)	0.1274(14)	0.1647(9)	0.420(3)	0.037(7)		
H(25)	0.1211	0.1425	0.4968		0.056	
C(26)	0.0602(13)	0.1818(8)	0.315(2)	0.026(6)		
H(26)	0.0083	0.1715	0.3216		0.038	
C(31)	-0.2389(12)	0.5062(8)	0.945(2)	0.017(5)		
C(32)	-0.2397(13)	0.5421(8)	1.054(2)	0.028(6)		
H(32)	-0.1925	0.5607	1.0969		0.041	
C(33)	-0.3104(14)	0.5515(9)	1.103(3)	0.037(7)		
H(33)	-0.3106	0.576	1.1776		0.056	
C(34)	-0.3787(14)	0.5245(9)	1.039(3)	0.036(7)		
H(34)	-0.4266	0.5311	1.0697		0.053	
C(35)	-0.3783(15)	0.4880(9)	0.932(3)	0.038(7)		
H(35)	-0.425	0.4686	0.8908		0.058	
C(36)	-0.3085(14)	0.4802(9)	0.887(3)	0.035(7)		
H(37)	-0.3088	0.4558	0.8113		0.052	
C(41)	-0.339(8)	0.406(4)	0.370(15)	0.00(5)		0.3(7)
C(42)	-0.375(2)	0.4514(18)	0.387(5)	0.02(2)		0.48(8)
H(42)	-0.3633	0.4803	0.3332		0.032	
C(43)	-0.428(3)	0.459(2)	0.480(5)	0.06(3)		0.62(11)
H(43)	-0.45	0.4926	0.4882		0.092	
C(44)	-0.445(3)	0.419(2)	0.556(6)	0.04(3)		0.58(14)
H(44)	-0.4813	0.4234	0.6173		0.065	
C(45)	-0.408(3)	0.369(4)	0.545(7)	0.03(3)		0.44(16)
H(46)	-0.4206	0.3405	0.5995		0.041	
C(46)	-0.356(3)	0.363(2)	0.456(5)	0.03(2)		0.56(11)
H(46)	-0.3304	0.3304	0.4513		0.039	
C(51)	-0.4719(13)	0.2848(9)	-0.124(3)	0.030(6)		
C(52)	-0.5080(16)	0.3313(11)	-0.164(3)	0.056(8)		
H(52)	-0.491	0.3621	-0.1107		0.085	
C(53)	-0.5766(17)	0.3314(13)	-0.297(3)	0.066(9)		
H(53)	-0.6041	0.3626	-0.3311		0.098	
C(54)	-0.5969(19)	0.2878(16)	-0.365(3)	0.073(9)		
H(54)	-0.6403	0.289	-0.4483		0.11	
C(55)	-0.5628(18)	0.2410(14)	-0.329(3)	0.068(9)		
H(55)	-0.5803	0.2104	-0.3832		0.102	
C(56)	-0.4984(16)	0.2411(11)	-0.203(3)	0.050(8)		
H(56)	-0.4725	0.2092	-0.1716		0.076	

(continued)

Atom	x	y	z	U_{eq}	U_{iso}	occupancy
C(61)	-0.334(6)	0.404(3)	0.358(12)	0.05(5)		0.7(7)
C(62)	-0.334(3)	0.3934(19)	0.499(6)	0.03(3)		0.53(12)
H(62)	-0.2842	0.3863	0.5654		0.047	
C(63)	-0.402(3)	0.392(3)	0.547(5)	0.02(3)		0.55(19)
H(63)	-0.3992	0.3849	0.6469		0.032	
C(64)	-0.473(3)	0.4014(18)	0.460(7)	0.03(3)		0.51(11)
H(64)	-0.5199	0.399	0.496		0.052	
C(65)	-0.479(5)	0.415(2)	0.309(8)	0.06(3)		0.45(11)
H(65)	-0.5297	0.4234	0.2475		0.09	
C(66)	-0.411(3)	0.4156(18)	0.257(6)	0.05(2)		0.57(10)
H(66)	-0.4138	0.423	0.157		0.071	
C(71)	0.293(6)	0.448(4)	0.494(8)	0.03(4)		0.4(2)
C(72)	0.348(3)	0.446(2)	0.421(6)	0.05(3)		0.60(14)
H(72)	0.3848	0.4741	0.4308		0.069	
C(73)	0.353(5)	0.409(2)	0.338(6)	0.02(3)		0.44(13)
H(73)	0.395	0.4111	0.2883		0.032	
C(74)	0.291(8)	0.354(6)	0.303(7)	0.08(3)		0.69(19)
H(74)	0.294	0.3251	0.2422		0.118	
C(75)	0.238(6)	0.363(3)	0.384(6)	0.03(3)		0.6(2)
H(75)	0.1986	0.3363	0.377		0.052	
C(76)	0.229(6)	0.402(4)	0.474(7)	0.02(2)		0.6(3)

Table 4.6b: Anisotropic displacement parameters for AlBzPO-2.

Atom	U_{11}	U_{22}	U_{33}	U_{23}	U_{13}	U_{12}
Al(1)	0.014(2)	0.012(2)	0.007(2)	-0.0001(16)	0.0043(16)	-0.0004(16)
Al(2)	0.018(2)	0.016(2)	0.012(2)	0.0003(17)	0.0061(17)	-0.0007(16)
Al(3)	0.018(2)	0.014(2)	0.010(2)	-0.0007(17)	0.0053(16)	-0.0013(16)
P(1)	0.016(2)	0.013(2)	0.007(2)	-0.0006(16)	0.0044(16)	-0.0001(15)
P(2)	0.015(2)	0.013(2)	0.009(2)	0.0001(16)	0.0047(16)	0.0006(15)
P(3)	0.020(2)	0.016(2)	0.011(2)	0.0005(16)	0.0062(16)	0.0007(16)
P(4)	0.017(2)	0.015(2)	0.010(2)	0.0001(16)	0.0058(16)	-0.0001(15)
P(5)	0.019(2)	0.018(2)	0.013(2)	0.0004(16)	0.0051(16)	0.0015(15)
O(1)	0.016(4)	0.016(4)	0.014(4)	0.0003(19)	0.004(2)	0.0001(19)
O(2)	0.018(4)	0.018(4)	0.017(4)	0.0000(19)	0.004(2)	-0.0003(19)
O(3)	0.020(4)	0.019(4)	0.018(4)	-0.0008(19)	0.005(2)	-0.0001(19)
O(4)	0.015(4)	0.015(4)	0.014(4)	0.0009(19)	0.004(2)	-0.0006(19)
O(5)	0.013(4)	0.013(4)	0.012(4)	-0.0001(19)	0.003(2)	-0.0002(19)
O(6)	0.013(4)	0.013(4)	0.011(4)	0.0000(19)	0.004(2)	-0.0001(19)
O(7)	0.022(4)	0.022(4)	0.021(4)	0.0001(19)	0.006(2)	-0.0001(19)
O(8)	0.020(4)	0.020(4)	0.018(4)	0.0001(19)	0.005(2)	0.0002(19)
O(9)	0.018(4)	0.017(4)	0.016(4)	0.0001(19)	0.004(2)	0.0001(19)
O(10)	0.013(4)	0.013(4)	0.012(4)	-0.0004(19)	0.003(2)	-0.0003(19)
O(11)	0.020(4)	0.020(4)	0.019(4)	0.0003(19)	0.006(2)	0.0000(19)
O(12)	0.019(4)	0.019(4)	0.018(4)	-0.0006(19)	0.005(2)	-0.0009(19)
O(13)	0.021(4)	0.020(4)	0.019(4)	-0.0005(19)	0.005(2)	0.0008(19)
O(14)	0.018(4)	0.018(4)	0.016(4)	-0.0002(19)	0.004(2)	0.0004(19)
O(15)	0.014(4)	0.013(4)	0.012(4)	0.0007(19)	0.004(2)	-0.0010(19)
O(16)	0.018(4)	0.017(4)	0.016(4)	-0.0001(19)	0.004(2)	0.0000(19)
C(1)	0.022(6)	0.022(6)	0.022(6)	0.0002(19)	0.005(2)	0.0003(19)
C(2)	0.015(5)	0.014(5)	0.014(5)	-0.0001(19)	0.004(2)	-0.0003(19)
C(3)	0.021(6)	0.020(6)	0.020(6)	0.0000(19)	0.005(2)	-0.0001(19)
C(4)	0.028(6)	0.028(6)	0.027(6)	0.000(2)	0.007(2)	0.0004(19)
C(5)	0.023(6)	0.023(6)	0.022(6)	-0.0002(19)	0.006(2)	0.0000(19)
C(11)	0.01(3)	0.01(3)	0.01(3)	0.000(2)	0.002(8)	0.000(2)
C(12)	0.03(4)	0.03(4)	0.03(4)	0.000(2)	0.007(9)	0.000(2)
C(13)	0.00(4)	0.00(4)	0.00(4)	0.000(2)	-0.001(9)	0.000(2)

(continued)

Atom	U_{11}	U_{22}	U_{33}	U_{23}	U_{13}	U_{12}
C(14)	0.03(2)	0.03(2)	0.03(2)	0.000(2)	0.006(5)	0.000(2)
C(15)	0.01(3)	0.01(3)	0.01(3)	0.000(2)	0.003(7)	0.000(2)
C(16)	0.03(2)	0.03(2)	0.03(2)	0.000(2)	0.007(6)	0.000(2)
C(21)	0.013(5)	0.013(5)	0.013(5)	-0.0006(19)	0.003(2)	0.0002(19)
C(22)	0.032(7)	0.032(7)	0.032(7)	0.000(2)	0.007(2)	0.000(2)
C(23)	0.037(7)	0.037(7)	0.037(7)	0.000(2)	0.009(2)	0.000(2)
C(24)	0.046(8)	0.045(8)	0.045(8)	-0.001(2)	0.010(3)	0.001(2)
C(25)	0.038(7)	0.038(7)	0.037(7)	0.000(2)	0.009(2)	0.000(2)
C(26)	0.026(6)	0.026(6)	0.026(6)	0.000(2)	0.006(2)	0.0003(19)
C(31)	0.017(6)	0.017(6)	0.017(6)	0.0001(19)	0.004(2)	0.0003(19)
C(32)	0.028(6)	0.028(6)	0.027(6)	0.000(2)	0.006(2)	0.0001(19)
C(33)	0.037(7)	0.037(7)	0.037(7)	0.000(2)	0.009(2)	0.000(2)
C(34)	0.036(7)	0.036(7)	0.035(7)	0.000(2)	0.009(2)	0.000(2)
C(35)	0.038(7)	0.038(7)	0.038(7)	0.000(2)	0.009(2)	0.000(2)
C(36)	0.035(7)	0.035(7)	0.034(7)	0.000(2)	0.008(2)	0.000(2)
C(41)	0.00(5)	0.00(5)	0.00(5)	0.000(2)	-0.004(12)	0.000(2)
C(42)	0.02(2)	0.02(2)	0.02(2)	0.000(2)	0.005(5)	0.000(2)
C(43)	0.06(3)	0.06(3)	0.06(3)	0.000(2)	0.014(6)	0.000(2)
C(44)	0.04(3)	0.04(3)	0.04(3)	0.000(2)	0.010(7)	0.000(2)
C(45)	0.03(3)	0.03(3)	0.03(3)	0.000(2)	0.006(7)	0.000(2)
C(46)	0.03(2)	0.03(2)	0.03(2)	0.000(2)	0.006(5)	0.000(2)
C(51)	0.030(6)	0.031(6)	0.030(6)	0.000(2)	0.007(2)	0.000(2)
C(52)	0.056(8)	0.057(8)	0.056(8)	0.000(2)	0.014(3)	0.000(2)
C(53)	0.065(9)	0.067(9)	0.065(9)	0.001(2)	0.016(3)	0.000(2)
C(54)	0.065(9)	0.132(9)	0.027(9)	0.000(2)	0.019(3)	0.000(2)
C(55)	0.066(9)	0.087(9)	0.052(9)	0.000(2)	0.017(3)	0.000(2)
C(56)	0.050(8)	0.051(8)	0.050(8)	0.000(2)	0.012(3)	0.000(2)
C(61)	0.05(5)	0.05(5)	0.05(5)	0.000(2)	0.011(12)	0.000(2)
C(62)	0.03(3)	0.03(3)	0.03(3)	0.000(2)	0.007(6)	0.000(2)
C(63)	0.02(3)	0.02(3)	0.02(3)	0.000(2)	0.005(6)	0.000(2)
C(64)	0.03(3)	0.03(3)	0.03(3)	0.000(2)	0.008(6)	0.000(2)
C(65)	0.06(3)	0.06(3)	0.06(3)	0.000(2)	0.014(8)	0.000(2)
C(66)	0.05(2)	0.05(2)	0.05(2)	0.000(2)	0.011(6)	0.000(2)
C(71)	0.03(4)	0.03(4)	0.03(4)	0.000(2)	0.007(9)	0.000(2)
C(72)	0.05(3)	0.05(3)	0.05(3)	0.000(2)	0.011(7)	0.000(2)
C(73)	0.02(3)	0.02(3)	0.02(3)	0.000(2)	0.005(7)	0.000(2)
C(74)	0.08(3)	0.08(3)	0.08(3)	0.000(2)	0.018(7)	0.000(2)
C(75)	0.03(3)	0.03(3)	0.03(3)	0.000(2)	0.008(7)	0.000(2)
C(76)	0.02(2)	0.02(2)	0.02(2)	0.000(2)	0.004(5)	0.000(2)

Table 4.7a: Bond lengths for AlBzPO-2 (in Å).

Al(1)-O(14)	1.836(15)	P(4)-O(12)	1.542(15)	C(33)-C(34)	1.38(3)
Al(1)-O(5)	1.865(14)	P(4)-C(4)	1.79(2)	C(34)-C(35)	1.38(3)
Al(1)-O(4)	1.869(13)	P(5)-O(15)	1.499(14)	C(35)-C(36)	1.38(3)
Al(1)-O(15)	1.902(13)	P(5)-O(14)	1.518(15)	C(41)-C(42)	1.34(16)
Al(1)-O(10)	1.924(14)	P(5)-O(13)	1.559(14)	C(41)-C(46)	1.45(14)
Al(1)-O(16)	1.964(14)	P(5)-C(5)	1.79(2)	C(42)-C(43)	1.42(6)
Al(2)-O(11)	1.715(14)	C(1)-C(11)	1.42(8)	C(43)-C(44)	1.33(7)
Al(2)-O(9)	1.722(15)	C(1)-C(76)	1.55(8)	C(44)-C(45)	1.45(12)
Al(2)-O(6)	1.726(14)	C(2)-C(21)	1.50(3)	C(45)-C(46)	1.39(7)
Al(2)-O(3)	1.741(15)	C(3)-C(31)	1.47(3)	C(51)-C(52)	1.36(3)
Al(3)-O(12)	1.708(15)	C(4)-C(61)	1.41(14)	C(51)-C(56)	1.37(3)
Al(3)-O(8)	1.719(15)	C(4)-C(41)	1.6(2)	C(52)-C(53)	1.51(4)
Al(3)-O(1)	1.730(14)	C(5)-C(51)	1.50(3)	C(53)-C(54)	1.30(4)
Al(3)-O(2)	1.737(15)	C(11)-C(12)	1.36(16)	C(54)-C(55)	1.35(4)
P(1)-O(2)	1.511(14)	C(11)-C(16)	1.5(2)	C(55)-C(56)	1.42(4)
P(1)-O(3)	1.522(15)	C(12)-C(13)	1.34(10)	C(61)-C(62)	1.35(13)

P(1)-O(1)	1.530(14)	C(13)-C(14)	1.55(12)	C(61)-C(66)	1.48(9)
P(1)-C(1)	1.77(2)	C(14)-C(15)	1.31(9)	C(62)-C(63)	1.37(7)
P(2)-O(5)	1.511(14)	C(15)-C(16)	1.43(8)	C(63)-C(64)	1.33(8)
P(2)-O(4)	1.519(14)	C(21)-C(22)	1.35(3)	C(64)-C(65)	1.44(9)
P(2)-O(6)	1.543(13)	C(21)-C(26)	1.41(3)	C(65)-C(66)	1.38(8)
P(2)-C(2)	1.771(19)	C(22)-C(23)	1.39(3)	C(71)-C(72)	1.30(10)
P(3)-O(7)	1.471(15)	C(23)-C(24)	1.38(3)	C(71)-C(76)	1.6(2)
P(3)-O(8)	1.544(14)	C(24)-C(25)	1.34(3)	C(72)-C(73)	1.26(10)
P(3)-O(9)	1.554(15)	C(25)-C(26)	1.41(3)	C(73)-C(74)	1.77(19)
P(3)-C(3)	1.79(2)	C(31)-C(36)	1.37(3)	C(74)-C(75)	1.35(11)
P(4)-O(10)	1.506(14)	C(31)-C(32)	1.39(3)	C(75)-C(76)	1.35(11)
P(4)-O(11)	1.530(14)	C(32)-C(33)	1.42(3)		

Table 4.7b: Bond angles for AlBzPO-2 (in °).

O(2)-P(1)-O(3)	109.7(8)	O(11)-Al(2)-O(9)	107.7(7)	C(21)-C(22)-C(23)	122(2)
O(2)-P(1)-O(1)	110.3(7)	O(11)-Al(2)-O(6)	113.3(7)	C(24)-C(23)-C(22)	119(2)
O(3)-P(1)-O(1)	112.4(8)	O(9)-Al(2)-O(6)	112.5(7)	C(25)-C(24)-C(23)	121(3)
O(2)-P(1)-C(1)	109.0(9)	O(11)-Al(2)-O(3)	108.0(7)	C(24)-C(25)-C(26)	120(2)
O(3)-P(1)-C(1)	109.4(9)	O(9)-Al(2)-O(3)	106.5(7)	C(21)-C(26)-C(25)	120(2)
O(1)-P(1)-C(1)	105.9(9)	O(6)-Al(2)-O(3)	108.6(7)	C(36)-C(31)-C(32)	118(2)
O(5)-P(2)-O(4)	114.7(7)	O(12)-Al(3)-O(8)	109.4(7)	C(36)-C(31)-C(3)	122(2)
O(5)-P(2)-O(6)	110.0(7)	O(12)-Al(3)-O(1)	111.5(7)	C(32)-C(31)-C(3)	120.2(19)
O(4)-P(2)-O(6)	108.0(7)	O(8)-Al(3)-O(1)	108.9(7)	C(31)-C(32)-C(33)	121(2)
O(5)-P(2)-C(2)	106.8(9)	O(12)-Al(3)-O(2)	108.4(7)	C(34)-C(33)-C(32)	119(2)
O(4)-P(2)-C(2)	109.7(9)	O(8)-Al(3)-O(2)	111.0(7)	C(33)-C(34)-C(35)	121(2)
O(6)-P(2)-C(2)	107.5(8)	O(1)-Al(3)-O(2)	107.7(7)	C(34)-C(35)-C(36)	119(2)
O(7)-P(3)-O(8)	112.8(8)	P(1)-O(1)-Al(3)	150.6(9)	C(31)-C(36)-C(35)	123(2)
O(7)-P(3)-O(9)	113.9(8)	P(1)-O(2)-Al(3)	150.9(9)	C(42)-C(41)-C(46)	117(10)
O(8)-P(3)-O(9)	105.1(8)	P(1)-O(3)-Al(2)	149.2(9)	C(42)-C(41)-C(4)	121(9)
O(7)-P(3)-C(3)	111.7(9)	P(2)-O(4)-Al(1)	141.9(9)	C(46)-C(41)-C(4)	122(10)
O(8)-P(3)-C(3)	105.6(9)	P(2)-O(5)-Al(1)	147.0(8)	C(41)-C(42)-C(43)	125(8)
O(9)-P(3)-C(3)	107.1(9)	P(2)-O(6)-Al(2)	131.9(8)	C(44)-C(43)-C(42)	119(5)
O(10)-P(4)-O(11)	113.2(8)	P(3)-O(8)-Al(3)	137.9(9)	C(43)-C(44)-C(45)	120(6)
O(10)-P(4)-O(12)	107.7(8)	P(3)-O(9)-Al(2)	136.1(9)	C(46)-C(45)-C(44)	120(8)
O(11)-P(4)-O(12)	109.0(8)	P(4)-O(10)-Al(1)	136.0(9)	C(45)-C(46)-C(41)	120(9)
O(10)-P(4)-C(4)	114.0(9)	P(4)-O(11)-Al(2)	163.7(10)	C(52)-C(51)-C(56)	120(3)
O(11)-P(4)-C(4)	105.1(10)	P(4)-O(12)-Al(3)	143.7(9)	C(52)-C(51)-C(5)	121(2)
O(12)-P(4)-C(4)	107.5(9)	P(5)-O(14)-Al(1)	157.8(9)	C(56)-C(51)-C(5)	119(2)
O(15)-P(5)-O(14)	115.6(8)	P(5)-O(15)-Al(1)	135.8(8)	C(51)-C(52)-C(53)	117(3)
O(15)-P(5)-O(13)	111.0(8)	C(11)-C(1)-C(76)	19(4)	C(54)-C(53)-C(52)	118(3)
O(14)-P(5)-O(13)	108.6(8)	C(11)-C(1)-P(1)	111(3)	C(53)-C(54)-C(55)	127(3)
O(15)-P(5)-C(5)	110.4(9)	C(76)-C(1)-P(1)	113(2)	C(54)-C(55)-C(56)	115(3)
O(14)-P(5)-C(5)	106.3(9)	C(21)-C(2)-P(2)	120.6(14)	C(51)-C(56)-C(55)	123(3)
O(13)-P(5)-C(5)	104.3(9)	C(31)-C(3)-P(3)	118.8(15)	C(4)-C(61)-C(62)	131(7)
O(14)-Al(1)-O(5)	178.0(7)	C(61)-C(4)-C(41)	2(5)	C(4)-C(61)-C(66)	110(8)
O(14)-Al(1)-O(4)	90.9(6)	C(61)-C(4)-P(4)	119(4)	C(62)-C(61)-C(66)	118(10)
O(5)-Al(1)-O(4)	88.8(6)	C(41)-C(4)-P(4)	118(4)	C(63)-C(62)-C(61)	122(6)
O(14)-Al(1)-O(15)	92.2(6)	C(51)-C(5)-P(5)	119.3(16)	C(64)-C(63)-C(62)	122(5)
O(5)-Al(1)-O(15)	88.0(6)	C(12)-C(11)-C(1)	131(10)	C(63)-C(64)-C(65)	120(6)
O(4)-Al(1)-O(15)	176.7(7)	C(12)-C(11)-C(16)	120(8)	C(66)-C(65)-C(64)	119(7)
O(14)-Al(1)-O(10)	90.3(6)	C(1)-C(11)-C(16)	109(10)	C(65)-C(66)-C(61)	119(8)
O(5)-Al(1)-O(10)	91.7(6)	C(13)-C(12)-C(11)	130(10)	C(72)-C(71)-C(76)	119(9)
O(4)-Al(1)-O(10)	93.2(6)	C(12)-C(13)-C(14)	108(9)	C(73)-C(72)-C(71)	122(8)
O(15)-Al(1)-O(10)	88.0(6)	C(15)-C(14)-C(13)	126(5)	C(72)-C(73)-C(74)	127(7)
O(14)-Al(1)-O(16)	89.9(6)	C(14)-C(15)-C(16)	121(6)	C(75)-C(74)-C(73)	103(9)
O(5)-Al(1)-O(16)	88.0(6)	C(15)-C(16)-C(11)	114(6)	C(74)-C(75)-C(76)	133(10)
O(4)-Al(1)-O(16)	88.8(6)	C(22)-C(21)-C(26)	118(2)	C(75)-C(76)-C(1)	119(10)
O(15)-Al(1)-O(16)	90.0(6)	C(22)-C(21)-C(2)	122.5(19)	C(75)-C(76)-C(71)	117(8)
O(10)-Al(1)-O(16)	177.9(6)	C(26)C(21)-C(2)	119.5(18)	C(1)-C(76)-C(71)	124(6)

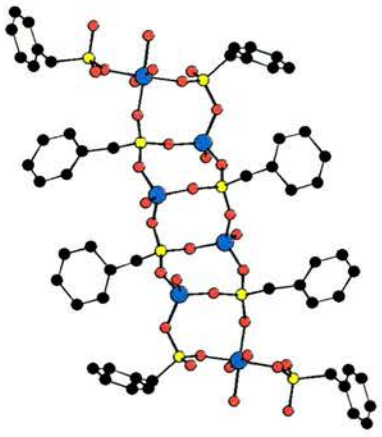

Figure 4.15: One of the four-ring units in AlBzPO-2. For clarity, only one orientation is shown for the disordered benzyl groups and hydrogen was omitted.
Key see pg. 4.

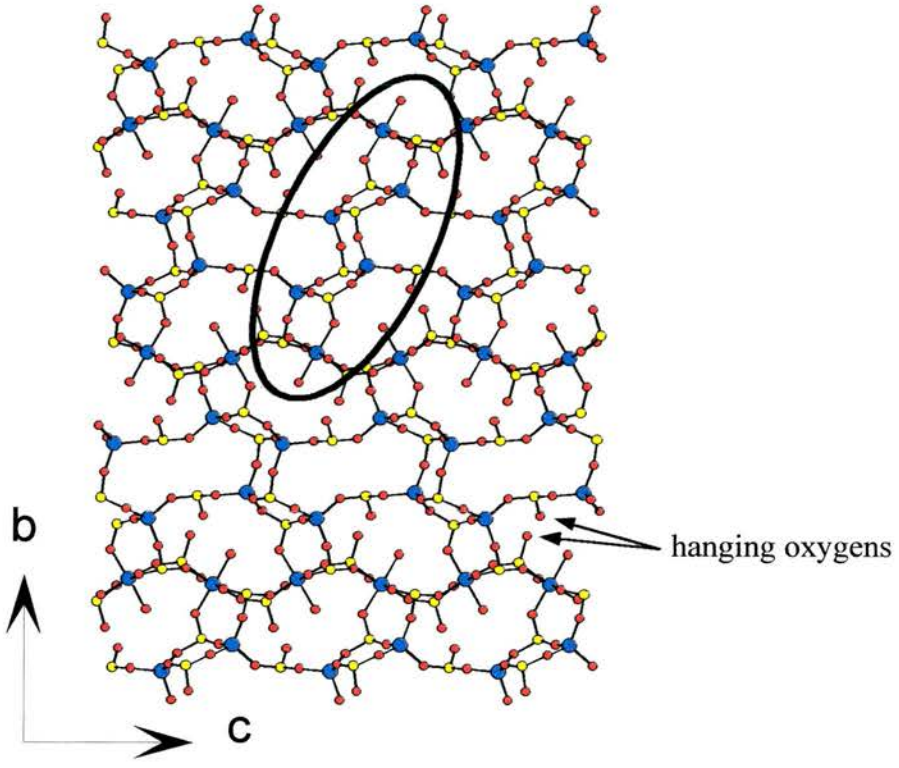

Figure 4.16: The inorganic structure of the layers of AlBzPO-2. For clarity, carbon and hydrogen atoms have been omitted. The position of one of the four-ring units shown in Figure 4.15 is circled.
Key see pg. 4.

Solid state MAS NMR spectroscopy of AlBzPO-2

As described above, AlBzPO-2 has only been synthesised as an impure sample in combination with other phases (see pp. 82), and so the analysis of the NMR spectra is complicated. However, the ^{31}P resonances of AlBzPO-1 and AlBzPO-3 can be identified from the spectra of pure AlBzPO-1 and of a mixture of only AlBzPO-1 and AlBzPO-3 (Figure 4.9 a and 4.9 b). Discounting these resonances leaves three resolvable peaks at 1.27, 16.79 and 19.75 ppm (Figure 4.9 c), which is at least not inconsistent with the multiple (five) phosphorus sites expected from the single crystal X-ray diffraction study. The ^{13}C spectrum (Figure 4.17) shows a broadening of the signals due to a mixture of different phases when compared with the spectrum of pure AlBzPO-1, while the complicated ^{27}Al MAS NMR spectrum (Figure 4.18) is caused by the presence of multiple aluminium environments, with both octahedral (at -22.6 pm) and tetrahedral (around 20 ppm) resonances visible.

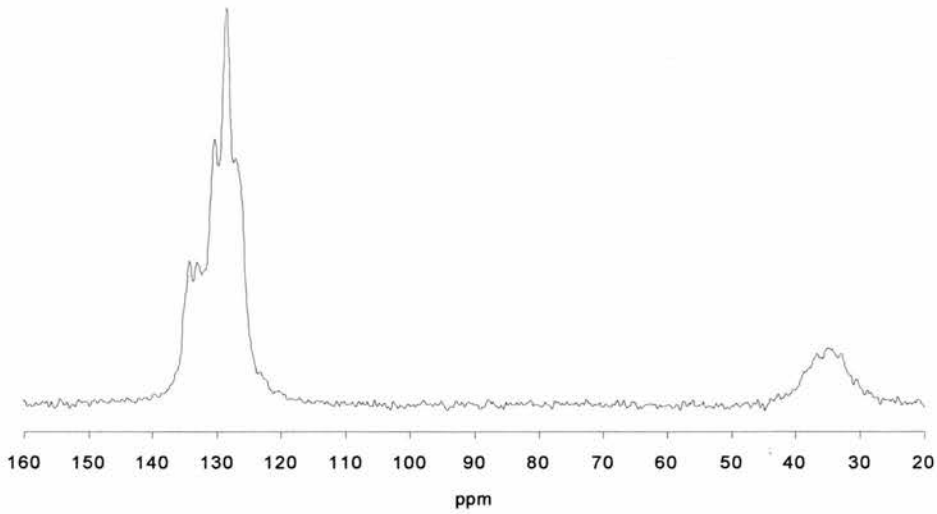

Figure 4.17: ^{13}C MAS NMR of a mixture of AlBzPO-1,-2 and -3 at 75.43 MHz.

4.1.3. AlBzPO-3 and AlBzPO-4

Since no pure phase or single crystal materials are available for AlBzPO-3, structural conclusions can be based only on NMR data. The ^{31}P NMR spectrum of a mixture of AlBzPO-3 and AlBzPO-1 (Figure 4.9b) shows three resonances at 4.64, 6.45 and 9.17 ppm (from AlBzPO-3), and a low field shoulder at about 10.3 ppm that can be identified as coming from AlBzPO-1. This indicates that there are at least three crystallographically independent P atoms present in the structure, and since the peak at 9.17 ppm seems significantly broader than the others it may be that there are more then three. The ^{27}Al spectrum shows clear evidence of the presence of both octahedral (around -40 ppm) and tetrahedral (around 15 ppm) aluminium (Figure 4.19). Since AlBzPO-1 contains only octahedral Al, it can be concluded that AlBzPO-3 contains tetrahedral aluminium and possibly some octahedral as well. The fact that it is synthesised from mixtures with high phosphorus concentrations, but not as high as those for AlBzPO-2, means that it is possible that the Al:P ratio in the solid could be somewhere between 1:1 and 3:5 (the Al:P ratios of AlBzPO-1 and –2 respectively).

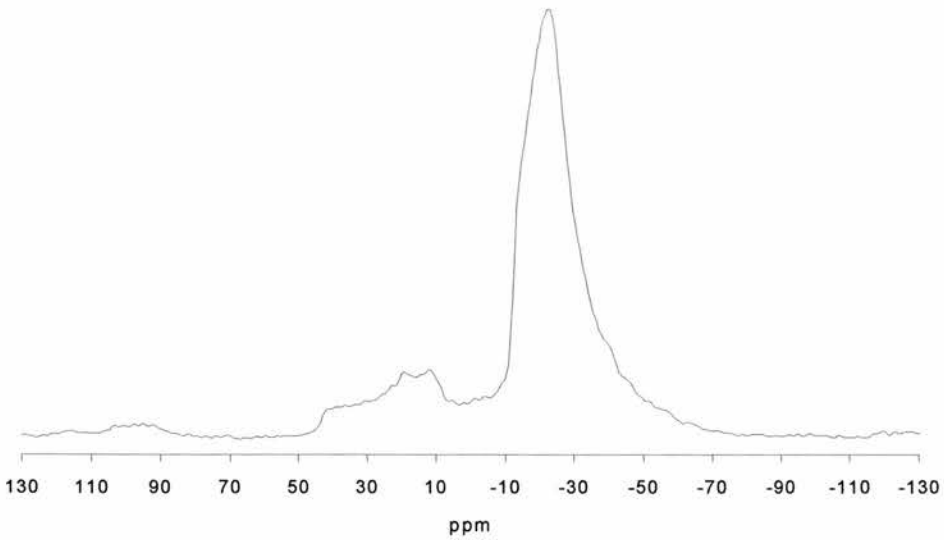

Figure 4.18: ^{27}Al MAS NMR of a mixture of AlBzPO-1, -2 and -3 at 78.13 MHz.

The ^{13}C MAS NMR spectrum of a mixture of AlBzPO-1 and -3 is shown in Figure 4.20. It also shows line broadening (see Chapter 4.1.2). The additional peak between 12 and 20 ppm is due to an unidentified organic impurity. In the case of AlBzPO-4, which is only ever found as a very minor phase, it is difficult to draw any conclusions on its composition and structure.

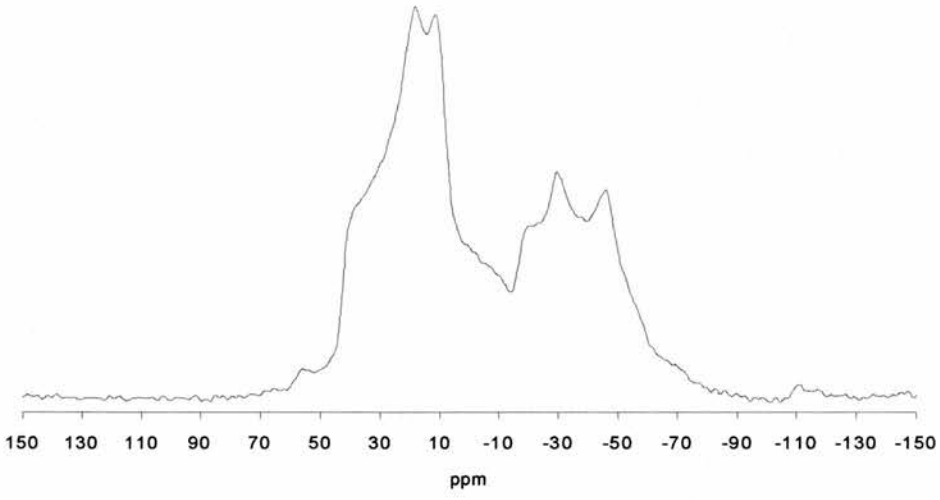

Figure 4.19: ^{27}Al MAS NMR spectrum of a mixture of AlBzPO-1 and -3 at 78.16 MHz.

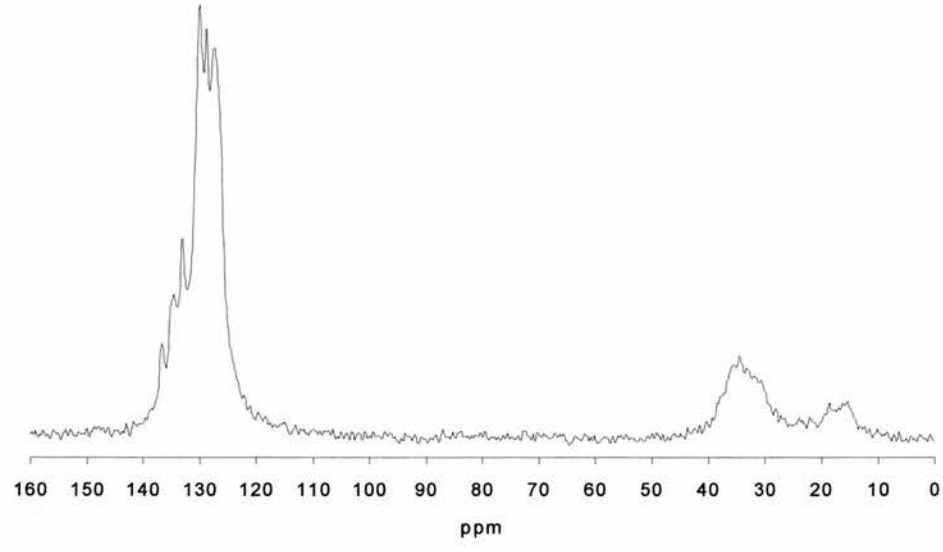

Figure 4.20: ^{13}C MAS NMR spectrum of a mixture of AlBzPO-1 and -3 at 75.43 MHz.

4.2. Synthesis of aluminium 3-aminopropylphosphonates

The preparation of aluminium 3-aminopropylphosphonates was attempted using four different aluminium sources (aluminium sulphate, chloride, nitrate and gibbsite), but only the use of aluminium sulphate produced any crystalline products. All other reactions yielded clear solutions.

When aluminium sulphate is used, the main product is aluminium aminopropyl-phosphonate-1 (AlaPrPO-1) for most reactions. Powder X-ray diffraction data give an indication that there are another three layered phases with different interlayer spacings (*d* approx. 15.5 Å, 9.5 Å and 14.6 Å for AlaPrPO-2, -3 and -4 respectively). However, these phases usually occur in mixtures with AlaPrPO-1 and could not be characterised further. Samples that consisted of mixtures of phases 2 and 3 only showed little crystallinity. AlaPrPO-4 generally occurred in presence of either AlaPrPO-2 or -3 or both, although on one occasion it was found in combination with AlaPrPO-1 only.

The formation of different phases/phase mixtures was influenced by the pH value at which the reaction was carried out. Reactions at pH 2.0 and 2.5 always yielded pure AlaPrPO-1. Reactions at pH 3.5 tended to yield mixtures of AlaPrPO-1 and -2 or -1 and -3 or of all three phases. Reactions between pH 4.5 and 5.5 led to a variety of mixtures between phases 1, 2, 3 and 4. Samples containing phase 4 generally had lower crystallinity than other samples. Reaction mixtures at pH values above 5.5 produced either amorphous materials or clear solutions. A survey of the products prepared at different pH values is given in Table 4.8. The X-ray powder patterns of pure AlaPrPO-1 and mixtures of AlaPrPO-1 and -2, -1 and -3 and -1 and -4 are shown in Figure 4.21a, b, c and d respectively.

The ratio of aluminium to phosphorus in the reaction vessel seemed to have little influence on the outcome of the reaction. An increase in the reaction time enhanced the crystallinity of the samples and in one case also led to an inversion of the respective relative amounts of two phases in a sample. The reaction temperature did not have any influence on the products. A few experiments carried out under reflux did not show any significant differences to similar samples prepared in an autoclave.

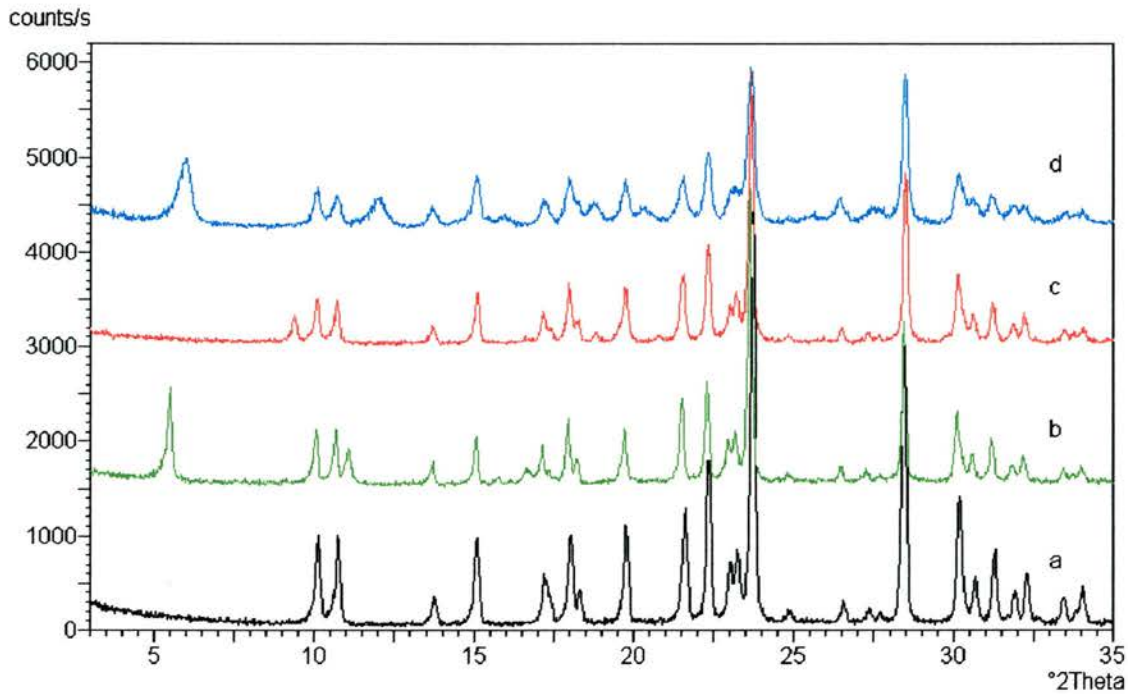

Figure 4.21: The X-ray powder patterns of pure AlaPrPO-1 (a) and mixtures of AlaPrPO-1 and -2 (b), -1 and -3 (c) and -1 and -4 (d). The values on the y-axis are arbitrary.

Table 4.8: Aluminium 3-aminopropylphosphonates prepared at different pH values.

pH value	***AlaPrPO phases***
2.0	1
2.5	1
3.5	1+2, 1+3, 1+2+3
4.5 - 5.5	1+2, 1+3, 1+4, 1+2+3, 1+3+4, 2+3, 2+3+4
>5.5	Amorphous materials or clear solutions

4.2.1. Structure of $Al(O_3P(CH_2)_3NH_3).SO_4.3H_2O$ (AlaPrPO-1)

Structural characterisation of AlaPrPO-1

Initially, only microcrystalline powders were available from the preparations described in (Section 3.3). The unit cell was therefore indexed using TREOR90[1] and the structure solved by direct methods *ab initio* from powder X-ray diffraction data using EXPO[10] by Dr. M.P. Attfield. Subsequently however, small single crystals (size 0.1 × 0.01 × 0.01 mm) of AlaPrPO-1 were recovered from one of the hydrothermal preparations, and data were collected using station 9.8 at the Daresbury Synchrotron Radiation Source. The data collected from a needle-shaped crystal were then used by Prof R.E. Morris to solve and refine the structure with direct methods and least-square techniques.[8]

The final crystal data for $Al(O_3P(CH_2)_3NH_3).SO_4.3H_2O$ (AlaPrPO-1) are; $M_r = 315.16$ g/mol, orthorhombic *Pnma*, a = 10.3082(10) Å, b = 6.2577(6) Å and $c = 16.486(2)$ Å. The final cycles of least-square refinement against F^2 included anisotropic thermal displacement parameters for Al, P, S, O, N and C atoms. Where possible, hydrogen atoms were placed using geometric methods and their positions recalculated at the end of each cycle of least-squares refinement. Their isotropic temperature factors were calculated based on the carbon atoms they are bonded to. Details of the structure determination can be found in Table 4.9. Fractional coordinates and equivalent isotropic temperature factors for AlaPrPO-1 are shown in Table 4.10 ((a) isotropic and (b) anisotropic displacement parameters). Bond lengths and angles are listed in Table 4.11.

Table 4.9: Details of the data collection and structure determination of AlaPrPO-1.

Identification code	AlaPrPO-1
Empirical formula	$Al(O_3P(CH_2)_3NH_3).SO_4.3H_2O$
Formula weight	315.16 g/mol
Temperature	293(2) °C
Wavelength	0.6887
Crystal system, space group	orthorhombic, *Pnma*
Unit cell dimensions	a = 10.3082(10) Å α = 90°
	b = 6.2577(6) Å β = 90°
	c = 16.486(2) Å γ = 90°
Unit cell volume	1063.4(2) $Å^3$
Z, calculated density	4, 1.97 g/cm^3
Absorption coefficient	0.65 mm^{-1}
$F_{(000)}$	595
Crystal size	0.1 × 0.01 × 0.01 mm
2Theta range for data collection	4.52° to 58.68°
Limiting indices	$-14 \le h \le 13$, $-8 \le k \le 8$, $-23 \le l \le 19$
Reflections collected / unique	7189 / 1632
Refinement method	Full-matrix least squares on F^2
Data / restraints / parameters	1632 / 0 / 97
Goodness-of-fit on F^2	1.073
Final R indices [$I>2\sigma(I)$]	$R_1 = 0.0717$, $wR^2 = 0.1929$
R indices (all data)	$R_1 = 0.0921$, $wR^2 = 0.2124$
Largest difference peak and hole	1.641 and -1.073 $eÅ^{-3}$

Table 4.10a: Atomic coordinates and temperature factors for AlaPrPO-1. Isotropic displacement parameters are given for hydrogen atoms, equivalent displacement parameters for all other atoms.

Atom	x	y	z	U_{eq}	U_{iso}
Al(1)	0.36908(14)	0.25	0.58443(9)	0.0142(4)	
S(1)	-0.11949(11)	0.25	0.61767(7)	0.0167(3)	
P(1)	0.56368(12)	0.25	0.42877(7)	0.0146(3)	
O(1)	0.2469(4)	0.25	0.6736(2)	0.0176(7)	
O(2)	0.2256(4)	0.25	0.5128(2)	0.0191(8)	
O(3)	0.4997(3)	0.25	0.6664(2)	0.0171(7)	
O(4)	0.5014(4)	0.25	0.5120(2)	0.0174(7)	
O(5)	0.3521(2)	-0.0521(4)	0.58399(14)	0.0156(5)	
O(8)	-0.0081(4)	0.25	0.6745(2)	0.0236(8)	
O(9)	-0.2393(4)	0.25	0.6661(2)	0.0336(11)	
O(10)	-0.1109(3)	0.0594(6)	0.5680(2)	0.0403(9)	
N(1)	0.0860(5)	-0.25	0.6200(3)	0.0238(10)	
C(1)	0.3734(5)	0.25	0.2072(3)	0.0201(10)	
H(1A)	0.3203(5)	0.1248	0.2174(3)		0.03
H(1B)	0.3203(5)	0.3752	0.2174(3)		0.03
C(2)	0.4872(5)	0.25	0.2663(3)	0.0164(9)	
H(2A)	0.5405(5)	0.3756	0.2572(3)		0.025
H(2B)	0.5405(5)	0.1244	0.2572(3)		0.025
C(3)	0.4371(5)	0.25	0.3532(3)	0.0158(9)	
H(3A)	0.3830(5)	0.1249	0.3612(3)		0.024
H(3B)	0.3830(5)	0.3751	0.3612(3)		0.024

Figure 4.10b: Anisotropic displacement parameters for AlaPrPO-1.

Atom	U_{11}	U_{22}	U_{33}	U_{23}	U_{13}	U_{12}
Al(1)	0.0145(7)	0.0137(7)	0.0145(7)	0	0.0003(5)	0
S(1)	0.0161(6)	0.0194(6)	0.0145(6)	0	-0.0010(4)	0
P(1)	0.0155(6)	0.0146(6)	0.0136(6)	0	0.0001(4)	0
O(1)	0.017(2)	0.021(2)	0.015(2)	0	0.0026(13)	0
O(2)	0.020(2)	0.017(2)	0.020(2)	0	-0.0062(14)	0
O(3)	0.016(2)	0.021(2)	0.014(2)	0	0.0005(13)	0
O(4)	0.020(2)	0.017(2)	0.015(2)	0	0.0039(13)	0
O(5)	0.0158(11)	0.0147(11)	0.0165(11)	0.0017(9)	0.0006(8)	0.0003(9)
O(8)	0.016(2)	0.037(2)	0.018(2)	0	-0.0002(14)	0
O(9)	0.018(2)	0.065(3)	0.018(2)	0	-0.0015(15)	0
O(10)	0.033(2)	0.037(2)	0.051(2)	-0.026(2)	-0.0082(14)	0.0000(14)
N(1)	0.023(2)	0.033(3)	0.015(2)	0	0.002(2)	0
C(1)	0.019(2)	0.022(3)	0.020(2)	0	-0.002(2)	0
C(2)	0.018(2)	0.018(2)	0.013(2)	0	0.001(2)	0
C(3)	0.016(2)	0.016(2)	0.015(2)	0	0.003(2)	0

Table 4.11: Bond lengths (in Å) and angles (in °) for AlaPrPO-1.

Al(1)-O(4)	1.813(4)	C(2)-C(3)	1.524(6)	O(10)-S(1)-O(9)	111.0(2)
Al(1)-O(2)	1.893(4)	O(4)-Al(1)-O(2)	100.2(2)	O(10)-S(1)-O(8)	108.1(2)
Al(1)-O(5)	1.898(3)	O(4)-Al(1)-O(5)	93.82(9)	O(9)-S(1)-O(8)	107.9(2)
Al(1)-O(3)	1.908(4)	O(2)-Al(1)-O(5)	85.74(9)	O(4)-P(1)-O(5)	111.45(13)
Al(1)-O(1)	1.935(4)	O(5)-Al(1)-O(5)	169.4(2)	O(5)-P(1)-O(5)	108.4(2)
S(1)-O(10)	1.449(3)	O(4)-Al(1)-O(3)	86.3(2)	O(4)-P(1)-C(3)	108.6(2)
S(1)-O(9)	1.470(4)	O(2)-Al(1)-O(3)	173.5(2)	O(5)-P(1)-C(3)	108.43(13)
S(1)-O(8)	1.482(4)	O(5)-Al(1)-O(3)	93.88(9)	P(1)-O(4)-Al(1)	156.3(3)
P(1)-O(4)	1.514(4)	O(4)-Al(1)-O(1)	171.8(2)	P(1)-O(5)-Al(1)	139.1(2)
P(1)-O(5)	1.527(3)	O(2)-Al(1)-O(1)	88.0(2)	N(1)-C(1)-C(2)	113.5(4)
P(1)-C(3)	1.804(5)	O(5)-Al(1)-O(1)	86.74(9)	C(1)-C(2)-C(3)	109.8(4)
N(1)-C(1)	1.498(7)	O(3)-Al(1)-O(1)	85.5(2)	C(2)-C(3)-P(1)	113.8(3)
C(1)-C(2)	1.525(7)	O(10)-S(1)-O(10)	110.7(4)		

The asymmetric unit of AlaPrPO-1 consists of an octahedrally coordinated aluminium atom and a tetrahedrally coordinated phosphorus atom. The phosphorus atom is connected to three different aluminium atoms *via* its three oxygen atoms. The aluminium is coordinated by three oxygens from three different phosphorus atoms and a further three oxygens from water molecules. The fourth bond of the phosphorus atoms is formed with the carbon of the aminopropyl chain (Figure 4.22). The sulphur is coordinated by four oxygens (Figure 4.23). Two of those oxygens form hydrogen bonds with neighbouring amino groups (distance 2.94 Å, Figure 4.24).

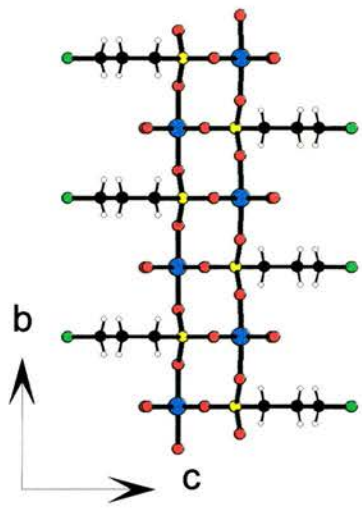

Figure 4.22: Ladder-like chain structure of AlaPrPO-1.
Key see pg. 4. Green spheres denote nitrogen.

The overall structure of AlaPrPO-1 consists of phosphonate chains along the b-axis, with the aminopropyl chains pointing along the c-axis. The sulphate groups lie between those chains, each of them close to a NH_3 group (Figure 4.23). The chains consist of edge-sharing four-membered ring units in a ladder-like arrangement (Figure 4.22). They are made up from alternating aluminium octahedra and phosphorus tetrahedra on each strand, connected by corner-sharing oxygens. The chains are held together by hydrogen bonding between the protonated amino groups, the sulphate ions, and the water molecules (Figure 4.24). Unlike in the powder XRD patterns of AlBzPO-1 and –2, in AlaPrPO-1 the first reflection does not equal the 100 % reflection (Figure 4.25), whichfurther suggests that AlaPrPO-1 does not have a layered structure like the first two samples. For the aluminium phosphonates investigated in this work, there seems to be a connection between a layered structure and the 100 % reflection being the first in the pattern.

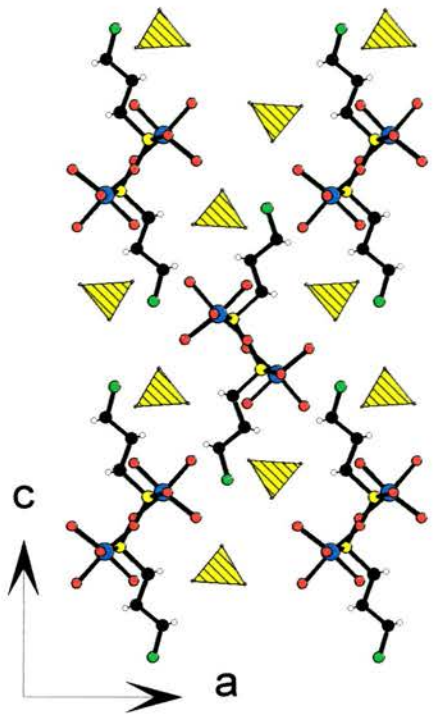

Figure 4.23: View along the AlaPrPO-1 chains. The position of the sulphate groups between the chains close to the nitrogen atoms is clearly visible.

Key see pg. 4. Green spheres denote nitrogen. Sulphate groups are shown as hatched yellow tetrahedra.

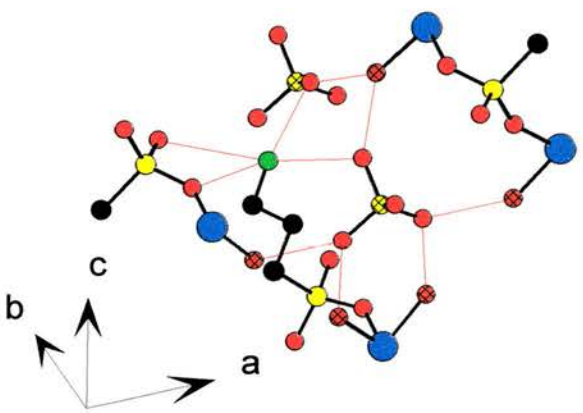

Figure 4.24: Hydrogen bonding around the sulphate groups in AlaPrPO-1.

Key see pg. 4. Hatched yellow spheres denote sulphur, red phosphonate and sulphate oxygen, hatched red water oxygen, and green nitrogen. Hydrogen bonds are shown in red. It can be assumed that the hydrogen atoms are situated somewhere on or close to these bonds.

Distances: Nitrogen - phosphonate oxygen atoms 3.0 Å,

Nitrogen - sulphate oxygen atoms 2.9 Å,

Sulphate oxygen - water oxygen atoms 2.6 Å.

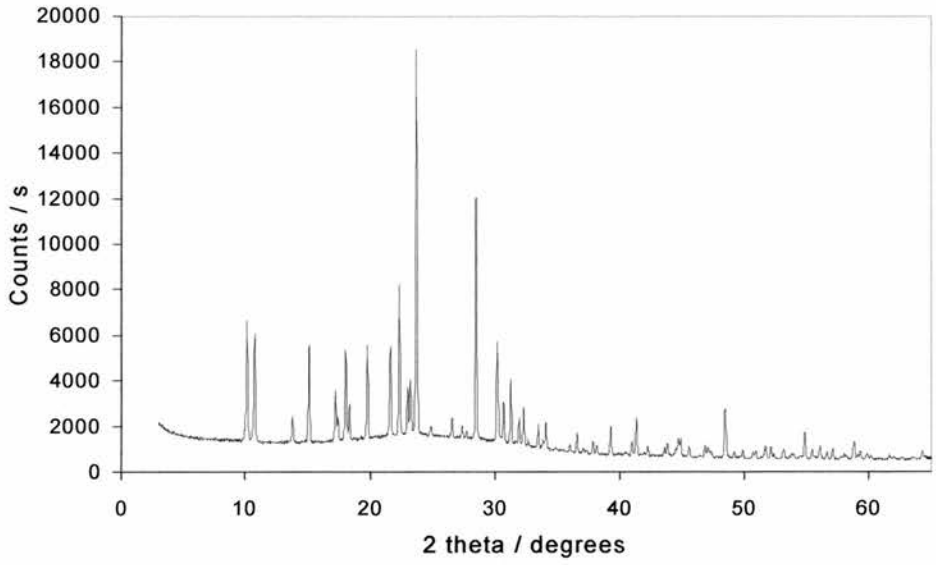

Figure 4.25: X-ray powder pattern of AlaPrPO-1.

Solid state MAS NMR spectroscopy of AlaPrPO-1

The symmetry of the X-ray diffraction model is consistent with the data collected from NMR experiments. The ^{27}Al MAS NMR spectrum (Figure 4.26) shows one aluminium site at δ -13.05 ppm). The ^{31}P NMR spectrum (Figure 4.27) also indicates only one independent phosphorus atom (δ 6.20 ppm), but there is a small impurity in the sample. The peak in the ^{15}N NMR spectrum (Figure 4.28) has a chemical shift of δ -346.6 ppm. This is within the range expected for protonated primary amines (δ -255...-355 ppm).[11] The ^{13}C NMR spectrum (Figure 4.29) consists of a singlet at 43.40 ppm, a doublet at 27.37 and 25.53 ppm respectively, and another singlet at 22.90 ppm. These peaks can be assigned as follows; the carbon that is deshielded by the nitrogen causes the singlet that is furthest downfield. The doublet results from coupling of the carbon to the phosphorus next to it. The remaining singlet is due to the carbon in the middle of the propyl chain.

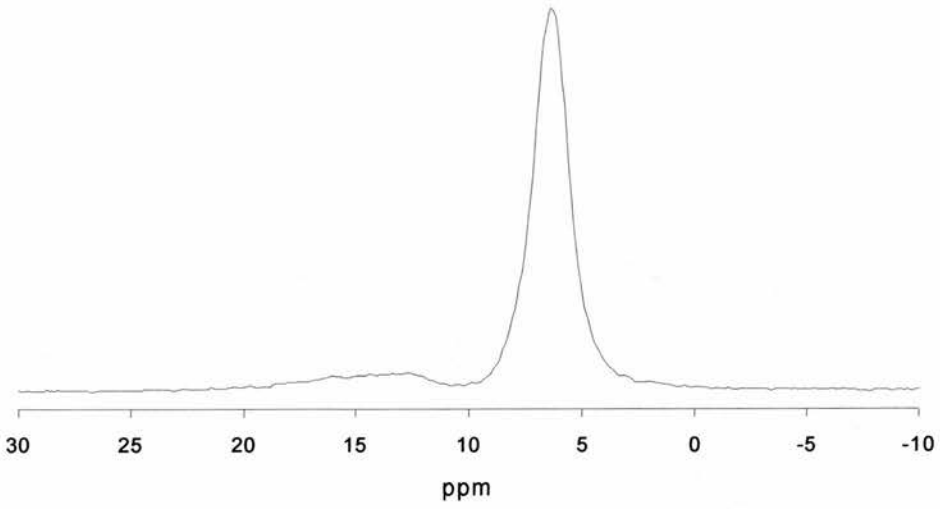

Figure 4.26: ^{27}Al MAS NMR spectrum of AlaPrPO-1 at 78.16 MHz.

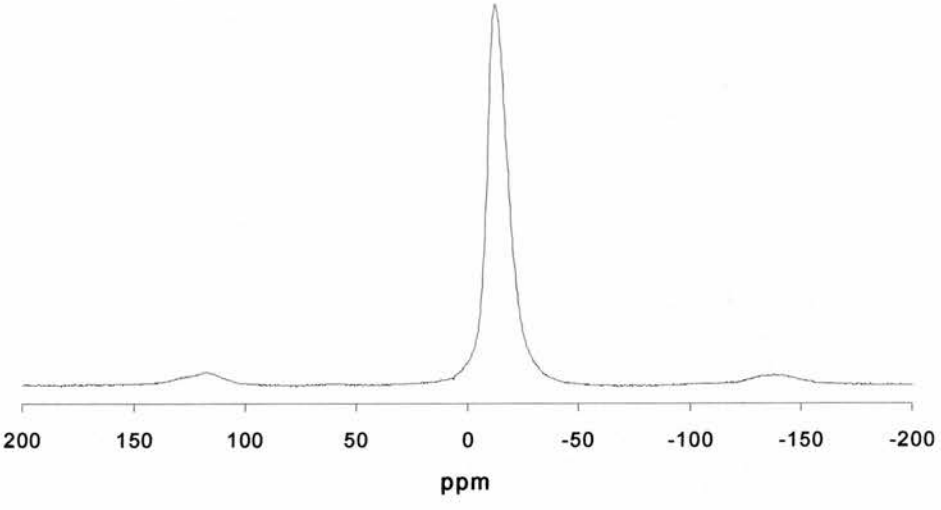

Figure 4.27: ^{31}P MAS NMR spectrum of AlaPrPO-1 at 121.42 MHz.

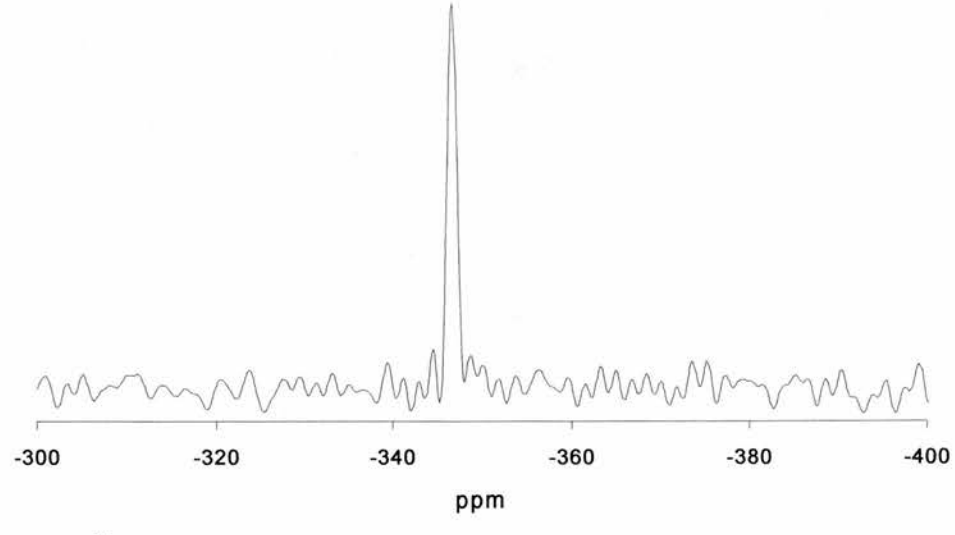

Figure 4.28: ^{15}N MAS NMR spectrum of AlaPrPO-1 at 30.40 MHz.

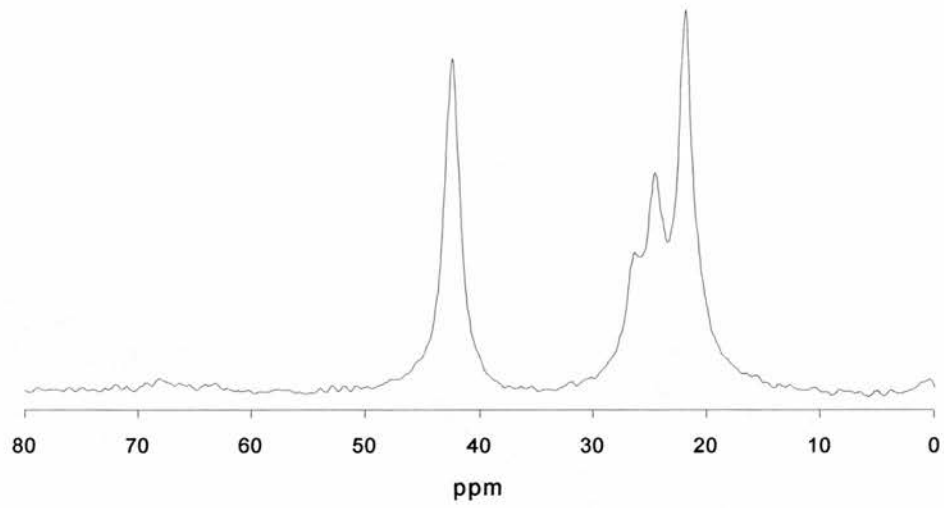

Figure 4.29: ^{13}C MAS NMR spectrum of AlaPrPO-1 at 75.43 MHz.

Thermogravimetric and CHN analysis of AlaPrPO-1

The results of the thermogravimetric analysis (Figure 4.30) are consistent with the X-ray diffraction structure. The first step at 200 °C was calculated to be 17.15 % for a loss of 3 molecules of water per formula unit, which is within 3.6 % of the observed value (20.69 %). The rather high temperature of the first loss also indicates that the

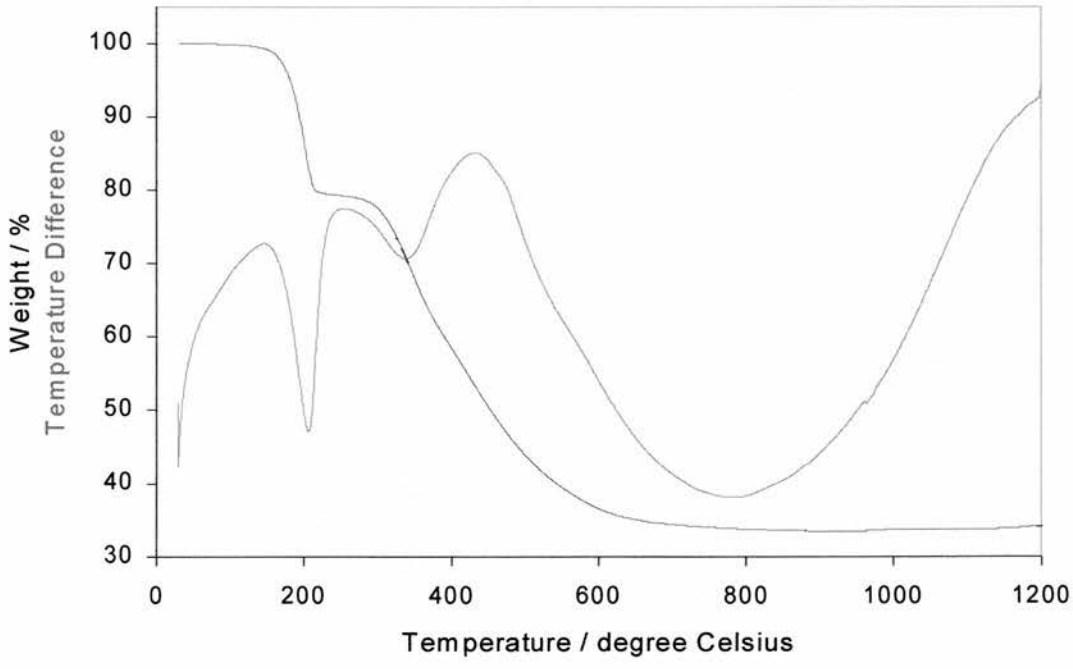

Figure 4.31: TGA trace of AlaPrPO-1.

water molecules are incorporated into the structure of the phosphonate. For the second step, a mass loss of 45.56 % was observed at 346 °C, compared with a calculated 44.16 % for the organic part of the material. The observed value for the residue is 33.75 %, compared with a calculated value of 38.69 % for one molecule of $AlPO_4$ per formula unit. X-ray powder diffraction on the TGA residue confirmed it to be $AlPO_4$. The results of the CHN analysis (10.85 % C, 4.80 % H, and 4.14 % N) are within 0.6 % of the values calculated for $Al(O_3P(CH_2)_3NH_3).SO_4.3H_2O$ (11.43 % C, 4.80 % H, and 4.44 % N).

The structure of AlaPrPO-1 is unusual in that it contains chains of aluminium phosphonate, rather than the much more common layered arrangements. Also unusual, by virtue of the protonation of the amine nitrogen atoms under the acidic reaction conditions, is that the aluminium phosphonate chain is positively charged. Normally in phosphonate chemistry the units are neutral or negatively charged.

In aluminium phosphates, the inorganic frameworks also tend to be either neutral or negatively charged (when doped with aliovalent M^{2+} cations or fluoride ions). This allows the use of positively charged structure directing agents to be occluded into the structure. In the case of AlaPrPO-1, the positive charge on the 3-aminopropylphosphonate unit is balanced by the occlusion of a negatively charged sulphate group between the chains. This type of synthetic approach to positively charged 'framework' aluminium phosphonate species opens up the possibility of using anions of different sizes as 'structure directing agents' in a similar fashion to the use of protonated/quaternary amines in the synthesis of chain, layered and microporous aluminium phosphates.

Furthermore, the inclusion of protonated amino groups enables a wide range of possible subsequent reactions on the material, such as ion exchange, amidation or intercalation. The presence of positive charges on the framework should thereby enable the introduction of negatively charged or polar compounds that could not previously be used in negatively charged or neutral frameworks. This would lead to a further diversification of the range and characteristics of aluminium phosphonates that are available either by direct synthesis or through post-synthetic modification.

4.2.2. Comparison of the IR spectra of AlAPrPO-1 and a mixture of AlaPrPO-2 and -3

There are some pronounced differences between the IR spectra of 3-aminopropyl PA and the corresponding phosphonates (see Figure 4.31). In the acid, there are no distinctive bands in the region for N-H stretching, although there is a very broad band with a maximum at approx. 3000 cm^{-1} (N-H··· stretching with H-bonds). However, the C-H stretching bands for CH_2 (2907 cm^{-1} and 2830 cm^{-1}) are clearly visible. There also are two (P-)O-H stretching bands at 2616 cm^{-1} and 2146 cm^{-1}, respectively. The spectrum for AlAPrPO-1 shows a broad maximum for the N-H··· stretching at approx. 3160 cm^{-1}, but no C-H stretching bands can be distinguished, presumably because they are overlapped by the broad N-H··· stretching band. In the spectrum of the mixture of AlAPrPO-2 and -3 there are three broad bands overlapping each other. The first two are situated at 3515 cm^{-1} (O-H··· stretching) and 3420 cm^{-1} (N-H stretching), respectively, and the third is centred at approx. 3040 cm^{-1} (N-H··· stretching). Two shoulders at 2905 cm^{-1} and 2812 cm^{-1} can be assumed to be due to C-H stretching vibrations.

In the fingerprint region, the three spectra have some common features, like the N-H deformation band at 1653 cm^{-1} (overlapped by a broad H_2O deformation band in

the spectrum of AlAPrPO-2/-3). In the region for the (P-)C-H bending vibration there are several bands. Its position was assumed to be 1467 cm^{-1} for the acid and approx. 1490 cm^{-1} for the phosphonates. A band at approx. 1240 cm^{-1} arises in all three spectra, as do four bands at approx. 1130 cm^{-1}, 1095 cm^{-1} (C-N stretching or O-P-O bending), 1055 cm^{-1} and 933 cm^{-1}. For the mixture of AlaPrPO-2 and -3 the first and the last of these bands are overlapped by the two middle bands. Variations between the two phosphonates could be due to different structures and to the broadness of the bands in the spectrum of AlAPrPO-2/-3, which leads to the overlapping of different bands. A summary of the three spectra is given in Table 4.12. Any bands due to the sulphate group[12] (a strong band between 1130 and 1080 cm^{-1} and a weak band between 680 and 610 cm^{-1} are obscured by strong bands arising from the phosphonate groups.

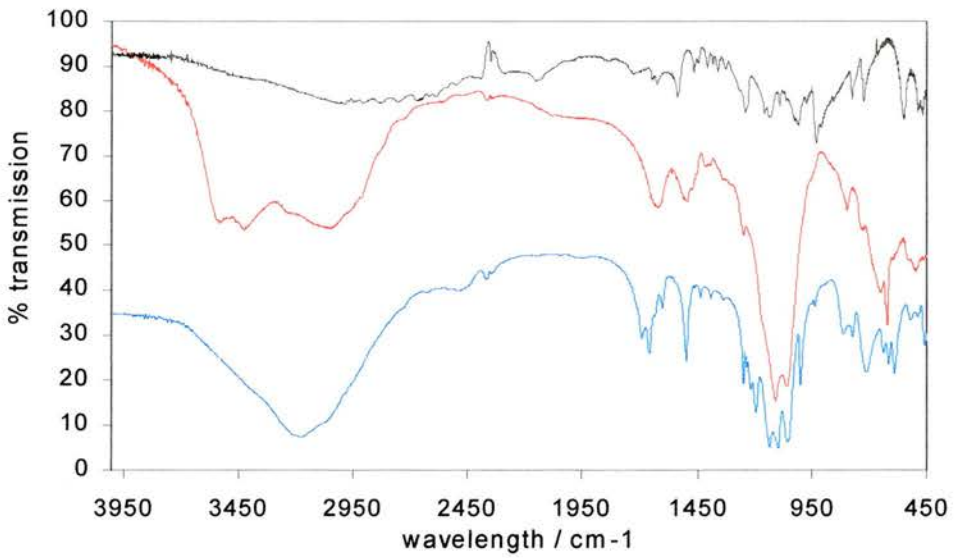

Figure 4.31: IR spectra of 3-aminopropylphosphonic acid (black), AlaPrPO-1 (blue), and a mixture of AlaPrPO-2 and -3 (red).

Table 4.12: Comparison of the IR spectra of 3-aminopropyl PA, AlAPrPO-1 and AlAPrPO-2/-3.

Assigned vibration	3-Aminopropyl PA	AlAPrPO-1	AlAPrPO-2/-3
O-H stretching/ H bonding			3515 cm^{-1}
O-H stretching/ H-bonding			3420 cm^{-1}
N-H stretching/ H bonding		3158 cm^{-1}	
N-H stretching/ H bonding	3015 cm^{-1}	3051 cm^{-1}	3040 cm^{-1}
C-H stretching/ CH_2	2907 cm^{-1}		2905 cm^{-1}
C-H stretching/ CH_2	2830 cm^{-1}		2812 cm^{-1}
(P-)O-H stretching	2612 cm^{-1}		
(P-)O-H stretching	2146 cm^{-1}		
N-H deformation	1652 cm^{-1}	1653 cm^{-1}	overlapped
C-H deformation/ P-CH_2	1467 cm^{-1}	1493 cm^{-1}	1489 cm^{-1}
	1240 cm^{-1}	1246 cm^{-1}	1243 cm^{-1}
	1136 cm^{-1}	1131 cm^{-1}	overlapped
C-N stretching or O-P-O bending	1092 cm^{-1}	1094 cm^{-1}	1105 cm^{-1}
	1061 cm^{-1}	1054 cm^{-1}	1053 cm^{-1}
	932 cm^{-1}	933 cm^{-1}	overlapped

4.3. Synthesis of aluminium 2-aminoethylphosphonates

Although the aluminium 2-aminoethylphosphonates have proved to be far more elusive than the corresponding 3-aminopropylphosphonates or the benzylphosphonates, it was possible to prepare a crystalline phase. The starting material for this reaction was aluminium chloride at an Al:P ratio of 1:1.5 and a pH value of 4.0. The hydrothermal reaction was performed at 150 °C and an increase in the reaction time from 3 to 17 days led only to a slight increase in crystallinity. The powder X-ray diffraction pattern of the material is shown in Figure 4.32. It was not possible to index this pattern. The *d*-spacing of 11.33 Å is shorter than the values found for the aluminium 3-aminopropylphosphonate phases AlAPrPO-2 and -3 (14.71 Å and 15.57 Å, respectively, see Section 4.2, pg. 110), and longer than the respective distance for aluminium aminomethylphosphonate (10.02 Å, see Section 4.4). The discontinuous increase could either be due to different structures or to odd/even effects in the conformation of the alkyl chains.[13]

Experiments with gibbsite, aluminium sulphate and aluminium nitrate either resulted in clear solutions or led to the recovery of gibbsite. Reactions with aluminium chloride under reflux were not successful either.

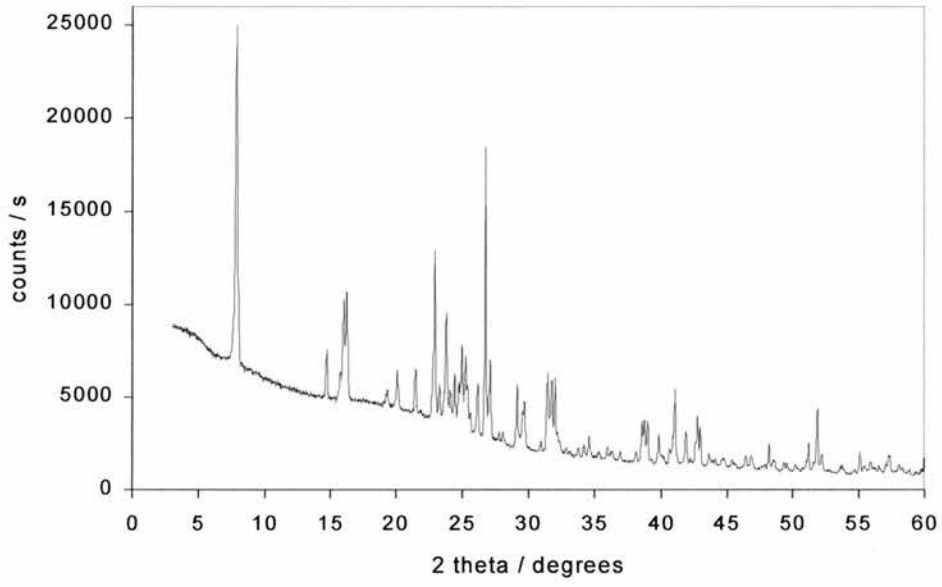

Figure 4.32: Powder XRD pattern of aluminium 2-aminoethylphosphonate.

Solid state MAS NMR spectroscopy of aluminium 2-aminoethylphosphonate

The ^{27}Al NMR spectrum of aluminium 2-aminoethylphosphonate shows one peak (-23.0 ppm) that indicates an octahedral environment for the aluminium (Figure 4.33). The phosphorus NMR spectrum (Figure 4.34) contains three peaks at 18.9, 17.5 and 14.5 ppm in a ratio of approx. 1:3:3. That could mean that two crystallographically independent phosphorus environment exist in this material if the weak peak at 18.9 ppm is due to an impurity. The ^{13}C MAS NMR contains a singlet at 38.60 ppm (the carbon that is next to and deshielded by the nitrogen) and a double doublet with peaks at 28.83, 26.94 and 24.61 ppm (Figure 4.35). It could therefore be possible that the material contains two 2-aminoethyl groups with different crystallographic environments.

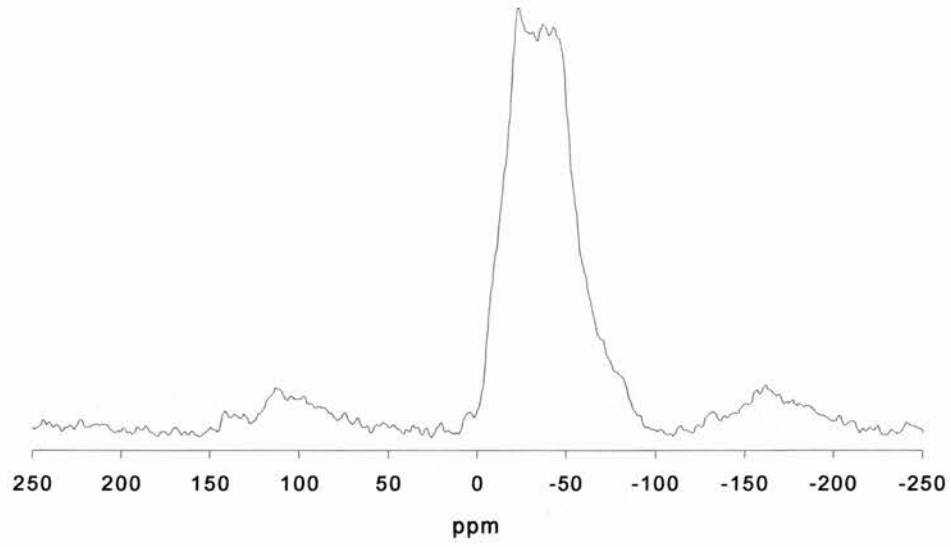

Figure 4.33: ^{27}Al MAS NMR spectrum of Al 2-aminoethylphosphonate at 78.16 MHz.

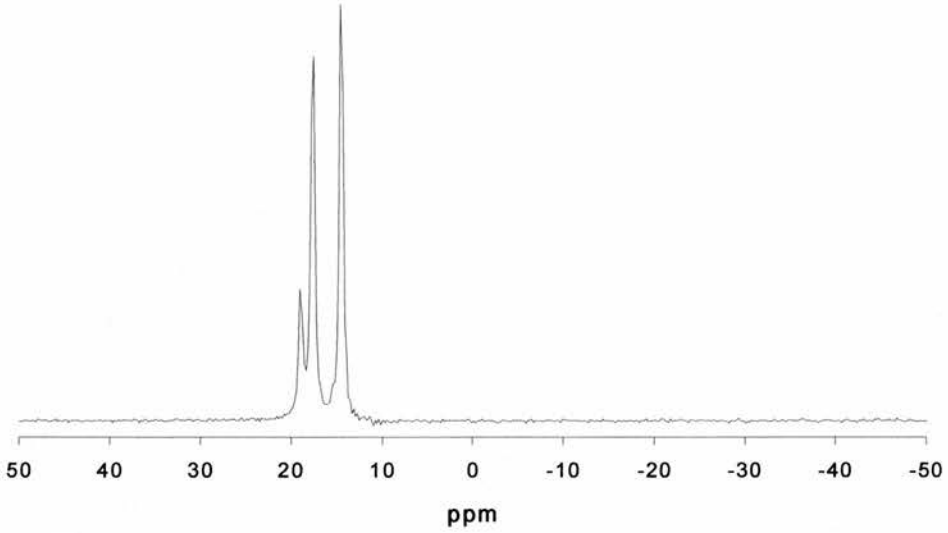

Figure 4.34: ^{31}P MAS NMR spectrum of Al 2-aminoethylphosphonate at 121.42 MHz.

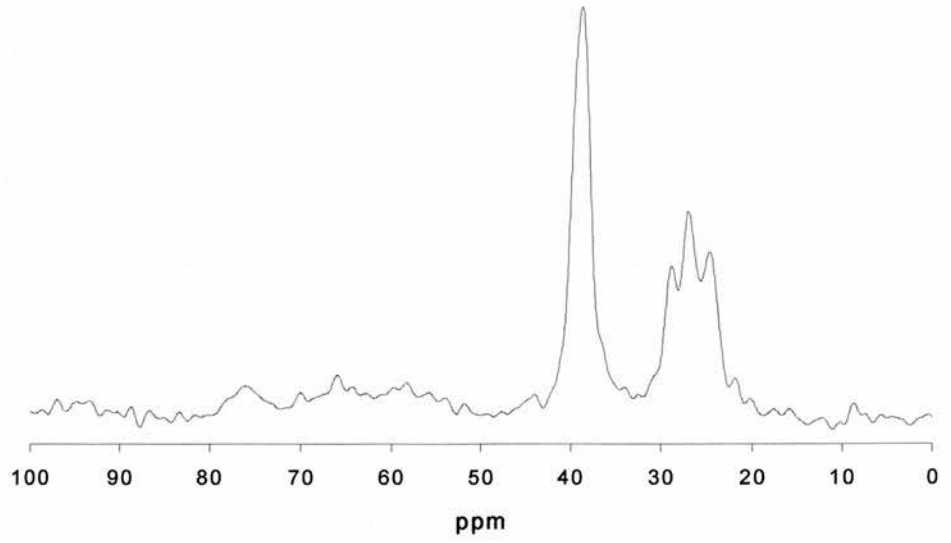

Figure 4.35: ^{13}C MAS NMR spectrum of Al 2-aminoethylphosphonate at 75.43 MHz.

Thermogravimetric and CHN analysis of aluminium 2-aminoethylphosphonate

The TGA of this phase (Figure 4.36) shows three distinct mass losses. The first and the second loss, at 200 °C (7.72 %) and 225 °C (3.49 %) respectively, could either be due to water molecules incorporated into the material or to a condensation reaction of hydroxyl groups. The third loss (22.66 %) takes place at 327 °C and is presumably caused by the combustion of the organic part of the molecule. The mass decreases by a further 10.28 % between 400 °C and 750 °C, which could be attributed to the loss of less volatile residues, leaving a residue of 55.85 % of the starting mass. The results of the CHN analysis are; 7.90 % C, 4.38 % H and 6.00 % N. However, the sample contained a small contamination of fibres from filter paper and therefore the results may be an underestimation of the real values.

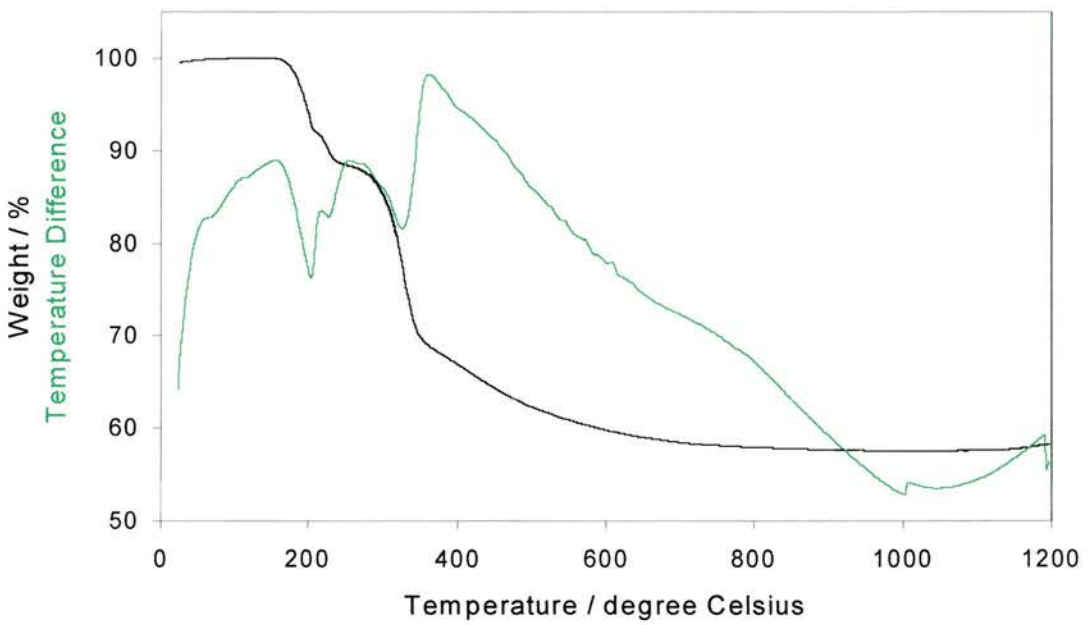

Figure 4.36: TGA trace of aluminium 2-aminoethylphosphonate.

Assuming a formula $Al(OH)(O_3P(CH_2)_2NH_3^+).Cl^-.H_2O$, the calculated values for the CHN analysis would be 10.84 % C, 4.55 % H and 6.32 % N. The corresponding TGA results could be calculated for the loss of one molecule of water (8.13 %), the

condensation of two OH groups equalling the loss of half a molecule of water (4.07 %) and the loss of the organic moiety (20.35 %). The fourth loss could be attributed to half a molecule of Cl_2 (16.00 %), leaving a residue of one molecule of $AlPO_4$ per formula unit (55.05 %). As it was not possible to index the X-ray powder pattern of the material, it was however impossible to prove or disprove this assumption.

IR spectroscopy of aluminium 2-aminoethylphosphonate

The spectrum for aluminium 2-aminoethylphosphonate shows a very broad band between 3600 and 2750 cm^{-1}. It can be expected that it consists of overlapping bands for O-H and N-H stretching with and without hydrogen bonding. Although there is a lot of noise in this area, two features could be interpreted as bands at 3541 cm^{-1} (O-H stretching with H bonding) and 3220 cm^{-1} (N-H stretching). In the 2-aminoethylphosphonic acid, the broad band is found between approximately 3400 and 2500 cm^{-1}. However, there are some distinct bands between 3026 cm^{-1} and 2500 cm^{-1}. The band at 3026 cm^{-1} is caused by N-H stretching with H bonding, while the bands at 2874 and 2860 cm^{-1} are caused by the C-H stretching of the CH_2 groups. The distinct bands at 2536 and 2176 cm^{-1} in the spectrum of the phosphonic acid arise from (P-)O-H stretching vibrations.

The N-H deformation vibration that can be found at 1644 cm^{-1} for the phosphonic acid is either overlapped or too weak in the phosphonate spectrum to be observed. C-H deformation vibrations can be found at 1480 cm^{-1} in the phosphonic acid and at 1490 cm^{-1} in the phosphonate. A band that appears at 1289 cm^{-1} in the phosphonate and at 1274 cm^{-1} in the phosphonic acid is common in aluminium phosphonates. Another band that commonly shows up in aluminium phosphonates is the one at 1142 cm^{-1} in the

phosphonic acid. However, it cannot be found in the phosphonate, although it may be overlapped by neighbouring strong bands there. A vibration at 1088 cm^{-1} (phosphonate) and 1072 cm^{-1} (phosphonic acid) could be assigned either to C-N stretching or O-P-O bending vibrations. The band at 1060 cm^{-1} in the phosphonate is also common, but only weak in the phosphonic acid (1056 cm^{-1}).

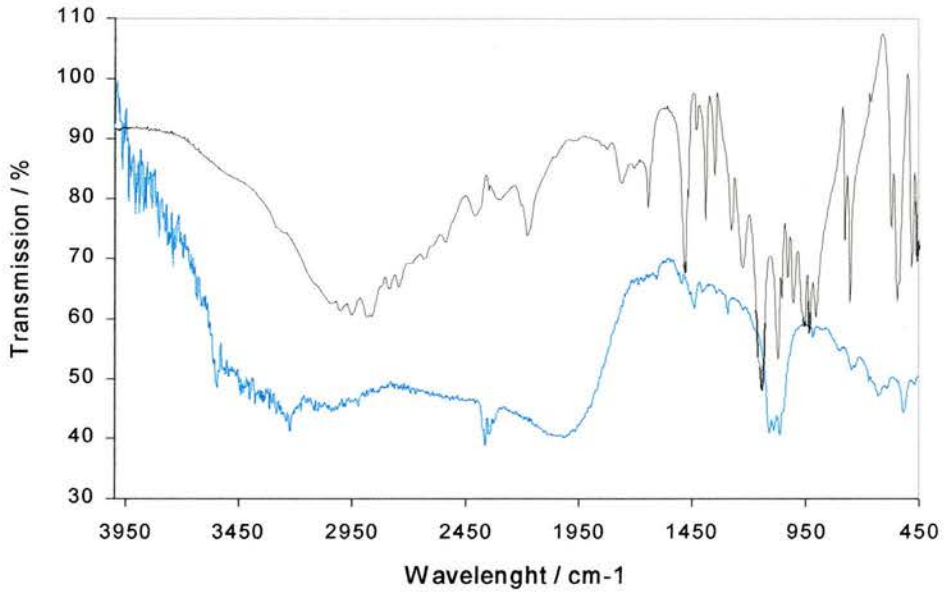

Figure 4.37: IR spectra of 2-aminoethylphosphonic acid (black) and aluminium 2-aminoethyl-phosphonate (blue).

Table 4.13: Comparison of the IR spectra of 2-aminoethylphosphonic acid and aluminium 2-aminoethylphosphonate.

Assigned vibration	**3-Aminopropyl PA**	**Phosphonate**
O-H stretching/ H bonding		3541 cm^{-1}
O-H stretching/ H-bonding		
N-H stretching/ H bonding		3220 cm^{-1}
N-H stretching/ H bonding	3026 cm^{-1}	3051 cm^{-1}
C-H stretching/ CH_2	2874 cm^{-1}	
C-H stretching/ CH_2	2860 cm^{-1}	
(P-)O-H stretching	2536 cm^{-1}	
(P-)O-H stretching	2176 cm^{-1}	
N-H deformation	1644 cm^{-1}	overlapped
C-H deformation/ P-CH_2	1480 cm^{-1}	1490 cm^{-1}
	1274 cm^{-1}	1289 cm^{-1}
	1142 cm^{-1}	overlapped
C-N stretching or O-P-O bending	1072 cm^{-1}	1088 cm^{-1}
	1056 cm^{-1}	1060 cm^{-1}

4.4. Synthesis of aluminium aminomethylphosphonates

An aluminium aminomethylphosphonates phase with *d*-spacings between 9.88 and 10.02 Å was prepared from gibbsite at Al:P ratios of 1:1.5 and 1:2 both under reflux and under hydrothermal conditions, although the reflux products had a lower crystallinity. The powder XRD patterns of this material (Figure 4.38) could not be indexed.

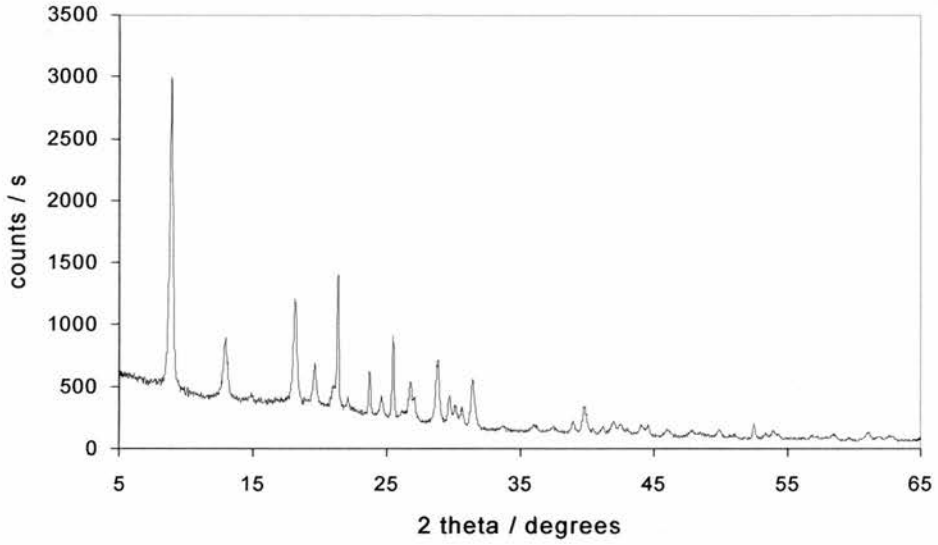

Figure 4.38: Powder XRD pattern of aluminium aminomethylphosphonate.

Solid state MAS NMR spectroscopy of aluminium aminomethylphosphonate

The position and shape of the peak in the ^{27}Al MAS NMR spectrum of the phosphonate (Figure 4.39) strongly indicates an octahedral environment for the aluminium. In the ^{31}P MAS NMR spectrum of the phosphonate (Figure 4.40) there are two very intense peaks at 1.8 ppm and 6.7 ppm. In addition, there is a weak peak further downfield at 10.3 ppm. The peaks have a ratio of approx. 3:3:1. This indicates at least two different phosphorus environments in the material, because the weak peak could be due to the presence of a small amount of a second component. The ^{13}C MAS NMR (Figure 4.41) contains only one peak at 37.1 ppm. The signal of the methyl carbon should be split due to its bond to the phosphorus atom, but the comparatively broad signal could be caused by two peaks that are not resolved.

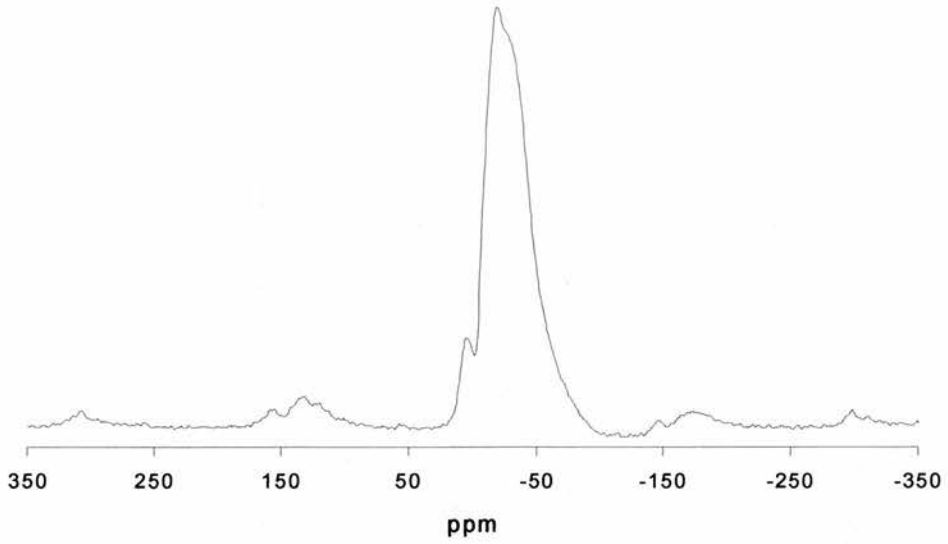

Figure 4.39: ^{27}Al MAS NMR spectrum of Al aminomethylphosphonate at 78.16 MHz.

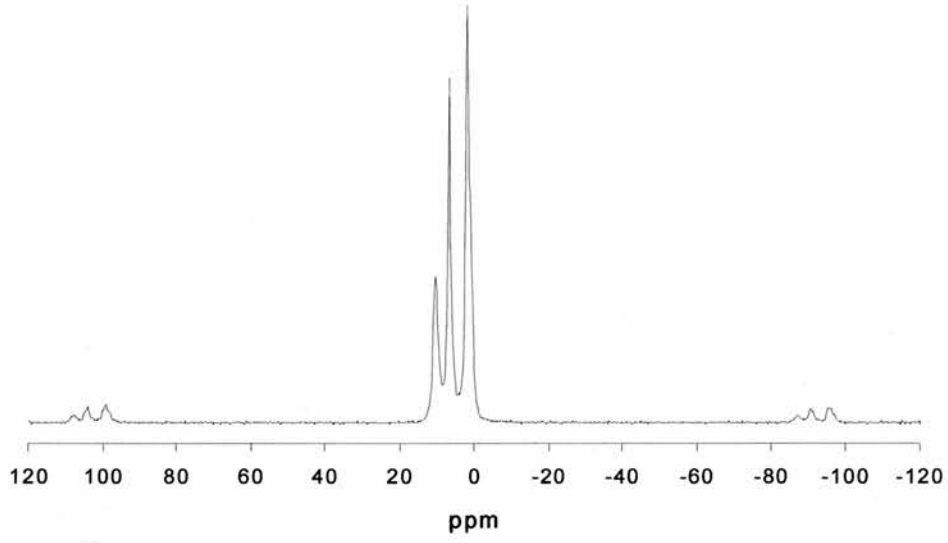

Figure 4.40: ^{31}P MAS NMR spectrum of Al aminomethylphosphonate at 121.42 MHz.

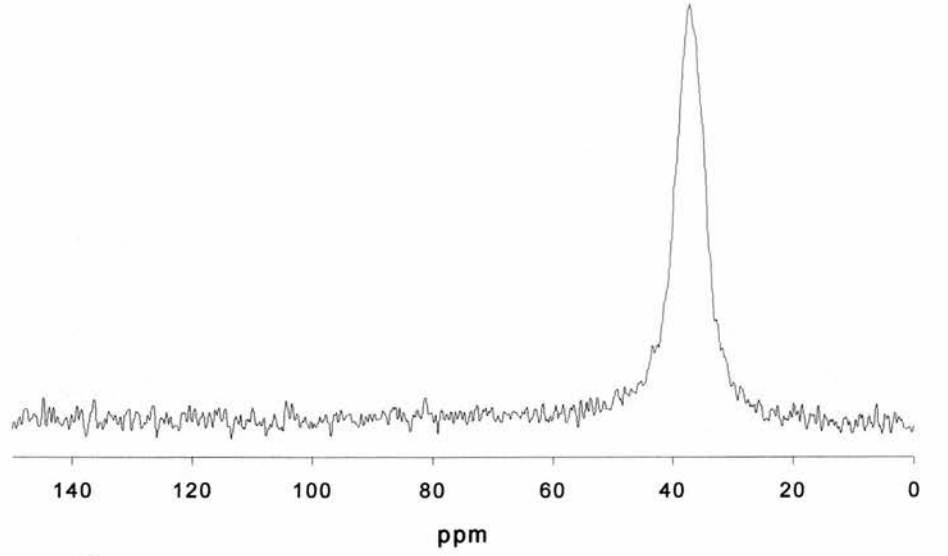

Figure 4.41: ^{13}C MAS NMR spectrum of Al aminomethylphosphonate at 75.43 MHz.

Thermogravimetric and CHN analysis of aluminium aminomethylphosphonate

The TGA of aluminium aminomethylphosphonate shows two mass losses, the first one at 94 °C and the second one at 349 °C. The compound then continues to release volatile material up to a temperature of 1200 °C (see Figure 4.42). The TGA was calculated for a compound with the formula $Al(O_3PCH_2NH_3)(OH).2H_2O$. The first loss can be calculated to be 9.48 % for one molecule of water per formula unit, which corresponds well to an observed value of 10.91 %. The second loss has an observed value of 24.48 %, compared with a calculation of 25.29 % for the combustion of the organic group, leaving a residue of one molecule of $AlPO_4$ per formula unit (observed 64.59 %, calculated 64.17 %). The values observed in the CHN analysis of the material were within 1.5 % of the values calculated for the above formula;

observed: 7.67 % C, 4.96 % H, 8.55 % N,

calculated for $Al(O_3PCH_2NH_3)(OH).3H_2O$: 6.32 % C, 5.30 % H, 7.37 % N.

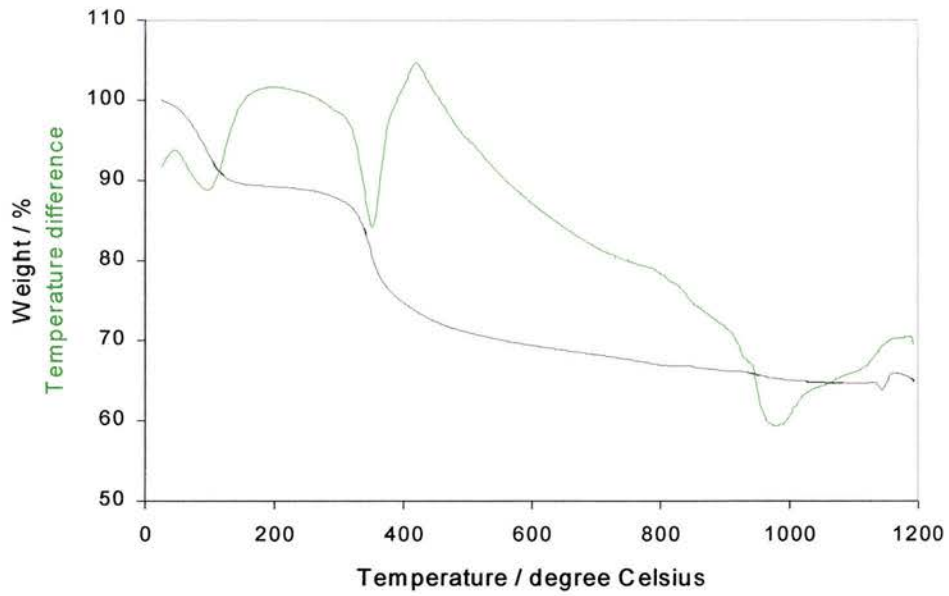

Figure 4.42: TGA trace of aluminium aminomethylphosphonate.

As it was not possible to index the powder pattern of the material, it is not possible to prove or disprove the above-mentioned empirical formula.

IR spectroscopy of aluminium aminomethylphosphonate

The IR spectra of aminomethyl PA and of aluminium aminomethylphosphonates have some features in common (see Figure 4.43), although broad bands in the spectrum of the phosphonate make a comparison less accurate in the fingerprint region. In contrast to the phosphonate (O-H stretching at 3404 cm^{-1}), the acid has no bands in the region for O-H stretching vibrations, but N-H··· and C-H stretching vibrations could be observed in both spectra (see Table 4.14). The presence of (P-)O-H stretching bands in the phosphonate at 2643 cm^{-1} and 2104 cm^{-1} points to a possible contamination of the material with a small amount of another compound, because the (P-)O-H stretching vibration for the acid can be found at 2621 cm^{-1} and 2121 cm^{-1}. However, it might also be the case that these bands are caused by (Al-)O-H vibrations instead of (P-)O-H vibrations. The N-H and (P-)C-H deformation vibrations are clearly visible in both spectra. A distinct band at 1216 cm^{-1} is present in the acid, but has either disappeared or is overlapped by a broad band at 1166 cm^{-1} in the spectrum of the phosphonate. This also happens to a band at 1112 cm^{-1} that is assigned to C-N stretching or O-P-O bending

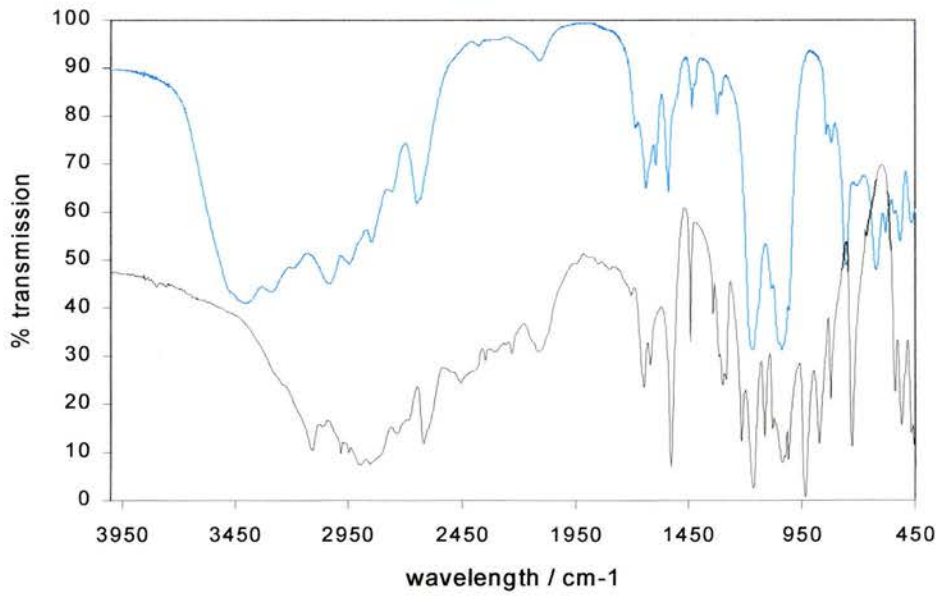

Figure 4.43: IR spectra of aminomethylphosphonic acid (black) and aluminium aminomethyl-phosphonate (blue).

in the acid, but does not appear in the spectrum of the phosphonate. Another band at 1022 cm^{-1} and 1032 cm^{-1} respectively can be found in both spectra, while a strong band at 931 cm^{-1} is not present in the phosphonate spectrum.

Table 4.14: Summary of the IR spectra of aminomethylphosphonic acid and aluminium aminomethylphosphonate.

Assigned vibration	Aminomethyl PA	Aminomethylphosphonate
O-H stretching/ H bonding		3403 cm^{-1}
N-H stretching		3288 cm^{-1}
N-H stretching/ H bonding	3112 cm^{-1}	3191 cm^{-1}
N-H stretching/ H bonding	2984 cm^{-1}	3028 cm^{-1}
C-H stretching/ CH_2	2901 cm^{-1}	overlapped
C-H stretching/ CH_2	2857 cm^{-1}	2845 cm^{-1}
(P-)O-H stretching	2621 cm^{-1}	2643 cm^{-1}
(P-)O-H stretching	2121 cm^{-1}	2104 cm^{-1}
N-H deformation	1649 cm^{-1}	1637 cm^{-1}
C-H deformation/ P-CH_2	1443 cm^{-1}	1431 cm^{-1}
	1216 cm^{-1}	
	1165 cm^{-1}	1167 cm^{-1}
C-N stretching or O-P-O bending	1112 cm^{-1}	
	1022 cm^{-1}	1032 cm^{-1}
	931 cm^{-1}	

4.5. Synthesis of aluminium 1-aminobutylphosphonates

The powder XRD patterns of the 1-aminobutylphosphonates prepared from gibbsite under hydrothermal conditions and under reflux showed small differences, although the products all had interlayer spacings of 14.25 Å and can be assumed to be layered. In the powder XRD pattern of the hydrothermal product, two reflections at 11.64 Å and 11.23 Å are absent. This could be due to preferred orientation or crystallinity effects, as all other reflections in the pattern of the reflux product were also present in the hydrothermal product, although preferred orientation effects would only be expected to affect one or the other but not both low angle peaks. Because of the

higher crystallinity of the hydrothermal product, several additional reflections could be found at higher angles.

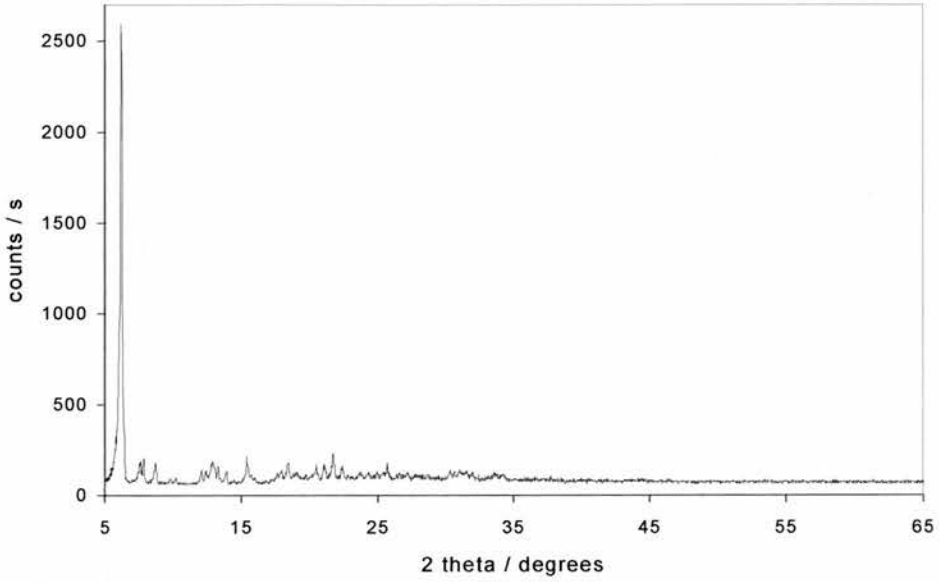

Figure 4.44: Powder XRD pattern of aluminium 1-aminobutylphosphonate prepared under reflux.

Solid state MAS NMR spectroscopy of aluminium 1-aminobutylphosphonate

The ^{27}Al MAS NMR spectrum contains a signal centred around -20 ppm *i.e.* in the area typical for octahedral aluminium environments (Figure 4.45). The ^{31}P MAS NMR spectrum shows a single peak at 6.5 ppm (Figure 4.46). Therefore, only one phosphorus environment should be present in the sample. The ^{13}C MAS NMR spectrum contains four peaks at 14.3, 20.0, 31.3 and 50.3 ppm (Figure 4.47). The peak at 50.3 ppm is broader than the other three peaks. It corresponds to carbon *(1)* that is connected to both the phosphorus and the nitrogen, leading to splitting and deshielding respectively. The broadening is presumably due to overlapping of the doublet caused by the phosphorus. The three peaks at 31.3 ppm, 20.0 ppm and 14.3 ppm are caused by C*(2)* to C*(4)*, respectively (numbering of 1-aminobutylphosphonic acid; $(OH)_2PO$-C*(1)*$H(NH_2)$-C*(2)*H_2-C*(3)*H_2-C*(4)*H_3).

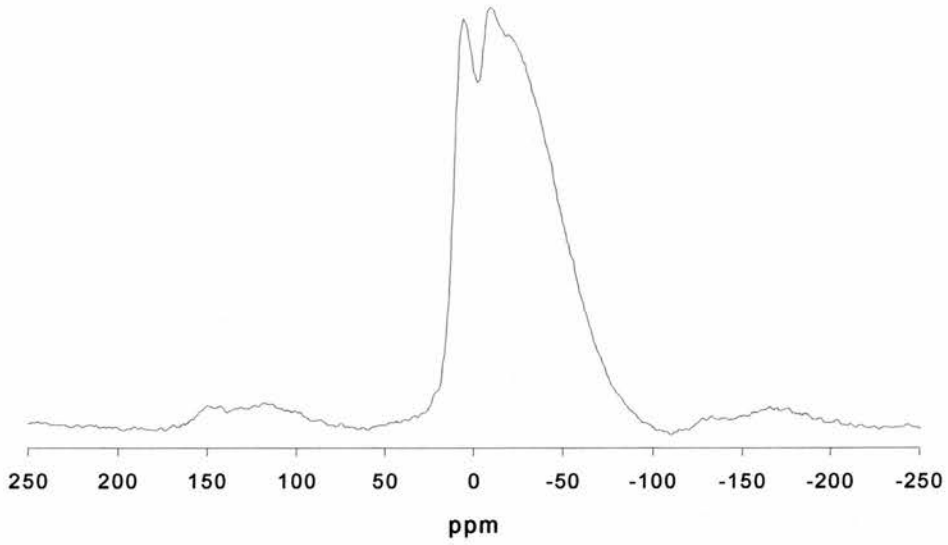

Figure 4.45: ^{27}Al MAS NMR spectrum of Al 1-aminobutylphosphonate at 78.16 MHz.

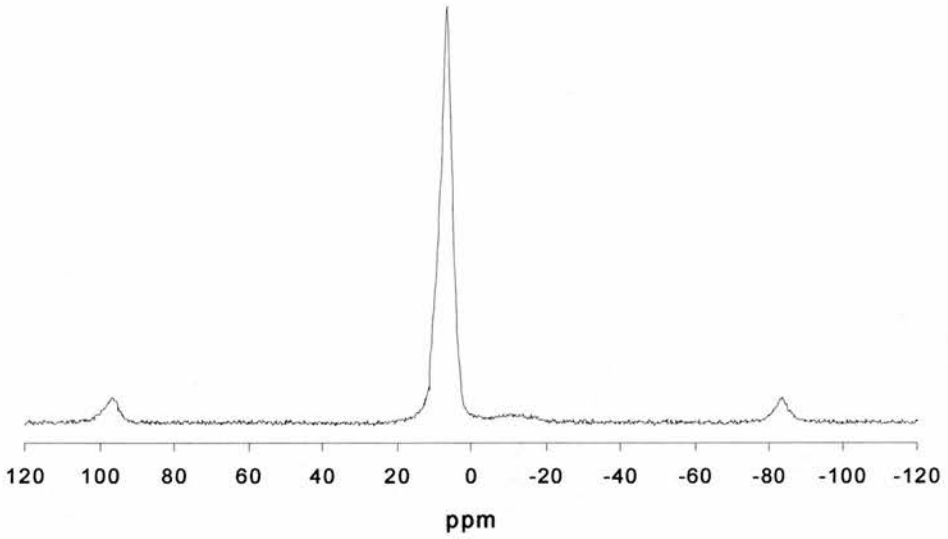

Figure 4.46: ^{31}P MAS NMR spectrum of Al 1-aminobutylphosphonate at 121.42 MHz.

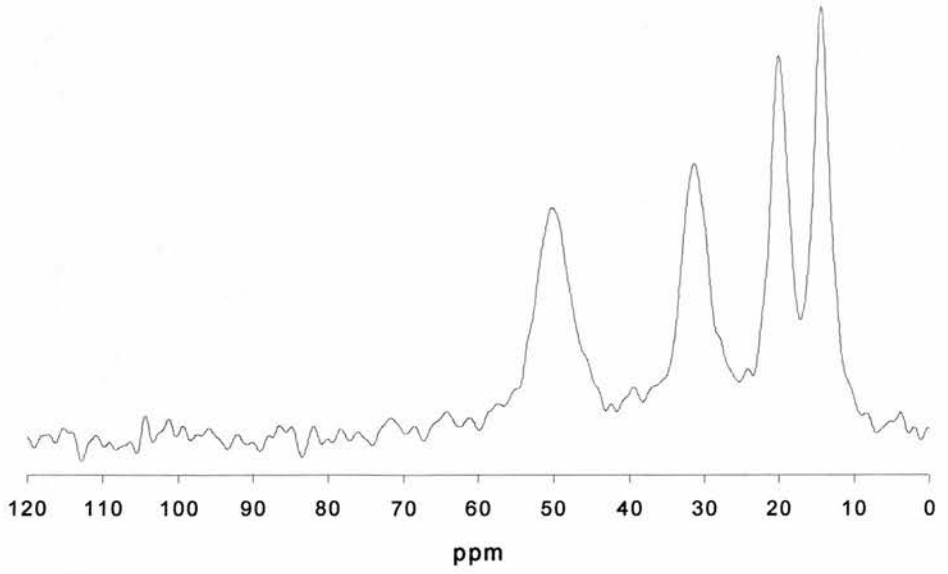

Figure 4.47: ^{13}C MAS NMR spectrum of Al 1-aminobutylphosphonate at 75.43 MHz.

Thermogravimetric and CHN analysis of aluminium 1-aminobutylphosphonate

In the TGA trace of aluminium 1-aminobutylphosphonate five consecutive mass losses can be observed. The first loss (10.02 %) at about 80 °C can presumably be associated with the loss of loosely attached water molecules. The second loss, 9.61 %, takes place around 150 °C. The third loss happens at 275 °C and accounts for another 12.03 %. The next loss (13.98 %) takes place over an extended temperature range between 320 and 930 °C. The last 5.64 % are lost around 1010 °C, leaving a residue of 48.70 %. In the CHN analysis, the following values could be observed; 21.65 % C, 7.74 % H and 6.19 % N.

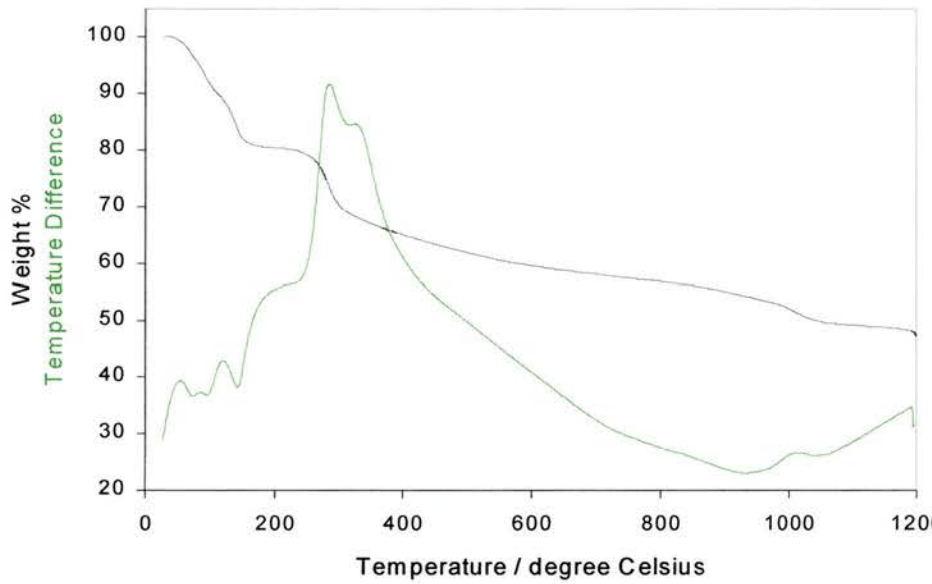

Figure 4.48: TGA trace of aluminium 1-aminobutylphosphonate.

IR spectroscopy of aluminium 1-aminobutylphosphonate

The IR spectrum of the 1-aminobutylphosphonic acid shows no distinct bands in the O-H and N-H stretching area, while for the phosphonate, there is a strong band at 3460 cm^{-1} (O-H··· stretching) and two shoulders at lower wavenumbers (3260 cm^{-1} and 3087 cm^{-1}) indicating N-H··· stretching bands (see Table 4.15 and Figure 4.49). However, the C-H stretching bands for CH_3 (2965 cm^{-1}) and CH_2 (2934 cm^{-1} and

2872 cm^{-1}) are clearly visible for both the acid and the phosphonate. In the fingerprint region, the spectrum of the acid is much clearer, because the bands are narrower. The (P-)O-H stretching bands only appear in the spectrum of the acid at 2703 cm^{-1} and 2288 cm^{-1}. The N-H and (P-)C-H deformation vibrations are visible in both spectra at approx. 1530 cm^{-1} and 1465 cm^{-1}. Two bands at 1220 cm^{-1}/1233 cm^{-1} and 1175 cm^{-1}/

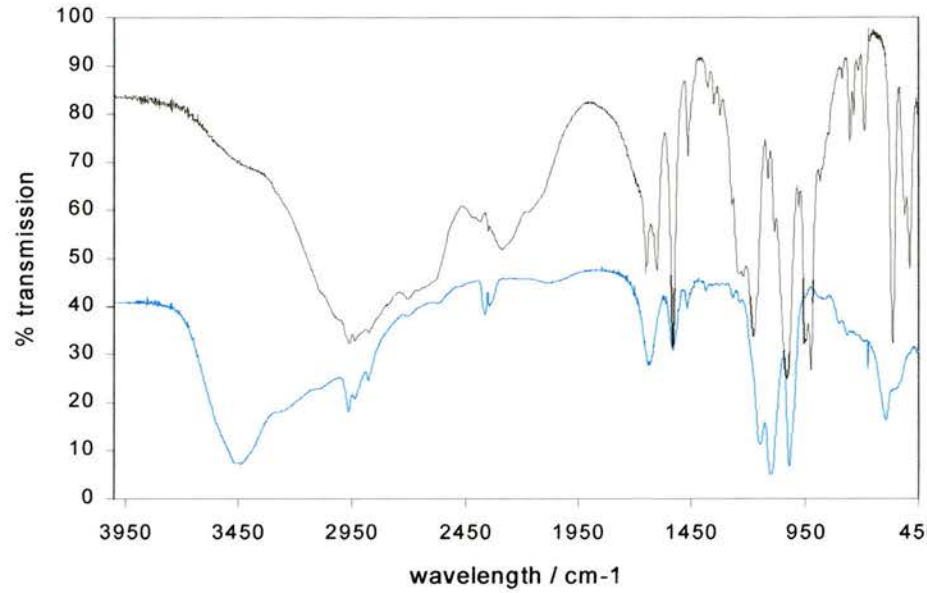

Figure 4.49: IR spectra of 1-aminobutylphosphonic acid (black) and aluminium 1-aminobutyl-phosphonate (blue).

Table 4.15: Summary of the IR spectra of 1-aminobutylphosphonic acid and aluminium 1-amino-butylphosphonate

Assigned vibration	**1-Aminobutyl PA**	**1-Aminobutylphosphonate**
O-H stretching/ H bonding		3440 cm^{-1}
N-H stretching		3260 cm^{-1}
N-H stretching/ H bonding		3086 cm^{-1}
C-H stretching/ CH_3	2962 cm^{-1}	2964 cm^{-1}
C-H stretching/ CH_2	2935 cm^{-1}	2934 cm^{-1}
C-H stretching/ CH_2	2875 cm^{-1}	2872 cm^{-1}
(P-)O-H stretching	2703 cm^{-1}	
(P-)O-H stretching	2288 cm^{-1}	
N-H deformation	1532 cm^{-1}	1528 cm^{-1}
C-H deformation/ P-CH_2	1466 cm^{-1}	1464 cm^{-1}
	1220 cm^{-1}	1233 cm^{-1}
	1175 cm^{-1}	1145 cm^{-1}
C-N stretching or O-P-O bending	1111 cm^{-1}	1097 cm^{-1}
	1027 cm^{-1}	1013 cm^{-1}
	923 cm^{-1}	

1145 cm^{-1} occur in the spectra of both 1-aminobutyl PA and the 1-aminobutylphosphonate respectively. The band due to either the C-N stretching or O-P-O bending vibration can be found at 1111 cm^{-1} in the acid and at 1097 cm^{-1} in the hydrothermal product, but not in the spectrum of the reflux product. A further band is present in all spectra; at 1027 cm^{-1} (acid) and 1013 cm^{-1} (phosphonate), while a distinct band at 923 cm^{-1} is only present in the spectrum of the acid.

4.6. Synthesis of aluminium 4-aminobenzylphosphonates

Most experiments with 4-aminobenzylphosphonic acid were done under reflux. The starting material for the majority of the reactions was gibbsite, although aluminium chloride was also used. Because of the insolubility of the acid in water, it was necessary to change the solvent for the reflux experiments. Preliminary solubility experiments with various organic solvents of different polarities failed to identify an appropriate solvent and therefore some experiments were carried out in an aqueous suspension and some in a mixture of water and dioxane. Later it was found that an increase in the pH value of the aqueous suspension *via* the addition of a mineral acid led to the dissolution of the 4-aminobenzylphosphonic acid. In contrast to the fact that all other aluminium phosphonates were white, the 4-aminobenzylphosphonates prepared under addition of mineral acids as well as the hydrothermal products turned out to be coloured in shades of pale yellow or brown. For reactions with aluminium chloride 4-aminobenzylphosphonic acid was recovered after the treatment.

Powder X-ray diffraction of aluminium 4-aminobenzylphosphonates

The powder XRD patterns of the products showed a range of interlayer spacings. The materials that had been treated with dilute mineral acids had *d* values of 14.80 Å, 14.84 Å, 15.04 Å and 15.35 Å that seemed to be distributed randomly over the different reaction conditions. The hydrothermal product had an interlayer spacing of 15.59 Å and the products prepared under reflux from an aqueous suspension and from a mixture of water and dioxane had their first reflections at 14.86 Å and 15.79 Å, respectively. The large *d* spacing is consistent with the large phosphonic acid used in the experiments. The powder XRD pattern of an aluminium 4-aminobenzylphosphonate is shown in Figure 4.50.

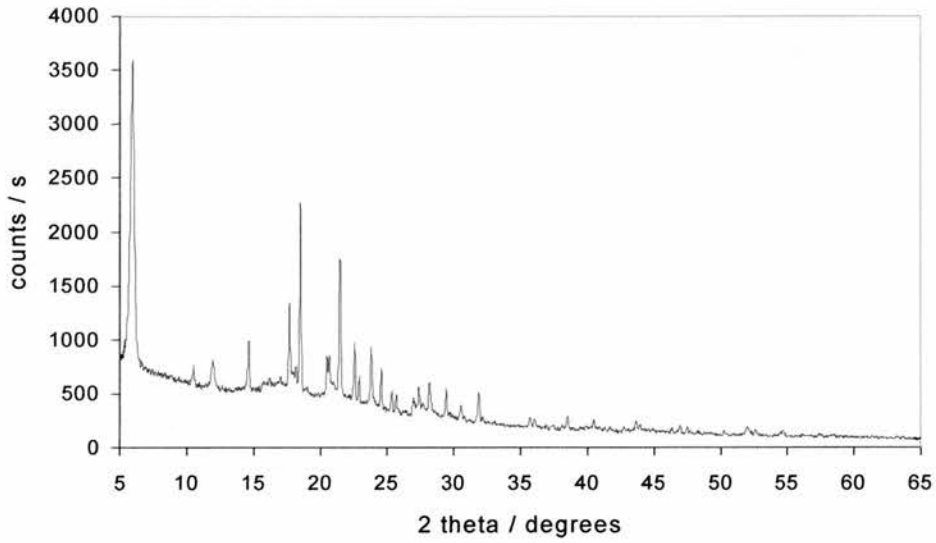

Figure 4.50: Powder XRD pattern of an aluminium 4-aminobenzylphosphonate prepared under addition of HCl.

Solid state MAS NMR spectroscopy of aluminium 4-aminobenzylphosphonates

The NMR spectra were acquired from samples prepared under addition of HCl. Samples prepared at different pH values showed only minor differences such as small contaminations. The signal in the ^{27}Al MAS NMR spectrum is caused by an octahedral aluminium site (Figure 4.51). It is similar in shift and shape to the peak in the

aluminium NMR of AlBzPO-1 (Figure 4.8). The ^{31}P MAS NMR spectrum (Figure 4.52) contains two peaks at 10.7 ppm and 22.3 ppm in a ratio of approx. 3:1. The 4-aminobenzylphosphonates therefore contain either two phosphorus sites in this ratio or only one site and a contamination by a second phase. The stronger peak has a very similar shift to the phosphorus in AlBzPO-1 (10.3 ppm, Figure 4.9a).

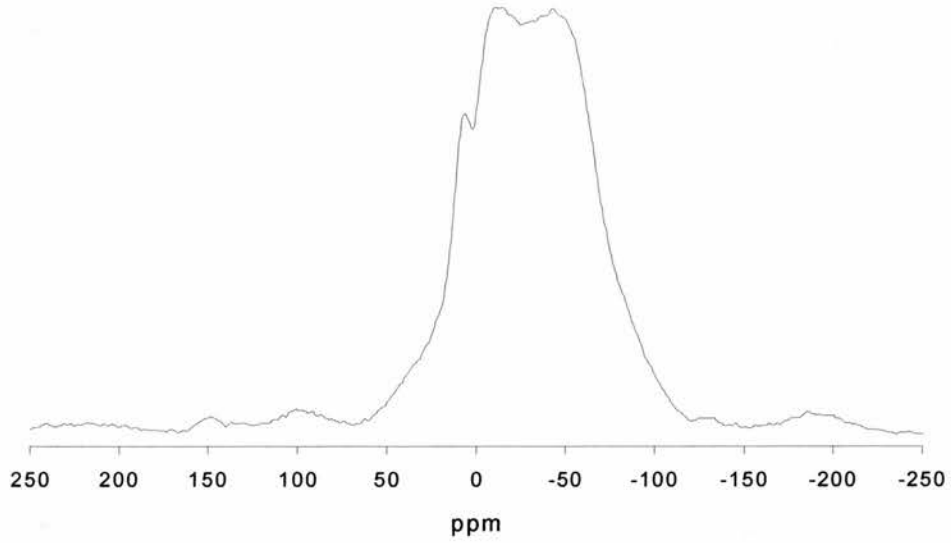

Figure 4.51: ^{27}Al MAS NMR spectrum of an aluminium 4-aminobenyzlphosphonate at 78.16 MHz prepared under addition of HCl.

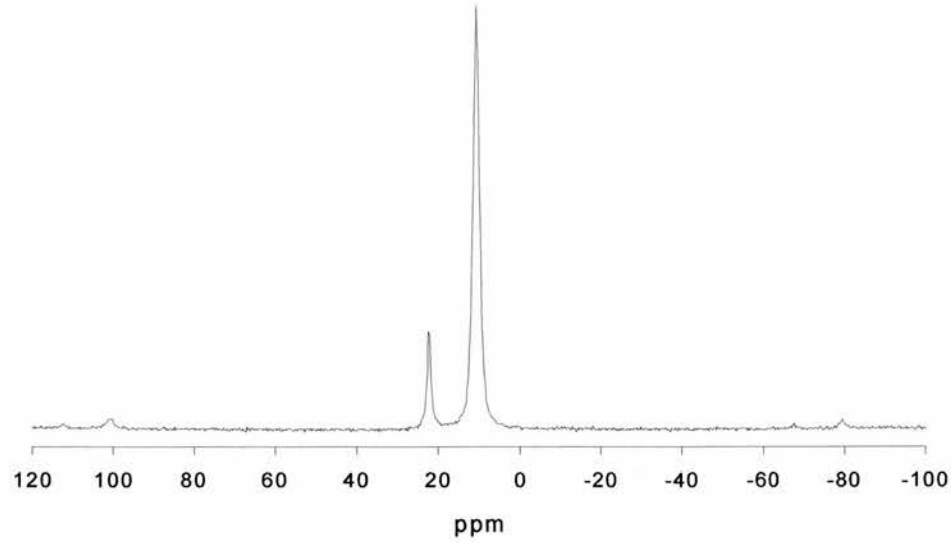

Figure 4.52: ^{31}P MAS NMR spectrum of an aluminium 4-aminobenyzlphosphonate at 121.42 MHz prepared under addition of HCl.

In the ^{13}C MAS NMR spectrum there are at least six peaks (Figure 4.53). A peak at 34.8 ppm is due to the methylene carbon. It should be split by the phosphorus atom to which it is connected, but the resolution may be too low to discern two peaks. The remaining peaks are in the range from 115 to 144 ppm and can be attributed to the benzyl group. The peak at 144.3 ppm is caused by the carbon (4) that is connected to the amino group. The signal at 115.7 ppm corresponds to carbon (1), which is connected to the methylene group. The signals at 125.6, 130.9 and 136.0 ppm are due to the remaining four benzyl carbons. As the peak at 136.0 ppm is weak compared to the other signals, it is possible that a second weak signal is hidden under the stronger ones. Again, the values are very similar to the shifts encountered in the spectrum of AlBzPO-1; there the methylene carbon can be found at 36.0 ppm and the carbons of the benzyl group give rise to signals between 120 and 140 ppm (Figure 4.10). Since the NMR shifts of AlBzPO-1 and aluminium 4-aminobenzylphosphonate are so similar and the two phosphonic acids are closely related to each other it seems possible that the two materials also have similar structures.

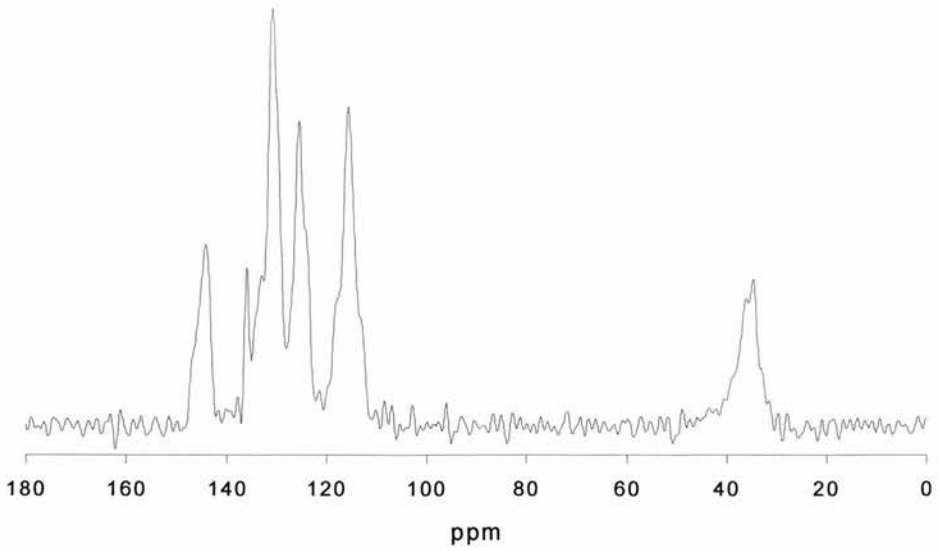

Figure 4.53: ^{13}C MAS NMR spectrum of an aluminium 4-aminobenyzlphosphonate at 75.43 MHz prepared under addition of HCl.

Thermogravimetric and CHN analysis of aluminium 4-aminobenzylphosphonates

The TGA's for the compounds prepared from pure water (1) and from a solution containing dilute HCl (2) showed major differences, even if their XRD patterns varied mainly in crystallinity and the intensity of the reflections and the interlayer distances differed only by 0.48 Å. However, this is not surprising since the interlayer distances are determined by the large 4-aminobenzyl groups. Water molecules could just fit in without changing the interlayer spacing.

In the TGA of compound (1) three mass losses occurred (Figure 4.54). The first loss at 113°C (endothermic) is quite likely due to a loss of water of crystallisation (4.08 %). At 327°C there is a mass loss of 26.89 % (exothermic), which is in the range for loss of water through condensation of hydroxyl groups. At 515°C another slightly exothermic loss can be observed (21.28 %), which is most likely due to the combustion of most of the organic groups. During further heating there is a slow weight loss up to 1200°C (observed 4.99 %). It is possible that the ratio of the losses at 327°C and 515°C

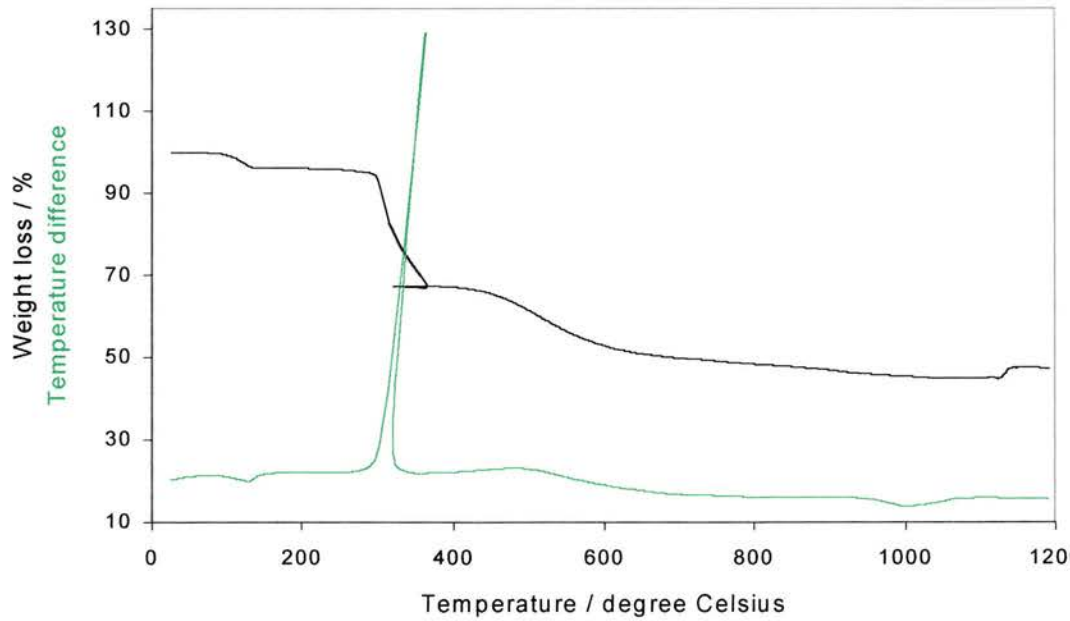

Figure 4.54: TGA trace of aluminium 4-aminobenzylphosphonate prepared in water (compound 1).

is obscured, as the first of these losses is strongly exothermic, leading to a sudden increase of temperature in the furnace. Subsequent cooling until the programmed temperature of the heating cycle is reached again leads to the graph moving backwards. A solution for this problem has not been found. The residue of 42.76 % is a mixture of $Al(PO_3)_3$ and $AlPO_4$.

In the TGA of compound (2) four mass losses occurred (see Figure 4.55). An endothermic loss of 4.43 % at 113°C most likely corresponds to the loss of water of crystallisation. An exothermic loss at 308°C could possibly be due to the condensation of hydroxyl groups or the loss of water that is more strongly bound to the framework (4.93 %). The third loss at 475°C is exothermic as well and can be attributed to the loss of the organic groups (38.60 %). The final exothermic loss at 687°C could result from the loss of volatile phosphorous oxides or chlorine (13.79 %). The residue (38.25 %) is composed of a mixture of $Al(PO_3)_3$, $AlPO_4$ and possibly a chlorine-containing

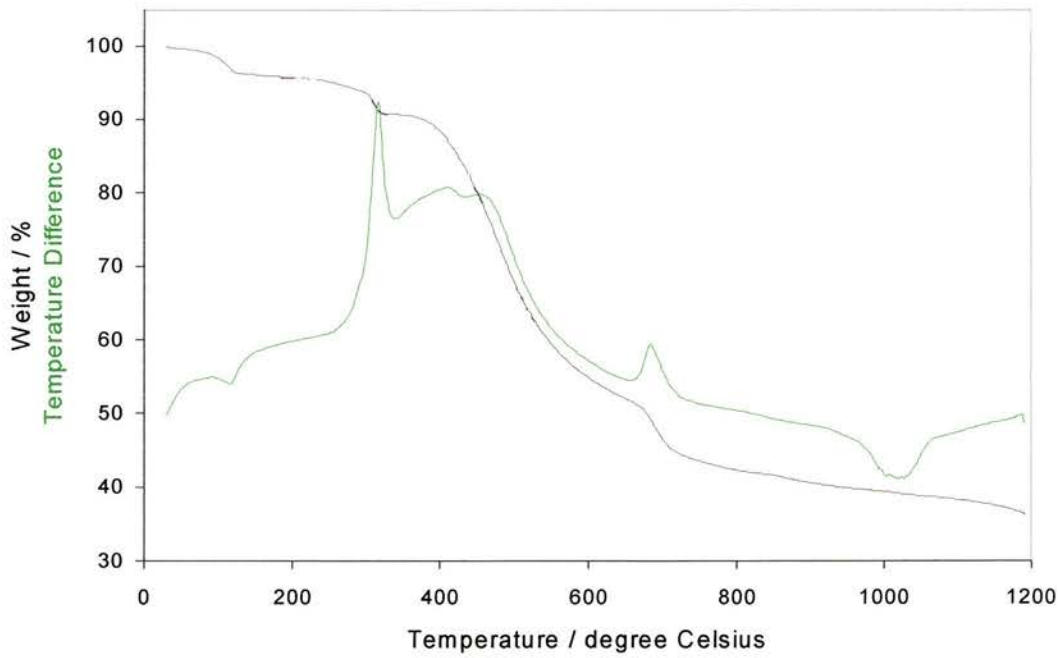

Figure 4.55: TGA trace of aluminium 4-aminobenzylphosphonate prepared in dilute HCl (compound 2).

compound with a structure similar to $Al(PO_3)_{2.4}F_{0.6}$. This was concluded from a comparison with known XRD patterns.

CHN analyses of both compounds resulted in the following values;

composition of compound (1)	38.56 % C	4.69 % H	6.27 % N
composition of compound (2)	38.90 % C	4.67 % H	6.44 % N.

Attempts to match the results of TGA and CHN to a variety of empirical formulae failed, which can be expected as the samples do not seem to be pure.

IR spectroscopy of aluminium 4-aminobenzylphosphonates

Although there are differences in the TGA for some of the 4-aminobenzylphosphonates, their IR spectra are very similar and they also have several bands in common with the IR spectrum of AlBzPO-1 (Figure 4.12 and Table 4.4). The O-H stretching vibration found in the spectrum of 4-aminobenzylphosphonate at 3651 cm^{-1} is also present in the spectrum of AlBzPO-1, as are the O-H··· stretching bands at 3495 cm^{-1} and 3352 cm^{-1}. The aromatic C-H stretching vibration has either shifted to 2965 cm^{-1} in the phosphonate or it is overlapped by a stronger band, because in the 4-aminobenzyl PA, it is situated at 3039 cm^{-1}, similar to the benzyl PA and the benzylphosphonate. The C-H stretching vibration of the CH_2 group is found at 2917 cm^{-1} and 2901 cm^{-1} for the 4-aminobenzyl PA and the corresponding phosphonate, respectively. There are two (P-)O-H stretching bands at 2623 cm^{-1}/ 2616 cm^{-1} and 2159 cm^{-1}/ 2126 cm^{-1} in the respective spectra of the acid and the phosphonate. Therefore, it can be assumed that the phosphonate contains either an impurity or that the bands are indeed due to (Al-)O-H vibrations instead. As the formula of the

4-aminobenzylphosphonate is yet unknown, this cannot be established with certainty.

The broad H_2O deformation vibration band is visible in both spectra at approx. 1628 cm^{-1} and the N-H deformation vibration can be found at 1566 cm^{-1}. The C-H deformation band of the CH_2 group can be found at 1438 cm^{-1} for acid and phosphonate and there is another band at 1229 cm^{-1} also present in both spectra. The C-H deformation vibration band for the monosubstituted aromatic ring seems to differ from the acid (1097 cm^{-1}) to the phosphonate (1122 cm^{-1}), while the O-P-O stretching vibration is in the same place in both spectra at 1090 cm^{-1}. A further three bands can be found in the same position for the acid as well as for the phosphonate; two unassigned ones at 1065 cm^{-1} and 931 cm^{-1} and another C-H deformation band of the monosubstituted aromatic ring at 829 cm^{-1} (see Figure 4.56 and Table 4.16).

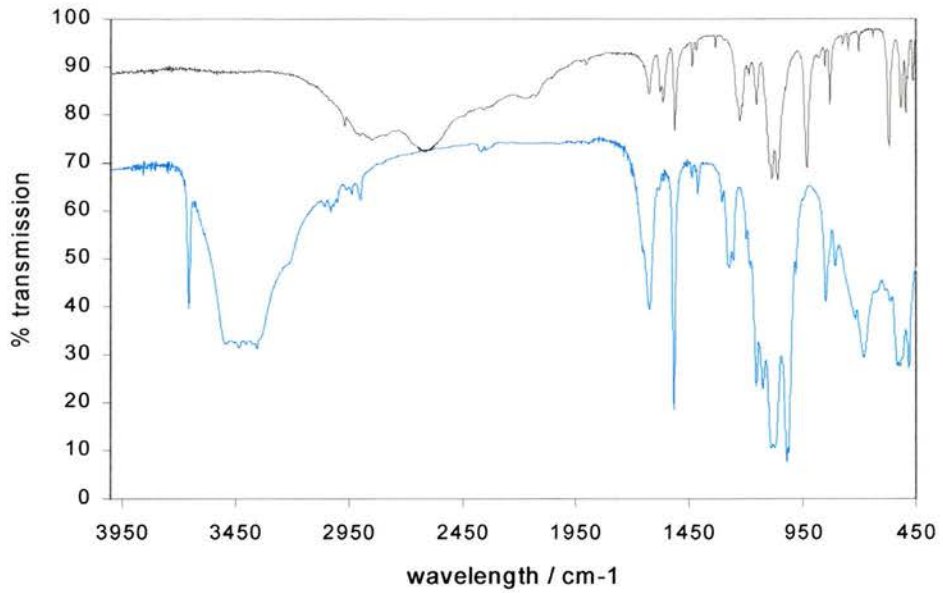

Figure 4.56: IR spectra of 4-aminobenzylphosphonic acid (black) and of aluminium 4-amino-benzylphosphonate (blue).

Table 4.16: Summary of the IR spectra of 4-aminobenzylphosphonic acid and aluminium 4-aminobenzylphosphonate.

Assigned vibration	4-Aminobenzyl PA	4-Aminobenzyl-phosphonate
Free O-H stretching		3651 cm^{-1}
O-H stretching/ H bonding		3495 cm^{-1}
O-H stretching/ H bonding		3352 cm^{-1}
C-H stretching/ aromatic	3039 cm^{-1}	2965 cm^{-1}
C-H stretching/ CH_2	2917 cm^{-1}	2901 cm^{-1}
(P-)O-H stretching	2623 cm^{-1}	2616 cm^{-1}
(P-)O-H stretching	2159 cm^{-1}	2126 cm^{-1}
H_2O deformation	1628 cm^{-1}	1626 cm^{-1}
N-H deformation	1566 cm^{-1}	1565 cm^{-1}
C-H deformation/ P-CH_2	1438 cm^{-1}	1438 cm^{-1}
	1229 cm^{-1}	1229 cm^{-1}
C-H deformation monosubstituted aromatic ring	1097 cm^{-1}	1122 cm^{-1}
O-P-O stretching	1090 cm^{-1}	1089 cm^{-1}
	1064 cm^{-1}	1066 cm^{-1}
	931 cm^{-1}	931 cm^{-1}
C-H deformation monosubstituted aromatic ring	829 cm^{-1}	829 cm^{-1}

In the NMR spectra, the shifts for all nuclei are very similar to the values found for AlBzPO-1 (Section 4.1.1). It is therefore fair to assume a similar structure for the aluminium 4-aminobenzylphosphonates. Differences could arise from the possible incorporation of chlorine into the structure and from hydrogen bonding due to the amino group. Further more, if the weak peak observed in the ^{31}P MAS NMR spectra is indeed due to an impurity, this would explain the problems in assigning the mass losses in the TGA and in indexing the X-ray powder patterns.

4.7. Synthesis of aluminium iminobis(methylphosphonates)

The synthesis of aluminium iminobis(methylphosphonates) was attempted under a variety of reaction conditions, but in no case the reaction product was crystalline enough to allow any characterisation by X-ray powder diffraction. The main features in the powder patterns are two broad peaks of very low intensity at approx. 11.2 Å and 3.7 Å,

with additional smaller peaks at 7.9, 7.2 and 5.8 Å (Figure 4.57). Neither variation of the aluminium source, nor of the reaction conditions (Al:P ratio, pH value, reaction time and reaction temperature) brought any change in the result of the experiments. It is therefore possible that the preparation of crystalline aluminium diphosphonates is only possible in the pyridine/HF system instead of an aqueous system.[14]

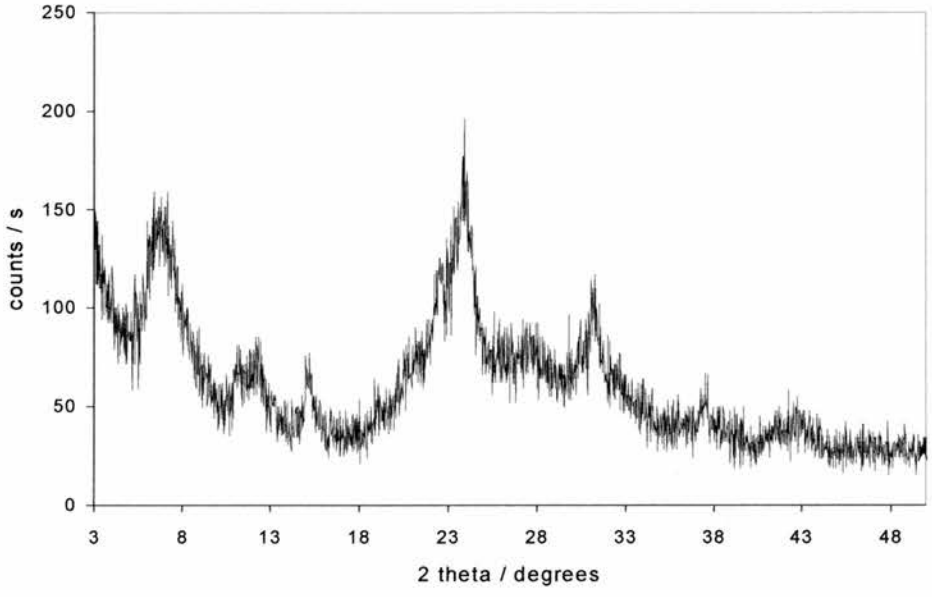

Figure 4.57: Powder XRD pattern of an aluminium iminobis(methylphosphonate).

Solid state MAS NMR spectroscopy of aluminium iminobis(methylphosphonate)

Due to the lack of a suitably crystalline material for X-ray diffraction the characterisation of aluminium iminobis(methylphosphonate) was only possible using solid state MAS NMR spectroscopy. In the ^{27}Al MAS NMR spectrum there is one peak at -19.3 ppm, which is caused by aluminium in octahedral coordination (Figure 4.58). In the ^{31}P MAS NMR spectrum there are three peaks, a strong one at -6.6 ppm and two weak peaks at -0.2 ppm and 3.2 ppm respectively (Figure 4.59). The two weak peaks could indicate two additional independent phosphorus environments or they could be due to a by-product contaminating the phosphonate. In the ^{13}C MAS NMR a single but rather broad peak can be found at 47.7 ppm (Figure 4.60). This is in the range of the

methylene carbon bound to nitrogen in aluminium 1-aminobutylphosphonate (50.3 ppm; Figure 4.47). In the ^{15}N MAS NMR spectrum there is a single peak at -342.1 ppm (Figure 4.61). This is surprisingly close to the value for AlaPrPO-1 (-346.6 ppm; Figure 4.28). As secondary amines have similar shifts to primary amines,[11] it may be possible that the nitrogen in the aluminium iminobis(methylphosphonate) is also protonated.

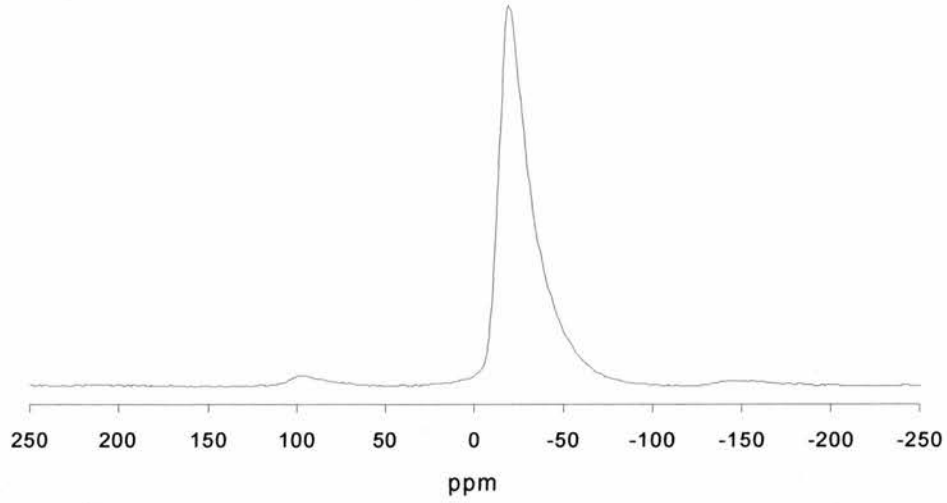

Figure 4.58: ^{27}Al MAS NMR spectrum of aluminium iminobis(methylphosphonate) at 78.16 MHz.

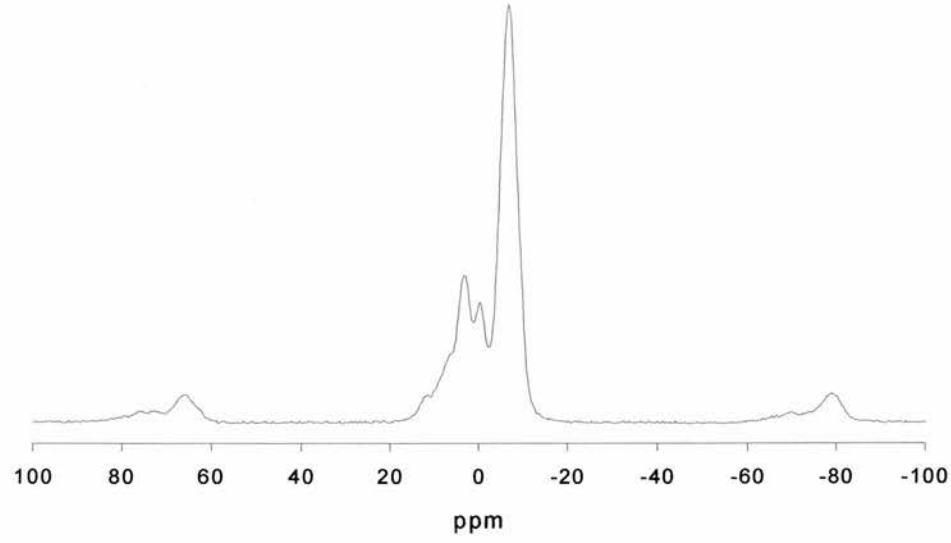

Figure 4.59: ^{31}P MAS NMR spectrum of aluminium iminobis(methylphosphonate) at 121.42 MHz.

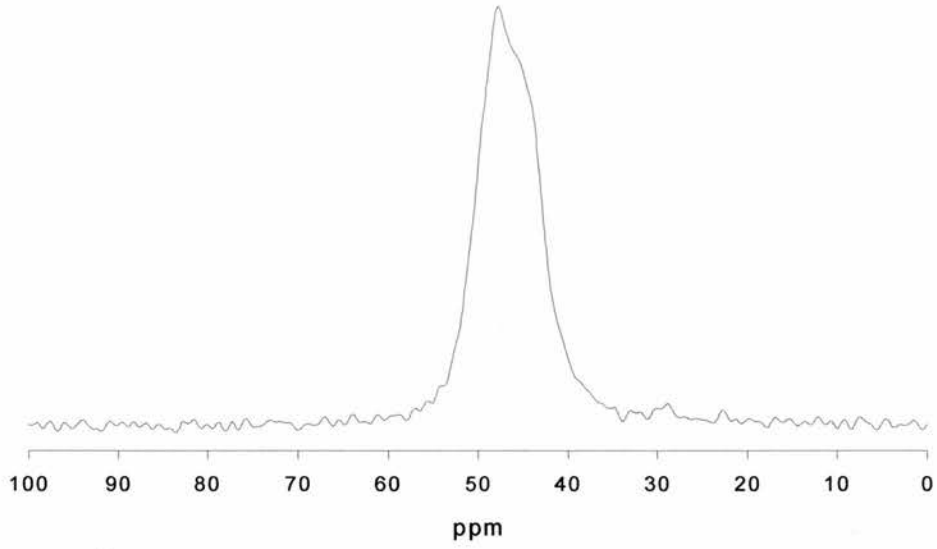

Figure 4.60: ^{13}C MAS NMR of aluminium iminobis(methylphosphonate) at 75.43 MHz.

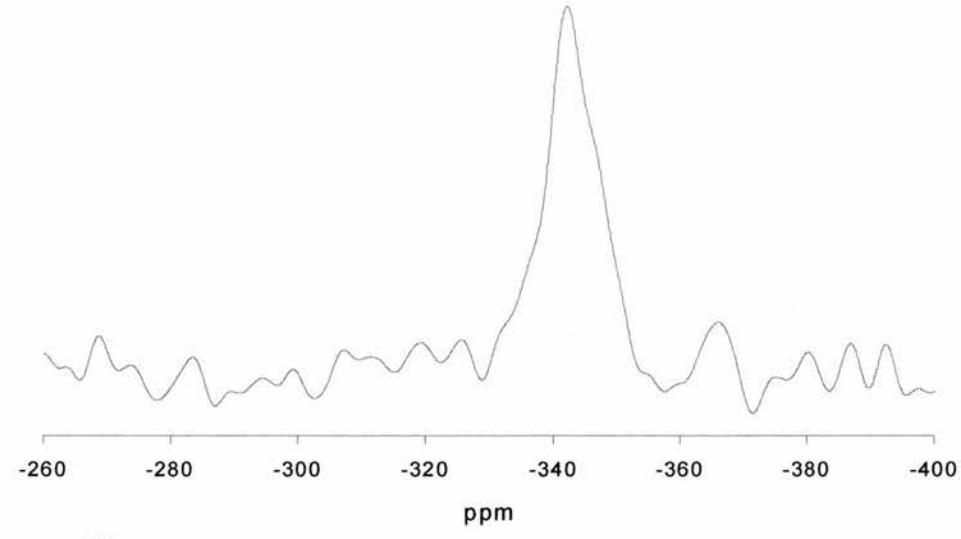

Figure 4.61: ^{15}N MAS NMR of aluminium iminobis(methylphosphonate) at 30.40 MHz.

Thermogravimetric and CHN analysis of aluminium iminobis(methylphosphonate)

The first mass loss in the TGA (7.63 %) takes place around 80 °C. It is presumably due to loosely attached water molecules in the material. The second mass loss (15.00 %) starts at about 350 °C and continues until 1050 °C, leaving a residue of 77.37 %. The results for the CHN analysis have the following values; 9.43 % C, 1,47 % H and 5.19 % N.

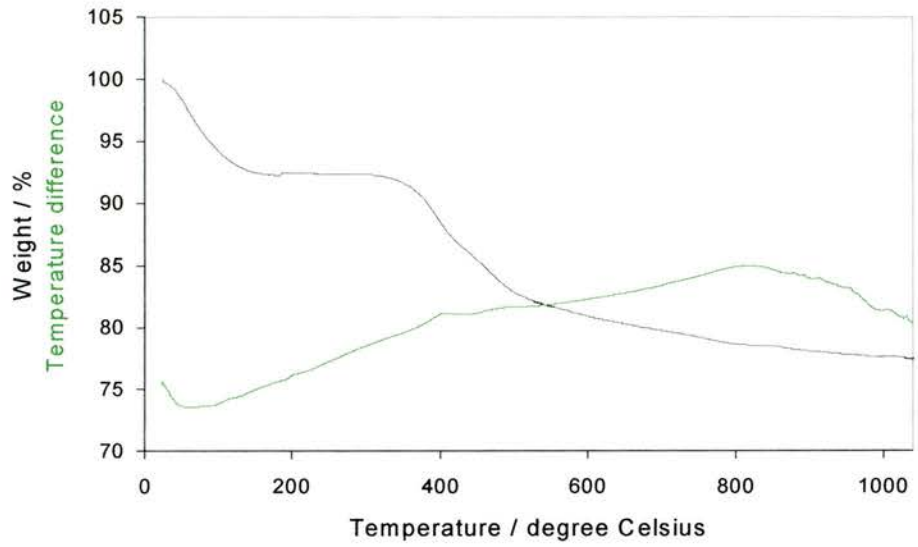

Figure 4.62: TGA trace of aluminium iminobis(methylphosphonate).

IR spectroscopy of aluminium iminobis(methylphosphonate)

In the spectrum of iminobis(methylphosphonic acid) the features are much clearer than in the spectrum of the corresponding phosphonate. Especially in the fingerprint region, the phosphonate spectrum contains a few broad bands that obliterate most of the bands that can be found in the spectrum of the acid, although some shoulders remain visible.

Between 3600 and 1950 cm^{-1} there are several broad bands in the spectrum of the aluminium iminobis(methylphosphonate) that are centred at approximately 3380 cm^{-1}, 3060 cm^{-1}, 2800 cm^{-1} and 2560 cm^{-1}. The first band can be attributed to O-H stretching vibrations with H-bonding, the second to N-H stretching with H-bonding and the third one to the C-H stretching of the methylene groups. In the fingerprint region a few strong bands can be found, together with a variety of weak bands and shoulders, indicated by *(w)*. The band at 1588 cm^{-1} is presumably due to N-H deformation vibrations. The C-H deformation could be either a band at 1437 cm^{-1} or at 1473 cm^{-1}

(w). Four bands that can also be found in most other phosphonates are situated at 1254 cm^{-1}, 1131 cm^{-1}, 1053 cm^{-1} *(w)* and 933 cm^{-1}.

In the spectrum of the iminobis(methylphosphonic acid), a broad band caused by O-H stretching vibrations with hydrogen bonding is centred at 3430 cm^{-1}. The band at 3013 cm^{-1} is due to N-H stretching with hydrogen bonding. A rather broad feature around 2790 cm^{-1} could stem from the C-H stretching vibrations. The band at 2660 cm^{-1} is caused by (P-)O-H stretching. N-H deformation vibrations may give rise to the band at 1602 cm^{-1}. The C-H deformation vibration could be either the band at 1509 cm^{-1} or at 1427 cm^{-1}. Three of the bands common for phosphonate groups can be found at 1223 cm^{-1}, 1127 cm^{-1} and 1053 cm^{-1}.

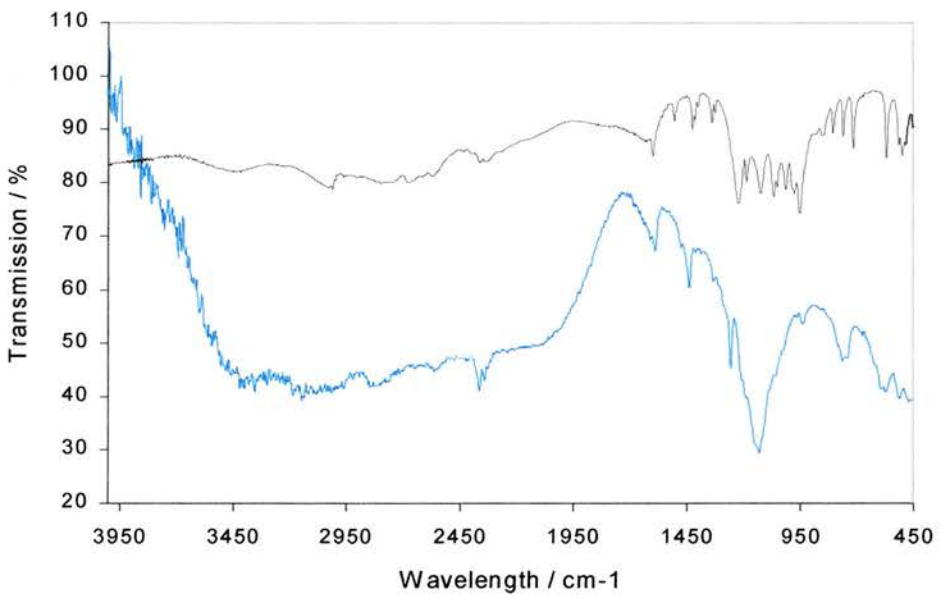

Figure 4.63: IR spectra of iminobis(methylphosphonic acid) (black) and aluminium iminobis-(methylphosphonate) (blue).

Table 4.17: Comparison of the IR spectra of iminobis(methylphosphonic acid) and aluminium iminobis(methylphosphonate).

Assigned vibration	Iminobis(methyl PA)	Al iminobis(methylphosphonate)
O-H stretching/ H bonding	3430 cm^{-1}	3380 cm^{-1}
N-H stretching/ H bonding	3013 cm^{-1}	3060 cm^{-1}
C-H stretching/ CH_2		2800 cm^{-1}
(P-)O-H stretching	2660 cm^{-1}	
N-H deformation	1602 cm^{-1}	1588 cm^{-1}
C-H deformation/ P-CH_2	1509 cm^{-1} or 1427 cm^{-1}	1473 cm^{-1} *(w)* or 1437 cm^{-1}
	1223 cm^{-1}	1254 cm^{-1}
	1127 cm^{-1}	1131 cm^{-1}
	1053 cm^{-1}	1053 cm^{-1}
		933 cm^{-1}

4.8. Synthesis of aluminium vinylphosphonates

Microcrystals of aluminium vinylphosphonate could be prepared under hydrothermal conditions (see Chapter 3.8) at an Al:P molar ratio of 1:1 when the reaction time was increased from 2.5 days (polycrystalline product) to 17 days. The powder XRD pattern of the microcrystalline product with a *d*-spacing of 9.67 Å is shown in Figure 4.64. An Al:P ratio of 1:1.5 yielded a product of low crystallinity with an interlayer spacing of 9.78 Å at 2.5 days. As the positions of the first 16 reflections in the powder XRD pattern of this material coincided with the more intense reflections in the pattern of the polycrystalline compound, only the more promising reaction conditions were investigated further in this work. Experiments concerned with the establishment of appropriate reaction conditions for the preparation of aluminium vinylphosphonates were carried out by G.B. Hix.[15]

The powder X-ray diffraction patterns suggested the layered structure of aluminium vinylphosphonate. Microcrystals were then investigated using the diffraction facilities at station 9.8 of the Synchrotron Radiation Source in Daresbury.

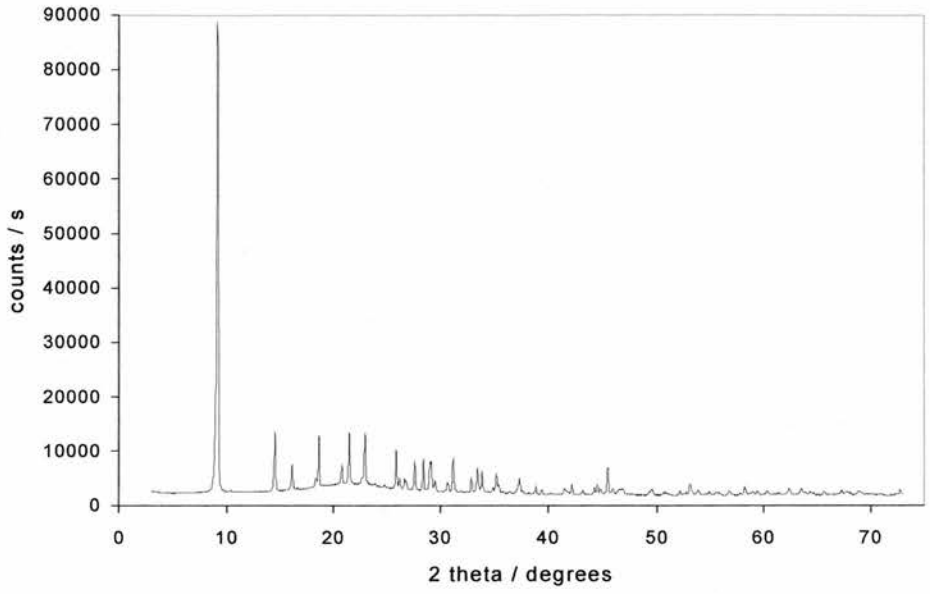

Figure 4.64: Powder XRD pattern of polycrystalline aluminium vinylphosphonate.

However, despite their regularity in two dimensions (presumably the inorganic layers) the third dimension (stacking of the layers) was disordered. Attempts to investigate the crystals by HRTEM failed because the material is not stable toward the electron beam. However, after initial failure to index the streaky patterns obtained from microcrystals at the Daresbury Synchrotron Radiation Source, high quality laboratory (Stoe STADIP) powder XRD data were collected. The pattern could be indexed as monoclinic with unit cell parameters of approximately a = 10.054 Å, b = 19.502 Å, c = 7.048 Å and β = 107.33° (FOM M(20) = 19) using the TREOR90 software.[1]

The systematic absences were consistent with the presence of a 2_1 screw axis, but there may also be glide plane absences, which are not easy to confirm in this pattern. Possible space groups would then be $P2_1/c$, $P2_1/a$, $P2_1/n$ and $P2_1/m$. Initial attempts to solve the structure form this data failed, so a high resolution synchrotron powder XRD pattern was collected on station 2.3 at the Daresbury Synchrotron Radiation Source. The pattern indexed using TREOR90[1] in the same monoclinic unit cell, but once again the systematic absences could not clearly distinguish between the space groups

mentioned above. The LeBail fit of the aluminium vinyl-phosphonate obtained with GSAS[3] is shown in Figure 4.65. Structure factors were extracted from the LeBail fit to the data, and were passed through the Direct Methods part of the program EXPO.[10] The most likely solution was found in spacegroup $P2_1/c$ (R_{EXPO} = 11.99 %). Further experiments are underway in order to complete the structure by Rietveld/Fourier methods.

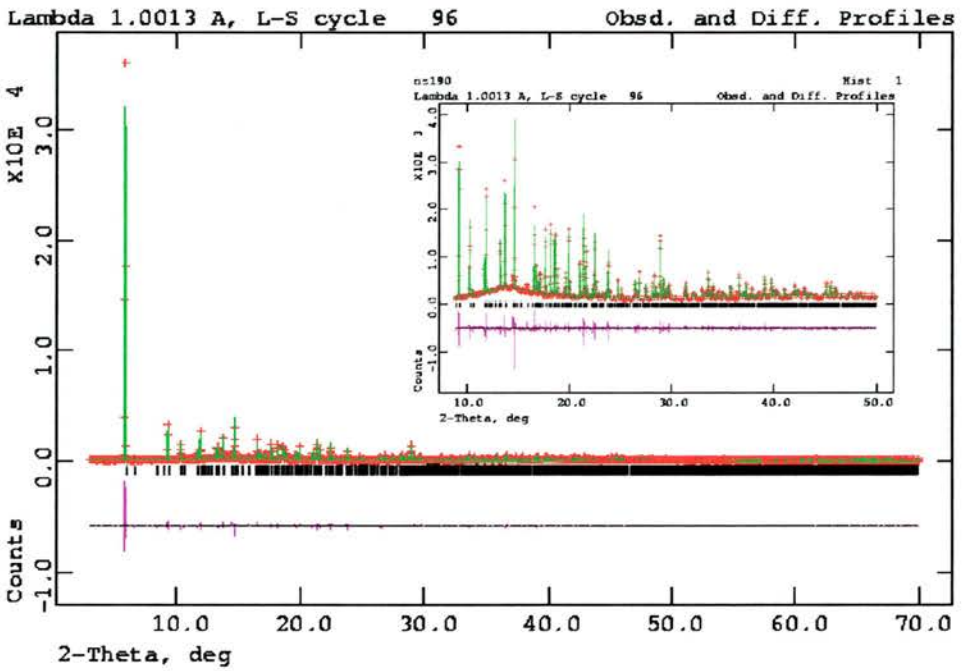

Figure 4.65: LeBail fit of the powder XRD pattern of aluminium vinylphosphonate.

Solid state MAS NMR spectroscopy of aluminium vinylphosphonate

The ^{27}Al NMR spectrum (Figure 4.66) corresponds to a single aluminium environment with an octahedral coordination. Its isotropic shift is close to 0 ppm. The ^{31}P NMR spectrum contains a single peak at 6.2 ppm and a small amount of an impurity (Figure 4.67), so the material contains only a single phosphorus environment. In the ^{13}C NMR spectrum three different peaks can be found at 129.9, 131.7 and 134.4 ppm (Figure 4.68). The peaks at 131.7 and 134.4 ppm are due to the carbon that is connected to the phosphorus atom. The peak at 129.9 ppm is caused by the other carbon atom of the vinyl group.

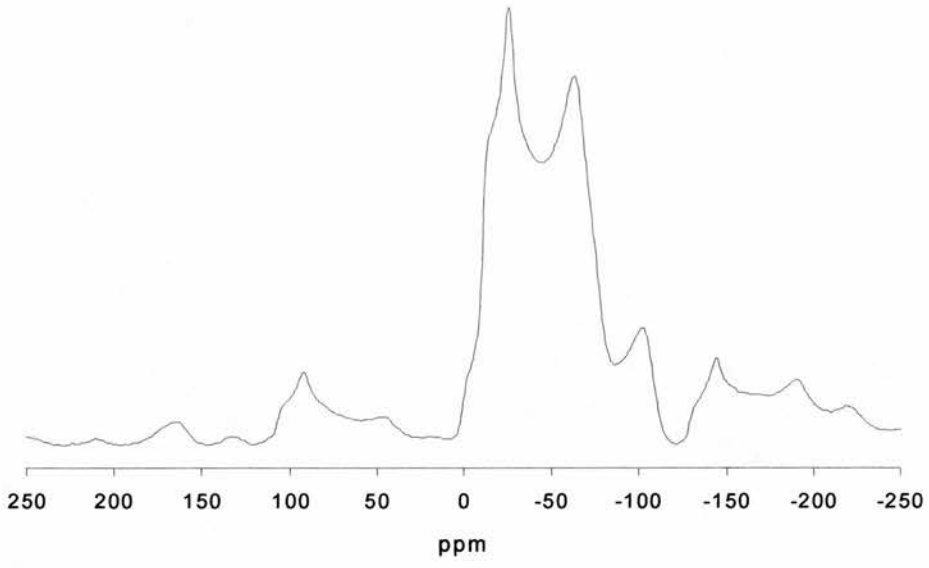

Figure 4.66: ^{27}Al MAS NMR spectrum of aluminium vinylphosphonate at 78.16 MHz.

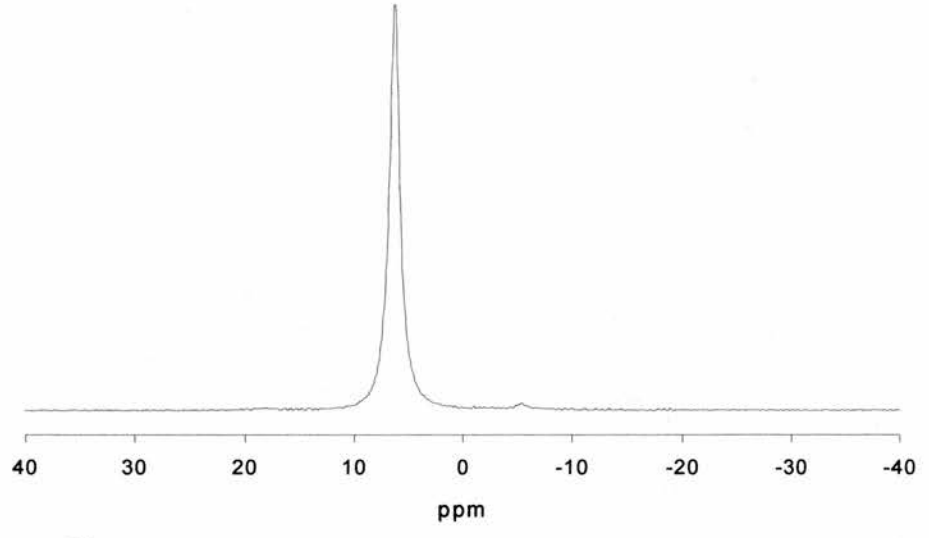

Figure 4.67: ^{31}P MAS NMR spectrum of aluminium vinylphosphonate at 121.42 MHz.

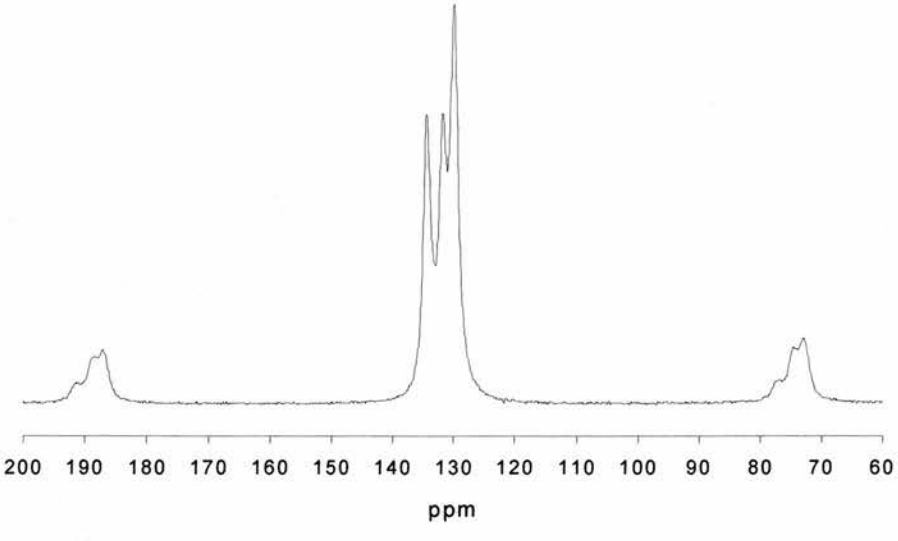

Figure 4.68: ^{13}C MAS NMR spectrum of aluminium vinylphosphonate at 75.43 MHz.

Thermogravimetric and CHN analysis of aluminium vinylphosphonate

In the TGA there are two distinctive mass losses at approx. 95 °C (8.26 %) and 145 °C (12.67 %) followed by a slight weight gain at 315 °C (0.88 %) and a final loss between 320 and 800 °C (9.23 %, Figure 4.69). As there is no definite idea concerning the empirical formula of the material, it is hard to make any assumptions regarding the events taking place during decomposition. However, it is fair to attribute the first mass loss to loosely attached water molecules. The TGA residue was found to be $AlPO_4$ from powder X-ray diffraction. The results of the CHN analysis are as follows; 6.93 % C and 4.17 % H.

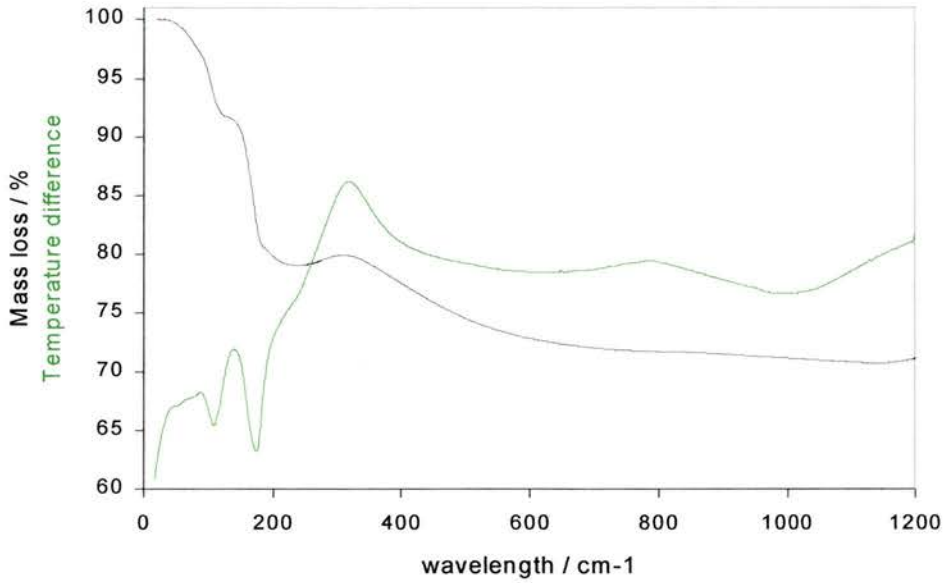

Figure 4.69: TGA trace of aluminium vinylphosphonate.

Further experiments were carried out trying to establish what happens when the material is heated. To this end, small samples were subjected to a series of TGA experiments with the final temperature staggered by 50 K. The results are shown in Figure 4.70. The powder pattern changes significantly between 100 and 150 °C, presumably due to the loss of water and ensuing changes in the structure. Apart from decreasing crystallinity the pattern then stays comparatively unaltered up to 500 °C,

with the first reflection at about 6° 2θ. However, it has to be mentioned that the patterns in Figure 4.70 are heavily scaled to allow comparison of graphs with widely differing crystallinity. The intensities of the original patterns range from 85000 for the 'as prepared' sample, to 1800 for the sample heated to 50 °C, to only 140 for the 400 °C sample.

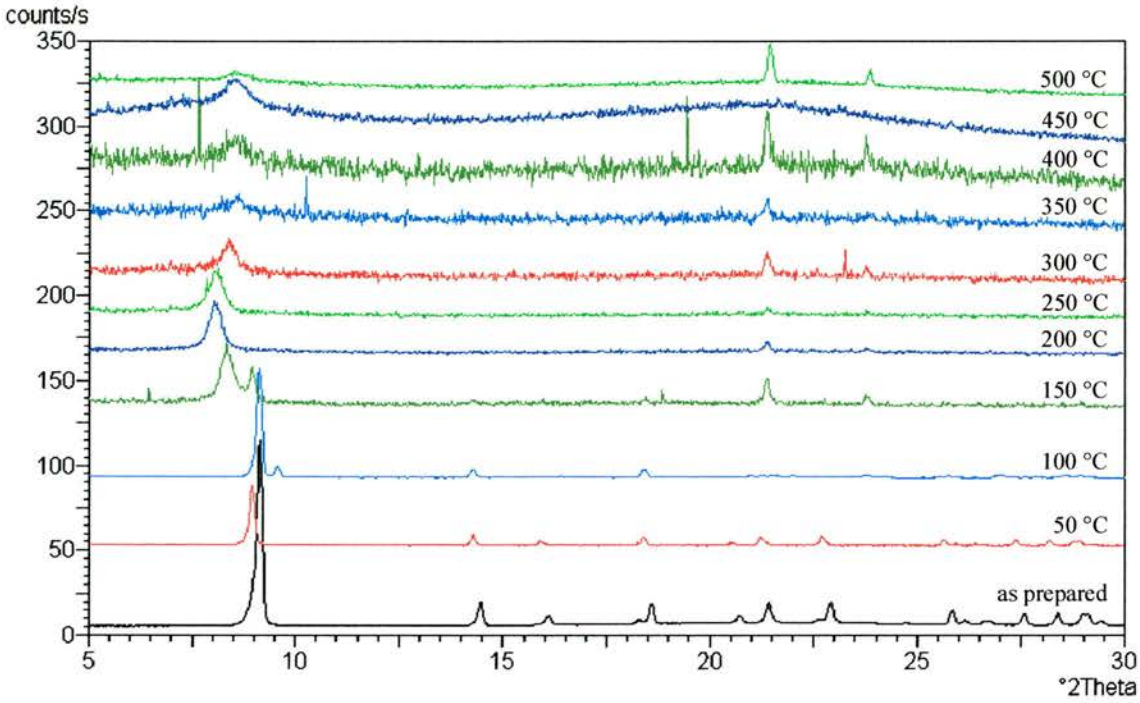

Figure 4.70: Powder XRD patterns for a succession of aluminium vinylphosphonate samples heated to different temperatures under oxygen. The scaling of the y-axis is arbitrary.

IR spectroscopy of aluminium vinylphosphonate

In the spectrum of the aluminium vinylphosphonate, there is a very broad band between 3670 cm^{-1} and 2900 cm^{-1}. It contains a shoulder at 3615 cm^{-1}, which is in the range for O-H stretching without H-bonding, and a distinct band at 3430 cm^{-1} that is caused by O-H stretching with H-bonding. A broad band centred at 1955 cm^{-1} could not be assigned. Vinyl groups should lead to two bands between 1800 and 1850 cm^{-1}. However, this area is still covered by the aforementioned broad band. The C=C

stretching of the vinyl group could cause the band at 1639 cm^{-1} although this is also the area of the water deformation vibration. The vinyl group also gives rise to the bands at 1411 cm^{-1} and 1274 cm^{-1} and the bands at 1156 cm^{-1} and 1058 cm^{-1} are common for phosphonates.

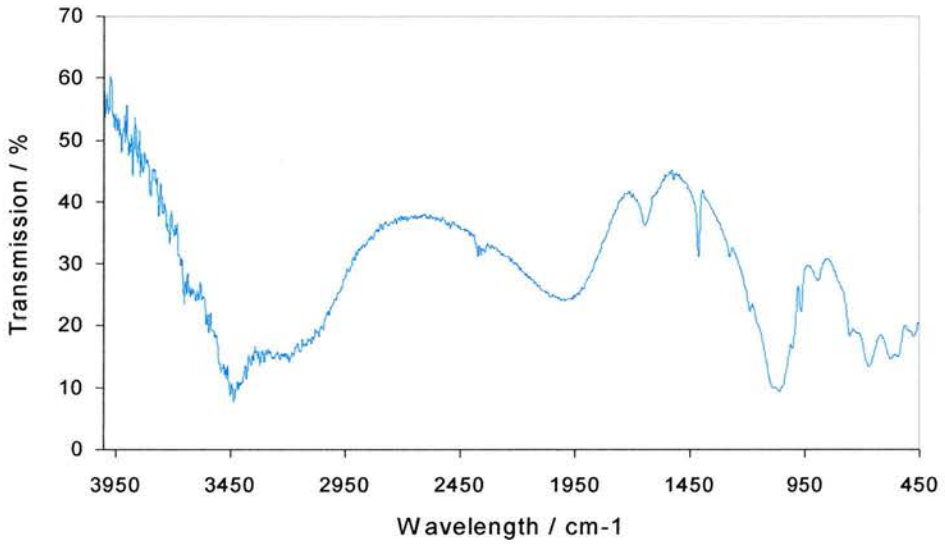

Figure 4.71: IR spectrum of aluminium vinylphosphonate.

Table 4.18: Summary of the main bands in the IR spectrum of aluminium vinylphosphonate.

Assigned vibration	**Al vinylphosphonate**
O-H stretching	3615 cm^{-1}
O-H stretching/ H bonding	3430 cm^{-1}
	1955 cm^{-1}
C=C stretching	1639 cm^{-1}
Vinyl group	1411 cm^{-1}
Vinyl group	1274 cm^{-1}
	1156 cm^{-1}
	1058 cm^{-1}

4.9. Synthesis of aluminium carboxymethylphosphonates

4.9.1. Aluminium carboxymethylphosphonate $Al(O_3PCH_2CO_2).3H_2O$

An aluminium carboxymethylphosphonate was successfully prepared using the method and reaction conditions that were unsuccessful in the case of aluminium

iminobis(methylphosphonate) (see Chapters 3.8 and 4.7). A powder XRD pattern is shown in Figure 4.72. The structure of the material was determined from single crystal data. Comparison of this structure with the literature proved it to be $Al(O_3PCH_2CO_2).3H_2O$, a compound previously published by Hix *et al.* (see Figure 1.20, pg. 39).[16] In their paper it was prepared from a different starting material using a structure directing agent (*n*-butylamine).

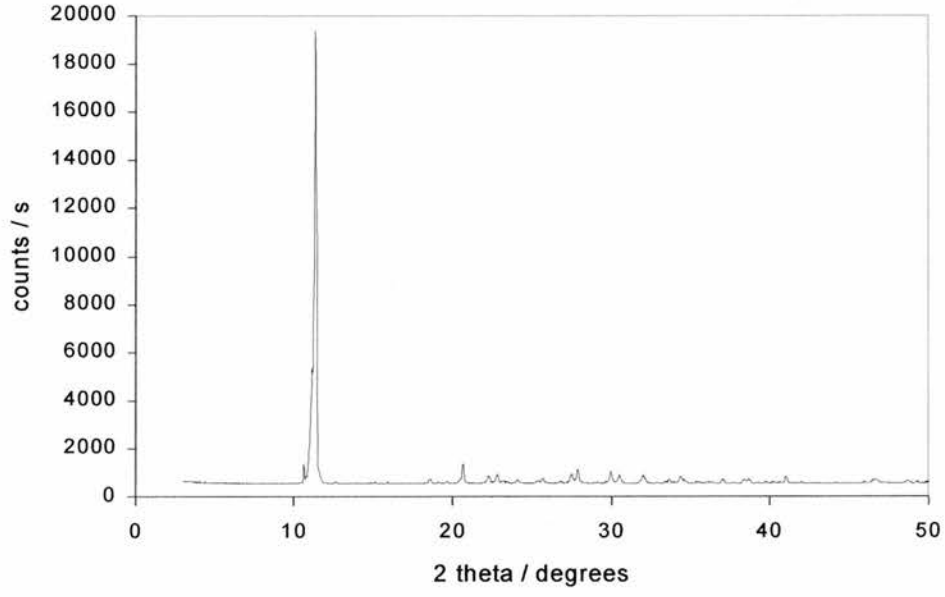

Figure 4.72: Powder XRD pattern of the aluminium carboxymethylphosphonate $Al(O_3PCH_2CO_2).3H_2O$.[16]

Solid state MAS NMR spectroscopy and IR spectroscopy of $Al(O_3PCH_2CO_2).3H_2O$

The products were further confirmed to be identical by the results of ^{31}P and ^{13}C MAS NMR (Figures 4.73 and 4.74 respectively) and IR spectroscopy (Figure 4.75). The ^{31}P MAS NMR spectrum has three peaks at -1.9, -4.4 and -7.5 ppm. The first and the last of these peaks are in good accord with the shifts for the two phosphorus sites mentioned in the paper. The peak at -4.4 ppm is much weaker than the other two and could be due to a contamination. In the ^{13}C MAS NMR spectrum there are four peaks at 35.2, 36.8, 174.1 and 177.0 ppm. The two peaks at 35.2 and 36.8 ppm can be

assigned to the methylene carbon, with the signal split by the adjacent phosphorus atom. The peak at 177.0 ppm is caused by the carbonyl carbon and the weak signal at 174.1 ppm could again be due to a contamination.

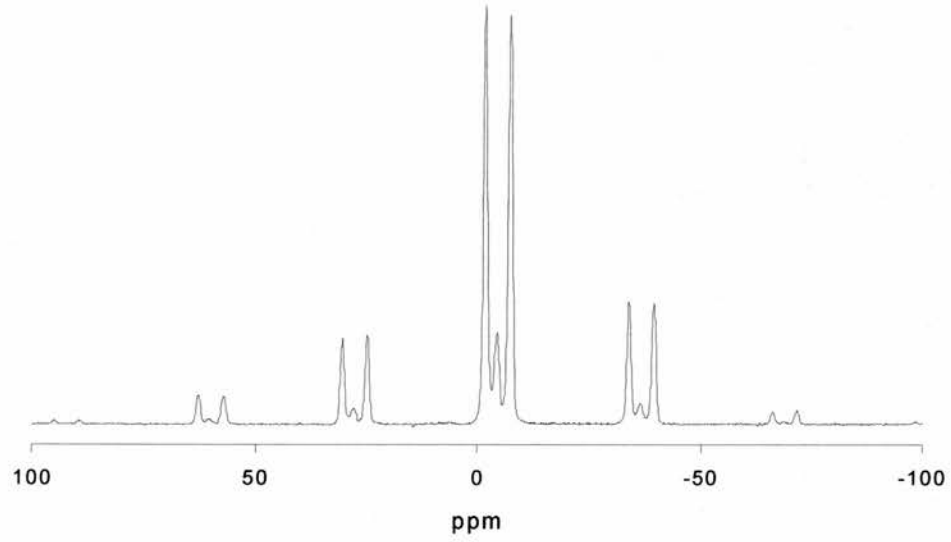

Figure 4.73: ^{31}P MAS NMR spectrum of the aluminium carboxymethylphosphonate $Al(O_3PCH_2CO_2).3H_2O$ at 121.42 MHz.

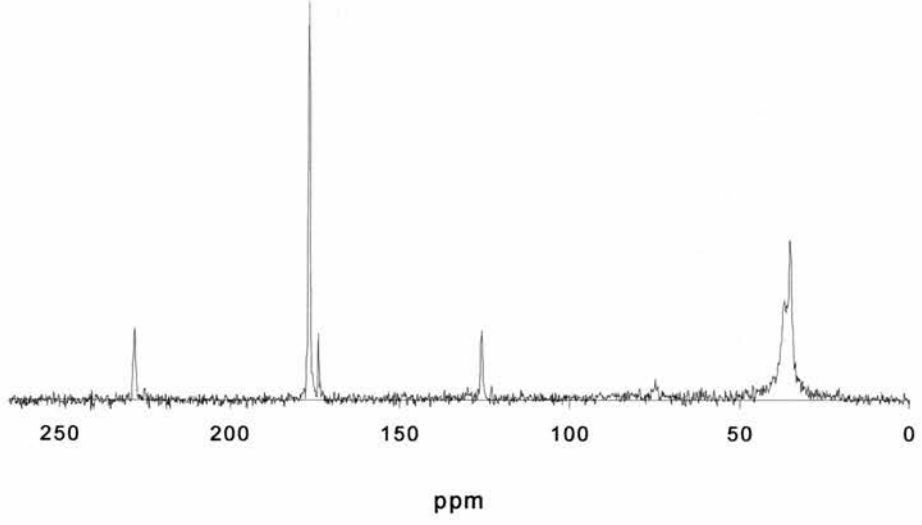

Figure 4.74: ^{13}C MAS NMR spectrum of the aluminium carboxymethylphosphonate $Al(O_3PCH_2CO_2).3H_2O$ at 75.43 MHz.

The IR spectrum of the material (Figure 4.75) exhibits the main features expected from a carboxylic acid. A broad feature between *ca.* 3650 and 2700 cm^{-1} indicates a

large amount of hydrogen bonding in the material, which can also be found in the spectrum of the corresponding phosphonic acid. The stretching of the C-O bonds causes two bands at 1626 cm^{-1} (in the phosphonate) and 1624 cm^{-1} (in the acid) and 1382 / 1388 cm^{-1} respectively. The spectrum of the phosphonate furthermore contains various bands that are common for phosphonates (see Table 4.19). The results of these experiments seem to indicate that $Al(O_3PCH_2CO_2).3H_2O$ is the dominant phase in this system. The IR spectrum of carboxymethylphosphonic acid is discussed below in Section 4.9.2, but a summary of the bands is given in Table 4.19.

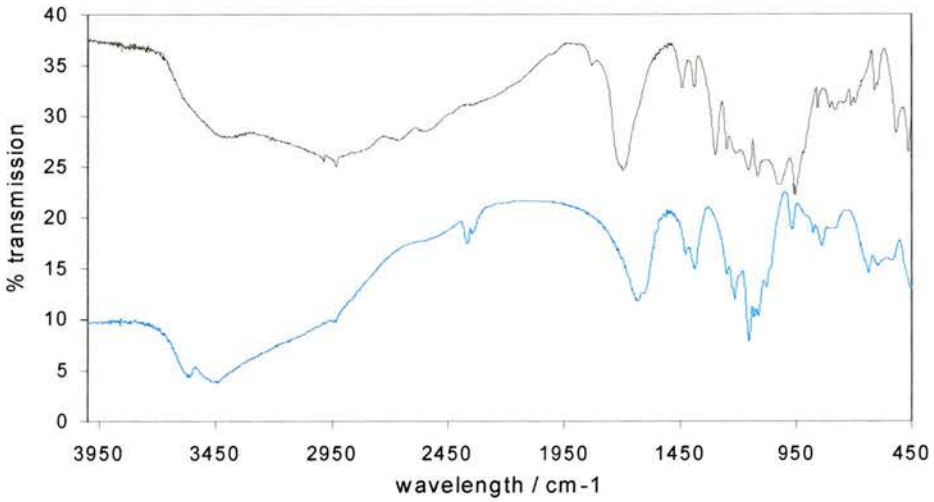

Figure 4.75: IR spectra of carboxymethylphosphonic acid (black) and the aluminium carboxymethylphosphonate $Al(O_3PCH_2CO_2).3H_2O$ (blue).

Table 4.19: Summary of the IR spectra of carboxymethylphosphonic acid and the aluminium carboxymethylphosphonate $Al(O_3PCH_2CO_2).3H_2O$.

Assigned vibration	**Carboxymethyl PA**	**$Al(O_3PCH_2CO_2).3H_2O$**
O-H stretching/ H bonding		3550 cm^{-1}
O-H stretching/ H bonding	3388 cm^{-1}	3435 cm^{-1}
C-H stretching/ CH_2	2985 cm^{-1}	
C-H stretching/ CH_2	2928 cm^{-1}	2928 cm^{-1}
(P-)O-H stretching	2652 cm^{-1}	
C=O stretching	1693 cm^{-1}	1626 cm^{-1}
C=O stretching	1387 cm^{-1}	1382 cm^{-1}
	1224 cm^{-1}	1229 cm^{-1}
	1152 cm^{-1}	1149 cm^{-1}
		1074 cm^{-1}

4.9.2. Aluminium carboxymethylphosphonate prepared according to Stucky and the corresponding zinc carboxymethylphosphonate

It was attempted to prepare the analogous aluminium compound to the zinc carboxymethyl-phosphonate recently published by Stucky *et al.*[17] In their paper, it was possible to prepare an open-framework zinc phosphonate with the carboxymethyl groups sticking out into 24-ring channels formed by this material. The reaction was carried out under hydrothermal conditions using zinc nitrate and carboxymethylphosphonic acid under addition of BTC and ethylendiamine in a mixture of water and ethylene glycol. Experiments on the zinc phosphonate showed that it was possible to prepare this material with high crystallinity under these reaction conditions. When a sample of the zinc carboxymethylphosphonate was prepared according to the procedure in the paper, the powder XRD pattern (Figure 4.76) closely matched both the powder XRD pattern and the theoretical pattern of the compound provided as supplementary material with the publication.

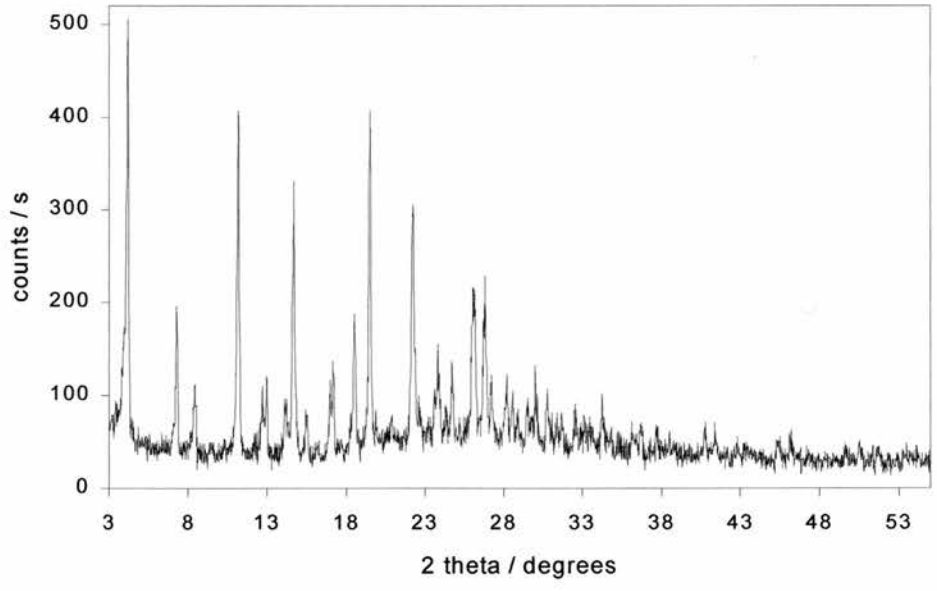

Figure 4.76: Powder XRD pattern of zinc carboxymethylphosphonate.

TGA experiments (Figure 4.77) and subsequent powder XRD done on the residues of the zinc phosphonate showed that its microporous structure broke down completely upon the removal of the organic molecules contained in the channels at 400 °C. Therefore, further experiments were not undertaken as a post-synthetic modification was impossible.

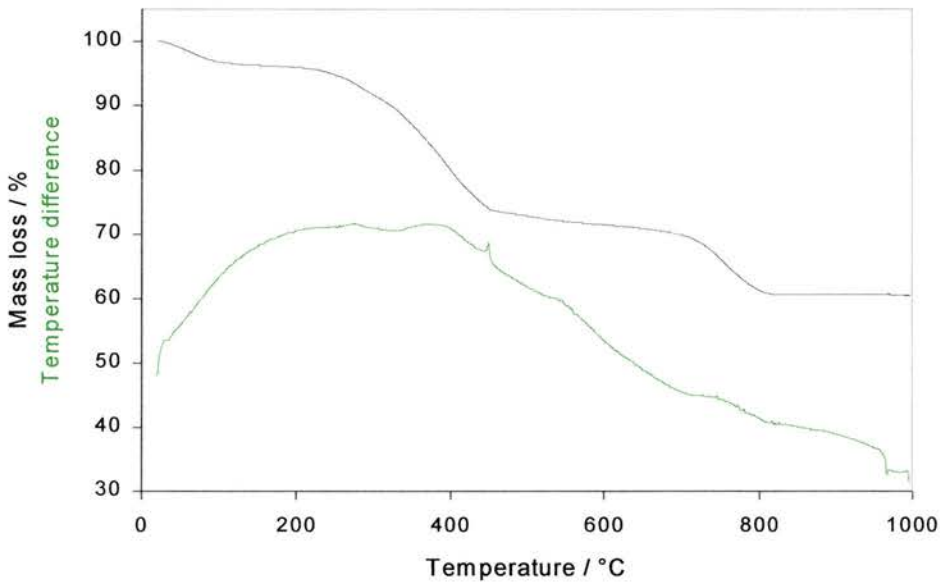

Figure 4.77: TGA trace of zinc carboxymethylphosphonate under oxygen.

For the analogous reaction, zinc nitrate was replaced by aluminium nitrate. However, the aluminium carboxymethylphosphonate turned out to have little crystallinity, with only two distinct peaks of low intensity at 14.5 Å and 6.2 Å (Figure 4.78, above).

Solid state MAS NMR spectroscopy of the aluminium carboxymethylphosphonate (Stucky)

In the ^{27}Al MAS NMR spectrum (Figure 4.79) there is a broad peak at -16.08 ppm and a weak peak at 38.90 ppm, indicating an octahedral environment for aluminium with an additional small amount of tetrahedral aluminium. In the ^{31}P MAS NMR spectrum there are also two peaks, a strong one at 1.93 ppm and a weak peak at

-15.87 ppm (Figure 4.80). The shift of the second peak is surprisingly small in comparison with other aluminium phosphonates (see Section 4.11, Comparison of the NMR shifts of different aluminium phosphonates). The ^{13}C MAS NMR spectrum contains three peaks, at 37.82 ppm, 134.30 ppm and 176.56 ppm (Figure 4.81). The first peak is due to the methylene carbon, which connected to the phosphorus. It is comparatively broad and could consist of an unresolved doublet. The peak at 176.56 ppm is caused by the carbonyl carbon that is deshielded by two oxygen atoms. The origin of the middle peak is doubtful, but it could be due to an impurity, as both the aluminium and the phosphorus NMR spectra do also contain peaks of low intensity (^{27}Al MAS NMR spectrum) or in unusual positions (^{31}P MAS NMR spectrum).

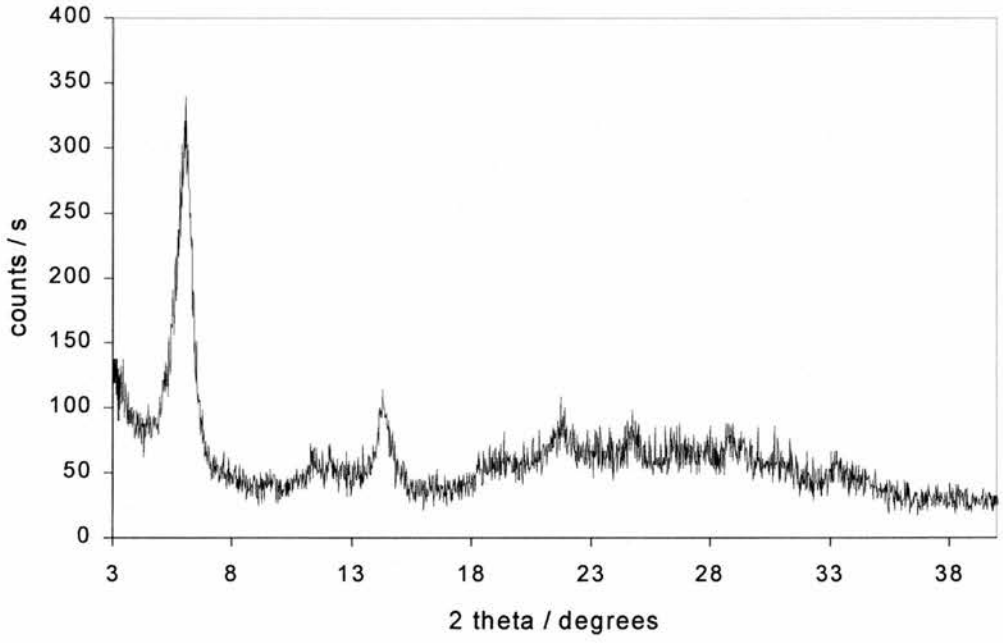

Figure 4.78: Powder XRD pattern of aluminium carboxymethylphosphonate (Stucky).

Thermogravimetric and CHN analysis of aluminium carboxymethylphosphonate (Stucky)

In the TGA (Figure 4.82), two mass losses can be observed. The first loss takes place at about 80 °C and should be due to loosely attached water molecules. The

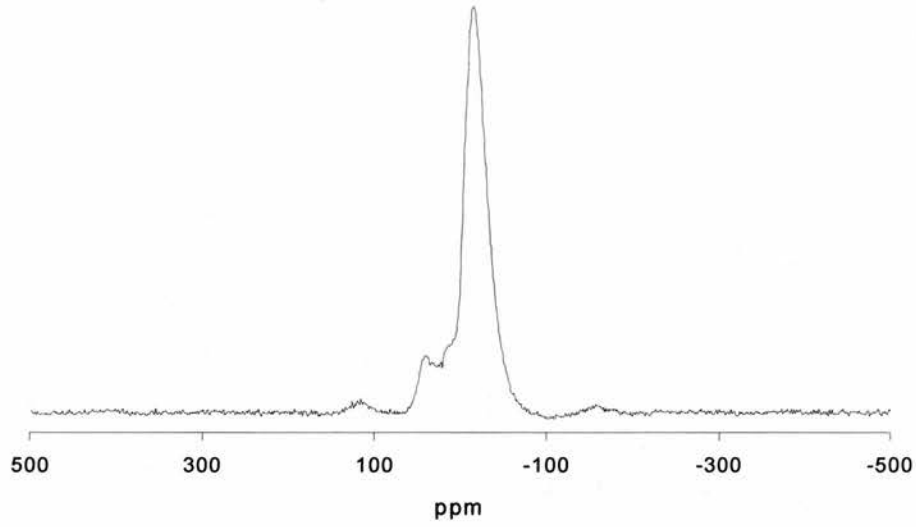

Figure 4.79: ^{27}Al MAS NMR of Al carboxymethylphosphonate (Stucky) at 78.16 MHz.

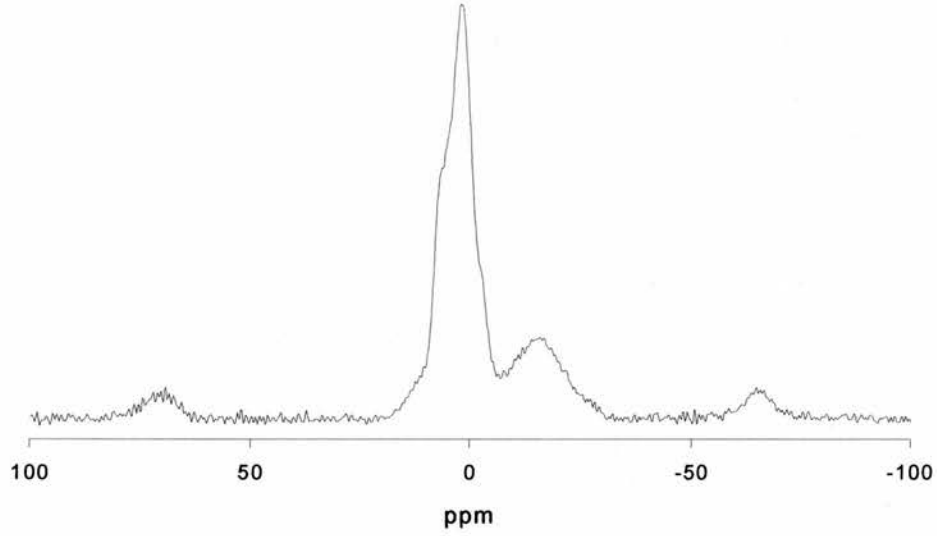

Figure 4.80: ^{31}P MAS NMR of Al carboxymethylphosphonate (Stucky) at 121.42 MHz.

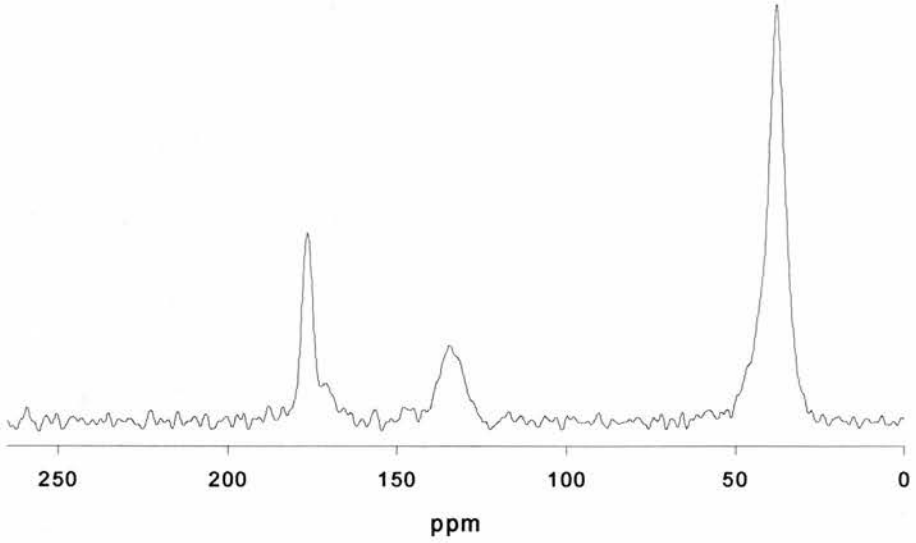

Figure 4.81: ^{13}C MAS NMR of Al carboxymethylphosphonate (Stucky) at 75.43 MHz.

second loss (42.05 %) happens between approximately 200 and 550 °C. The residue weighs 46.70 % of the original mass of the sample. As one of the starting materials was aluminium nitrate, the microanalysis was carried out for nitrogen as well as carbon and hydrogen. The results are; 17.64 % C, 3.45 % H and 5.52 % N.

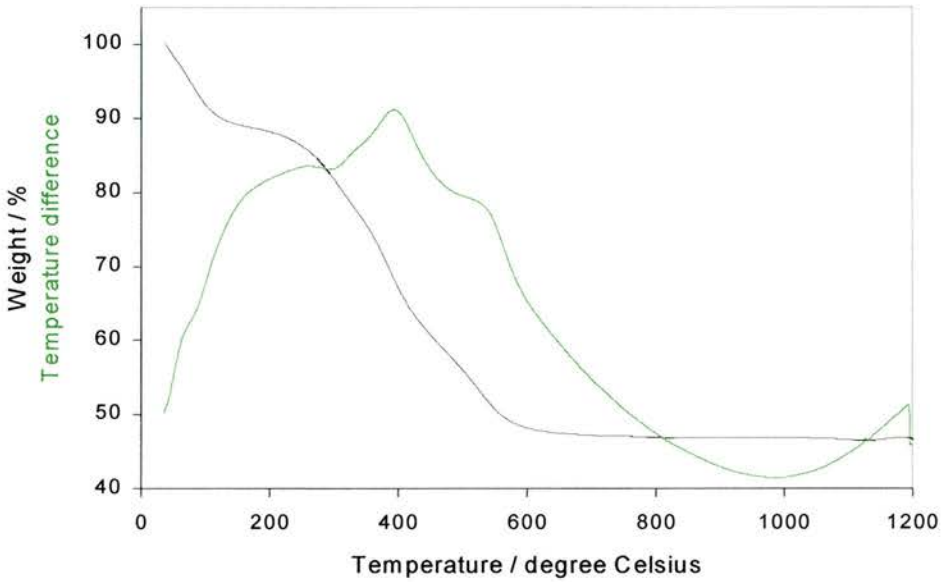

Figure 4.82: TGA trace of aluminium carboxymethylphosphonate Stucky.

IR spectroscopy of aluminium carboxymethylphosphonate (Stucky)

The spectrum of the phosphonate has a broad band at 3415 cm^{-1} in the area associated with O-H stretching vibrations with hydrogen bonding. An unassigned broad band is found at 1985 cm^{-1}. A band at 1636 cm^{-1} can be attributed to C=O stretching, as can another broad peak centred at 1380 cm^{-1}. The last major feature of the spectrum is a broad band at 1086 cm^{-1}, which is common for phosphonates. The spectrum of the phosphonic acid contains a broad peak at 3388 cm^{-1} (O-H stretching with H-bonding). There are also two bands at 2985 and 2928 cm^{-1} that could be due to C-H stretching vibrations. The band at 2652 cm^{-1} is caused by (P-)O-H stretching. A strong band at 1693 cm^{-1} stems from the C=O stretching vibration, as does the band at 1387 cm^{-1}.

Some of the common phosphonate bands can also be found; at 1224 cm^{-1} and 1152 cm^{-1}.

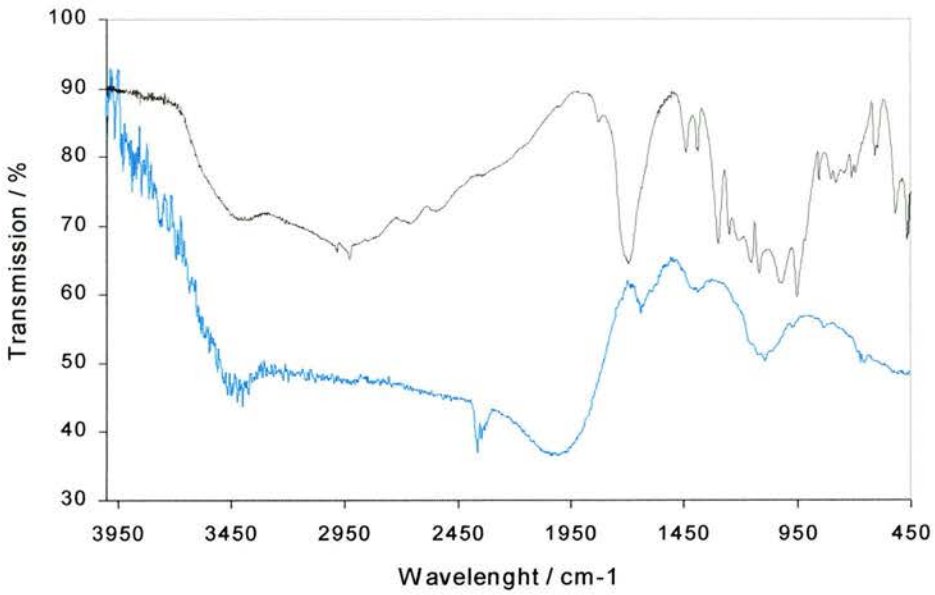

Figure 4.83: IR spectra of carboxymethylphosphonic acid (black) and aluminium carboxy-methylphosphonate (Stucky) (blue).

Table 4.20: Summary of the IR spectra of carboxymethylphosphonic acid and aluminium carboxymethylphosphonate (Stucky).

Assigned vibration	Carboxymethyl PA	Al carboxymethylphosphonate (Stucky)
O-H stretching/ H bonding	3388 cm^{-1}	3415 cm^{-1}
C-H stretching/ CH_2	2985 cm^{-1}	
C-H stretching/ CH_2	2928 cm^{-1}	
(P-)O-H stretching	2652 cm^{-1}	
C=O stretching	1693 cm^{-1}	1636 cm^{-1}
C=O stretching	1387 cm^{-1}	1380 cm^{-1}
	1224 cm^{-1}	
	1152 cm^{-1}	
		1086 cm^{-1}

4.10. Amidation of the amino-functionalised aluminium phosphonates with functionalised carboxylic acids

The amidation was carried out with aminomethyl-, 1-aminobutyl- and 4-aminobenzylphosphonates. All products were white. Sometimes the products

contained polycrystalline needles of an approximate length of 0.7 mm in addition to the usual powdered product. The needles were neither soluble neither in water or acetone (like the pure carboxylic acids) nor in dioxane (like DCC) and their nature could not be elucidated in the course of this work.

Powder X-ray diffraction

The different products prepared from aluminium aminomethyl- and 4-aminobenzylphosphonate share a common reflection at approximately 11.40 Å (see Table 4.21). The reflections at lower angles that occur in some of the X-ray patterns all had a very low intensity. Reflections below 9 Å were not listed in the table.

Table 4.21: Reflections in the powder XRD patterns of the amidation products.

Starting material/ phosphonate	Interlayer spacing of the starting material	Carboxylic acids	Reflections of the product in Å
Aminomethyl-[(a)]	9.88 Å	Oct.	12.48; 11.75; 10.02
Aminomethyl-[(a)]	9.88 Å	3-Hydr.	11.72; 9.86
Aminomethyl-[(a)]	9.88 Å	Imid.	11.72; 9.97
Aminomethyl-[(b)]	9.99 Å	4-Hydr.	11.41; 9.77
Aminomethyl-[(b)]	9.99 Å	Imid.	11.37; 9.84
Aminomethyl-[(b)]	9.99 Å	Oct.+4-Hydr.+Imid.	11.40; 9.80
1-Aminobutyl-[(a)]	14.29 Å	Oct.+4-Hydr.+Imid.	13.92; 11.42
1-Aminobutyl-[(b)]	14.10 Å	Oct.+4-Hydr.+Imid.	11.39
4-Aminobenzyl-[(b)]	15.79 Å	Oct.+4-Hydr.+Imid.	11.39
4-Aminobenzyl-[(a)]	15.59 Å	Oct.+4-Hydr.+Imid.	14.91; 11.46

[(a)] synthesised hydrothermally
[(b)] synthesised under reflux
Oct. ... Octanoic acid
3-Hydr. ... 3-Hydroxybenzoic acid
4-Hydr. ... 4-Hydroxybenzoic acid
Imid. ... Imidazolecarboxylic acid

For the products obtained from the aminomethylphosphonates a noticeable increase of the interlayer spacing occurred. The interlayer spacing for the starting material was 9.88 Å and 9.99 Å respectively, depending on the synthetic conditions. The main reflections for the products corresponded to interlayer spacings of approximately 11.70 Å and 11.40 Å, respectively. An additional weak reflection corresponding to an

interlayer spacing of 12.48 Å could be found in the product treated with octanoic acid. However, this reflection did not occur in the product prepared from a mixture of all three acids. The powder XRD patterns of aluminium aminomethylphosphonate prepared under reflux and of its amidation product with imidazolecarboxylic acid are shown in Figure 4.84.

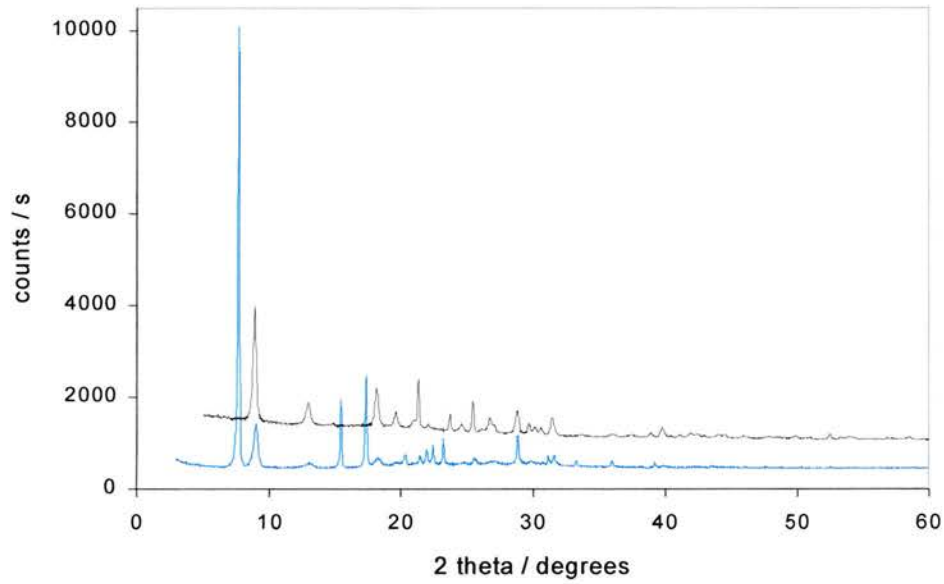

Figure 4.84: Powder XRD patterns of aluminium aminomethylphosphonate (black) and of its amidation product with imidazolecarboxylic acid (blue).

As it can be seen from Table 4.21, neither of the interlayer spacings of the products derived from the 1-aminobutylphosphonate by hydrothermal treatment or reflux could be increased by amidation. In the case of the hydrothermal product the interlayer spacing decreased from 14.29 Å to 13.92 Å. However, the first reflection corresponding to this interlayer spacing was rather weak and the first strong reflection was found at 11.42 Å. The interlayer spacing of the reflux product (14.10 Å) decreased to 11.39 Å. The amidation products of the 4-aminobenzyl-phosphonate also showed no increase in the interlayer spacings. There are no additional reflections at lower angles.

IR spectroscopy

The polycrystalline needles obtained from the products treated with imidazolecarboxylic acid were separated from the powdered product. Both the powder and the needles were examined. The IR spectra showed in no case any difference between the two products.

The product amidated with a mixture of three acids (4-hydroxybenzoic, octanoic and imidazolecarboxylic acid) exhibited exactly the same IR spectra as the products prepared with pure 4-hydroxybenzoic and imidazole carboxylic acid, respectively. There were no distinct features depending on the character of the acid or the starting material. The amidation with octanoic acid was not always successful. All products showed the Amide bands I, II and III. A comparison of the IR spectra of aluminium aminomethylphosphonate and of its amidation product with imidazolecarboxylic acid is given in Table 4.22, with their spectra shown in Figure 4.85.

Both spectra contain bands caused by O-H stretching vibrations with H bonding at 3403 and 3325 cm^{-1} for the phosphonate and the amidation product respectively. Both do also have bands in the area of N-H stretching vibrations (3028 and 3036 cm^{-1}, as before). This means that the amino groups in the amidation product did not fully react. There are also C-H stretching bands, at 2832 cm^{-1} for the phosphonate and at 2928 and 2849 cm^{-1} for the amidation product. The Amide I band can be found at 1626 cm^{-1} in the amidation product, with the N-H deformation vibration in the phosphonate in the same range (1616 cm^{-1}). The Amide II band is situated at 1574 cm^{-1}. The C-H deformation leads to bands at 1426 cm^{-1} and 1436 cm^{-1} in the phosphonate and the amidation product respectively. The Amide III vibration gives rise to a band at

1311 cm^{-1} in the amidation product and in this spectrum a band can also be found at 1087 cm^{-1} that is either due to C-N stretching or O-P-O bending. Furthermore, there are two of the bands that are commonly found in phosphonates in each of the spectra; at 1173 cm^{-1} and 1027 cm^{-1} in the phosphonate and at 1178 cm^{-1} and 1028 cm^{-1} in the amidation product.

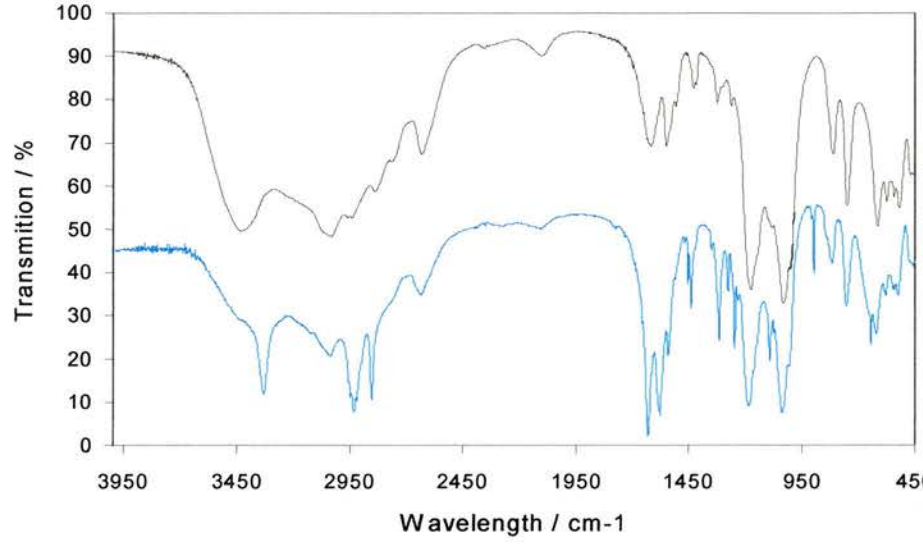

Figure 4.85: IR spectra of aluminium aminomethylphosphonate (black) and of its amidation product with imidazolecarboxylic acid (blue).

Table 4.22: Comparison of the IR spectra of aluminium aminomethylphosphonate and of its amidation product with imidazolecarboxylic acid.

Assigned vibration	**Al aminomethylphosphonate**	**Amidation product**
O-H stretching/ H bonding	3403 cm^{-1}	3325 cm^{-1}
N-H stretching/ H bonding	3028 cm^{-1}	3036 cm^{-1}
C-H stretching/ CH_2	overlapped	2928 cm^{-1}
C-H stretching/ CH_2	2832 cm^{-1}	2849 cm^{-1}
(P-)O-H stretching	2630 cm^{-1}	
(P-)O-H stretching	2090 cm^{-1}	
Amide I		1626 cm^{-1}
N-H deformation	1616 cm^{-1}	
Amide II		1574 cm^{-1}
C-H deformation/ P-CH_2	1426 cm^{-1}	1436 cm^{-1}
Amide III		1311 cm^{-1}
	1173 cm^{-1}	1178 cm^{-1}
C-N stretching or O-P-O bending		1087 cm^{-1}
	1027 cm^{-1}	1028 cm^{-1}

Most of the amidation products were lacking wetability, which caused them to float on the reaction solution and made it hard to recover them. This problem was partly overcome by the addition of acetone to the reaction mixture.[18] The increase in the interlayer distance for the product prepared from aluminium aminomethylphosphonate and the presence of amidation bands in the IR spectra of the amidation products implies that a post-synthetic modification of the material was indeed possible. However, as the structures of the starting materials are not known, few assumptions can be made as to the nature of their products. Furthermore, there is a possibility that the crystalline needles found in the products are due to recrystallisation or precipitation of the acids, although their solubility did not suggest this. EDX analysis would be a suitable tool for further investigation into the nature of the needles.

4.11. Comparison of the ^{27}Al and ^{31}P MAS NMR spectra of aluminium phosphonates

The ^{27}Al and ^{31}P MAS NMR shifts of all aluminium phosphonates prepared in the course of this work and of all previously known aluminium phosphonates (as far as published in the respective articles) are listed in Table 4.23. In the ^{27}Al MAS NMR spectra there are two ranges in which signals can be observed; 41 to 51 ppm for tetrahedrally coordinated aluminium and –63 to 6 ppm if the aluminium is octahedrally coordinated. These shifts for 4- and 6-coordinated aluminium are well known.[19,20,21]

It can be noted for the phosphorus spectra that there are various peaks that occur in several patterns at approximately the same shift, although not necessarily all at the same

time. A peak at 6.6 ± 0.4 ppm appears in the spectra of a diverse range of phosphonates such as;

aluminium aminomethylphosphonate ($-CH_2-NH_2$),

aluminium 1-aminobutylphosphonate ($-CH(NH_2)-CH_2-CH_3$),

AlaPrPO-1 ($Al(O_3P(CH_2)_3NH_3).SO_4.3H_2O$),

AlMePO-β[6] ($-CH_3$),

aluminium vinylphosphonate ($-CH=CH_2$), and

$Al_2(O_3PC_6H_5)_3.2H_2O$.[22]

The formula of the organic group connected to the phosphorus is shown in brackets.

Another peak can be found at 10.5 ± 0.2 ppm. However, it also occurs in various materials, some of which have organic groups with widely different structures such as;

$Al(OH)(O_3PCH_2C_6H_5).H_2O$ (AlBzPO-1),

aluminium 4-aminobenzylphosphonate ($-CH_2-C_6H_4-NH_2$),

aluminium aminomethylphosphonate ($-CH_2-NH_2$), and

AlMePO-β[6] ($-CH_3$).

Thus it becomes obvious that generalisations cannot be made that easily as the phosphorus environments vary profoundly between most of these materials. It seems that phosphonates with different environments can accidentally have the same shift. However, it is reasonable to assume similar phosphorus environments if all phosphorus shifts in the spectrum are similar and not just one of them. This is the case for

AlBzPO-1 and aluminium 4-aminobenzylphosphonate. Nevertheless, it is also true for AlaPrPO-1, aluminium vinylphosphonate (both have one peak at 6.2 ppm) and aluminium 1-aminobutylphosphonate (one peak at 6.5 ppm), which have chemically very different organic groups connected to the phosphorus. Still, in these cases there is only one peak in each spectrum, making an accidental agreement of the shifts more likely than for the aluminium benzyl- and 4-aminobenzylphosphonate with two peaks in their respective spectra.

Table 4.23: Comparison of ^{27}Al and ^{31}P NMR shift of aluminium phosphonates

Al Phosphonate	**^{27}Al**				**^{31}P**						
aminomethyl~ (Section 4.4)		4.5	-19.9				10.3	6.7	1.8		
2-aminoethyl~ (Section 4.3)			-23.0		18.9	17.5 14.5					
$Al(O_3P(CH_2)_3NH_3).SO_4.3H_2O$ (AlaPrPO-1, Section 4.2.1)			-13.0					6.2			
1-aminobutyl~ (Section 4.5)		5.1	-9.3					6.5			
iminobis(methyl~) (Section 4.7)			-19.3						3.0 -0.4	-6.6	
vinyl~ (Section 4.8)			-26.2	-63.7				6.2			
carboxymethyl~ (Stucky) (Section 4.9.2)	38.9		-16.8						1.9		-15.9
$Al(O_3PCH_2CO_2).3H_2O$ [16]									-1.8	-7.4	
AlMePO-β[6]	41.2		-17.6			14.7 13.1	10.3	6.9	1.5		
$Al(OH)(O_3PCH_3).H_2O$[2]		- 0.2				13.6					
4-aminobenzyl~ (Section 4.6)			-14.9	-48.0	22.3		10.7				
$Al(OH)(O_3PCH_2C_6H_5).H_2O$ (AlBzPO-1, Section 4.1.1)		0.0					10.3				
$Al(OH)(O_3PCH_2C_6H_4Br).H_2O$ [23]		1.1					11.1				
$Al_3H(PO_3CH_2C_6H_5)_5.H_2O$ (AlBzPO-2, Section 4.1.2)					19.8	16.8			1.3		
$Al_2(O_3PC_6H_5)_3.H_2O$[23]	51.4		-13.4						2.0 -1.2		
$Al_2(O_3PC_6H_5)_3.2H_2O$[22]	44		-21						-3	-6 -8	
$Al_2(O_3PC_6H_5)_3.4H_2O$[24]									0		
$Al(HO_3PC_6H_5)_3.H_2O$[22]			-20					5.1	1.7		
$AlH(O_3PC_6H_5)_2.H_2O$[25]			-16								
α- $Al(HO_3PC_6H_5)(O_3PC_6H_5).H_2O$ [22]			-13.1						1.5 0.3		

A comparison of ^{31}P MAS NMR spectra of aluminium phosphonates therefore seems to be possible only if the whole spectrum is taken into account and not just single peaks. It is moreover necessary to be careful not to compare phosphonates with organic groups that have widely different chemical structures. It was not possible to compare the phosphorus shifts of aluminium phosphonates with respect to their connectivities as it was done by Massiot *et al.* for zinc phosphonates.[26] The lack of suitable data from different phases within one aluminium phosphonate system pre-empted any such attempts.

4.12. References for Chapter 4

[1] TREOR90, P.E. Werner, University of Stockholm, Sweden, **1990**

[2] L.-J. Sawers, V.J. Carter, A.R. Armstrong, P.G. Bruce, P.A. Wright and B.E. Gore, *J. Chem. Soc., Dalton Trans.*, **1996**, 3159-3161

[3] GSAS, R.B. von Dreele and A.C. Larson, Regents of the University of California, USA, **1995**

[4] G. Chaplais, J. Le Bideau, D. Leclercq, H Mutin and A. Vioux, *J. Mater. Chem.*, **2000**, 10, 1-10

[5] J.D. Gale, *Faraday Discuss.*, **1997**, 106, 219

[6] K. Maeda, Y. Kiyozumi and F. Mizukami, *Angew. Chem. Int. Ed. Engl.*, **1994**, 33, 1335-1337

[7] K. Maeda, J. Akimoto, Y. Kiyozumi and F. Mizukami, *J. Chem. Soc., Chem. Commun.*, **1995**, 1033-1034

[8] SHELX97, G.M. Sheldrick, Institut für Anorganische Chemie der Universität Göttingen, Tammanstr. 4, Göttingen, Germany, **1998**

[9] J. LeBideau, A. Jouanneaux, C. Payen and B. Bujoli, *J. Mater. Chem.*, **1994**, 4, 1319-1323

[10] EXPO, A. Altomare *et al.*, University of Bari, Italy, **1997**

[11] Encyclopedia of Nuclear Magnetic Resonance, eds. D.M. Grant and R.K. Harris, John Wiley & Sons, Chichester, **1996**, vol. 5, pp. 3230

[12] C.N.R. Rao, *Chemical applications of infrared spectroscopy*, Academic Press, London, **1963**

[13] G. Alberti, U. Costantino, M. Casciola and R. Vivani; *Solid State Ionics*, **1991**, 46, 61-68

[14] H.G. Harvey, S.J. Teat and M.P. Attfield; *J. Mater. Chem.*, **2000**, 10, 2632-2633

[15] G.B. Hix, unpublished work

[16] G.B. Hix, D.S. Wragg, R.E. Morris and P.A. Wright; *J. Chem. Soc,. Dalton Trans.*, **1998**, 3359-3361

[17] J. Zhu, X. Bu, P. Feng and G.D. Stucky, *J. Am. Chem. Soc.*, **2000**, 122, 11563-11564

[18] S. Yamanaka, K. Sakamoto and M. Hattori, *J. Phys. Chem.*, **1984**, 88, 2067-2070

[19] C.S. Blackwell and R.L. Patton, *J. Phys Chem.*, **1988**, 92, 3965-3970

[20] *Encyclopedia of inorganic chemistry*, ed. R.B. King, John Wiley & Sons, Chichester, **1994**, vol. 5, pg. 2645-2646

[21] C.A. Fyfe and R.E. Wasylishen, *High-resolution solid-state MAS NMR investigations of inorganic systems, in* Solid State Chemistry – Techniques, eds. A.K.Cheetham and P.Day, Oxford University Press, **1988**, pg. 220

[22] A. Cabeza, M.A.G. Aranda, S. Bruque, D.M. Poojary, A. Clearfield and J. Sanz, *Inorg. Chem.*, **1998**, 37, 4168-4178

[23] G. Chaplais, J. Le Bideau, D. Leclercq, H Mutin and A. Vioux, *J. Mater. Chem.*, **2000**, 10, 1-10

[24] L. Raki and C. Detellier, *Chem. Commun.*, **1996**, 2475-2476

[25] J.E. Haky, J.B. Brady, N. Dando and D. Weaver, *Mater. Res. Bull.*, **1997**, 32, 297-303

[26] D. Massiot, S. Drumel, P. Janvier, M. Bujoli-Doeuff and B. Bujoli, *Chem. Mater.*, **1997**, 9, 6-7

Chapter 5. Conclusions and future work

During the investigation into new aluminium phosphonate materials it was found that aluminium phosphonates generally do not crystallise well. The one exception to this was aluminium carboxymethylphosphonate, $Al(O_3PCH_2CO_2).3H_2O$ (Chapter 4.9.1). The structure determination was thus greatly complicated, as even microcrystals are a rare occurrence. Powder data did only in one case (AlBzPO-1, $Al(OH)(O_3PCH_2C_6H_5).H_2O$, Chapter 4.1.1) yield enough data for the full structural characterisation of a material and even there it was necessary to use information from a previously known compound. For aluminium vinylphosphonate the lack of data has so far prevented the unambiguous allocation of a space group (Chapter 4.8). Yet even when microcrystals were obtained, the structure solution could be complicated by their small size (AlBzPO-2, $Al_3H(O_3PCH_2C_6H_5)_5.H_2O$, Chapter 4.1.2).

The structure of AlaPrPO-1 ($Al(O_3P(CH_2)_3NH_3).SO_4.3H_2O$, Chapter 4.2.1) is highly interesting as it comprises an inversion of the conditions normally found in aluminium phosphates, where the inorganic framework tends to be neutral or negatively charged and protonated/quaternary amines are used as structure directing agents. The appearance of a material with a positively charged framework balanced by occluded sulphate anions opens a whole new range of possible structures. AlaPrPO-1 could be the first of a new range of aluminium phosphonates with an inverse charge distribution. In addition, the presence of positive charges in the framework should allow the intercalation of new species such as negatively charged ions.

The protonated amino groups in AlaPrPO-1 also make it a good starting point for the post-synthetic modification of aluminium phosphonates. Experiments on post-synthetic amidation in

this work were hampered by the lack of knowledge about the structure of the starting materials. With a fully characterised amino-functionalised aluminium phosphonate now available, more in-depth experiments could be conducted in this area.

Another area of interest is the aluminium vinylphosphonate (Chapter 4.8). It may be rewarding to investigate the structural changes occurring at elevated temperatures, especially whether or not the vinyl groups polymerise. However, previous knowledge of the phosphonate structure would be necessary for this.

Chemicals

Acetone	Bamford Laboratories, 99.5 %
Aluminium sulphate hydrate	Aldrich, 98 %
Aluminium nitrate	BDH, 99 %
Aluminium chloride	Aldrich, 98 %
4-Aminobenzylphosphonic acid	Aldrich, 97 %
1-Aminobutylphosphonic acid	Aldrich, 98 %
2-Aminoethylphosphonic acid	Aldrich, 99 %
Aminomethylphosphonic acid	Aldrich, 99 %
3-Aminopropylphosphonic acid	Aldrich, 99 %
Carboxymethylphosphonic acid (Phosphonoacetic acid)	Aldrich, 98 %
Dicyclohexylcarbodiimide	Aldrich, 99 %
Diethyl benzylphosphonate	Aldrich, 99 %
Dioxane	Avocado, 98 %
Gibbsite	ACROS
Hydrochloric acid	Fisher, 37 %
3-Hydroxybenzoic acid	Fluka, 98 %
4-Hydroxybenzoic acid	Aldrich, 99 %
Imidazolecarboxylic acid	Aldrich, 98 %
Iminobis(methylphosphonic acid)	Aldrich, 97 %
Nitric acid	BDH, 69 %
Octanoic acid	BDH, 97.5 %
Potassium bromide	Aldrich, 99+ %, FT-IR grade
Sodium hydroxide	Fisher Chemicals, 97 %
Sulphuric acid	Prolabo, 95 %
Vinylphosphonic acid	Aldrich, 97 %